WEATHERING OF BASALT:
GEOTECHNICAL & GEOCHEMICAL ASPECTS

Thesis
submitted in partial fulfilment of
the requirements for the Degree
of
Doctor of Philosophy
in
Earth Sciences
by

Merennage Padma Jayanthi Jayawardane

University of Waikato
2002

ABSTRACT

Geochemical influences on the geotechnical parameters of weathered Karamu Basalt are determined and the likely processes involved in basalt weathering are investigated. Geochemical and geotechnical parameters of basalt at different stages of weathering are evaluated; possible relationships between these two sets of parameters are determined and quantified; models are formulated based on statistical analysis; and an hypothesis is postulated to explain the weathering processes.

At an abandoned basalt quarry, materials belonging to different weathering grades are observed and described. *In situ* geotechnical tests such as Schmidt rebound hardness, penetration resistance and vane shear and laboratory tests such as uniaxial compressive strength, point load, direct shear, Shore scleroscope hardness, California Bearing Ratio, water content, density, particle size distribution, Atterberg limits, permeability, X-ray fluorescence and diffraction, abrasion pH, electrical conductivity, petrography, and scanning electron microscopy are carried out. Using statistical methods, comparisons between geochemical and geotechnical parameters are determined, and their relationships shown in graphical form. Model equations, which depict these relationships quantitatively, are evaluated.

Geochemical results show the following major element concentrations in fresh Karamu Basalt: SiO_2 42.39 ± 1.66%; Al_2O_3 12.04 ± 0.23%; MgO 12.53 ± 0.59%; CaO 10.82 ± 0.31%; FeO 10.34 ± 0.35%; Fe_2O_3 3.09 ± 0.10%; TiO_2 2.41 ± 0.11%; Na_2O 1.30 ± 0.35%; K_2O 0.70 ± 0.26%; MnO 0.18 ± 0.00%; and loss on ignition 3.68 ± 0.99 %. In this study, the loss on ignition was assumed to be the structural water (H_2O+) concentration. As weathering proceeds, there is a reduction in CaO, MgO and FeO and an increase of Al_2O_3, Fe_2O_3 and H_2O+. When the chemical concentrations are recalculated assuming a constant Al concentration, these trends remain the same for CaO, MgO, FeO, Fe_2O_3 and H_2O+. The following trace elements are also identified: V, Cr, Ni, Zn, Ga, Rb, Sr, Y, Zr, Nb, Ba, La, Ce, Nd, Pb and Th. At the slight stage of weathering, an increase in concentration is shown by : V, Cr, Ni, Zn, Ga, Y, Zr, Nb, Ba, La, Ce, Nd, Pb and Th. Some trace elements follow the abundance patterns of the major elements containing similar charges and compatible ionic radii (Ba follows Ca while Ga follows Al). Principal component analysis indicates that CaO amd MgO values serve as discriminators of fresh basalt.

Petrographic studies show that fresh basalt is holocrystalline to hypocrystalline, fine grained, porphyritic with phenocrysts of olivine, titanaugite, plagioclase and rare titanomagnetite set in a groundmass composed of plagioclase laths, titanaugite, olivine, glass and titanomagnetite; approximately olivine 33%, titanaugite 28%, plagioclase 34 %, glass 2 % and titanomagnetite 2%. Apatite and chromite are accessory minerals. As weathering proceeds the mineral assemblage changes and finally the completely weathered basalt consists of only secondary minerals (clays, hematite and goethite).

The weathering profile was divided into five grades according to the New Zealand Geomechanics Society Standards: fresh, slightly weathered, moderately weathered, highly weathered and completely weathered. Only some geotechnical results could be obtained for all grades of weathering due to the varying nature

of the testing materials. They are California Bearing Ratio (CBR), density, porosity and water content. Fresh rock is strong (uniaxial compressive strength ~ 262 MPa) with near-vertical columnar jointing. Along joint planes, discolouration occurs at slightly weathered stage. From fresh to slightly weathered stage, there is a dramatic drop in strength parameters (average point load strength index 5.59 for fresh rock, 0.41 for slightly weathered basalt; CBR drops from 100 % to 45 %), and horizontal joints develop. From fresh to completely weathered CBR drops from 100 % to 1 %; density drops from 2902 kg m^{-3} to 1502 kg m^{-3}; and porosity increases from 0.18% to 27.19 %. From slight to completely weathered stage cohesion and water content increase (cohesion 0 to 7 kPa; water content 12 % to 59 %). From the moderately weathered stage, corestones are reduced in size and a clayey matrix develops. The material shows plastic behaviour, but Atterberg limits show no consistent trends with weathering grade.

Based on chemical analyses, an easily calculable "new weathering index" (NWI):

$$NWI = (MgO+CaO+FeO)/(Al_2O_3+Fe_2O_3+H_2O+)$$

which may be used to define the degree of weathering of Karamu Basalt, is proposed. It correlates well with compressive strength, water content, density, porosity, and California Bearing Ratio but does not correlate well with shear strength, Atterberg limits, cohesion or angle of internal friction.

Abrasion pH value is indicative of the degree of weathering. It is higher in fresh rock (8.5) and gradually decreases to 4 due to weathering. Abrasion pH has good positive correlations with compressive strength, density, and California Bearing Ratio and negative correlations with water content, cohesion, and porosity. By obtaining the abrasion pH of Karamu Basalt material, its degree of weathering can be determined.

Several chemical predictors of geotechnical parameters are formulated. Predictor "x", given by:

$$x = 225\ pH + 283\ TiO_2 + 7.4\ Sr - 80\ Fe_2O_3$$

provides the best prediction of geotechnical properties of Karamu Basalt. Its suitability for other lithologies could not be evaluated due to unavailability of data regarding trace element content and abrasion pH value. Modified versions with fewer components were tested against other lithologies, with some success for specific parameters. Obtaining trace element analysis and abrasion pH values is thus crucial for predicting geotechnical parameters from geochemical data.

A causal relationship between the loss of cations Mg and Ca and initial loss of strength is hypothesised. The early stage of weathering is diffusion controlled (with some hydrolysis) whereby cations are lost from the constituent primary minerals and are replaced by H^+ and possibly Al^{3+}. This process affects the lattice structure due to radius to charge ratio imbalances, thus causing a marked loss of strength, leading to microfractures and later macrofracturing following stress release. Later weathering is controlled by hydrolysis, dissolution, Redox and leaching, leading to the development of clay minerals.

Based on the results of this study, it is suggested that the basalt weathering profile be divided into only 3 categories as follows: fresh rock, weathered rock and saprolitic soil. Fresh rock should remain as it is; slightly weathered, together with moderately weathered material should be called weathered rock; highly and completely weathered material should be included in the saprolitic soil. This is a simpler classification, and better reflects the geotechnical behaviour of the materials. Further investigation may indicate the suitability of this simpler classification for other lithologies.

ACKNOWLEDGMENTS

I have great pleasure in thanking my supervisors Dr. V. G. Moon, Dr. A.P.W. Hodder and Prof. R. M. Briggs for helping me in carrying out this project, for marking the manuscript and timely advice.

It would not have been possible for me to write a Ph.D. thesis if not for the kind guidance of Professors, C.S.Nelson, M.J.Selby and David Lowe and I take this opportunity to thank them. Dr Ray Littler of the Department of Statistics is gratefully remembered for the help given in carrying out statistical analysis.

My gratitude is extended to Dr Jock Churchman and Dr. Leah Moore both of Australia for the help given in interpreting my results.

While I received technical support from Mike Vennard, Steve Bergin, Yuang Ji and Alf Harris, and student support from Loretta Garett and Rodney Milner to whom I am grateful, I also received encouragement from Penny Cooke, Frank Bailey, Sydney Wright and Elaine Norton to whom I wish to say a big "Thank You".

The project site belonged to Ron and Sue Thompson, at the time the field investigations were carried out, and I wish to thank them both for their hospitality.

A very special vote of gratitude is offered to Renat Radosinsky and Thesara Jayawardane for assisting me in many ways, especially with the presentation techniques.

Jayanthi

LIST OF CONTENTS

LIST OF FIGURES

LIST OF TABLES

CHAPTER 1: INTRODUCTION

Rocks and soils of varied degrees of weathering are being used in the roading and building industry. Phenomenon of weathering may be considered to be one of the greatest sources of potential difficulties in geotechnical engineering (Price, 1995). The weathered nature of the ground can lead to special problems at every stage of an engineering project (Hencher and McNicholl, 1995). Mineral composition and chemistry of rocks and soils are known to affect geotechnical parameters but few attempts (as given in section 1.3) have been made to determine their exact influences. The purpose of this research is to attempt to quantify the geochemical influences on the geotechnical parameters of weathered basalt of North Island, New Zealand, and to develop an understanding of the likely processes involved in basalt weathering.

1.1 Aims of the study

In a broad sense, this project is an attempt: a) to determine the precise role geochemistry plays in controlling the geotechnical properties of rock materials derived from weathering of basalt; b) to investigate the possibility of establishing models of relationships between geochemical and geotechnical parameters; and c) to present the most suitable of the geochemical predictors of geotechnical parameters.

Specific objectives of the project are: a) to evaluate the geochemical and geotechnical parameters of basalt at different stages of weathering; b) to determine possible relationships between these two sets of parameters; c) to quantify these relationships and formulate models based on statistical analysis; and d) to formulate a hypothesis to explain the weathering processes.

1.2 Scope of the study

Since basalt is a common rock type in New Zealand, chemically weathered basalt was selected as the testing material for this research. Due to availability of an exposed weathering profile, an abandoned basalt quarry at Karamu was chosen for the study. Karamu is a village which lies 17 km southwest of Hamilton (Figure 1.1).

1.3 Previous work

Few previous studies have considered both geochemical and geotechnical aspects of rocks and soils and attempted at determining relationships between geochemical and geotechnical parameters (Table 2.6). Some key studies are outlined below:

(a) Nutter and Otton (1969) correlated degree of weathering with porosity.

(b) Aires-Barros (1978) made an attempt to link physical (microhardness and reflectivity) and chemical measurements (Parker and Miura Indices) of weathering.

(c) Malomo (1980) correlated abrasive pH of feldspars with the physical properties such as porosity, absorption and specific gravity of granites.

(d) Hodder (1984) made a thermodynamic interpretation of weathering indices and its application to engineering properties of rocks.

(e) Obermeier and Langer (1986) studied the correlation between the degree of weathering and permeability.

(f) Veldkamp *et al.* (1990), working on alkali basalt gravel, determined how the bulk density can be predicted from the chemical compositions of three elements: silicon, magnesium and potassium.

(g) Hodder and Hetherington (1991) correlated Hodder susceptibility index with physical durability tests and demonstrated that there is a close relationship between chemical and physical indices for which a thermodynamic justification was claimed.

(h) Ohtsubo *et al.* (1995) found that in marine clays, sensitivity and overconsolidation ratio depended on the iron oxide content.

(i) Bassett (1998) determined correlation between California Bearing Ratio, point load strength index, water content, density and porosity with the geochemical parameters.

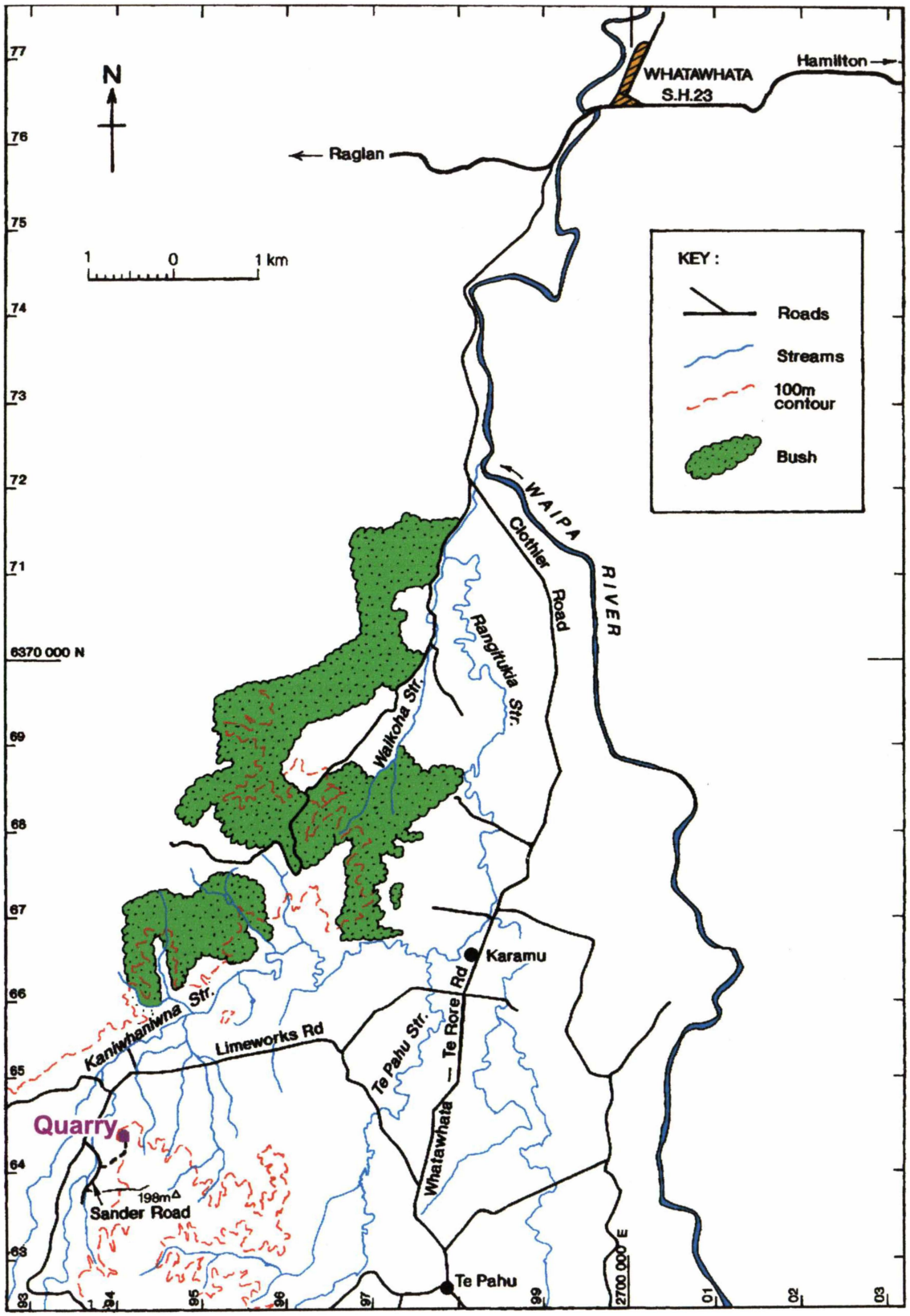

Figure 1.1 Location Map of Karamu Quarry

1.4 Geology of the study area

Karamu is a volcanic centre of the Okete Volcanics, which is part of the Alexandra Volcanics Group (Briggs and Goles, 1984). This group is the southernmost of the Pliocene-Quaternary (2.7 to 1.6 Ma) basalt fields of northern North Island. Okete Volcanics form a basalt field of monogenetic volcanoes scattered around the Raglan - Pirongia area. The Okete Volcanics have compositions which include basanites, alkali-olivine basalts and hawaiites (Briggs & Goles 1984). Karamu volcanic centre consists of basaltic lava flows and associated scoria material. The age of the lava flows is estimated at 2.03 ± 0.03 Ma (Stipp 1968). The basaltic lavas are overlain by a thick sequence of weathered rhyolitic tephra and alternating paleosols belonging to the Hamilton Ash Formation (Horrocks, 2000). The oldest of these beds, called "H1", is 0.35 ± 0.04 Ma (Kohn *et al.* 1992). This implies that the Karamu Basalt was exposed for an approximate period of 1.65 Ma before being covered by tephra.

1.5 Methods

At the outset of the project, an abandoned basalt quarry at Karamu which showed a complete weathering profile starting from fresh basalt, through slightly weathered, moderately weathered, highly weathered to completely weathered basalt was selected (Figure 1.2). The materials at different depths were observed and described.

In situ tests such as Schmidt rebound hammer hardness, vane shear and penetration resistance were carried out in the field. Samples of each unit in the profile, in quantities of up to 10 kg, were then collected and prepared for laboratory examination. In the laboratories, tests were carried out to determine the following geotechnical parameters: uniaxial compressive strength, point load strength index, Shore scleroscope hardness, California Bearing Ratio, water content, bulk density, dry density, particle density, particle size distribution, cohesion and angle of internal friction, Atterberg limits and permeability.

In order to determine the geochemical parameters of these materials, the following studies were carried out: X-ray fluorescence for chemical analyses, X-ray diffraction for mineral identification, abrasion pH values, electrical conductivity, petrographic descriptions on thin and polished sections, and scanning electron microscopy.

Distribution patterns of geochemical and geotechnical parameters as well as mineralogy throughout the weathering profile, with emphasis on the depth, were studied in detail. Attention was given to any possible patterns or trends of these parameters, with regard to the degree of weathering. Weathering indices were calculated based on the results of chemical analyses, and a weathering index suitable for the Karamu Basalt was formulated.

Using statistical methods, comparisons between geochemical and geotechnical parameters were determined, and their relationships shown in graphical form. Model equations, which depict these relationships quantitatively, were evaluated. Based on these findings, a conceptual model and a hypothesis were proposed which explain the processes and changes taking place in weathering of Karamu Basalt. Several chemical predictors of geotechnical parameters were formulated, and their applicability to other rock types from New Zealand and overseas was tested.

1.6 Thesis Outline

Chapter 1 introduces the project objectives and thesis content. Chapter 2 gives a literature review on chemical weathering of basaltic rocks: definitions of important terms, classifications of weathering, mineralogy of basalt, and previous studies on establishing relationships between chemical and geotechnical properties. Chapter 3 gives details of the methodology used in carrying out this research project: field investigations, geochemical investigations and laboratory geotechnical investigations.

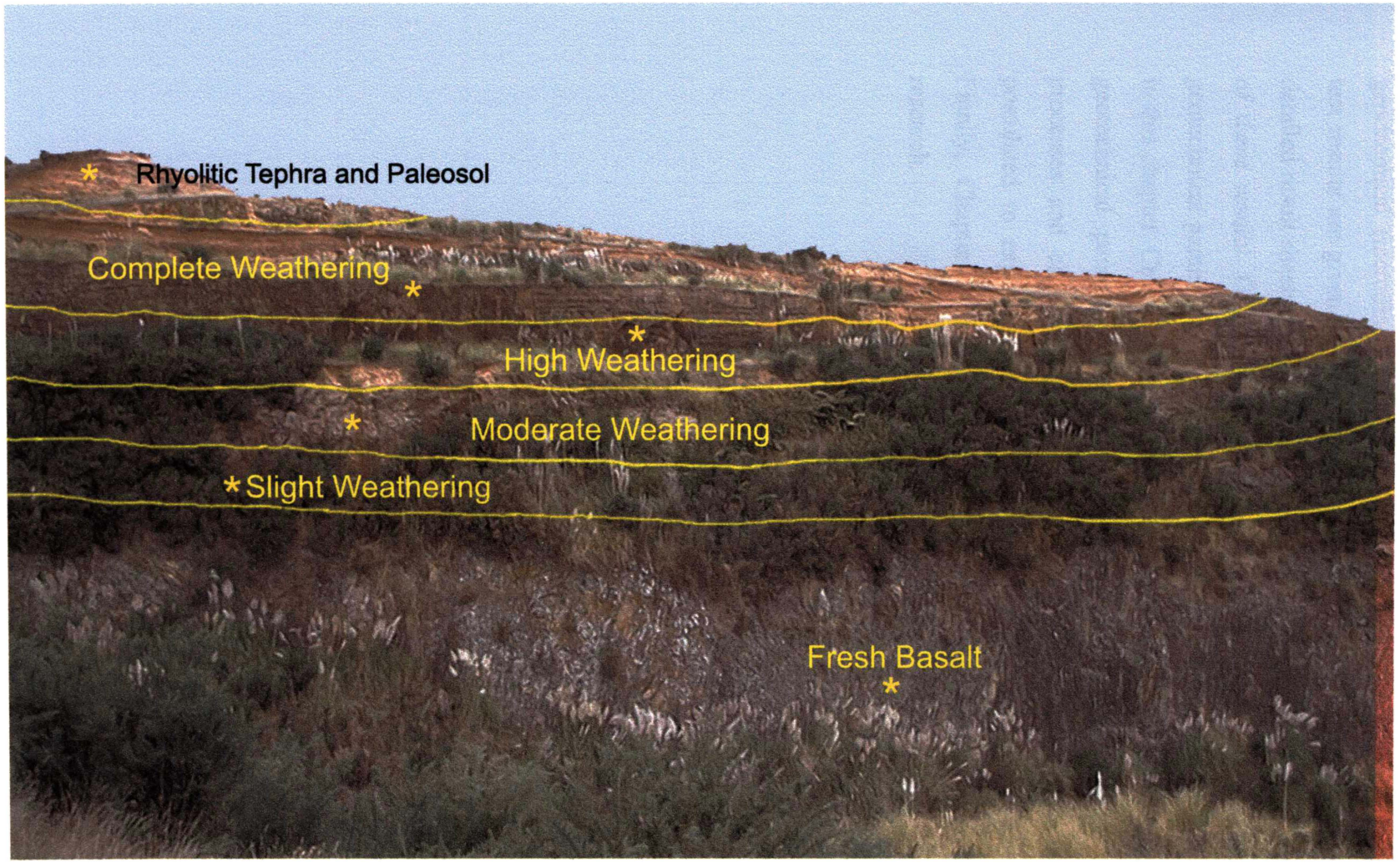

Figure1.2 Photograph of weathering profile at Karamu quarry (overall face height 80 m). Weathering grades according to the New Zealand Geomechanics Standards (1988).

Chapters 4 and 5 cover the observations made and the results obtained from geochemical (including mineralogy) and geotechnical investigations respectively. Most test results are given in the form of tables and graphs within the chapters, and some detailed result sheets are included as appendices. Chapter 6 contains statistical analyses of these results. Graphical presentations of relationships between geochemical and geotechnical parameters and comparisons made with other lithologies also are included in this chapter. Chapter 7 gives a detailed conceptual model and chemical predictors of geotechnical parameters, proposed by the author, which explain the weathering processes and changes that have taken place. Chapter 8 discusses a hypothesis postulated to explain the weathering processes that take place in Karamu Basalt. Finally, Chapter 9 presents conclusions and recommendations made for further research.

CHAPTER 2: WEATHERING OF BASALT: A LITERATURE REVIEW

2.1 Introduction

This chapter is a collection of information pertaining to the weathering of basalt published by different authors. The importance of studying weathering in detail can be expressed by quoting Price (1995, p.243):

> "The shallow domain of geotechnical engineering in the Earth's crust happens to be that zone in which the processes of weathering, erosion, transportation and deposition are conspicuously active. Weathering modifies the mineralogy and texture of the geological materials within this zone and thus the phenomenon of weathering may be considered to be one of the greatest sources of potential difficulties in geotechnical engineering".

2.1.1 Definition of Weathering

Weathering is defined in a number of ways depending on the standpoint of each different author:

(a) According to Reiche (1950), weathering is the response of materials which were in equilibrium within the lithosphere to conditions at or near to its contact with the atmosphere, the hydrosphere, and perhaps more importantly, the biosphere.

(b) Ollier (1984, p.1) states "Weathering is the breakdown and alteration of materials near the Earth's surface to products that are more in equilibrium with newly imposed physico-chemical conditions".

(c) Later, Ollier (1991) redefines weathering as the alteration and breakdown of rocks near the Earth's surface, mainly by reaction with water and air, to form clay, iron oxides and other weathering products.

(d) Selby (1993) describes weathering as the process of alteration and breakdown of soil and rock materials at and near the Earth's surface by physical, chemical and biotic processes.

(e) Price (1995) gives weathering a definition suitable for geotechnical applications as the irreversible response of soil and rock materials and masses to their natural and artificial exposure to the near surface geomorphologic or engineering environment.

(f) Eggleton (2001) refers to weathering as any process, which, through the influence of gravity, the atmosphere, hydrosphere and/or biosphere at ambient temperature and atmospheric pressure, modifies rocks, either physically, or chemically.

Definitions given above show the diversity of the understanding of weathering. Some researchers consider mainly the chemical processes as important (as in a & c), some take into account the physical control of weathering also (as in b, d and e), yet others consider engineering environmental aspects of it as relevant (as in f).

2.1.2 Occurrence and Rates of Weathering

It is important to find out where, how and at what speed weathering occurs. The following statements attempt to explain these aspects:

(a) Weathering depends upon the external environmental agents acting to promote weathering (e.g. climate, plant growth) which will vary from place to place and through time, and upon the properties of the rock material (e.g. mineralogy & chemical composition) and rock mass (e.g. joint spacing) (Price, 1995).

(b) Weathering occurs most rapidly at sites of excess free energy such as crystal defects, dislocations, twinning boundaries, or microfractures (Berner, 1978).

(c) Physical and chemical weathering commonly act together, the progress of chemical weathering usually relying on fractures opened or formed partly as a result of physical weathering. Similarly, fractures may develop in response to changes in volume and weakening induced by chemical weathering (GSEGWP Report, 1995).

(d) Chemical weathering below the surface takes place via water movement through mass and materials. Movement through the mass is via joints and other discontinuities and the distribution of mass weathering may reflect both minor and major joint spacing and orientation and the presence of faults (Taylor, 1988).

(e) Chemical weathering is usually initiated along primary cracks, pores and open cleavages (Baynes and Dearman, 1978).

(f) Behaviour of cations during weathering is dependent upon the particular mineral being weathered, the ability of the cation to be transported in solution - effectively the ionic potential, and the ease of its incorporation into or adsorption onto secondary minerals. The Goldich stability series (Goldich, 1938) was later reconstituted to express the thermodynamic ease of mineral dissolution in the order: feldspar<mica<amphibole<pyroxene<olivine. This is effectively the reverse of Bowen's reaction series.

(g) The composition and structure of olivine, amphiboles, pyroxenes and other ferromagnesian minerals make them susceptible to rapid chemical weathering in most environments, although the effect of iron on weathering rates is complex (Colman, 1982).

(h) Weathering of hornblende and pyroxene causes etching, disaggregation, and eventual depletion of these minerals in weathering profiles (Berner *et al.*, 1980).

(i) Weathering rate depends on the free energy of formation of the mineral (Keller, 1954). Keller's idea is more applicable to feldspar and other non-iron-bearing minerals.

(j) Weathering rinds develop in basaltic and andesitic clasts (Colman and Pierce, 1981) at rates as high as 20 micrometers per 1000 years, averaging 5 in the western US over the past 500,000 years.

(k) Whitehouse *et al.* (1986) report initial rates of rind development as high as 1000 micrometers per 1000 years in medium grained sandstone from the Southern Alps of New Zealand. It is generally understood that in many cases, the rate decreases with time.

(l) Fast or slow, chemical and mechanical alterations occur everywhere at the Earth's surface. Disintegration, which is the mechanical break-up of rocks, exposes additional surfaces to air and water. Therefore, disintegration can accelerate decomposition (Bortz and Wonneberger, 2000).

(m) Ultimately, weathering rate will depend on the mechanism whereby the weathering agents break the bonds between the atoms of a crystal. This mechanism will itself be affected by the bond strength, the chemical reactivity of the agents, and the crystal structure. Cleavage cracks and fractures provide the first pathways for the entry of weathering agents into a crystal. Such avenues obviously increase the weathering rate by increasing the effective surface area of crystals open to attack. Optical examinations show, however, that weathering can invade uncracked and uncleaved regions of silicate minerals via submicroscopic diffusion avenues (Colman and Dethier, 1986).

2.1.3 Saprolites

The term saprolite is often used by scientists and engineers when referring to weathered rock material. The following examples show how the term has become gradually more complicated:

(a) Little (1969) defined saprolites as the zones of completely weathered or highly weathered rock that contain soil-like material but retain the original rock structure.

(b) Brand (1985) proposed a similar definition: saprolites are weathering products of rocks, in which the degree of weathering and the extent to which the original structure of the rock mass is destroyed vary from the ground surface to depth.

(c) Massey and Pang (1988) stated that saprolitic soils generally do not exhibit properties normally associated with soils, and present problems in analysis and design because of their different engineering properties and extreme variability.
(d) Selby (1993) used the term saprolite for the chemically weathered material lying in a weathering profile, below the solum and above the rock.

The term "saprolite" can be defined as weathered rock material, which could be at different stages of weathering but retaining at least parts of the original rock material and structure.

2.1.4 Description and Classification of Weathering Profiles

Description and classification of weathered rocks for engineering purposes has been a subject of debate since engineering geologists first produced standards and codes. However, there is consensus on the following key points:

(a) Different lithologies weather in different ways in the same climatic regime.
(b) Lithological heterogeneity or joints and faults can give rise to complex weathering fronts or profiles.
(c) Weathered rocks are difficult to classify unless the fresh end member is seen (particularly in the case of weak rocks).
(d) Attempts are often made to apply the same weathering classification in all situations, even when clearly not appropriate to certain rocks.

The literature contains many respected classifications, which are being used successfully. Anon (1981) proposed a code of practice for site investigations which was later adapted by British Standards Institution. Figure 2.1 gives an overview of several such classifications of rock materials and masses for the period 1957 – 1995 as given in Geological Society Engineering Group Working Party (GSEGWP) Report (1995). They were used for classifying granites, mudstones, chalk and crystalline limestone and the material or mass was divided into 4 to 7 zones, classes or grades depending on the classification criteria.

Dearman (1974, 1995) produced idealised diagrams of the stages of weathering of a rock mass (Figure 2.2). The British Standards (BS 5930) present descriptive terms for the weathering of rock material, and a scale of weathering grades of rock mass which incorporate Dearman's (1976) classification (Tables 2.1 and 2.2).

Geological Society Engineering Group Working Party Report (1995) gives elaborate approaches to weathering description and classification (Figure 2.3).

The New Zealand Geomechanics Society (1988) scale of rock mass weathering (Table 2.3), which is compatible with the British Standards scale and the International Society of Rock Mechanics suggested methods (Table 2.4) as given in Brown (1981), was used in this study of the Karamu Basalt weathering profile. These classifications are based on the field criteria only.

The regolith glossary of surficial geology, soils and landscapes, edited by Eggleton (2001), gives a recent classification of the weathering profile (Table 2.5). This classification not only describes the field criteria but elaborates on the alteration mineral assemblages and some changes in the chemical composition. However, there is a slight difference in the field criteria from the previously mentioned ones: there is no "residual soil" grade.

At the time the Karamu Basalt weathering profile was described in this study, this recent source was not yet published. If this classification was used in this study, the "completely weathered" grade would have been further divided into "very highly weathered" and "intensely weathered" grades.

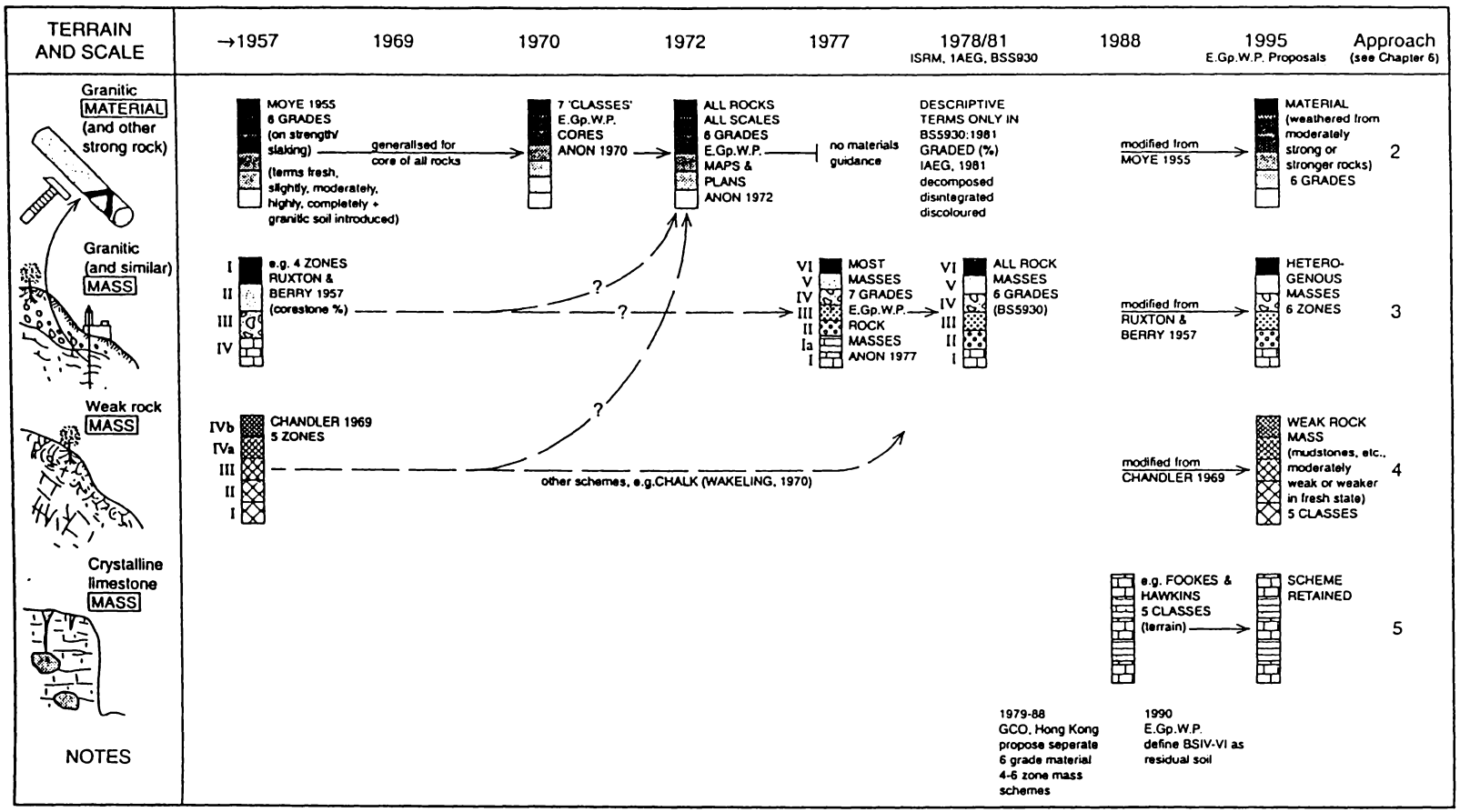

Figure 2.1 Outline Representation of the Evolution of Weathering Classifications for Rock for Engineering Purposes (GSEGWP Report, 1995).

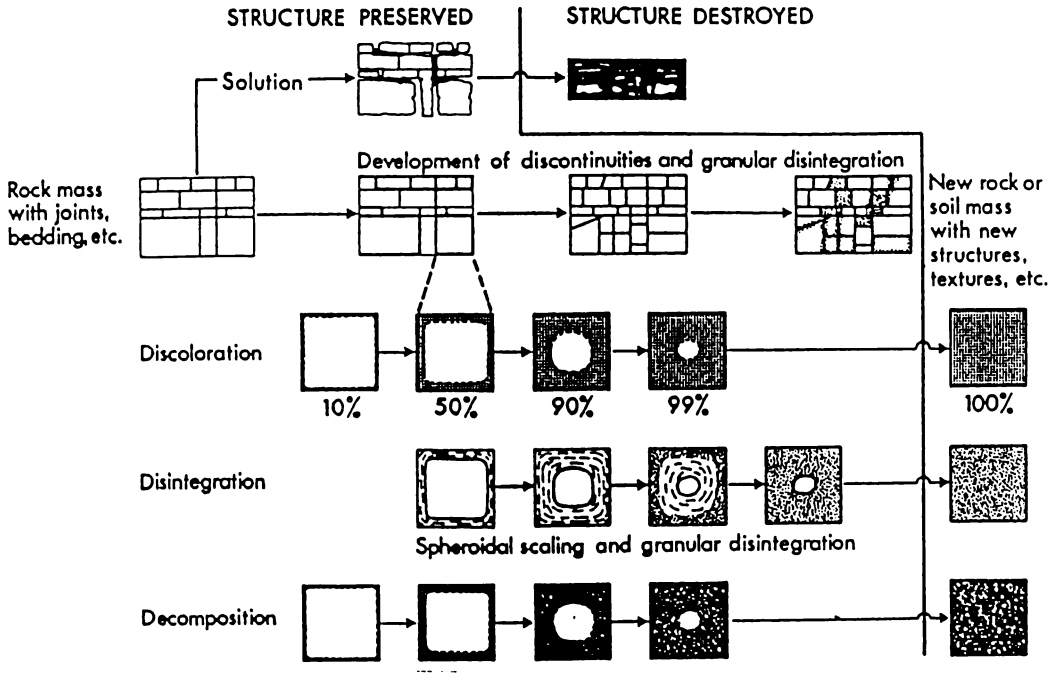

Figure 2.2 Idealised Diagram of the Stages of Weathering of Rock Mass (Dearman, 1974).

TABLE 2.1 DESCRIPTIVE TERMS FOR THE WEATHERING OF ROCK MATERIAL (BRITISH STANDARDS 5930, DEARMAN, 1976).

Term	Description
Fresh	No visible sign of weathering of the rock material.
Discoloured	The colour of the original fresh rock material is changed and is evidence of weathering. The degree of change from the original colour should be indicated. If the colour change is confined to particular mineral constituents this should be mentioned.
Decomposed	The rock is weathered to the condition of a soil in which the original material fabric is still intact, but some, or all, of the mineral grains are decomposed.
Disintegrated	The rock is weathered to the condition of a soil in which the original material fabric is still intact. The rock is friable, but the mineral grains are not decomposed.

TABLE 2.2 SCALE OF WEATHERING GRADES OF ROCK MASS (BRITISH STANDARDS 5930, DEARMAN, 1976).

Term	Description	Grade
Fresh	No visible sign of rock material weathering; perhaps slight discoloration on major discontinuity surfaces.	I
Slightly weathered	Discoloration indicates weathering of rock material and discontinuity surfaces. All the rock material may be discoloured by weathering.	II
Moderately weathered	Less than half of the rock material is decomposed or disintegrated to a soil. Fresh or discoloured rock is present either as a continuous framework or as corestones.	III
Highly weathered	More than half of the rock material is decomposed or disintegrated to a soil. Fresh or discoloured rock is present either as a discontinuous framework or as corestones.	IV
Completely weathered	All rock material is decomposed and/or disintegrated to soil. The original mass structure is still largely intact.	V
Residual soil	All rock material is converted to soil. The mass structure and material fabric are destroyed. There is a large change in volume, but the soil has not been significantly transported.	VI

TABLE 2.3 SCALE OF ROCK MASS WEATHERING (NEW ZEALAND GEOMECHANICS SOCIETY, 1988).

TERM	GRADE	ABBREVIATION	DESCRIPTION
Fresh (unweathered)	I	UW	Rock material shows no discolouration, loss of strength or any other effects due to weathering. There may be slight discolouration on major discontinuity surfaces.
Slightly weathered	II	SW	Rock material may be slightly discoloured. Discontinuities have discoloured surfaces and may be open. The rock material is not significantly weaker than the fresh rock material.
Moderately weathered	III	MW	Rock material is discoloured. Discontinuity surfaces will have a greater discolouration, which also penetrates slightly into the rock material. The rock material is significantly weaker than the fresh rock and part of the rock mass may have been changed to a soil.
Highly weathered	IV	HW	Rock material is discoloured and more than half the rock mass is changed to a soil. Weathering adjacent to discontinuities penetrates deeply into the rock material but lithorelicts or core stones of fresh or slightly weathered rock may still be present.
Extremely (completely) weathered	V	CW	All the rock mass is decomposed and externally changed to a soil, but the original rock fabric is mainly preserved.
Residual weathered (residual soil)	VI	RW	Rock is completely changed to a soil with the original fabric completely destroyed but the resulting soil is not significantly transported.

APPROACH 1 : FACTUAL DESCRIPTION OF WEATHERING (MANDATORY)

Standard descriptions should always include comments on the degree, extent and nature of any weathering effects at material or mass scales. This may allow subsequent classification and provides information for separating rock into zones of like character. Typical indications of weathering include:

- Changes in colour
- Reduction in strength
- Changes in fracture state
- Presence, character and extent of weathering products

These features should be described using standard terminology, quantified as appropriate, together with non-standard 'English' descriptors as necessary to describe the results of weathering. At the mass scale, the distribution and proportions of the variously weathered materials (e.g. corestones vs matrix) should be recorded.

Can classification be applied unambiguously ? — No → DO NOT CLASSIFY

Yes

Rock is moderately strong or stronger in fresh state

APPROACH 2 : CLASSIFICATION FOR UNIFORM MATERIALS

Grade	Classifier	Typical Characteristics
I	Fresh	• Unchanged from original state
II	Slightly Weathered	• Slight discolouration, slight weakening
III	Moderately Weathered	• Considerably weakened, penetrative discolouration • Large pieces cannot be broken by hand
IV	Highly Weathered	• Large pieces can be broken by hand • Does not readily disaggregate (slake) when dry sample immersed in water
V	Completely Weathered	• Considerably weakened • Slakes • Original texture apparent
VI	Residual Soil	• Soil derived by in situ weathering but retaining none of original texture or fabric

Is a zonal classification appropriate and is there enough information available? — No → Use Rock Mass Classification if appropriate

Yes

APPROACH 3 : CLASSIFICATION FOR HETEROGENOUS MASSES

ZONE	PROPORTIONS OF MATERIAL GRADES	TYPICAL CHARACTERISTICS
1	100% G I - III (not necessarily all fresh rock)	Behaves as rock; apply rock mechanics principles to mass assessment and design
2	>90% G I - III <10% G IV - VI	Weak materials along discontinuities. Shear strength, stiffness and permeability affected
3	50 to 90% G I - III 10 to 50% G IV - VI	Rock framework still locked and controls strength and stiffness; matrix controls permeability
4	30 to 50% G I - III 50 to 70% G IV - VI	Rock framework contributes to strength; matrix or weathering products control stiffness and permeability
5	<30% G I - III >70% G IV - VI	Weak grades will control behaviour. Corestones may be significant for investigation and construction
6	100% G IV - VI (not necessarily all residual soil)	May behave as soil although relict fabric may be still be significant

Rock is moderately weak or weaker in fresh state

APPROACH 4 : CLASSIFICATION INCORPORATING MATERIAL AND MASS FEATURES

Class	Classifier	Typical Characteristics
A	Unweathered	Original strength, colour, fracture spacing
B	Partially Weathered	Slightly reduced strength, slightly closer fracture spacing, weathering penetrating in from fractures, brown oxidation
C	Distinctly Weathered	Further weakened, much closer fracture spacing, grey reduction
D	Destructured	Greatly weakened, mottled, ordered lithorelicts in matrix becoming weakened and disordered, bedding disturbed
E	Residual or Reworked	Matrix with occasional altered random or "apparent" lithorelicts, bedding destroyed. Classed as reworked when foreign inclusions are present as a result of transportation

APPROACH 5 : SPECIAL CASES

For rocks whose weathering state does not follow the other patterns indicated here, such as karst in carbonates and the particular effect of arid climates

FIGURE 2.3 Approaches to Weathering Description and Classification (GSEGWP Report, 1995).

TABLE 2.4 INTERNATIONAL SOCIETY OF ROCK MECHANICS SUGGESTED METHODS FOR THE QUANTITATIVE DESCRIPTION OF DISCONTINUITIES (BROWN, 1981).

Term	Description	Grade
Fresh	No visible sign of rock material weathering; perhaps slight discolouration on major discontinuity surfaces.	I
Slightly weathered	Discolouration indicates weathering of rock material and discontinuity surfaces. All the rock material may be discoloured by weathering and may be somewhat weaker externally than in its fresh condition.	II
Moderately weathered	Less than half of the rock material is decomposed and/or disintegrated to a soil. Fresh or discoloured rock is present either as a continuous framework or as corestones.	III
Highly weathered	More than half of the rock material is decomposed and/or disintegrated to a soil. Fresh or discoloured rock is present either as a discontinuous framework or as corestones.	IV
Completely weathered	All rock material is decomposed and/or disintegrated to soil. The original mass structure is still largely intact.	V
Residual soil	All rock material is converted to soil. The mass structure and material fabric are destoyed. There is a large change in volume, but the soil has not been significantly transported.	VI

TABLE 2.5 WEATHERING PROFILE (EGGLETON, 2001).

	Field criteria	Alteration assemblage/composition
unweathered	Having no visible signs of weathering.	None.
slightly weathered	Core-stones, if present, are interlocked, few microfractures, is easily broken with a hammer. Sediments have traces of weathering on the surfaces of sedimentary particles. Some clay or iron oxides may be present, filling voids between coarse particles.	Weak iron staining; slight weathering of feldspars. Primary minerals very prominent; some smectite and minor goethite may be present. Ca, Mg, Na appreciably depleted; K, Si show slight depletion.
moderately weathered	Marked iron staining common; up to 50% secondary minerals; core-stones rectangular and interlocked. Larger particles have thick weathering skins. Can be broken by a kick (with boots on), but not by hand.	Most feldspars in larger particles are weathered. Most alkalis and alkaline earths have been lost. Primary minerals still dominant, with smectite, kaolin ± iron oxides and oxyhydroxides present.
highly weathered	Strong iron staining, and more than 50% secondary minerals; core-stones are free and rounded, and there are numerous microfractures. The material can be broken apart in the hands with difficulty.	Nearly all feldspars are weathered. Appreciable silica has been lost; mineralogy includes kaolin ± goethite ± hematite with significant amounts of primary minerals
very highly weathered	Retains structures from the original rock; may be pale coloured, and is composed completely of secondary minerals and resistates from the parent material. Core-stones, if present, are rare and rounded. It can easily be broken by hand.	All feldspars are weathered, mineralogy is dominated by kaolin ± goethite ± hematite with or without residual quartz. Other primary minerals in low abundance or absent.
intensely weathered	Only major parent rock features discernable, such as lithological changes or resistant veins; resistate minerals may remain in a matrix of secondary minerals.	Mineralogy is essentially ± goethite/ hematite/maghemite ± quartz ± kaolinite ± gibbsite. High levels (>50%) of sesquioxides; negligible alkalis and alkaline earths; significant titania.

2.1.5 Indices of Chemical Weathering

Over 30 chemical indices have been proposed since the beginning of the 20th century. Most of these indices are reviewed by Duzgoren-Aydin *et al.* (2002) and they are given, together with their limitations and/or assumptions, in a table which is reproduced here as Appendix 2.1. However, some weathering indices were missed out by them and they are added as Appendix 2.2. These added indices are as follows: Vogt Ratio (Vogt, 1927; in Roaldset, 1972), Ruxton's Ratio (Ruxton, 1968), Miura Weathering Index (Miura, 1973), Hodder Weatherability Index (Hodder, 1984), Silica Titania Index (Jayawardena and Izawa, 1994), Weathering Index (Bland and Rolls, 1998) and Mobility Index (Guan *et al.*, 2001).

The five weathering indices discussed below are calculated in this study for the material comprising the weathering profile of Karamu Basalt. They were selected on the basis that they represent, to some extent, the changes in the chemical compositions of the Karamu Basalt. These were easily calculable. The results of these calculations and their significance as weathering indices of Karamu Basalt are later discussed in Chapters 4, 6 and 7.

Reiche (1943) stated that the simplest measurement of weathering is absolute change, paramount in deciphering the processes and degree of weathering, stability of minerals and mobility of elements. He proposed the Weathering Potential Index (WPI) and a Product Index (PI) which were tested for sedimentary rocks. These are:

$$WPI = \frac{\sum BASES - H_2O}{\sum BASES + SiO_2 + R_2O_3} X100 \qquad 2.1$$

where R includes all trivalent cations.

$$PI = \frac{SiO_2}{SiO_2 + Al_2O_3 + Fe_2O_3 + FeO + TiO_2} X100 \qquad 2.2$$

WPI and PI suggested by Reiche (1943) consider the loss of silica and mobile cations along with the increase of alumina and structural water.

Ruxton (1968) suggested the Ruxton's Ratio (RR) which was tested for granites.

$$RR = \frac{SiO_2}{Al_2O_3} \qquad 2.3$$

Ruxton's Ratio considers changes in the concentrations of alumina and silica. Ruxton proposed this weathering index as a measure of the degree of chemical weathering of rocks.

According to Ruxton (1968), Ruxton's Ratio is especially suitable for acid and intermediate rocks and is valid for well-drained, acid and humid environments where the end products are kaolin group minerals.

However literature (e.g. Duzgoren-Aydin *et al.* , 2002) indicates that silica alumina ratio proposed by Ruxton (1968) was earlier (in 1926) proposed by Harrassowitz as a molecular ratio of mobile (SiO_2) to immobile (Al_2O_3) elements.

Parker (1970) considered the loss of bases relative to their respective bond strength to oxygen and proposed the Parker Weathering Index (W_p).

$$W_p = \frac{a_{Na}}{0.35} + \frac{a_K}{0.25} + \frac{a_{Mg}}{0.90} + \frac{a_{Ca}}{0.70} \qquad 2.4$$

where a_E is the atomic proportion of the element E and the denominators are the relative oxygen to element bond strengths.

Parker proposed this as an index of weathering for silicate rocks.

Miura (1973) devised an alternative called the Miura Weathering Index (Wm):

$$W_m = \frac{MnO + FeO + CaO + MgO + Na_2O + K_2O}{Fe_2O_3 + Al_2O_3 + H_2O} \qquad 2.5$$

In this case, the ratio of concentrations of mobile elements to the concentrations of immobile elements are taken into account. The concentrations are percentages by weight.

Miura Weathering Index was tested for weathered plutonic rocks in Japan. It enabled the differentiation of different grades of weathering.

2.2 Geology of the Project Area

Briggs (1983), Briggs & Goles (1984) and Briggs *et al.* (1989) have reviewed the geology of this area. The following description was obtained from these sources. Alexandra is the southernmost Pliocene-Quaternary (2.7 to 1.6 Ma) basalt field of the northern North Island of New Zealand and the most voluminous of the basalt fields (55 km^3), covering an area of 450 km^2 and forming a 65 km-long volcanic chain.

The Alexandra Volcanic Group consists of 3 basaltic magma series:

(a) An alkalic intraplate series called the Okete Volcanics;

(b) A calcalkalic series called Karioi, Pirongia, Kakepuku, Tokanui and Te Kawa Volcanics; and

(c) A minor K-rich mafic cap lava series on Pirongia.

Okete Volcanics have erupted from at least 27 volcanic centres and form either eroded scoria mounds surrounded by an apron of several lava flows, or tuff rings. Karamu rocks belong to the Okete Volcanics. The distribution of Okete volcanic centres shows no apparent spatial patterns, although Karamu and a few others have centres aligned along N and NE striking Cenozoic faults. The Okete Volcanics have compositions which include basanites, alkali-olivine basalts and hawaiites, and most lavas contain ultramafic xenoliths.

Three major volcanic materials are contained in the Okete Volcanics at Karamu:

(a) pyroclastic fall (ash) deposits;

(b) pyroclastic flow deposits (ignimbrites); and

(c) lava flows.

The Karamu quarry contains predominantly basalt comprising mainly olivine, titanaugite and plagioclase. At Karamu quarry, there is a section through Okete lava flows, dated by K/Ar methods at 2.03 ± 0.03 Ma (Stipp, 1968), that are overlain by weathered tephra. The tephra belong to Hamilton Ash Formation which is rhyolitic. The oldest bed "H1" is typically pale yellowish brown with a sharp lower boundary marked by a coarse-grained yellow, quartz-rich sandy layer forming a prominent marker bed.

Based on correlations with other tephra deposits in the central and southern North Island, H1 has been identified as the Rangitawa tephra (Horrocks, 2000), which has an age of 0.38 ± 0.04 Ma (Lowe *et al.,* 2001) and 0.35 ± 0.04 Ma based on fission track analysis of zircons (Kohn *et al.* 1992). The remaining Hamilton Ash beds, all clayey in texture (~ 60 – 85 % clay), range from friable to firm in consistence with reddish-yellow to strong brown colours, and have the lowest age estimated at 0.07 Ma (Horrocks, 2000).

2.3 Development of Stress Release Fractures in Rocks

2.3.1 Tensile Crack Development

The development of fractures in brittle rock under compressive (and tensile) stresses has been studied and described by many authors (Hoek and Bieniawski, 1965; Bieniawski, 1983; Attewell and Farmer, 1979; Hoek, 1983). Crack initiation represents the stress level where microfracturing begins. Unstable crack growth continues until the microfractures have coalesced and the rock can no longer support an increase in load (Eberhart *et al.,* 1998). At this stage the rock fails along well developed macrofractures.

The first fractures in a uniaxially loaded brittle material are tensile microcracks: these cracks grow through tensile failure at their tips (Lambe and Whitman, 1969). Development of the microfractures is thus dependent upon the tensile stress at the tips of the fractures being greater than the tensile strength of the material. Microfractures themselves will result in stress concentrations at the tips (Hoek and Bieniawski, 1965), so the stress at the tips is also not necessarily the average stress in the material as a whole.

As cracks increase in both number and size, they begin to interact with each other: crack development becomes complex as the local stress directions become influenced by the presence of neighbouring cracks. Eventually, directions of crack propagation are influenced by the surrounding cracks, and they begin to coalesce by developing

an *en echelon* arrangement (Eberhart *et al.,* 1998). Macroscopic fractures result from brittle fracturing which is the inevitable result of unstable crack development and coalescence.

2.3.2 Residual Stresses

When rock is formed some stress is retained within the intact rock (Krinsley and Smalley, 1972). Bock (1979) presents an analysis of the residual stresses within a basalt column, which shows that there are regions of both compressive and tensile stress within the rock material which are irregular, but in a stable state of static equilibrium. These stresses reach high magnitudes (> 12 MPa in tension; > 15 MPa in compression), and Bock (1979) suggests that they are large enough to account for the extension of microfractures if the equilibrium is disturbed. Stresses measured axially were considered to be insignificant, but the author conceded that insufficient and inadequate measurements had been made to determine these. As the rock formed at or near the Earth's surface and is not significantly weathered, it is assumed that these stresses are a relict of the original cooling of the lava flow.

The development of a low-stress surface, such as an artificial excavation or exposure through erosion and weathering, in a stressed rock mass will lead to stored internal energy being relaxed (Jumikis, 1982). This leads to displacement of the rock material, which continues until a new state of equilibrium is reached. Relaxation and deformation can lead to fracturing of the intact rock, as evidenced by rock bursts or "popping" which involves the separation of thin rock slabs from an excavation or tunnel (Jumikis, 1982).

In a natural slope, stress-release joints develop parallel to the low-stress ground surface, especially following unloading of the profile by erosion of laterally confining rock masses (Selby, 1993). Relaxation of the rock body towards the low stress region results in the development of high outward, or tensile, stresses. The development of microcracks, and hence macrofractures, occurs in the direction perpendicular to the maximum tensile stress. Fractures parallel to the low-stress surface thus result. These are particularly common in granitic rock bodies where large-scale sheeting occurs after erosion of the overlying material (Selby, 1993).

2.4 Weathering of Constituent Minerals of Basalts

Olivine $(Mg,Fe)_2SiO_4$ is the least resistant to weathering of the common rock-forming silicates. According to Baker and Haggerty (1967), weathering produces "iddingsite"; iddingsite is commonly a mixture of montmorillonite, saponite, chlorite, hematite and goethite, showing an orientation in relation to the parent olivine. Included in olivine's weathering products may be serpentine, chlorite, smectite, goethite, maghemite and hematite. Nahon *et al.* (1982) found that under conditions of tropical weathering, olivine weathers in two stages; an initial smectite later gives way to iron hydroxides and oxyhydroxides, mainly goethite. Many olivines in basalts have been partly iddingsitised before exposure to weathering, which is thought to be formed by the reaction between olivine and water contained in the glass during the cooling of lava (Eggleton, 1984).

Augite $Ca(Mg,Fe,Al)[(Si,Al)_2O_6]$ is a clino pyroxene. Pyroxene minerals such as augite have SiO_4 tetrahedra which are joined together in very long chains. Pyroxene hydration studies show strong evidence for lattice coherence between pyroxene and its alteration products such as clays, goethite and hematite. Veblen and Buseck (1980, 1981) have shown examples of layer silicate minerals, primarily talc, serpentine, and brucite, crystallising in the solid state as alteration products of augite.

Plagioclase is an isomorphous series between albite ($Na[AlSi_3O_8]$) and anorthite ($Ca[Al_2Si_2O_8]$) feldspar. Feldspars such as plagioclase, have a framework structure, in which up to 50% of the Si^{4+} ions (ionic radius = 0.42 Å) have been replaced by Al^{3+} (ionic radius = 0.51 Å). This replacement creates a negative charge, which requires the presence of cations such as Ca^{2+} (ionic radius = 0.99 Å) and Na^{+} (ionic radius = 0.64 Å) to balance it. Feldspars develop "speckly material" or turbidity in the first stages of weathering due to sericitisation. Oriented etch pits develop, generally in positions related to twin planes. According to Smith and Eggleton (1983), TEM examination of weathered plagioclase in basalt shows that twin planes are a site for early formation of clay minerals. Hochella and Banfield (1995) state that, during incipient weathering, dissolution and crystallisation of secondary minerals occur throughout the feldspar, not just at grain boundaries with other phases.

Magnetite Fe_3O_4 crystallises as black octahedra that are quite resistant to weathering but slowly weathers to maghemite and or to hematite (Eggleton, 2001).

Volcanic glass is not a mineral, yet it is a constituent of the Karamu Basalt. It is the irregular shaped amorphous substance which is formed due to quick solidification of lava. Glass varies widely in composition and lacks any regular arrangement of constituent particles (Bishop, 1967). Glass is metastable and hydrates quite easily (White and Brantley, 1995), leading to the formation of smectities.

2.4.1 Views of Different Authors on the Changes in Crystal Structures of Primary Minerals in Basalt and Subsequent Weakening of Rocks

According to Bland and Rolls (1998), olivine contains the $[SiO_4]^{4-}$ unit with divalent cations Mg^{2+} and Fe^{2+}; and it is most easily weathered owing to the simple structure and low lattice energy.

Ultimately weathering reactions consist of detachment and attachment of atoms at a mineral surface (White and Brantley, 1995).

According to Colman and Dethier (1986), cleavage cracks and fractures provide the first pathways for the entry of weathering agents into a crystal. Such avenues increase the weathering rate by increasing the effective surface area of crystal open to attack. Optical examinations show, however, that weathering can invade uncracked and uncleaved regions of silicate minerals via submicroscopic diffusion avenues (Colman and Dethier, 1986).

Loughnan (1969) made the following observations:

(a) Hydrogen ions produced by the hydrolysing action of mineral surfaces play an important role in the breakdown of silicate structures. The size of these ions permits easy penetration into crystal lattices and, once they have gained admission, the high charge-to-radius ratio, which is greater than for any other ion, has a marked disrupting effect on the charge balance within the lattice.

(b) The persistence of aluminium in tetrahedral coordination and the retention of highly mobile cations in the secondary mineral products indicate that much of the parent mineral structure is inherited by the secondary products.

Eggleston and Hellmann (1989) note that mineral dissolution can have two models:

(a) a diffusion model; and

(b) a surface reaction model.

Experimentally, they show that dissolution must proceed by rupturing various bonds at mineral surfaces, which are in contact with water. In albite, Na-O, Al-O and Si-O bonds have different strengths, therefore, the rupture will be differential. At the surface, Na^+ is exchanged for H^+ or H_3O^+. From diffraction patterns they see no disruption in the feldspar meaning that the bonds are intact (at the surface). During hydrolysis, the oxygen which bonds two Si–O tetrahedra (bridging oxygen) is important. Water plays a major role in breaking this bond so that the H-atom is then attached to an O-atom at the end of each tetrahedron.

Frye (1974) gives the following for the breakdown of plagioclase to kaolinite:

$$CaAl_2Si_2O_8 + 2H_2O \rightarrow Al_2Si_2O_5(OH)_4 + Ca^{2+} + O^{2-} \qquad 2.6$$

which is a hydration process.

Berner *et al.* (1980) and Berner and Schott (1982) discuss the dissolution of pyroxenes and amphiboles during weathering and describe surface features associated with dissolution including:

(a) etch pits;

(b) microcaves; and

(c) "teeth" formed by etch-pit coalescence.

Similar features were displayed by the ferromagnesian minerals studied by Hodder *et al.* (1991), who also ascribed blunted grains and deeply embayed or skeletal grains to dissolution processes.

According to Bland and Rolls (1998), olivine can undergo weathering by hydrolysis, the oxygen atoms are protonated, and silicic acid is released. Under good drainage conditions, Fe^{2+} is oxidised and redistributed typically as hematite or goethite along any fractures. Chemical weathering of pyroxenes is guided by their good cleavage. Under conditions of slow leaching, smectites are formed in cleavages and fissures. Good drainage leads to the total loss of Ca^{2+}, Mg^{2+} and Si^{4+}, resulting in a neoformation consisting mainly of oxyhydroxides like goethite. They also identified Redox weathering reactions which commonly occur in aqueous solutions.

According to Stegena (1983), during a diffusion process, the medium in which the diffusion takes place does not move, only the unequally distributed materials move. According to Hochella and Banfield (1995), a common feature to most inter-granular weathering reactions is the confined space that connects the primary/secondary mineral interface with fluids external to the grain. These conduits must be at least 3 Å across to pass a water molecule or partially coordinated aqueous metal, and approximately twice that to pass a fully coordinated aqueous metal. When weathering reactions occur on internal surfaces, chemical constituents released from the primary dissolution process and not needed for the secondary mineral crystallisation process must be transported by diffusion to the external zone for removal. On the other hand, the chemical constituents not available from the breakdown of the primary mineral, but needed for the growth of the secondary phase (including water, hydrogen or hydroxyls), must follow the reverse path.

Schott and Berner (1984) studied the dissolution mechanisms of pyroxenes and olivines and concluded that in the absence of oxygen, the minerals underwent congruent dissolution after the initial formation of a thin (> 10 Å) protonated layer depleted in Fe, Ca and Mg relative to Si. These results, combined with findings of high activation energies, rule out a control of dissolution by a solution-transport mechanism. Dissolution is strictly a surface process and occurs by a H^+ (or H_3O^+) exchange reaction at the surface. Under oxygenated conditions, dissolution of iron-rich minerals results in the formation of two surface layers. The outer layer is hydrated ferric oxide. The inner layer is probably a Fe^{3+} - Mg silicate and is protective towards silica release.

According to Nahon *et al.* (1982) weathering of olivine crystals develops either from contacts with the neighbouring minerals such as pyroxene, or from cracks and fissures within the crystals. Two main stages of weathering can be recognised: first the ephemeral development of smectites; and second, the widespread formation of iron oxyhydroxides.

According to Carrol (1970) water at pH 7 and exposed to air has an oxidising potential of 810 mV which is well above the value necessary to oxidise ferrous iron to ferric iron in typical occurrences near the earth's surface. In thin sections of rocks, oxidation can be recognised by the presence of iron staining.

Wollast and Chou (1984) experimented with dissolution of feldspars and concluded that when freshly ground feldspars are exposed to aqueous solutions, a large amount of alkali ions are released to solution with an increase in pH, suggesting that the main process occurring during this initial stage is the exchange of alkali ions on the feldspar surface for protons. This exchange reaction proceeds continuously at a decreasing rate, involving deeper layers. According to Frederickson (1951), the small hydrogen ions from the water enter and upset the neutrality of the crystal. The crystal attempts to become neutral again by rejecting the Na^+, which is less strongly held than the invading hydrogen. The ion substitution causes the crystal to expand (Frederickson, 1951), and the chemical activity is increased, which hastens the eventual collapse of the crystal.

Berner (1995) points out that weathering of Ca- and Mg- bearing silicates withdraws CO_2 from the atmosphere and ultimately precipitates it in the oceans as carbonate minerals.

Clayton and Pearce (2000) state that products of low temperature alteration in basalt show the presence of early Fe-rich dioctahedral mica with some smectite and Fe oxyhydroxides, followed by saponite, carbonates and zeolites.

2.5 Clay Minerals Formed due to Weathering of Basalt

The term "clay" is used in two senses as explained below:

(a) as a particle size grade less that 2 microns in diameter; Lambe and Whitman (1969, p 40) state "Clay is used to describe a fine-grained soil having plasticity. But we can avoid confusion by employing 'clay size' to denote a particle smaller than 2 microns".

(b) as a group of minerals with a specific range of composition and crystallographic structures. According to Whitten and Brooks (1972), clay minerals have plastic properties, their atomic structure is a layer-lattice, and they generally occur as minute, platy, more rarely fibrous crystals.

When describing the geochemical characteristics, the author uses the term "clay" as a group of minerals and when considering the geotechnical parameters, it is considered as a particle size grade.

The ultimate solid product of weathering is the material called soil, and chief among the constituents of most soils are the clay minerals (Krauskopf, 1979).

Clay mineralogy is important, because the amount and type of clay minerals present will greatly affect the mechanical properties and behaviour of saprolite. Most clay minerals are platy and have a low coefficient of inter-particle friction. They can orientate under shearing, resulting in polished shear surfaces and a low residual frictional strength. Clay minerals impart cohesion to the rock or soil material (Lupini *et al.*, 1981).

2.5.1 Clay Mineralogy

Clay minerals are phyllosilicates, silicates with continuous sheet structures. Chemically, the clay minerals are best described as hydrous aluminium silicates (Betekhtin, 1972). This needs qualifying, by adding that many clays contain other cations, particularly magnesium and iron, and some types have no aluminium at all. Crystallographically, clays are divided into two-layer and three-layer types: those with one tetrahedral and one octahedral sheet (e.g. kaolinite) and those with an octahedral sheet between two tetrahedral sheets (e.g. montmorillonite).

The following descriptions are given based on Betekhtin (1972):

(a) *Kaolinite* $Al_4[Si_4O_{10}][OH]_8$ is commonly the chief clay mineral in soils of humid climates on well-drained slopes, where abundant vegetation makes soil solutions acid and cations are effectively leached away. Kaolinite occurs as books of plates (verm structure).

(b) Halloysite $Al_4[Si_4O_{10}][OH]_8 .4H_2O$ occurs mainly in the weathering crust of rocks. It usually forms small lenticular masses and concretions, often associated with other minerals of this group, as well as with montmorillonite. Halloysite occurs as tubes, needles and spheres.

(c) *Montmorillonite* $m\{Mg_3[Si_4O_{10}][OH]_2\}.p\{(Al,Fe)_2[Si_4O_{10}][OH]_2\}.nH_2O$ is characteristic of soils in less humid climates, where soil solutions are slightly alkaline and the cations are removed less rapidly. Montmorillonite occurs as flakes. Montmorillonite is the principal mineral in the smectite group. *Smectite* is usually considered to be formed in environments of restricted drainage conditions. Smectite formation depends on the microenvironment too.

(d) *Saponite* $Mg_3[Si_4O_{10}][OH]_2.nH_2O$ is a layer silicate which develops on olivine crystals and other iron bearing minerals due to weathering. It is a common occurrence in iddingsite rims.

(e) *Illite* $K_{0-1}Al_2[(Si,Al)_4O_{10}][OH]_2.nH_2O$ is the common clay mineral in alkali soils of desert areas and in soils formed from igneous rocks, especially those rich in potassium. *Illite* is also called *hydromuscovite* in Russia and *hydromica* in Europe.

In addition to montmorrillonite and saponite, the smectite group of clays contain beidellite and nontronite. Smectites, particularly beidellite and nontronite, are often found (mixed with illites) in soils deriving from the weathering of basic rocks (Deer *et al.*, 1992). According to Deer *et al.* (1992), magnesium ions in montmorrillonite are replaced by aluminium ions in the case of beidellite and by ferric irons in the case of nontronite.

Chichester *et al.* (1969) attributed smectite formation in a well-drained pumice soil in Oregon to restricted microdrainage conditions within the pumice fragments due to their microporosity. Glassman (1982) also pointed to smectite formation in wet soils on andesitic pyroclasts as a result of microenvironments with restricted drainage conditions in contrast to adjacent well-drained soil material where halloysite forms.

2.5.2 Other Clay Minerals Pertaining to the Study Area

Allophane $m Al_2O_3 . n SiO_2 . p H_2O$, is found in many soils derived from volcanic ash, basic rocks or finely communited parent materials. Allophane, along with halloysite, is the most abundant secondary mineral occurring in the clay fraction of tephra in the North Island of New Zealand. The climate is moist and temperate with rainfall usually exceeding evapotranspiration for most of the year. These conditions favour the formation of allophane (Parfitt and Kimble, 1989).

2.6 Other Secondary Minerals Formed due to Weathering of Basalt

Iddingsite, a familiar petrographic description of olivine alteration products, has been shown to be a mixture of goethite and hydrosilicates with a large degree of structural orientation inherited from the parent olivine (Brown and Steven, 1959). They also showed that the layer silicates in iddingsite develop with their close packed octahedral sheet parallel to the close packed (100) plane of olivine, and that most goethite crystals grow with x, y and z axes parallel to x, y and z axes of the parent olivine.

Chabazite $Ca_2[Al_4Si_8O_{24}].12H_2O$ is a zeolite. Zeolites are considered to be the result of late-stage fluids that permeated the basalts after their extrusion, eg. chabazite and analcite (Deer *et.al.*, 1992). Zeolite minerals are common constituents of weathered volcanic rocks (Ming and Mumpton, 1989).

Hematite Fe_2O_3 has two natural polymorphs: trigonal and stable α - Fe_2O_3 and cubic and unstable γ - Fe_2O_3. Hematite can be formed in small amounts as a sublimation product in crusts on the walls of craters and in cracks in lavas (Betekhtin, 1972).

Goethite α-FeO.OH commonly occurs as a weathering product of iron-bearing minerals (Deer *et al.*, 1992). $HFeO_2.nH_2O$ is called *hydrogoethite* which can have a water content as high as 14 %.

Manganosite (MnO) forms as a result of weathering of minerals with a considerable quantity of manganese. It appears as opaque, black and earthy nodules.

2.7 Relationships Between Chemical and Engineering Properties

Some researchers have attempted to find relationships between chemical and engineering properties of different rocks and soils. These studies are outlined in Table 2.6.

From the information in Table 2.6, the following general conclusions can be drawn:

TABLE 2.6 RELATIONSHIPS PREVIOUSLY ATTEMPTED AT BETWEEN CHEMICAL AND ENGINEERING PARAMETERS

Authors	Rock/Soil Type	Chemical Parameter	Engineering Parameter	Relationship Obtained
Nutter and Otton, 1969	igneous rocks, USA	visually estimated degree of weathering	porosity	porosity increases with weathering
Aires-Baros, 1978	greywacke, Portugal	Parker and Miura Weathering Indices	microhardness, density, sonic velocity, porosity, permeability, swelling & reflectivity	a) microhardness, density, sonic velocity & reflectivity decrease with increased weathering; and b) porosity, permeability & swelling increase with weathering
Malomo, 1980	granites, Nigeria	abrasive, pH	porosity, absorption & specific gravity	porosity and absorption decrease with increasing abrasive pH; specific gravity increases with weathering
Sahasrabudhe and Vaidyanath, 1981	laterites, India	iron oxide content	Atterberg Limits	could not determine any relationship
Hodder, 1984	various rocks (data from text books)	(Hodder) Chemical Weatherability Index	Los Angeles abrasion value	negative correlation between Hodder Chemical Weatherability Index and LA abrasion value
Hind, 1986	ignimbrites, New Zealand	chemical composition (major element)	uniaxial compressive strength, cohesion &angle of internal friction	could not determine any relationship
Obermeier and Langer, 1986	metamorphic & igneous rocks, USA	clay content (percentage by weight)	field permeability	in weathered material, permeability decreases with increasing clay content
Stevenson, 1986	rhyolites, New Zealand	chemical composition (major element)	compressive strength, density & porosity	could not determine any relationship
Conca and Cubba, 1986	weathered tonalite, USA	kaolinite content (percentage by weight)	field abrasion resistance hardness value (H_a)	abrasion resistance hardness value decreases with increasing kaolinite content
Veldkamp *et al.*, 1990	basaltic gravels, France	silicon, magnesium & potassium content (XRF)	bulk density	bulk density can be predicted from the contents of three elements: silicon, magnesium & potassium (using a regression equation)
Hodder and Hetherington, 1991	andesite, New Zealand	Miura Weathering Index	Los Angeles abrasion resistance & Shore scl. hardness	Shore scleroscope hardness & Los Angeles abrasion Value decrease with increasing Miura W.I.
Ulusay *et al.*, 1994	sandstone, Turkey	chemical composition	engineering properties	could not determine any relationship
Jayawardena and Izawa, 1994	garnet-sillimanitic gneiss, Sri Lanka	Silica Titania Index	point load strength index & uniaxial compressive strength	two strength parameters increase with increasing Silica Titania Index values
Ohtsubo *et al.*, 1995	marine clays, Japan	iron oxide & smectite content	sensitivity, overconsolidation ratio & Atterberg Limits	sensitivity and overconsolidation ratio depend on iron oxide content; smectite content governs Atterberg Limits.
Macari and Hoyos, 1996	basaltic residual soils, Puerto Rico	degree of weathering determined by depth	shear modulus	shear modulus decreases with the intensity of weathering
Bassett, 1998	greywacke & andesite, New Zealand	Miura Weathering Index	California Bearing Ratio, point load strength index, water content, density & porosity	California Bearing Ratio, point load strength index and density decrease with increased Miura W.I., while porosity and water content increase
Gupta and Rao, 1998; 2001	granite, basalt & quartzite, India	intensity of chemical weathering (field observations)	tensile & uniaxial compressive strengths	chemical weathering negatively influences the tensile strength and to a lesser degree the uniaxial compressive strength
Tugrul and Zariff, 1999	granite, Turkey	quartz to feldspar ratio	dry unit weight, tensile & uniaxial compressive strengths	unit weight, tensile and uniaxial compressive strengths increase with quartz to feldspar ratio
Arel and Tugrul, 2001	granite, Turkey	Reiche Weathering Potential Index	uniaxial compressive strength	uniaxial compressive strength has a positive ($r = 0.81$) correlation with Reiche Weathering Potential Index

(a) Several authors note negative correlations between intensity of weathering and hardness, strength, density, elasticity and indices of surface hardness and abrasive resistance.

(b) As a result of decreased density in weathered rock, both the porosity and permeability have been seen to increase with weathering.

(c) At later stages of weathering, with increased clay content, permeability may decrease while swelling potential and water content increase; clay content governs the Atterberg Limits.

(d) Some chemical indices such as abrasion pH and weathering indices (e.g. Reiche W.P.I.; Miura W.I.) have been proposed as predictors of physical properties such as porosity and strength.

These previous attempts made at correlating chemical parameters with engineering parameters do not provide a comprehensive explanation of the relationship between geochemistry and strength, especially at early stages of weathering. In particular, most studies have concentrated on deriving statistical relationships between various parameters without suggesting the causes of the relationships discovered. This gap in knowledge is to be partially closed in this investigation.

2.8 Summary

This chapter covered definitions of weathering; occurrence and rates of weathering; description and classification of weathering profiles; indices of weathering; geology of the project area; development of stress release fractures; weathering processes of constituent minerals of basalt; secondary minerals formed due to weathering of basalt; and attempts that have been made to correlate chemical and engineering properties.

Few previous attempts have been made at correlating chemical parameters with geotechnical parameters and this is further addressed in this investigation.

CHAPTER 3: METHODOLOGY

3 .1 Introduction

This research was a combination of field and laboratory investigations followed by statistical analysis and interpretation. In the field, the weathering profile of the Karamu Basalt was studied in detail and *in situ* tests were carried out. Samples were then collected for laboratory investigations, both geochemical and geotechnical. Results of all tests were recorded and later statistically analysed. Relationships have been sought between geochemical and geotechnical parameters. Attention was also given to determining suitable indices of weathering and chemical predictors of geotechnical parameters for Karamu Basalt. Attempts were then made to understand the weathering process from aspects of mineralogy, chemistry and geomechanics.

3.2 Field Investigations

Reconnaissance studies for the project suggested the suitability and availability of an abandoned basalt quarry at Karamu which exposed a complete weathering profile from fresh basalt, through slightly weathered, moderately weathered, highly weathered to completely weathered basalt. Exposure of rocks and soils was extremely good on the north wall of the quarry. A cross section of the north wall was prepared by using general survey methods and observations made by visual studies of material at different depths of the profile (Figure 4.1).

Sample collection was not undertaken at regularly spaced intervals. Where there were apparent changes in colour, grain size or structure, the sample locations were more closely spaced, and where there were no visible changes, a greater distance between sample locations was allowed. Altogether 60 sample locations were selected which aimed to sample all of the observed variability within the exposure (Figure 4.1). The preliminary sample descriptions were done mainly in the field using Munsell colour charts. In identifying the degree of weathering for each sample, the New Zealand Geomechanics Society (1988) scale of rock mass weathering (Table 2.3) was used.

In situ tests such as Schmidt rebound hammer hardness determinations, vane shear tests and hand-penetrometer tests were carried out in the field. The Schmidt rebound hardness test could be carried out only for fresh and slightly weathered basalt, for a total of 11 sample locations. In other cases, the values obtained were below the detectable limit. The vane shear tests and the hand penetrometer tests could be carried out on moderately to completely weathered basalt. The hand penetrometer tests were conducted for a total of 27 sample locations and the vane shear tests for a total of 28 sample locations.

Rock samples were collected in the form of blocks of an average diameter of 0.3 m, controlled by the joint spacing. In the case of weathered material, attempts were made to collect samples of at least two kilograms in weight. Although samples of some joint fillings were small, they were very useful for identification purposes. Special cylindrical samplers were used to collect specimens for the determination of bulk density and permeability, and also for the direct shear test. Later, up to ten kilograms of sample material was collected in locations where special tests such as California Bearing Ratio were proposed.

3.2.1 Schmidt Rebound Hardness

The Schmidt rebound hammer measures the distance of rebound of a known mass impacting on a rock surface (Brown, 1981). The plunger of the hammer is placed against the rock face and depressed into the hammer by pushing the hammer against the specimen. Advantages of this method are the instrument's light weight, ease of carrying and use, relatively low cost, minimal time consumption, and that data can be collected from a variety of rock surfaces. A disadvantage is that it is extremely sensitive to discontinuities in a rock mass: even fine fractures can result in a substantially reduced reading.

Following the procedure given in Brown (1981), the L type hammer (impact energy = 0.74 Nm) was used for measuring the hardness of the rock masses and materials in the Karamu weathering profile. Figure 3.1 shows the conversion chart (Brown, 1981) used

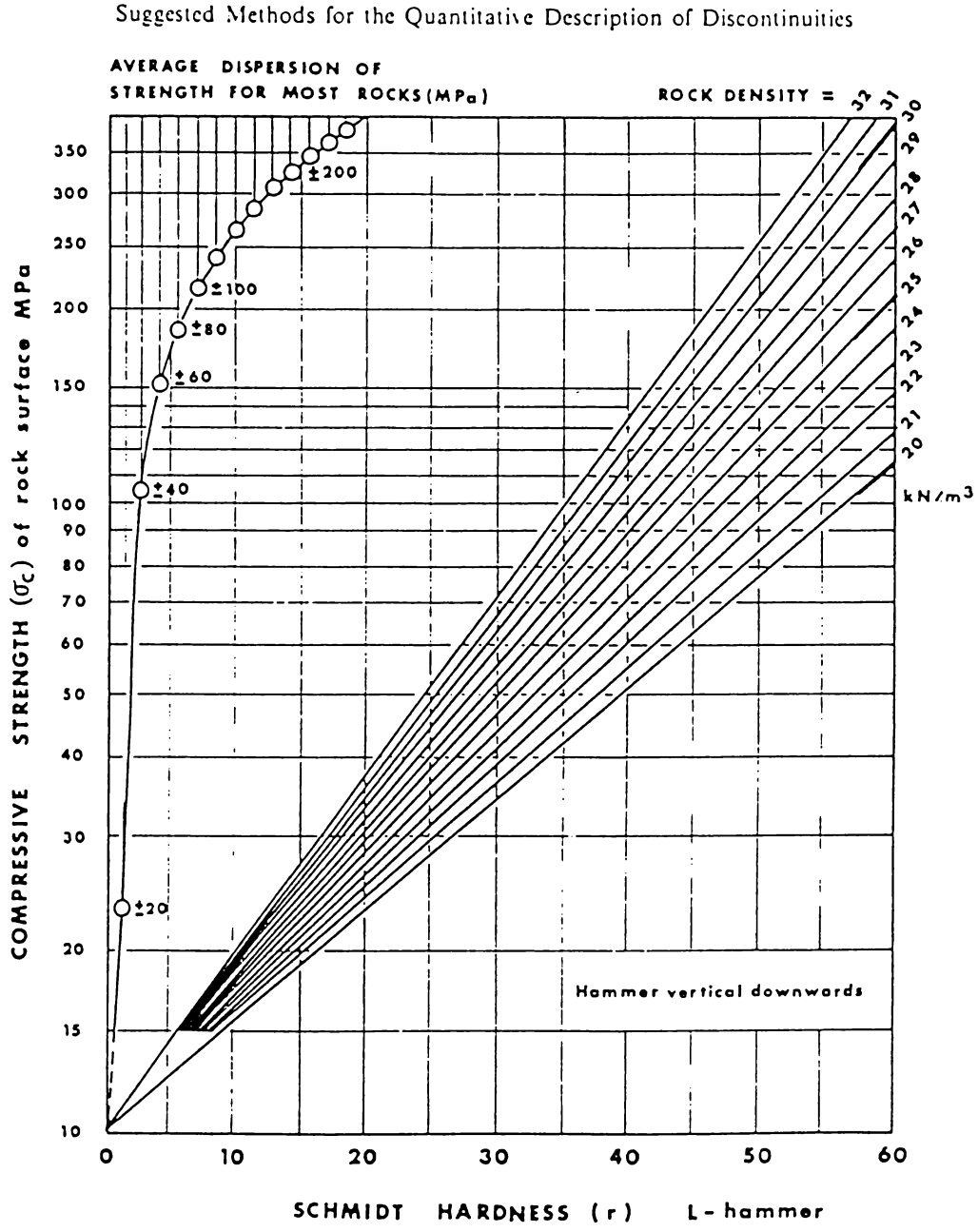

Figure 3.1 Conversion Chart to Estimate Compressive Strength from Schmidt Rebound Hardness (Miller, 1965 reproduced by Brown, 1981)

for obtaining the compressive strength from the rebound number R. Eleven sample locations of fresh and slightly weathered basalt were tested, and for each location twenty readings were recorded with the average of the ten highest values calculated. Using the chart, the average compressive strength was estimated.

3.2.2 Vane Shear Strength

Shear strength can be obtained by *in situ* testing, using the Geonor Hand-held Vane Tester H-60 (Figure 3.2) which comprises a torque head, with direct reading scale and non-return pointer. The vane, which consists of four thin rectangular blades with a depth to width ratio of 2:1, is screwed into the rear of the torque head. The vane is pushed into the undisturbed material and rotated through a calibrated spring, until the soil failure occurs. Torque, which is necessary to turn the vane, is automatically recorded on the shear strength scale attached to the calibrated spring.

The shear strength range of the instrument is from 0 to 260 kPa. Three different sized vanes are used: 16x32 mm, 20x40 mm and 25x50 mm. To obtain the shear strength in kPa, the values on the scale are taken as they are in the case of the medium sized (20x40 mm) vane, multiplied by two in the case of the smaller vane, and divided by 2 in the case of the larger vane.

Following instructions of Geonor (1966), undrained shear strength of soft weathered material was obtained using the hand vane tester for 28 sample locations. 20 readings were taken for each sample location, and the average of the ten highest values was calculated.

3.2.3 Penetrometer Test

A pocket penetrometer (Figure 3.3), a lightweight device for determining the approximate unconfined compressive strength, was used to determine the penetration resistance. A stainless steel plunger is pushed into the soil until the penetration mark is reached. Equivalent unconfined compressive strength of the material can be read in kgf/cm^2 from the maximum load indicator provided (Engineering Laboratory Equipment Ltd. Catalogue, 1993).

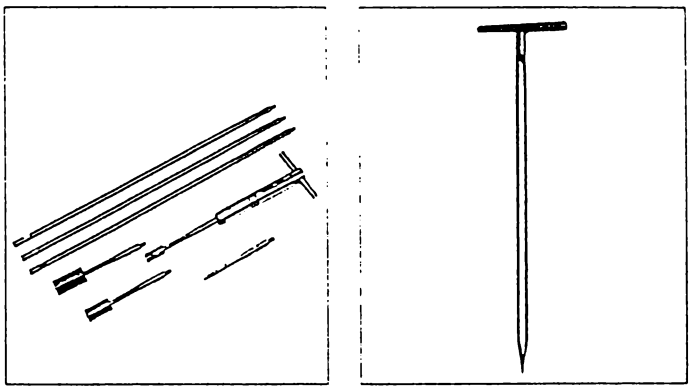

Original Geonor Hand-Held Vane Tester

Figure 3.2 Geonor Hand—held Vane Tester H-60

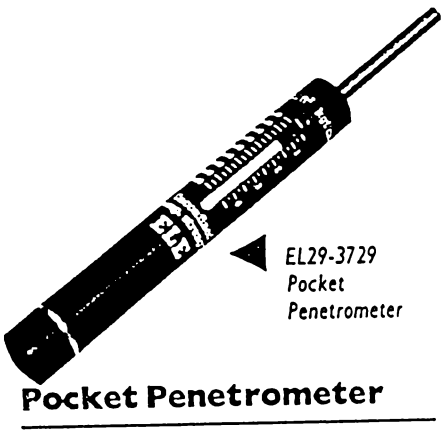

Figure 3.3 Pocket Penetrometer EL 29-3729

In the field, 20 readings for each of 27 sample locations were taken and the average values of the ten highest readings were calculated and converted to SI units using the following conversion equation: 1 kgf/cm^2 = 0.098 MPa. Where the weathering was only slight, readings could not be obtained by this method.

3 .3 Laboratory Geochemical Investigations

Sealed samples were brought to the laboratories for further investigations. From each sample oven-dried powders were prepared for chemical tests, crushed in a ring mill. Thin sections were prepared for microscopic studies. Samples of about 25 mm in diameter were selected for all grades of weathering. These were cut in the middle with the rock saw, and one half was polished in order to determine the Shore sclerescope hardness. The other half was used to prepare thin sections, in order to examine the thickness of olivine rims, if any. Later, polished sections were prepared for the sections with opaque minerals.

In order to evaluate the chemistry of these materials, the following studies were carried out: chemical analyses by X-ray fluorescence (for constituent major and trace elements), X-ray diffraction for mineral identification, abrasion pH values of the finely ground material dissolved in water in 1:2.5 ratio by weight, electrical conductivity (which in turn indicates the amount of soluble salts present), petrography on thin and polished sections, and scanning electron microscopy.

3.3.1 X-Ray Fluorescence Method of Chemical Analysis

The X-ray fluorescence method was used to determine the chemical components of all samples. Samples were oven-dried at 105 °C for over 24 hours and finely powdered in the ring mill before testing. XRF analyses were carried out by Geoscience Laboratories, Sudbury, Ontario, Canada. Major and trace element analyses were carried out. In addition, X-ray fluorescence studies were later carried out at the University of Canterbury, New Zealand in order to check any previously unidentified trace elements.

3.3.2. X-Ray Diffraction Method for Mineral Analysis

The X-ray diffraction method was used to identify minerals present in samples. Philips MPD x'pert system was used with Cu α K21 at 0.02° 2θ/step and with the automatic optical setting of with 45 kV; 40 mA. The range of 2θ (2 theta) taken was 1° to 100°.

Karamu Basalt specimens of all weathering grades were tested. Samples from all available locations were taken. However, moderately weathered basalt contained 12 specimens and out of them only ten were tested. One sample each of tephra and paleosol and two inclusions (containing brown, black and white components) were also tested. A total of 39 samples were tested.

These samples were crushed sufficiently so that individual crystals of material could be separated in order to get the crystal faces to diffract the X-rays and produce peaks at respective angles. Bulk samples, core stones and matrix / joint infill were separately tested where appropriate in order to get a better understanding of the constituent minerals. Special attention was given to the samples, or fractions of samples, for which the mineral composition could not be clearly obtained with the use of a polarising microscope i.e. cryptocrystalline or microcrystalline minerals.

3.3.3 Abrasion pH

Abrasion pH is measured in suspensions or solutions of powdered material. Water has always been the suspension or solution medium for pH determination of soils and rocks. The International Society of Soil Science committee has suggested a one part of soil to 2.5 parts of water ratio for the preparation of suspensions (Blakemore *et al.*, 1987).

According to NZS 4402 (Standards Association of New Zealand, 1986), a pH meter consisting of two electrodes and a digital monitor was used for this purpose. Powdered samples were mixed with distilled water, to the ratio by weight of 1:2.5, stirred at high speed and then were allowed to stand overnight. Electrodes were thoroughly washed with distilled water, and the samples positioned on the instrument so that both electrodes were well covered. Without stirring, the pH value was measured and recorded.

3.3.4 Electrical Conductivity

Electrical conductivity of solutions can be used to indirectly evaluate the amount of soluble salts present in a rock or soil sample. Samples were dried, powdered and then dissolved in water in the ratio by weight of 1:2.5. They were then stirred and left to stand overnight. The conductivity meter electrode was inserted into the solution and the reading (measurement) displayed on the monitor was recorded. The measurements were recorded in the units microsiemens per centimetre (μS / cm).

"There is no clear relationship between electrical conductivity and total soluble salts due to the different ionic conductivities of the various salts and to the influence of soil particles" (Rayment & Higginson, 1992 p 15). However, according to Rayment & Higginson (1992) an approximate value for percentage total soluble salts may be obtained by multiplying, by 0.34, the electrical conductivity given in decisiemens per metre (dS / m).

In order to obtain the approximate percentages of soluble salts, the measurements obtained in this study in microsiemens per centimetre (μS / cm), were multiplied by 0.34×10^{-3} taking into consideration the conversion ratios of microsiemen to decisiemen and centimetre to metre.

3.3.5 Polarising Microscopic Studies

Rock samples were sliced, and sections of 0.03 mm thickness were prepared and mounted on to glass plates using Hillquist resin. Where the samples were weathered, and the material tended to disintegrate when cut, an epoxy resin was used to hold the particles together. In the case of very loose material, some temporary mounts were prepared by sprinkling the grains on a glass slide with a drop of clove oil (Refractive Index = 1.53-1.54) and covering with a cover slip. For such material, permanent mounts were also made using Hillquist resin. Thus, transparent and translucent minerals both of primary and secondary origin were studied. Point counting was carried out on fresh basalts.

Special attention was paid to the iddingsite rims of olivine crystals from basalt of varying weathering degrees. The rim thickness was measured using an accessory tool,

which measures distances on thin sections to an accuracy of 0.01 microns. As mentioned earlier, specimen preparation for this was as follows: each sample from all grades of weathering were cut in the middle and one half was used to prepare thin sections for iddingsite rim thickness determination and the opposite half was used to determine the Shore scleroscope hardness. This way, for each average olivine rim thickness, there is a corresponding average value of Shore scleroscope hardness. Twenty readings of each parameter were taken for each specimen.

3.3.6 Reflected Light Microscopic Studies

In order to understand the nature of the opaque minerals found in the samples, polished sections were prepared. From these polished sections, minerals such as magnetite, hematite and goethite could be identified and studied.

3.3.7 Scanning Electron Microscopy

A polarising microscope was not sufficient to study clay minerals and some other layer silicates. A Kevex Scanning Electron Microscope, with a delta class analyser, was used for this purpose, since magnifications upto X20,000 could be achieved with this instrument. Identification of clay minerals and differentiation between some of them was made possible with this method. Micrographs taken were later sent to CSIRO, Melbourne, for confirmation of identification.

3.3.8 Detection of Presence of Allophane

According to the NZ Standards 4402 (1986), the presence of allophane in the samples was checked. The procedure was to place a small amount of crushed material (~10 mg) on the indicator paper (ordinary filter paper previously treated with phenolphthalein indicator and allowed to dry); add a drop of saturated sodium fluoride solution to wet the sample; observe for 3 minutes and report any colour change in the indicator paper. Pink or red colours indicate the presence of allophane.

3.4 Laboratory Geotechnical Investigations

In the laboratories, the following tests were carried out to determine geotechnical parameters: uniaxial compressive strength, point load strength index, Shore scleroscope hardness, California Bearing Ratio, water content, dry density, particle density, particle size distribution, direct shear test, Atterberg limits and permeability. NZ Standards 4402 (1986) were used wherever available. In other cases, ISRM (International Society of Rock Mechanics) suggested methods of testing (Brown, 1981) were preferred over the ASTM (American Society for Testing of Materials) methods of testing (Lambe, 1951).

Once the samples were collected, sealed and brought to the laboratory, test specimens were prepared by ISRM suggested methods for geotechnical examination. Blocks of rocks were cored, in order to obtain NX (54 mm diameter) core size cylindrical specimens of 125-150 mm height, for uniaxial compressive strength determination. For point load tests, rock lumps of an average diameter of 50 mm were prepared, with the help of geological hammers. For California Bearing Ratio, samples of about 6 kg were required. Loose material of high to completely weathered grades, at natural water content, was placed in the moulds for testing. In the less weathered basalt, the samples were crushed to obtain a minimum grain size of 10 mm. The specimens for bulk density, permeability and direct shear tests were already in special cylindrical samplers. Atterberg limits, water content and particle density were carried out on samples stored in plastic bags.

3.4.1 Uniaxial Compressive Strength Determination

This test method is intended to measure the uniaxial compressive strength of a rock sample, using specimens of regular geometry (Brown, 1981). A suitable machine is used for applying to the specimen and measuring the axial load. Steel platens in the form of discs and having a Rockwell hardness of not less than HRC58 are placed at the specimen ends.

From blocks of rocks, cylindrical specimens were cored with a hydraulic corer. Test specimens were right circular cylinders with diameters of NX core size (approximately 54 mm) with a height to diameter ratio of 2.5 to 3.0. The ends were flattened and smoothed. Load on the specimen was applied continuously, at a constant stress rate,

such that failure occurred within 10 minutes of loading. The maximum load on the specimen was then recorded. Uniaxial compressive strength of the specimen was calculated by dividing the maximum load carried by the specimen during the test by the original cross-sectional area.

Uniaxial compressive strength testing requires large blocks of rocks from which to core multiple cylinders. As the quarry walls are near-vertical, and vehicle access is restricted to the base of the slope, sampling large blocks was hazardous, and considered inadvisable. Therefore, samples large enough for preparation of cylindrical core specimens could be obtained only from the location MPJ 1 (No. 1 in Figure 4.1), and a total of 10 specimens was tested.

3.4.2 Point Load Strength Index

The point load strength test is an index test for the strength classification of rock materials. It may be used to predict other strength parameters such as uniaxial compressive strength. ISRM suggested methods for determining point load strength index (Franklin, 1985) were followed. The test measures the point load strength index $I_{s(50)}$ of rock specimens. The testing machine (Figure 3.4) consists of a loading system (comprising a loading frame, pump, ram and platens), a system for measuring the load (P) required to break the specimen, and a system for measuring the distance (D) between the two platen contact points.

Point load strength index, I_s, is calculated as:

$$I_s = P/D_e^2 \quad \ldots 3.1$$

where D_e, the equivalent core diameter, is given by:

$$D_e^2 = 4A/\pi \quad \ldots 3.2$$

where A = WD where W is the width of specimen and D is the minimum distance between platen points.

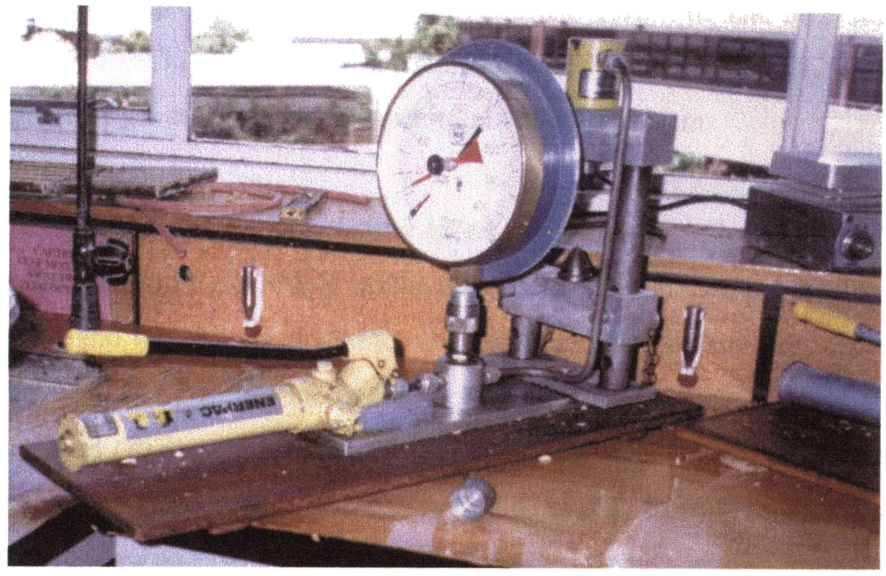

Figure 3.4 Point Load Tester

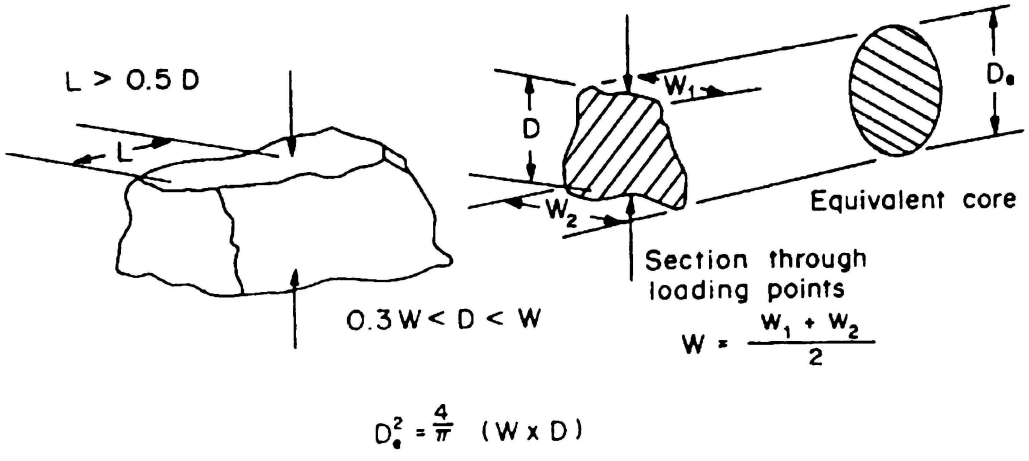

Figure 3.5 Specimen shape requirements for Point Load (irregular lump) test. (ISRM Testing Method)

Since I_s is dependent on the geometry of the test specimen, a size adjustment is required when irregular lumps are used instead of cylindrical core samples. Size-corrected point load strength index $I_{s(50)}$ of a rock sample, is defined as the value of I_s that would have been measured by a diametrical test specimen with D = 50mm.

Twenty irregular lump specimens were taken from each sample (Figure 3.5). Callipers were used to measure the width W of the specimens. The specimen was inserted into the test machine and the platens closed to make contact with the smallest dimension of the lump. The load was steadily increased such that failure occurred within a minute, and the failure load (P) was then recorded. For Karamu Basalt, Point load index $I_{s(50)}$ was calculated using standard conversions (Franklin, 1985) from I_s to $I_{s(50)}$. Following the method of Bieniawski (1975), uniaxial compressive strength was estimated as $24.I_{s(50)}$.

3.4.3 Shore Scleroscope Hardness Determination

As suggested by Brown (1981), Shore scleroscope model C-2 was used. It consists of a vertically disposed barrel containing a precision bore glass tube. A scale graduated from 0 to 140 is set behind the barrel and is visible through the glass tube. A pneumatic actuating head, affixed to the top of the barrel, is manually operated by a rubber bulb and a tube. A hammer drops from a specified height and rebounds within the glass tube. When a reading is required, the specimen is placed below the barrel, and the rubber bulb is squeezed so that it causes the hammer to go up to the specified height and then drop from there and rebound within the glass tube.

Tests were carried out on specimens with flat surfaces, ground smooth using abrasive powder. The instrument was set in a vertical position, with the bottom of the barrel in firm contact with the test specimen, and normal to the surface of the specimen. The hammer was brought to the elevated position by squeezing the rubber bulb and then was allowed to fall and strike the test surface and the height of rebound was measured. The height to which the hammer rebounds on the first bounce indicates the Shore scleroscope hardness of the material. Prior to testing of the samples, at least 5 readings were taken on the standard test blocks provided. For each specimen 20 readings were taken at different points. The average of these 20 values was taken as the Shore scleroscope hardness.

3.4.4 California Bearing Ratio Determination

California Bearing Ratio test, or CBR test as it is usually called, is an empirical test for estimating the bearing value of material (Figure 3.6). According to the New Zealand Standards 4402 (1986), the test is performed by pushing, at a fixed rate of penetration (1 mm/min), a standard plunger of 1935 mm^2 cross section into the test material held in a special container (CBR mould), and measuring the force required to maintain that rate. Ratio of the force required by the tested sample to that required by a sample of crushed fresh rock is the CBR and it is given as a percentage. By definition, the fresh rock will have a CBR value of 100 %.

Loose samples of weathered material compacted with a standard compaction effort (New Zealand Standards 4402, 1986), at their natural water contents (determined simultaneously) were tested. The CBR was determined at penetrations of 2.5 mm and 5 mm, and the higher value was used. The CBR values were calculated as follows: for CBR values over 20 %, to the nearest 5 %; for values 5 to 20 %, to the nearest 1 % and for values < 5 %, to the nearest 0.5 %.

3.4.5 Direct Shear Test

The direct shear test was carried out according to Lambe (1951). The specimen is stressed to failure by moving one part of the specimen relative to the other, forcing it to be ruptured along a horizontal plane at mid-height. A shear box is used for this purpose. It is a square box, without a top or a bottom, split horizontally at the level of the centre of the soil sample. A horizontal force is applied to the lower part of the box at a constant rate until the sample fails. For determining the shear resistance under a normal stress, a vertical load is applied to the sample by means of a dead weight (Selby, 1993).

Whenever possible undisturbed cylindrical specimens of 60 mm in diameter were collected for direct shear testing, but for samples of weathered material which contained original rock fragments only the matrix was taken and remoulded (material manually placed in the sampling rings) specimens were used for testing. The tests were carried out at unconsolidated, undrained conditions with a shearing rate of 0.61 mm/min. Plots of normal stress versus peak shear stress for each sample gave the values of angle of internal friction (ϕ) and cohesion (c).

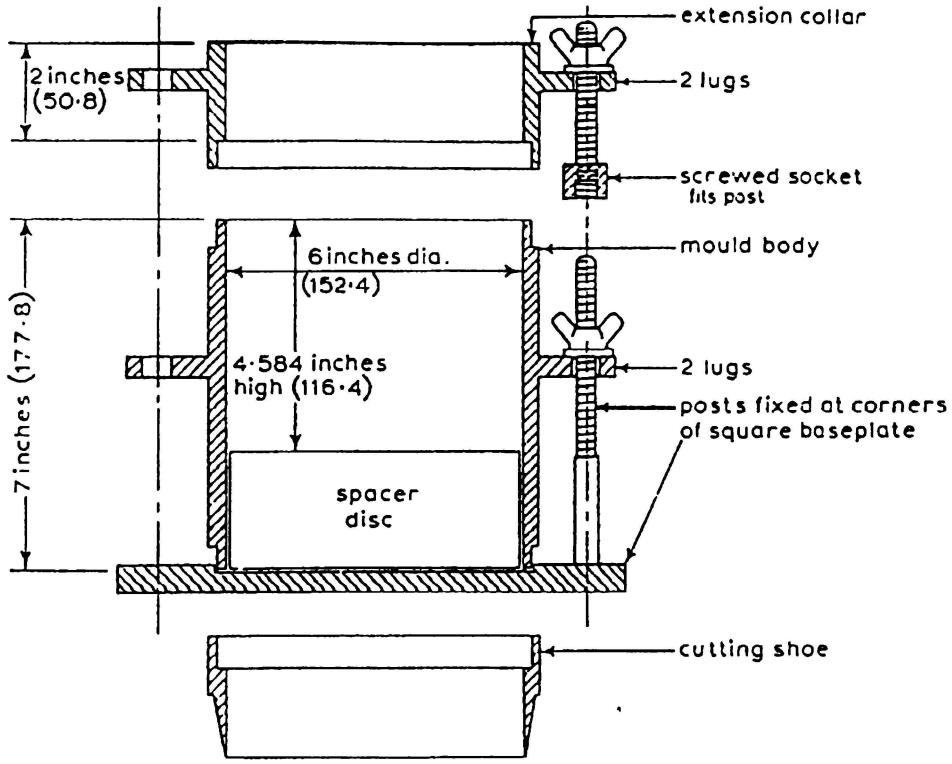

Figure 3.6 Arrangement of CBR mould and fittings (ASTM type) (dimensions in brackets are mm)

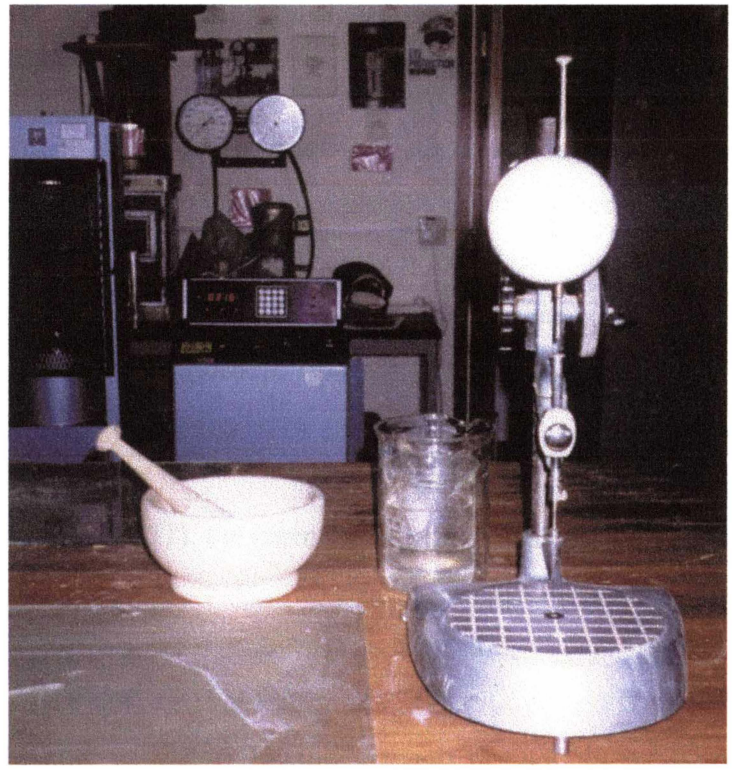

Figure 3.7 Cone Penetrometer

3.4.6 Atterberg Limits Determination

Atterberg limits (liquid limit, plastic limit and plasticity index) were determined using the cone penetrometer which is usually used for obtaining the cone penetration limit which is related to (and sometimes identical to) the liquid limit. The decision to use this easier and faster method was made after some results thus obtained were checked against respective values obtained by tests using the liquid limit device (Casagrande apparatus) and the plastic limit plate. Since there was an acceptable calibration adjustment (an increase by ~ 5 % in both liquid limit and plastic limit in the cone penetrometer values) this method was adopted. The plasticity index remained constant. This calibration check is given as Appendix 3.1.

The cone penetrometer, as per NZS 4402 (1986) (Figure 3.7), consists of:

(a) A cone of stainless steel 35 mm long, with a smooth polished surface, and an angle of 30 °.
(b) A penetrometer with an indicator dial readable and accurate to 0.1 mm over a 40 mm travel length of cone.
(c) A metal cup, 55 mm in diameter and at least 40 mm deep, with the rim parallel to the base.

Samples with different water contents were used to fill the cup and the penetration was recorded five times for the same sample at each water content. The water content values were plotted against the average cone penetration values. A water content value corresponding to the penetration of 20 mm was taken as the cone penetration limit (equivalent to the liquid limit). The water content value corresponding to 2.8 mm was taken as the plastic limit (Allbrook, 1980).

3.4.7 Permeability Test

According to Lambe (1951), the permeability can be calculated using Darcy's Law:

$$Q = kPA \qquad \ldots 3.3$$

where Q is the rate of water flowing through the soil in m^3/s ; P is the hydraulic gradient; A is the cross-sectional area of the sample in m^2 and k is the permeability in m/s.

For the falling head situation, where a volume of water is supplied at the start of the test and the head is allowed to fall as the test proceeds, the following equation can be used to calculate the coefficient of permeability (k) in m/s (Lambe, 1951):

$$k = 2.3[\, aL / A(t_1 - t_0)]\log_{10}(h_0 / h_1) \quad \ldots 3.4$$

where:

a = cross sectional area of the standpipe, in m^2;

L = length of the soil in the permeameter, in m ;

A = cross sectional area of the permeameter, m^2;

h_0 and h_1 = heads between which the permeability is determined, in m; and

t_0 and t_1 = corresponding times in s.

The falling head permeability test was carried out on samples collected in special cylindrical samplers of 54 mm diameter and 100 mm height. The procedure was as follows:

(a) Samples were placed in the permeameter and locked and placed in water overnight so that saturation could take place.

(b) The permeameter was connected to the standpipe tube (of known internal diameter) of the permeability apparatus.

(c) Level of water in the standpipe and the elapsed time was recorded at different time intervals depending on the rate of flow.

A total of 10 readings were taken for each sample and the full range of the height (1000 mm) was used. The coefficient of permeability was calculated in metres per second.

3.4.8 Particle Size Distribution Analysis

Grain size analysis is performed on soils as a routine test in most soil mechanics laboratories. There are a number of possible methods for determining particle size distribution including sieves, sedimentation, electrozone sensing, microscopy and laser diffraction (Rawle, 1993).

In this study, wet sieve analysis (using sieves 2 mm and 0.6 mm) was carried out on samples of materials in order to determine the particle size distribution, but for fractions smaller than 0.6 mm diameter the Malvern Mastersizer - X was used as per Rawle (1993), and weight percentages of fine fractions were thus obtained. The Mastersizer operates with a laser beam that goes through the suspension of particles in water. The rays reflect and refract at different angles depending on the particle size. These angles are interpreted and a computer calculates the relative quantity of particles in each size range. The samples were mixed with water and thoroughly shaken before testing and a deflocculant (10 ml of 5 % calgon) was added to ensure that the individual clay particles were separated.

3.4.9 Determination of Natural Water Content; Bulk-, Dry- and Particle-Density

New Zealand Standards 4402 (1986) were followed for these tests.

The water content (w): A container was weighed (M_1); then the rock material was added in its natural condition and weighed (M_2); and then it was oven dried overnight and weighed again (M_3). This measurement was repeated after oven-drying overnight once again (M_4) to see if it had the same value as M_3 in order to make sure the sample has dried completely. The water content (w) was calculated as:

$$(M_2 - M_4)/(M_4 - M_1) \times 100\% \quad \ldots 3.5$$

The bulk density (ρ) was determined in natural moisture conditions, using the special samplers of 50mm diameter and 60mm height for weathered material and right cylindrical cores for rocks. The samples were weighed (W) and the volume (V) was calculated from length (L) and diameter (D) measurements using callipers. The formula used is:

$$V = \pi D^2 L/4 \quad \ldots 3.6$$

The bulk density (ρ) in kg/m^{3}was taken as the weight divided by volume (W/V).

The dry density (ρ_d) was calculated from the values of bulk density and water content:

$$\rho = \frac{100\rho_d}{100 + w} \quad \ldots 3.7$$

where ρ is the bulk density in kg/m^3; ρ_d is the dry density in kg/m^3; and w is the water content as a percentage.

The particle density (ρ_s) was determined using oven-dried and crushed samples. A simple pycnometer was used for this purpose. The weight of the empty pycnometer (M_1), weight of it with the sample (M_2), weight of it with sample plus water (M_3), and the weight of the pycnometer filled with water alone (M_4) were measured. The particle density in kg/m^3 was calculated as:

$$\rho_s = \frac{(M_2 - M_1)}{(M_4 - M_1)} \times \rho_w \quad \ldots 3.8$$

where ρ_s is the particle density and ρ_w is the density of water at room temperature.

3.5 Presentation of Observations and Results

Most observations and results are presented in tabular form. Where appropriate the average values are presented with error estimates being the standard deviation. Geochemical and geotechnical test results are separately presented. Wherever available, test results of tephras, paleosols and inclusions were included. Using the chemical analysis results, several weathering indices were calculated and they too are presented in the tables. Where appropriate, sketches and photographs were made to make the observations easier to understand. Graphical presentations of relationships between parameters are also available.

3.6 Analysis of Results

Observations made, and results obtained by field and laboratory investigations, were statistically analysed. A major objective of many statistical investigations is to establish

relationships which make it possible to predict one or more variables in terms of others (Freund, 1974). The computer software Minitab 13 was used in statistical analysis. At the outset, geochemical parameters were correlated with each other using linear, logarithmic and curvilinear regression analysis. Similarly, geotechnical parameters were correlated with each other. The next step was to correlate geochemical parameters with geotechnical parameters using regression analysis. According to Johnson (1984), $R^2 = 0.64$ is considered significant at 95% confidence level. Therefore, $R^2 = 0.64$ was considered as the minimum value for acceptance of a possible relationship. Throughout this study, relationships showing acceptable correlations ($R^2 \geq 0.64$) are given as plots. However, relationships with high R^2 values that did not produce convincing plots, in terms of spread of data points or clusters, were excluded.

Principal component analysis was then carried out. The object of the analysis is to take *p* variables $X_1, X_2, \ldots X_P$ and find linear combinations of these to produce indices $Z_1, Z_2, \ldots Z_P$ that are uncorrelated. The lack of correlation is a useful property because it means that the indices are ordered so that index Z_1 displays the largest amount of variations, index Z_2 displays the second largest amount of variation, and so on. Z_i are called the principal components. The best results are obtained when the original variables are very highly correlated, positively and negatively. If that is the case it is quite conceivable that 20 or 30 original variables can be adequately represented by two or three principal components (Manly, 1994). Some chemical parameters were thus identified as representatives explaining the whole range of variations in values of chemical parameters.

Once this was completed best subsets regression analysis was carried out taking all geochemical parameters as independent variables and the geotechnical parameters as dependent variables or responses. The objective of the best subsets regression analysis is to determine individual or groups of independent variables that can predict the variations in the values of dependant variables. Based on some geotechnical parameters, which covered a wide range of the weathering grades, best geochemical subsets were determined with the use of Minitab 13 computer software. According to their regression coefficients and the number of components in a subset, a few of them were selected as suitable for the prediction of geotechnical parameters of Karamu Basalt. The validity of these predictors was tested for other rock types using works of other authors.

CHAPTER 4: GEOCHEMICAL RESULTS AND OBSERVATIONS

4.1 Introduction

After a preliminary reconnaissance study, field investigations were carried out. The north wall of the Karamu quarry was surveyed and mapped. Figure 4.1 is a section drawn along the north wall. Sixty locations were selected for sampling. These 60 sample locations are marked in the cross section for reference. Their field description is given in Appendix 4.1. The locations were numbered in the sequence the samples were collected, therefore the numbers do not express the degree of weathering, depth or any other parameter. Chapter 5 five deals with the geotechnical properties of Karamu Basalt, and the weathering profile is described in geotechnical detail there (a brief outline is given here in order to understand the profile). Mineralogical and chemical investigations, observations and results are given in this chapter. Chemical indices were calculated for each sample based on their chemical analyses and they too are discussed here.

4.1.1.Weathering Profile

The bottom of the Karamu Basalt profile consists of dark grey, columnar-jointed fresh basalt. Grading upwards, slightly weathered basalt has additional horizontal fractures, which seem to turn the rock into angular blocks with brown discolouration at the joints and fractures. This is followed by moderately weathered basalt consisting of less angular corestones surrounded by a yellowish brown clay, which in turn is followed by highly weathered basalt consisting of smaller corestones in a matrix of clayey material. On top of this, is brown coloured, completely weathered basalt where the original structure could be seen but the original minerals have been altered beyond recognition. Several layers of weathered tephra and their associated paleosols cover these layers in some places. Photographs of the weathering profile at each weathering grade are given as Figures 4.2 to 4.7. Their locations are indicated by stars in Figure 1.2.

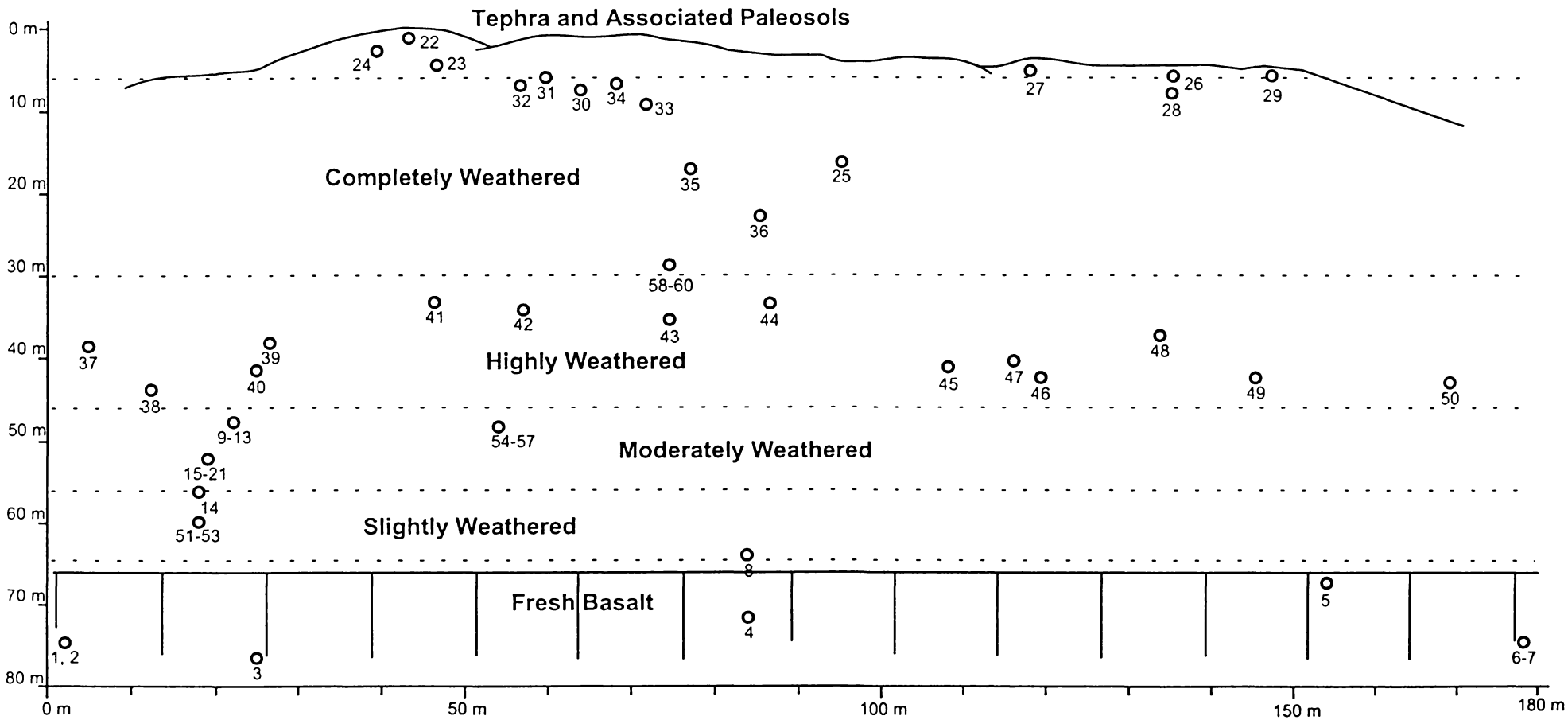

Figure 4.1 Schematic Weathering Profile at Karamu North Wall. Dotted Lines Indicate Average Depth of Boundaries Between Adjacent Weathering Grades. Numbers Indicate Sample Locations.

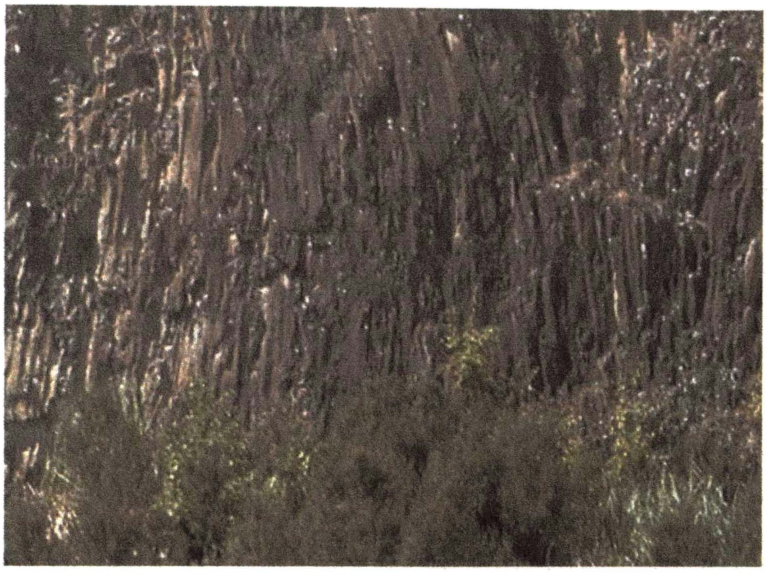

Figure 4.2 Fresh Karamu Basalt Showing Columnar Jointing (scale 1:50)

Figure 4.3 Slightly Weathered Karamu Basalt Showing Discolouration At Joint Apertures (scale 1: 10)

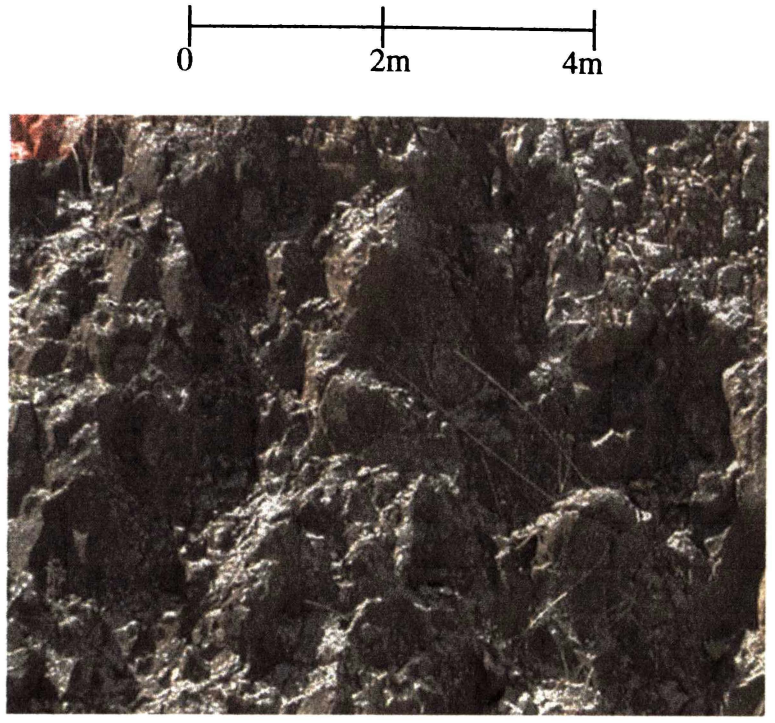

Figure 4.4 Moderately Weathered Basalt Showing Angular Corestones in a Clayey Matrix

Figure 4.5 Highly Weathered Basalt Showing Near-horizontal Joint Fillings (scale 1: 25)

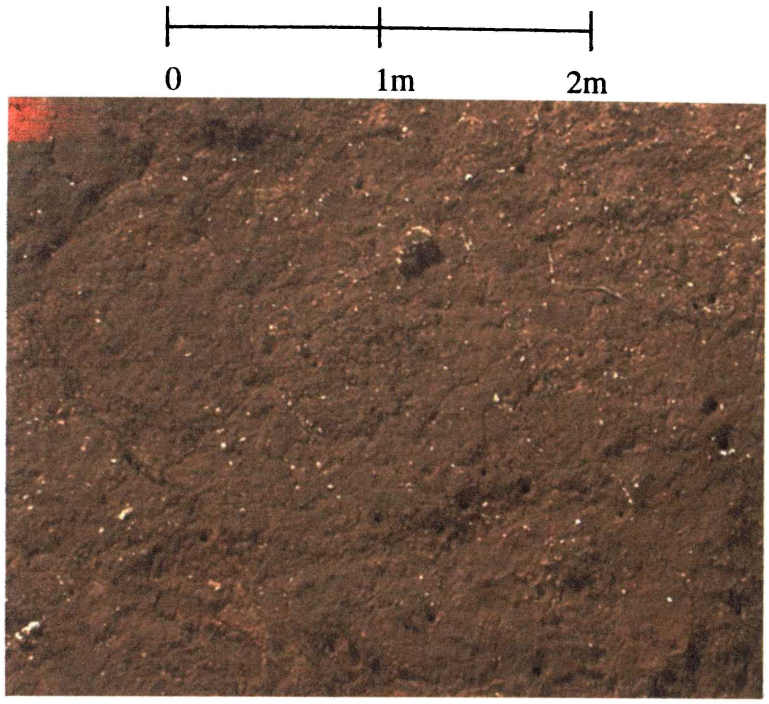

Figure 4.6 Completely Weathered Basalt Showing White Inclusions Consisting mainly of Clays

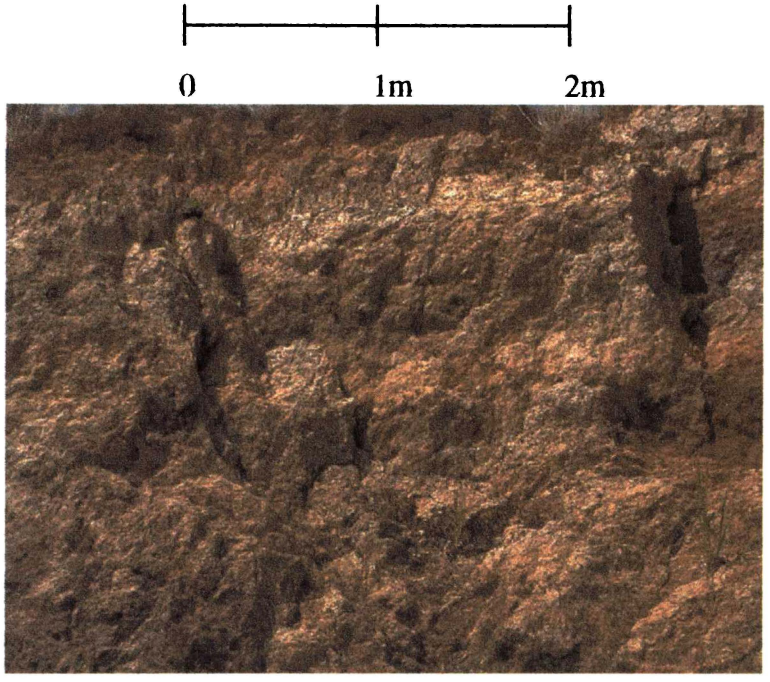

Figure 4.7 Alternating Layers of Tephra (pale brown) and Paleosol (dark brown) on Top of the Karamu Basalt. Evidence of Near-vertical Slides (Scale 1: 75)

4.2 Mineralogical Observations

Petrographical observations of the samples made under the polarising microscope, both in thin sections and polished sections, are given in Appendix 4.2. A summary of the textural and mineralogical observations for each grade of weathering of Karamu Basalt was prepared (Table 4.1). The percentages of minerals given in Table 4.1 are modal percentages determined by point counting method. In fresh basalt, holocrystalline to hypocrystalline porphyritic texture was predominant and in weathered samples the relict porphyritic texture was retained. Gradual development of a network of cracks and their widening was observed from fresh to weathered samples. The following minerals were identified in different grades of weathering: olivine, titanaugite, plagioclase, titanomagnetite, volcanic glass, clays, apatite, chromite, hematite, goethite, manganosite and zeolites.

The X-ray diffraction method produced diffractograms for the mineral assemblage present in all samples. Using the powder diffraction files (Bigelow and Smith, 1966) and the user guidelines to the files (Johnson and Vand, 1966), minerals present were identified. This confirmed the presence of the minerals optically identified in thin sections in the Karamu Basalt weathering profile (except for apatite and zeolites, probably due to low concentrations). In addition, the clay minerals present were distinguished as montmorillonite, nontronite, saponite, beidellite, kaolinite, illite and halloysite. Small quantities of phlogopite and vermiculite were detected in some weathered basalt samples. Diffractograms depicting the changes in mineralogy from fresh basalt to different grades of weathering are given in Figure 4.8.

According to Bertin (1975), a semiquantitative analysis could be carried out using the areas of peaks for each mineral. The percentage mineral content was calculated as mineral peak area / total peak area x 100 % (Appendix 4.3). The average mineral percentages which were calculated by this method are given in Table 4.2. These values may not be similar to the modal percentages obtained by the point counting method (p.c.m.) on thin sections: in fresh basalt, percent augite remains the same (~28 %) but the percent olivine is reduced to 20 % (from 33 % in p.c.m.) while plagioclase is increased to 39 % (from 34 % in p.c.m.).

Table 4.1 SUMMARY OF PETROGRAPHIC OBSERVATIONS

Unit	Petrographic Description
Fresh Basalt Sample Nos: MPJ 1, MPJ 2, MPJ 3, MPJ 4, MPJ 5, MPJ 6, MPJ 7	Holocrystalline to hypocrystalline, fine grained, porphyritic with abundant euhedral to subhedral phenocrysts of olivine, titanaugite, plagioclase and rare titanomagnetite set in a groundmass composed of plagioclase laths, titanaugite, olivine, glass and tiny granular titanomagnetite crystals. Accessory minerals are apatite and chromite. Vesicles present. Olivine 33.14 ± 2.54 %; titanaugite 28.43 ± %; plagioclase 34.07 ± 1.10 %; glass 2.43 ± 2.44 % and titanomagnetite 2.07 ± 1.30 %. Occasional pale yellow outlines on olivine crystals. Evidence of microfracturing. Zeolites identified in two samples.
Slightly Weathered Basalt Sample Nos: MPJ 8, MPJ 14, MPJ 51, MPJ 52, MPJ 53	Porphyritic texture of the fresh basalt is retained. Alteration of olivine crystals shown by development of orange coloured iddingsite rims of up to 17 μm thickness. Titanaugite crystals reduced in size from the fresh basalt due to breaking off of parts. Plagioclase crystals show turbid and speckly appearance due to development of clay. Titanomagnetite abundant. Interstitial positions show alteration of glass to smectites. Fractures more visible and frequent. Clays appear on fracture surfaces.
Moderately Weathered Basalt Sample Nos: MPJ 9, MPJ 10, MPJ 11, MPJ 12, MPJ 13, MPJ 15, MPJ 16, MPJ 17, MPJ 18, MPJ 19, MPJ 20, MPJ 21	Relict porphyritic texture. Olivine crystals have thicker iddingsite rims (30 μm) than slightly weathered basalt. Along fracture planes, olivine and titanaugite crystals in parts (in some places completely) removed. Plagioclase and glass absent. Titanomagnetite unaltered. A network of cracks in the rock filled with clays, goethite and hematite.
Highly Weathered Basalt Sample Nos: MPJ 38, MPJ 41, MPJ 44, MPJ 47, MPJ 49, MPJ 50	Relict porphyritic texture. Olivine and augite phenocrysts altered to goethite and hematite. Only a small fraction of olivine can be seen in relict phenocrysts. Pyroxenes in the groundmass broken down to clays. Clays abundant. Extensive crack network.
Completely weathered Basalt Sample Nos: MPJ 31, MPJ 32, MPJ 33, MPJ 34, MPJ 36, MPJ 58, MPJ 60	Relict porphyritic texture. Only relict outlines of olivine and titanaugite crystals visible. Clay minerals, hematite and goethite constitute the material.
Rhyolitic Tephra: Sample Nos: MPJ 22, MPJ 23, MPJ 25, MPJ 26, MPJ 27, MPJ 28, MPJ 30, MPJ 35	Clay minerals and goethite predominant in tephra. Fine grained or earthy texture.
Paleosols: Sample Nos: MPJ 24, MPJ 29	Clay minerals and hematite predominant in paleosols. Fine to medium grained texture.
Clayey infill in weathered basalt Sample Nos: MPJ 37, MPJ 39, MPJ 40, MPJ 42, MPJ 43, MPJ 45, MPJ 46, MPJ 48, MPJ 54, MPJ 55, MPJ 56, MPJ 57, MPJ 59	Clays sometimes as white spots or lenses, sometimes mixed thoroughly with hematite (reddish brown) and goethite (orangish brown); black manganese oxide in nodule form distributed unevenly in weathered rock material. These can be identified on polished sections.

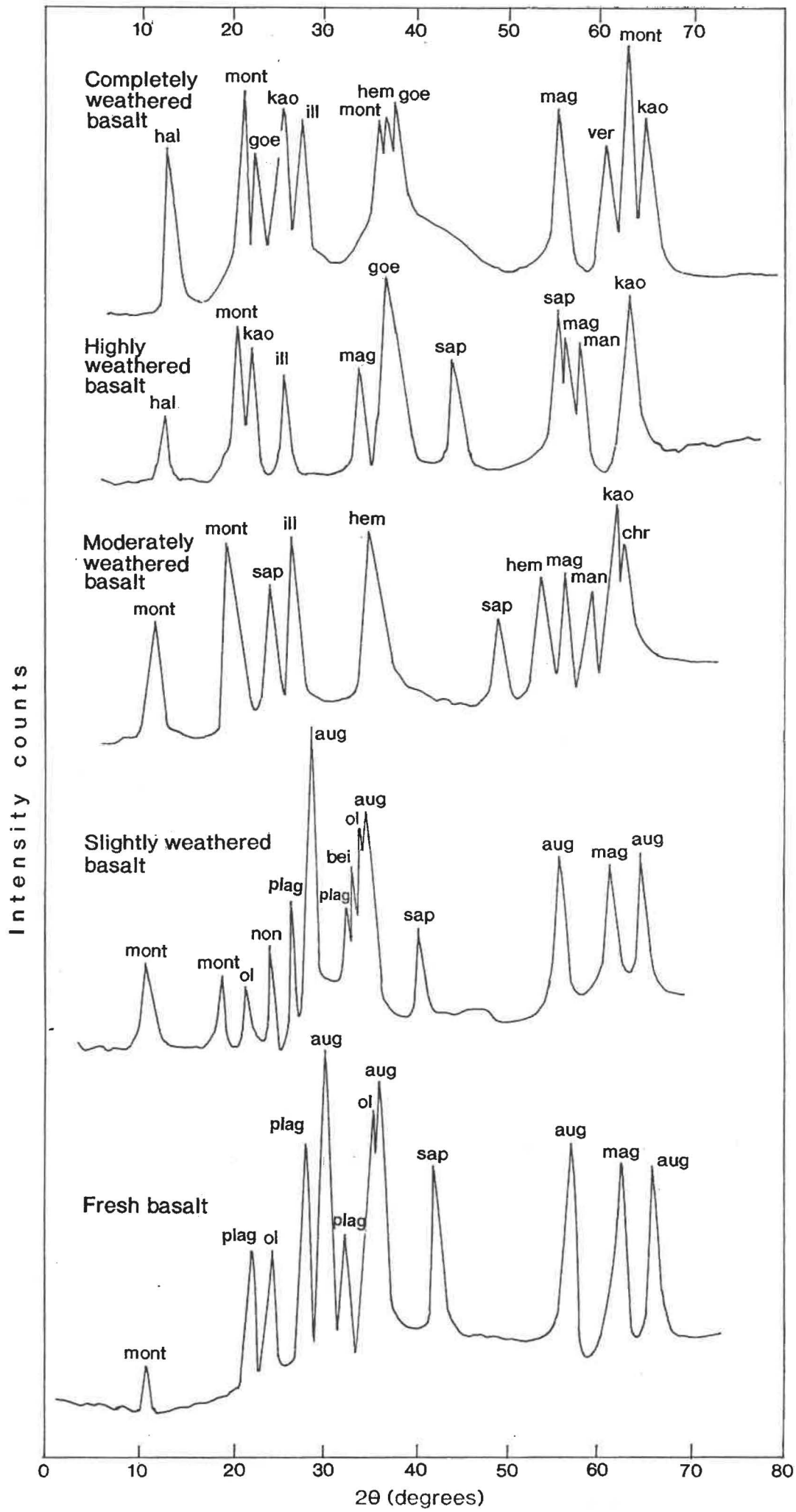

Abbre-viation	Mineral Name
aug	titanaugite
bei	beidellite
chr	chromite
goe	goethite
hal	halloysite
hem	hematite
ill	illite
kao	kaolinite
mag	titanomagnetite
man	manganosite
mont	montmorillonite
non	nontronite
ol	olivine
plag	plagioclase
sap	saponite
ver	vermiculite

Figure 4.8 X-ray Diffractograms of Karamu Basalt Samples from Different Grades of Weathering.
Fresh basalt shows the peaks of primary minerals olivine, titanaugite, plagioclase, titanomagnetite and a hump indicating the presence of glass. Small amounts of saponite and montmorillonite are present in iddingsite rims of olivine. From slightly to completely weathered stages, secondary minerals appear in larger quantities.

TABLE 4.2 PERCENTAGES OF MINERALS DETECTED BY X-RAY DIFFRACTION ANALYSIS

Description	Karamu Basalt					Tephra	Paleosol	Inclusions	
	Fresh	Slightly weathered	Moderately weathered	Highly weathered	Completely weathered	MPJ 22	MPJ 29	MPJ 54	MPJ 57
Mineral Name	Average of 7 samples	Average of 5 samples	Average of 10 samples	Average of 6 samples	Average of 7 samples				
olivine	20.3 ± 1.2	24.8 ± 14	16.3 ± 22.4	1.8 ± 3.1				11.6	12.5
titanaugite	28.5 ± 0.9	21.8 ± 3.6	5.4 ± 5.7	2.8 ± 1.4				2.6	8.5
plagioclase	39.1 ± 0.8	3.6 ± 8.0							
volcanic glass	7.4 ± 0.4	2.9 ± 2.8							
titanomagnetite	2.2 ± 0.1	4.1 ± 4.9	3.6 ± 5.1	6.9 ± 11.1	4.3 ± 5.9				
chromite			1.6 ± 3.4						
hematite			6.4 ±11.1		3.2 ± 4.0			6.4	7.2
goethite			6.5 ± 7.5	5.0 ± 3.7	7.7 ± 5.3		51.3		
manganosite		1.3 ± 1.8	1.3 ± 3.4	2.5 ± 3.2	2.3 ± 6.1				
phlogopite		1.3 ± 2.7						4.8	4.6
montmorillonite	1.3 ± 1.2	12.1± 6.5	26.8 ±19.6	8.4 ± 11.4	31.5 ± 6.5	41.1		47.0	44.6
nontronite		0.9 ± 2.0							
beidellite		1.6 ± 3.5		12.9 ± 10.3	6.3 ± 6.1				
saponite	1.2 ± 1.2	8.0 ± 3.3	6.2 ±10.0		4.7 ± 6.0				
kaolinite		12.7 ± 6.2	11.4 ±13.4	24.1 ± 3.0	8.9 ±14.1	22.4		6.8	8.9
vermiculite		0.7 ± 1.7			3.0 ± 3.8			1.1	1.0
illite		1.5 ± 3.3	8.4 ± 13.5	20.6 ± 10.6	15.7 ± 8.1		48.7	19.8	12.8
halloysite		4.7 ± 6.5	5.8 ± 7.6	14.1 ± 7.3	12.3 ±11.9	30.6			
allophane						5.9			
TOTAL	100	100	100	100	100	100.0	100.0	100.0	100.0
% clay minerals	2.5 ± 0.3	42.2 ± 11.7	58.9 ± 27.4	81.0 ± 15.2	82.5 ± 2.7	100.0	48.7	74.6	67.2

Presence of a 2.5 % clay content in fresh basalt is probably from the montmorillonite and saponite which partly constitute the iddingsite rims of olivine. However, based on thin section observations, it is believed this value 2.5 % is exaggerated. This exaggeration of clay percentage is true for other weathering grades also.

Scanning electron microscopy was useful in identifying and confirming the X-ray diffraction identifications of clay minerals such as montmorillonite (flaky and webby), kaolinite (elongate verm structure consisting of books of plates) and halloysite (needle- and rod- shaped crystals).

Based on petrographical observations, X-ray diffraction method and scanning electron microscopy, general observations could be made regarding each unit of the weathering profile.

4.2.1 Fresh Basalt

The fresh basalt is holocrystalline to hypocrystalline, fine grained, porphyritic with phenocrysts of euhedral to subhedral olivine, subhedral titanaugite and rare plagioclase set in a groundmass composed of laths of plagioclase, tiny granular titanomagnetite and glass. Apatite and chromite are present as accessory minerals. Average modal analyses of constituent minerals are: olivine 33.14 ± 2.54 %, titanaugite 28.43 ± 1.81 %, plagioclase 34.07 ± .10 %, glass 2.43 ± 2.44 % and titanomagnetite 2.07 ± 1.30 %. In the fresh basalt, the minerals are unaltered except for slight discolouration of olivine crystal edges to iddingsite, indicating either incipient weathering or possible hydration at the time of mineral formation. Pale yellow outlines on some olivine crystals could contribute to the presence of montmorillonite and saponite which were detected by X-ray diffraction method. Fine linear fractures can be observed in the matrix throughout the rock (Figures 4.9 a –c).

4.2.2 Slightly Weathered Basalt

In slightly weathered basalt, the fracturing of the rock becomes more visible due to an increase in the frequency. Porphyritic texture of the fresh basalt is retained. Olivine crystals start to develop yellow- to orange- coloured rims (thickness ~17 μm) of iddingsite (Figure 4.9d).

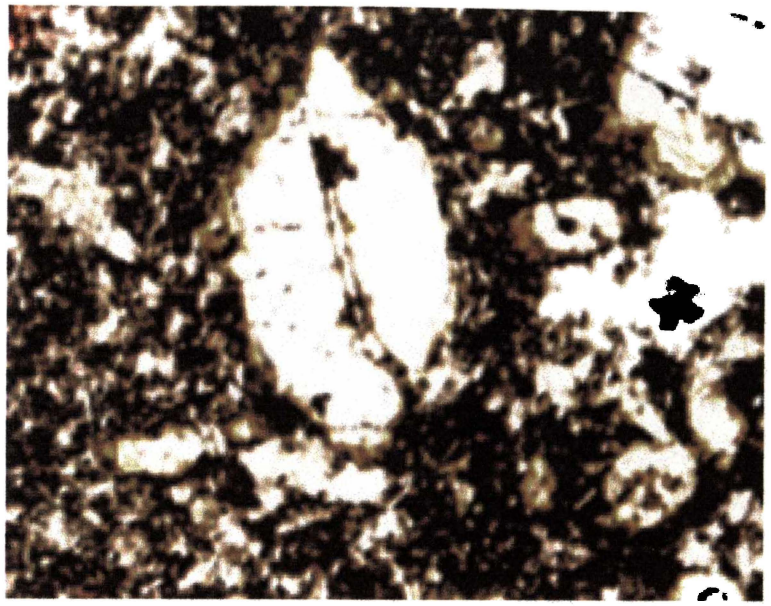

Figure 4.9a Micrograph of **fresh** basalt showing an **olivine** phenocryst in a groundmass of other minerals and glass. Pale yellow outline on olivine is iddingsite (X 400)

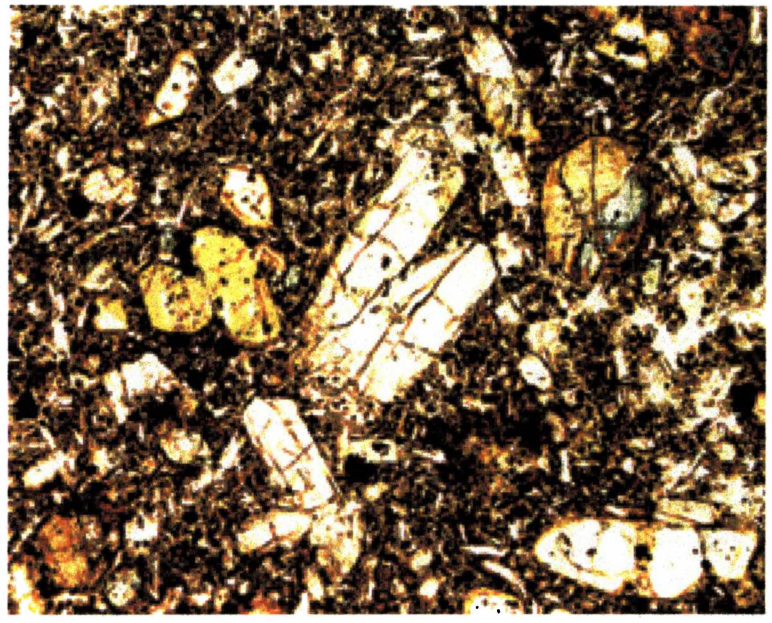

Figure 4.9b Micrograph of **fresh** basalt showing euhedral **titanaugite** phenocrysts in a groundmass of plagioclase laths, opaque minerals and glass. Opaque titanomagnetite is present as black spots (X 400)

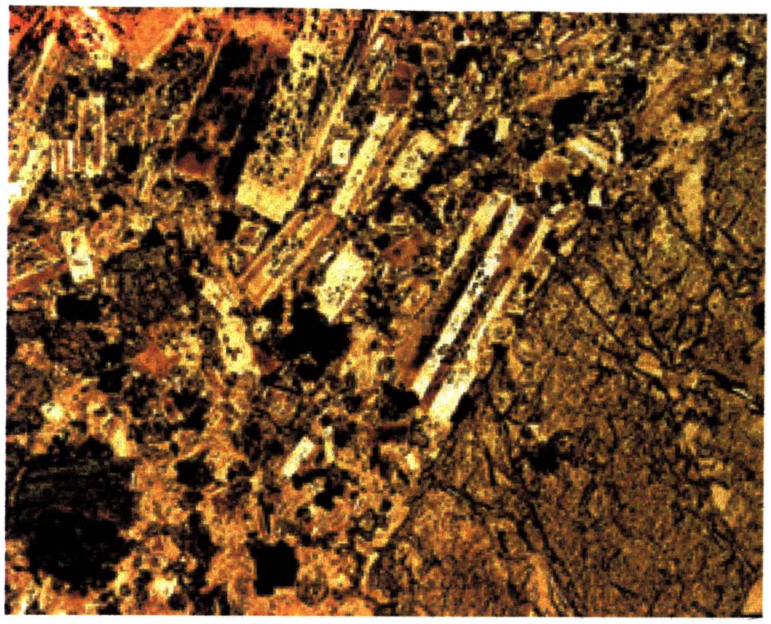

Figure 4.9c Micrograph (XP) of **fresh** basalt showing **plagioclase** phenocrysts indicating polysynthetic twinning (X 1000)

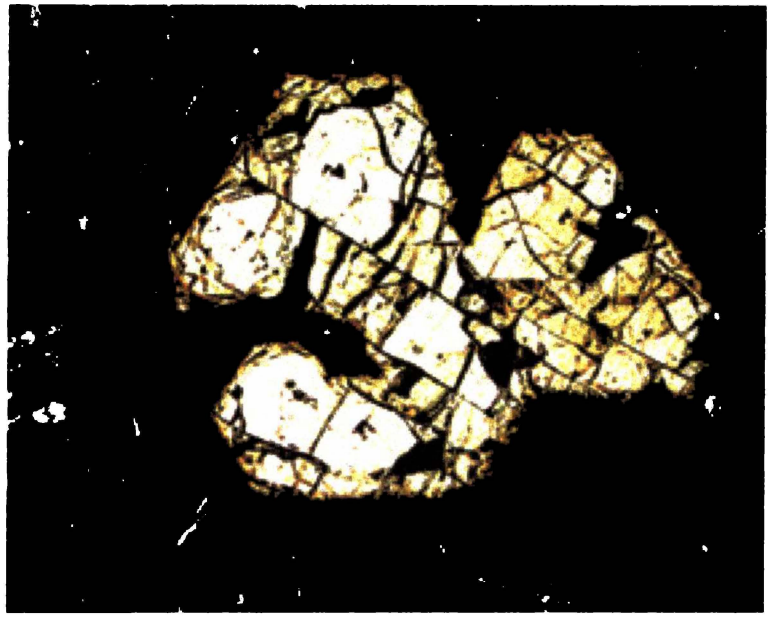

Figure 4.9d Micrograph of **slightly weathered** basalt showing development of cracks and yellow iddingsite rims on an **olivine** crystal (X 400)

Opaque minerals, mainly titanomagnetite, are abundant and occur as scattered grains in the groundmass. Titanaugite crystals develop cracks, possibly along cleavage planes, and break off in parts (Figure 4.9e). Plagioclase shows mottled appearance indicating seritisation i.e. changes to smectite or illite (Figure 4.9f). Interstitial glass shows alteration to pale yellow to bright yellow smectite. X-ray diffraction studies indicate that the smectites are mainly montmorillonite and saponite. Phlogopite and manganosite are also present in the groundmass. In thin sections of slightly weathered basalt, cryptocrystalline substances are present in the cracks. X-ray diffraction studies indicate the presence of clay, mainly smectites and kaolinite. Electron microscopy confirms presence of smectites.

4.2.3 Moderately Weathered Basalt

In moderately weathered basalt, relict porphyritic texture is preserved (Figure 4.9g). Parts of the olivine crystals develop orange to brown coloured iddingsite rims up to 30 μm in thickness, and also become altered to smectite. Titanaugite phenocrysts show evidence of alteration to hematite in the form of change of colour from pale purplish grey to reddish brown (Figure 4.9h). Plagioclase is completely altered to clays. Goethite, hematite and manganosite are also present as secondary minerals after olivine and titanaugite. Appearance of a network of cracks in the rock filled with clays, goethite and hematite is significant. In moderately weathered basalt, clay mineral formation is more intense than in slightly weathered basalt. Clay minerals, mainly smectites and, in lesser quantities, illite and kaolinite were detected by X-ray diffraction. The presence of smectites was confirmed by scanning electron microscopy that shows flaky and webby smectites (Figure 4.9i).

4.2.4 Highly Weathered Basalt

Highly weathered basalt is a mixture of titanomagnetite, goethite, manganosite and clays (Fig 4.9 j and k) with remnants of the original rock preserved. Because of these remnants of rock, the matrix, although very weak, appears to retain the relict porphyritic texture. Titanaugite is replaced completely but relict traces of the outlines of olivine crystals are still visible. An extensive crack network exists. The X–ray diffraction studies show the presence of clay minerals, mainly kaolinite, illite, halloysite, beidellite and montmorillonite. Scanning electron microscopy shows needle- and rod- shaped crystals of halloysite confirming its presence (Figure 4.9l).

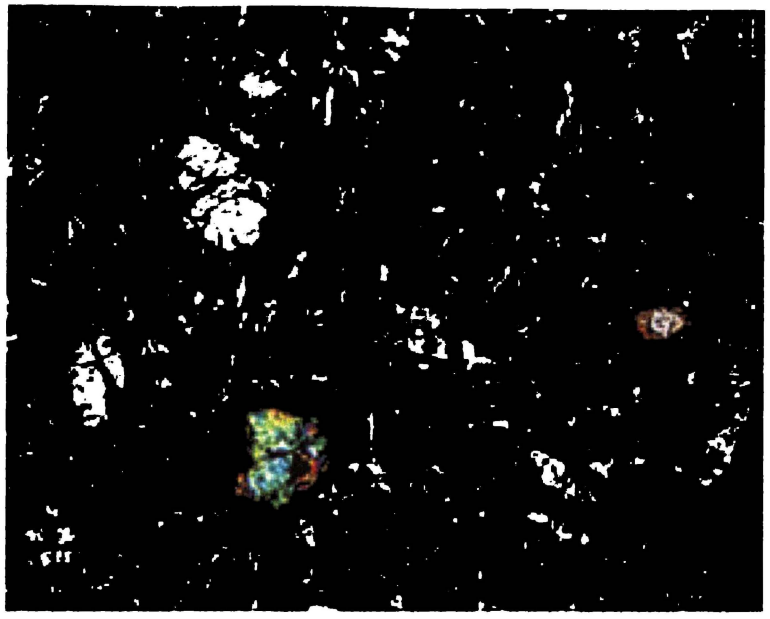

Figure 4.9e Micrograph (XP) of **slightly weathered** basalt showing alterations and cracks in **augite** and **olivine** crystals (X 400)

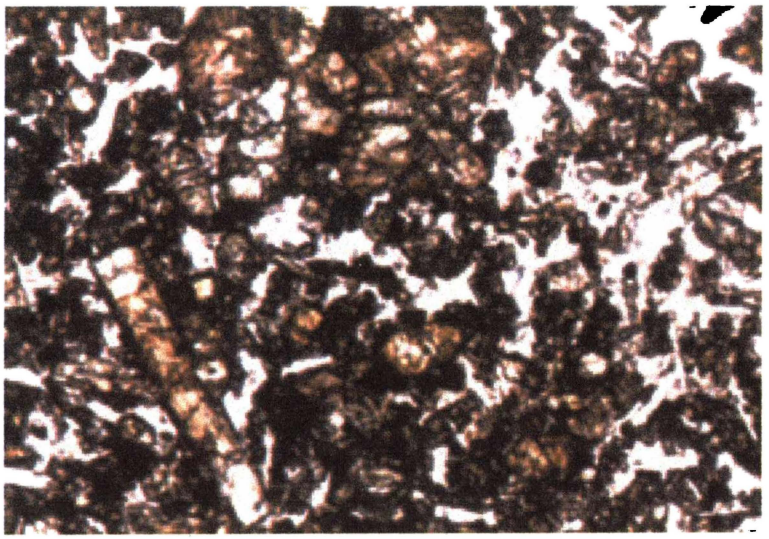

Figure 4.9f Micrograph of **slightly weathered** basalt showing altered **plagioclase** laths with speckly appearance and cracks (X 400)

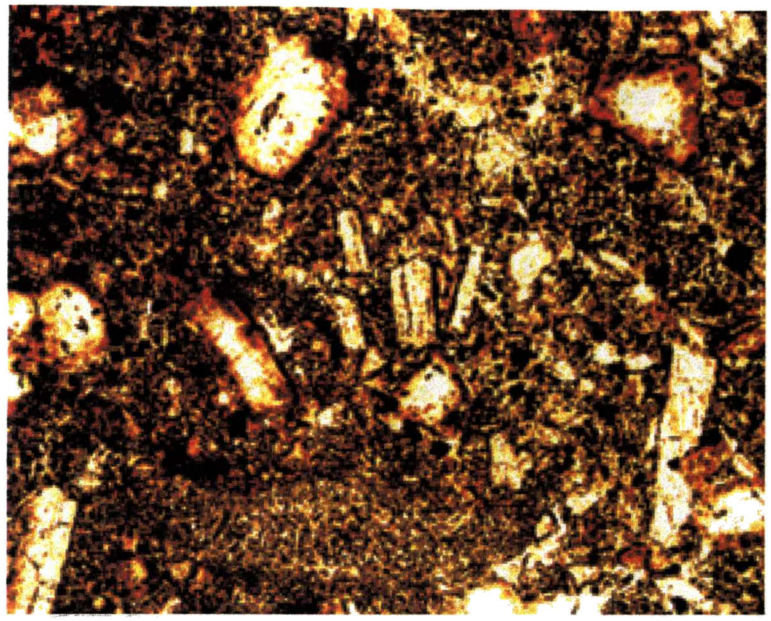

Figure 4.9g Micrograph of **moderately weathered** basalt showing altered **olivine** crystals with thick iddingsite rims, comprising predominantly reddish brown goethite (X 400)

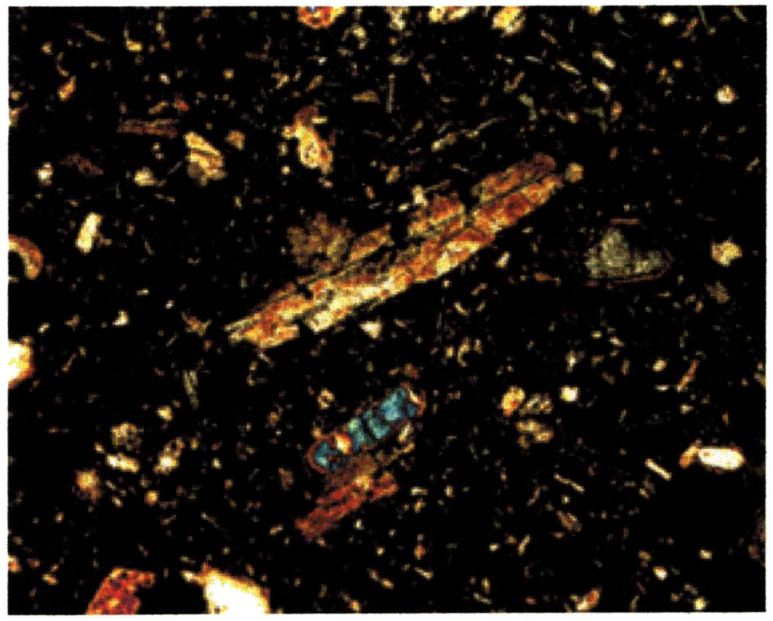

Figure 4.9h Micrograph (XP) of **moderately weathered** basalt showing an altered **augite** crystal with broken edges (X 400)

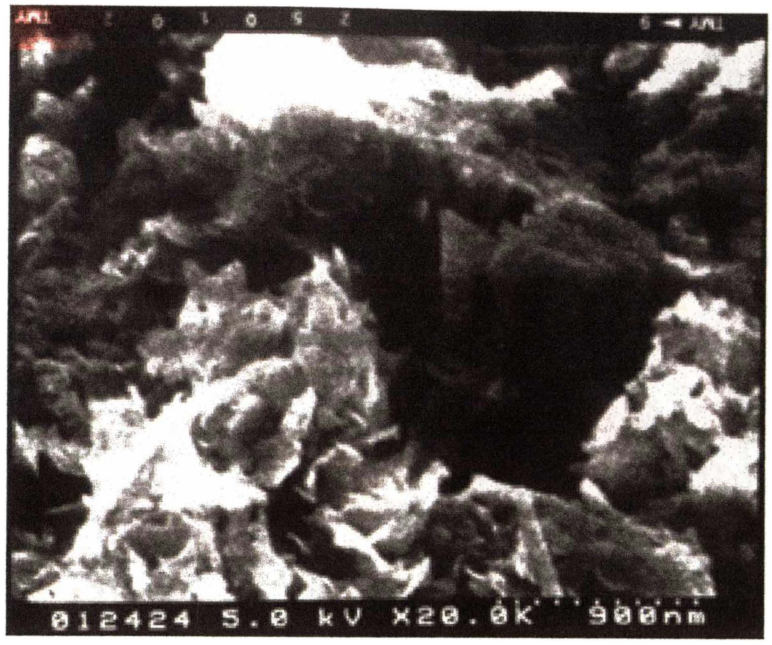

Figure 4.9i Electron micrograph of **moderately weathered** basalt showing **flaky** crystals of **smectite** formations (X 40,000)

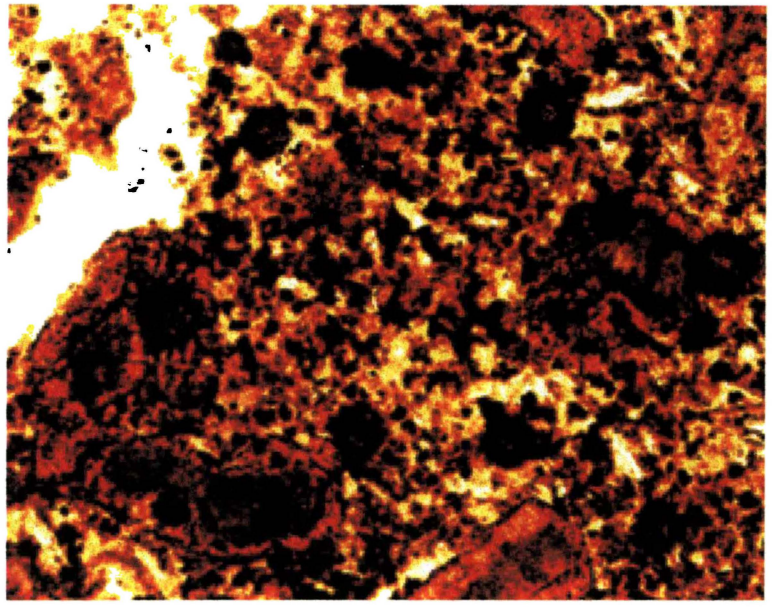

Figure 4.9j Micrograph of **highly weathered** basalt showing olivine crystals altered to reddish brown hematite and other secondary minerals (X 400)

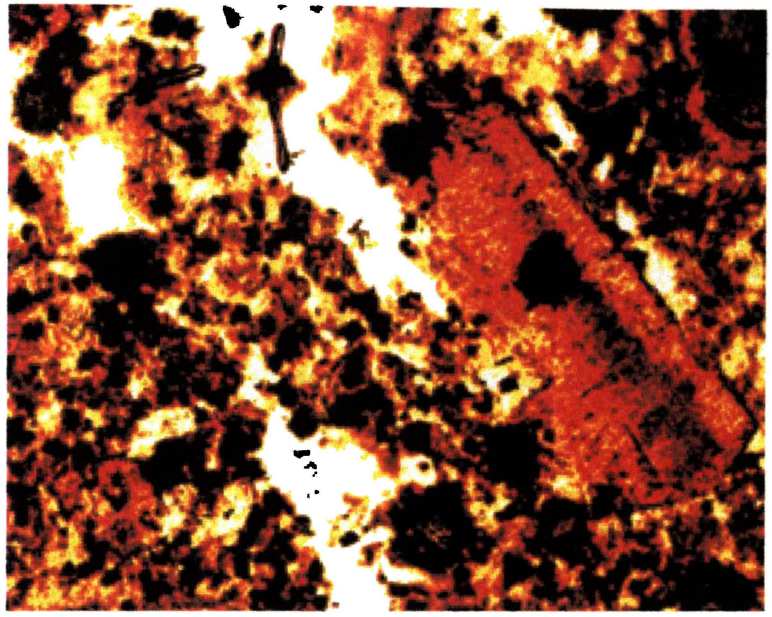

Figure 4.9k Micrograph of **highly weathered** basalt showing augite crystals altered to reddish brown hematite and other secondary minerals (X 400)

Figure 4.9l Electron micrograph of **highly weathered** basalt showing rod-like and needle shaped halloysite crystals (X 40,000)

4.2.5 Completely Weathered Basalt

Mineralogy of the completely weathered basalt is complex with clays predominating; only relict outlines of olivine and titanaugite are left. As is the case throughout the weathering profile, titanomagnetite remains unaltered. The original porphyritic texture is present as traces only and the matrix cannot hold the remaining parts of phenocrysts together. Goethite and hematite are present in patches (Fig 4.9 m and n). The clay minerals are montmorillonite, illite, halloysite, kaolinite, beidellite, saponite and vermiculite. An elongate verm structure typical of kaolinite was observed in electron micrographs (Figure 4.9o).

4.2 6 Tephra and Paleosol

Allophane detection test results indicated the absence of allophane in Karamu Basalt in all weathering grades. Weathered tephra were the only samples with measurable allophane content. As per the colour scale of Fieldes and Perrot (1966), all tephra samples have 5-7 % allophane. According to X-ray diffraction method, tephra has substantial quantities of smectites, halloysite, kaolinite and allophane while paleosols seem to consist of goethite and illite.

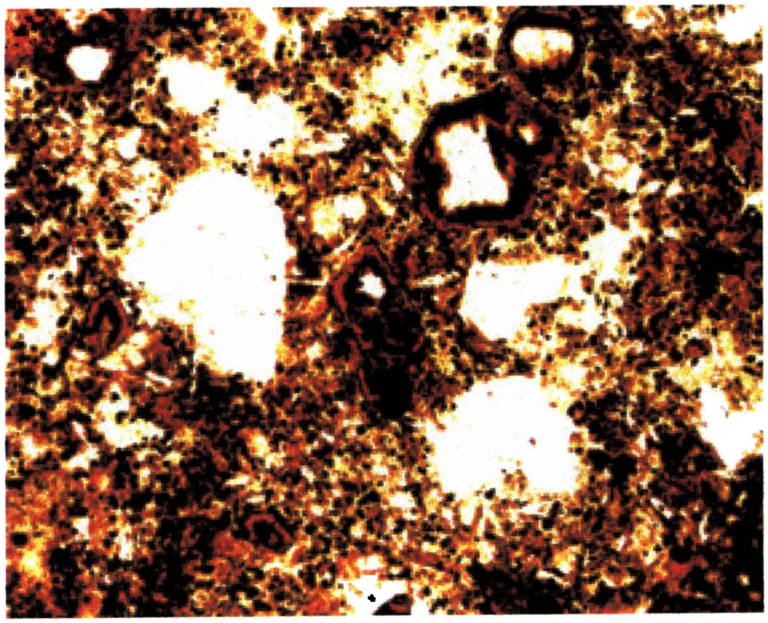

Figure 4.9m Micrograph of **completely weathered** basalt showing relict outtlines of olivine crystals (X 400)

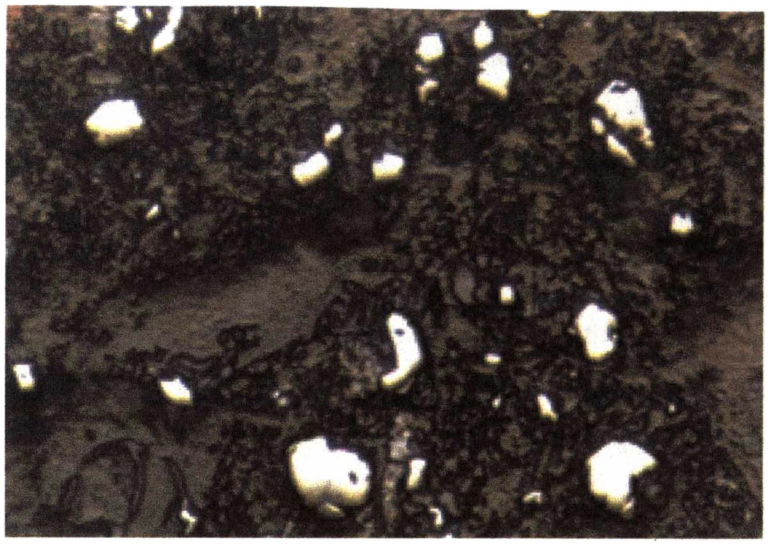

Figure 4.9n Micrograph of a polished section of **completely weathered** basalt showing the opaque minerals. The white areas are mainly hematite and goethite developed on primary minerals (X 200)

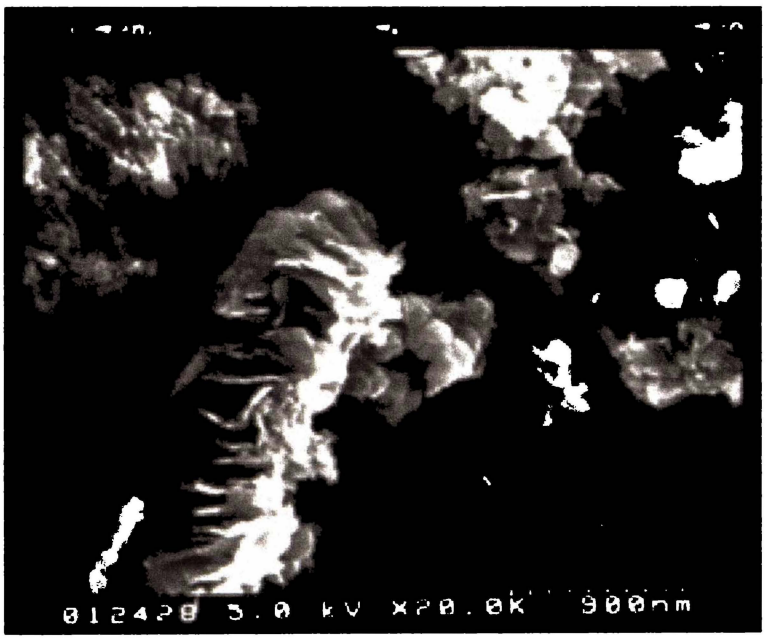

Figure 4.9o Electron micrograph of **completely weathered** basalt showing kaolinite crsytals with "verm" strcuture (X 40,000)

4.3 Geochemical Information

The chemical analyses of 57 samples were obtained by X-ray fluorescence method (Appendix 4.4). Major elements detected were SiO_2, Al_2O_3, MnO, MgO, CaO, FeO, Fe_2O_3, TiO_2, Na_2O, K_2O and P_2O_5. Sixteen trace elements were detected: Nb, Zr, Th, Sr, Ba, Rb, V, Cr, Ni, Zn, La, Ce, Nd, Ga, Pb.and Y.

The value of loss on ignition is assumed in this study to be the water retained within the mineral structures (H_2O+) which is released on ignition at temperatures over 110 °C (Rollinson, 1993). The samples were oven-dried at 105 °C prior to the chemical analysis, therefore H_2O-, which is the pore water content, is not included in the chemical analyses results. However, H_2O- was determined as the geotechnical parameter water content.

4.3.1 Iso-con Contour Cross-sections

The spatial distribution of element concentration values can be expressed in the form of a map using equal-concentration contours called iso-con contours (Govett, 1983). This is usually done in the form of maps rather than cross-sections. However, Koksoy and Bradshaw (1969) plotted the distribution of mercury on a cross-section of residual soils down to bedrock over a cinnabar mineralisation.

The concentrations of major and trace elements of Karamu Basalt were plotted on the cross section of the weathering profile. Then iso-con plots were drawn as lines of best fits by interpolated contouring, to study their distribution pattern (Figure 4.10).

The plots of the concentrations of MgO, CaO and FeO show a decrease of these oxides upwards through the weathering profile but show no significant lateral change (Figures 4.10 a-c). The decrease is more intense at the slightly and moderately weathered stages and the values are very small at highly and completely weathered stages. Al_2O_3, Fe_2O_3 and structural water (H_2O+) increase upwards; Al_2O_3 and Fe_2O_3 do not show much lateral change; Fe_2O_3 shows a decrease at the completely weathered stage (Figures 4.10 d-f).

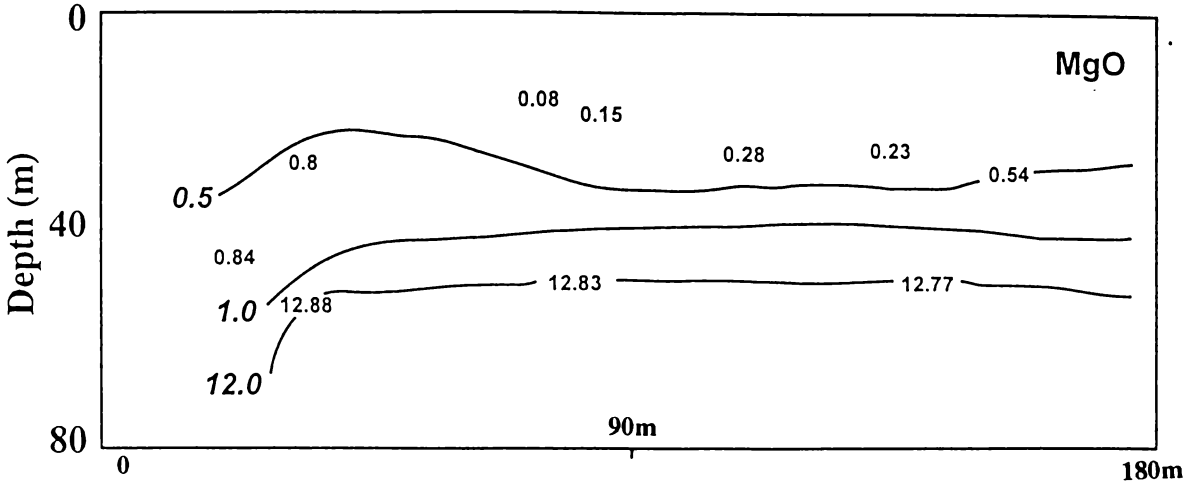

Figure 4.10a Iso-con Contour Cross Sections of MgO in the Karamu Weathering Profile

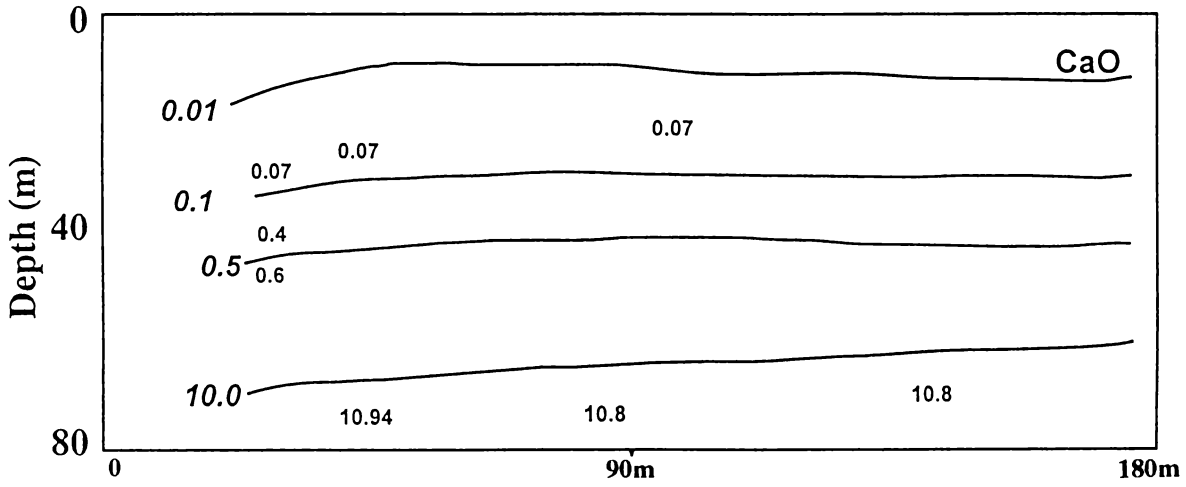

Figure 4.10b Iso-con Contour Cross Sections of CaO in the Karamu Weathering Profile

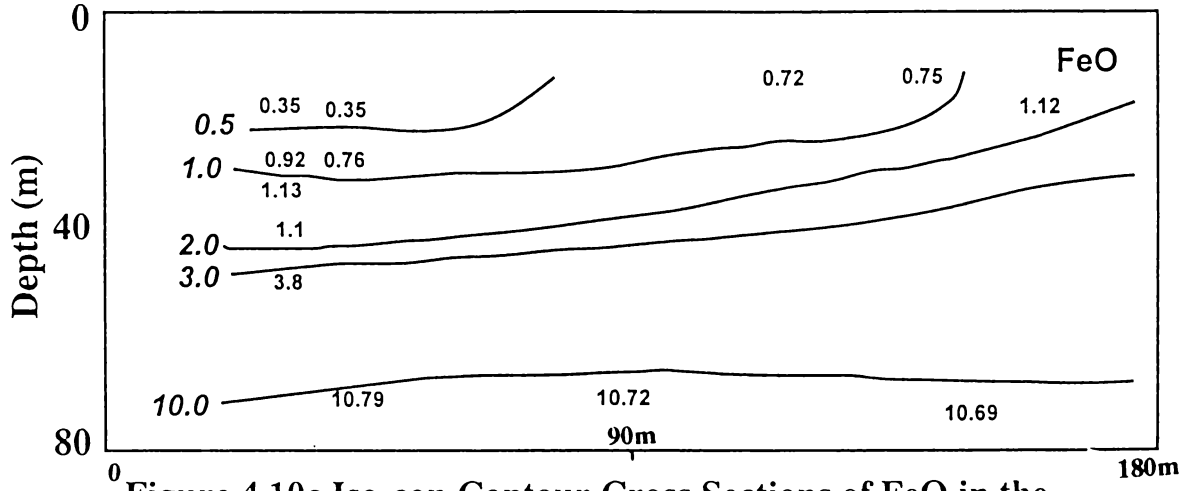

Figure 4.10c Iso-con Contour Cross Sections of FeO in the Karamu Weathering Profile

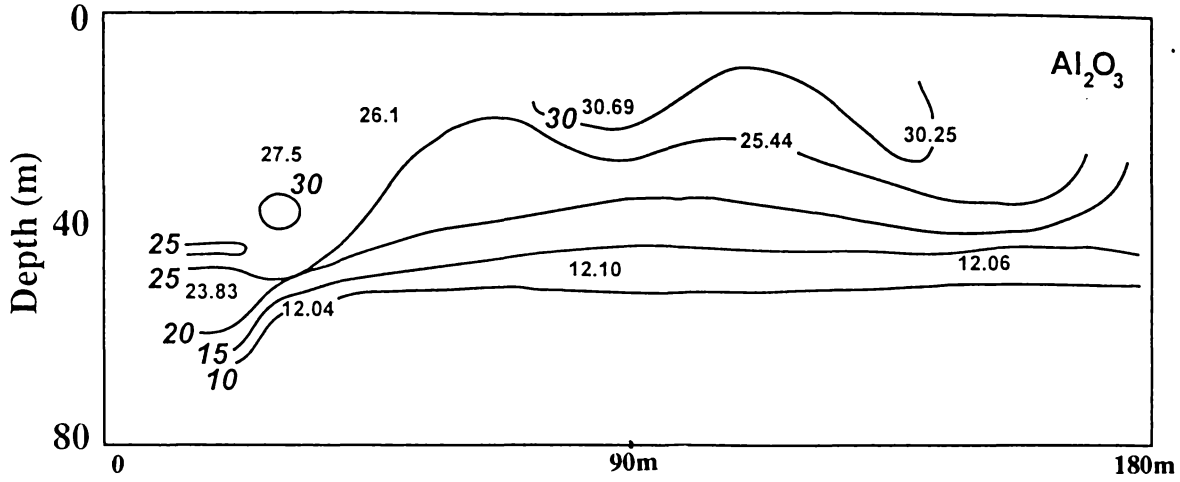

Figure 4.10d Iso-con Contour Cross Sections of Al_2O_3 in the Karamu Weathering Profile

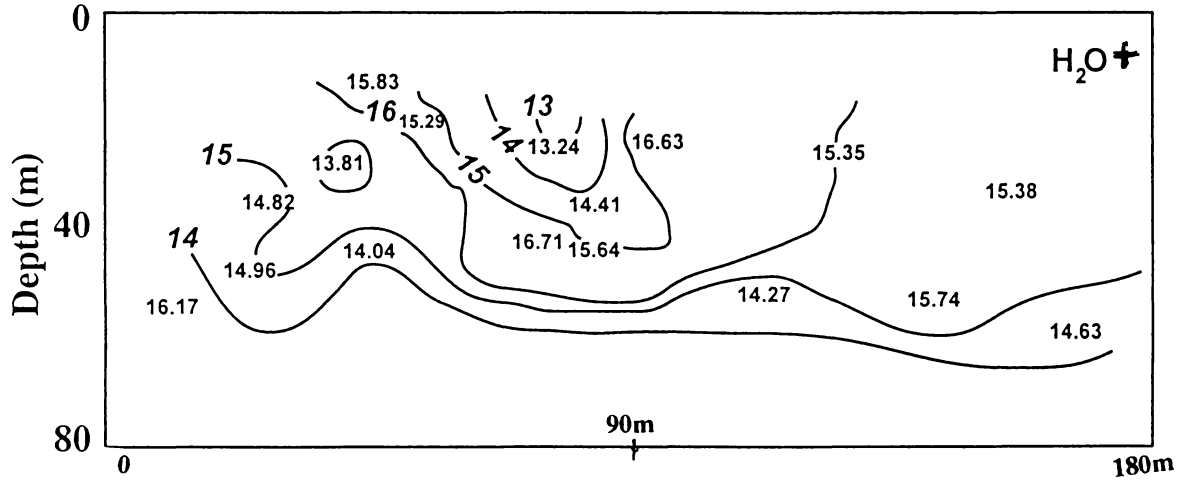

Figure 4.10e Iso-con Contour Cross Sections of H_2O+ in the Karamu Weathering Profile

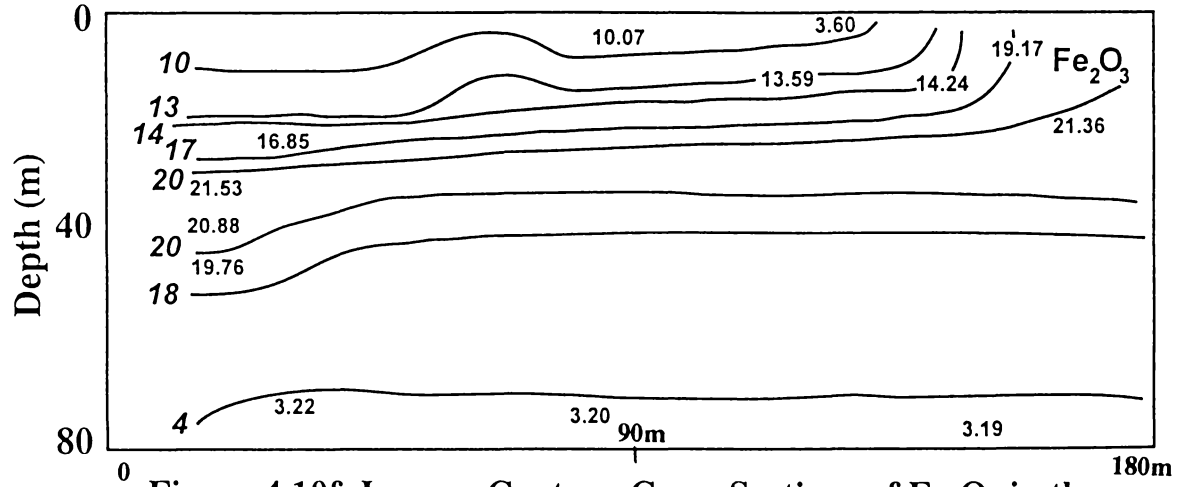

Figure 4.10f Iso-con Contour Cross Sections of Fe_2O_3 in the Karamu Weathering Profile

Plots of concentrations of SiO_2, MnO and TiO_2 show a variation with depth as well as laterally, but there is no particular pattern of distribution (Figures 4.10 g-i). Iso-con contours of other major elements could not be plotted because in many locations their contents have zero values.

Some trace elements show a variation in concentration along the profile (figures are included in Appendix 4.5). Ga follows the same pattern as Al_2O_3, the major element containing similar charges and compatible ionic radii. Ba and Y have a sudden increase at the earliest stage of weathering then gradually decrease.

Taking all this into consideration it can be concluded that the iso-con plots show that due to weathering:

(a) There is a decrease in the contents of MgO, CaO and FeO. This is true also for Na_2O and K_2O as well as the trace element Y.
(b) There is an increase in the contents of Al_2O_3, Fe_2O_3, H_2O+ and Ga.
(c) SiO_2, MnO, TiO_2, and P_2O_5, and the trace elements Pb and Th do change within the profile but not in a particular direction.

4.3.2 Regression Analysis

In order to determine relationships among different chemical elements present, regression analysis was carried out using all chemical results. Linear and polynomial regression coefficient R^2 values at 95% confidence level were obtained for the relationships and the highest value of these for each correlation is included in Table 4.3. Graphical plots of geochemical parameters showing acceptable ($R^2 \geq 0.64$) correlations and convincing plots, in terms of spread of data points or clusters, are included.

Regression analysis shows most elements, except for Fe_2O_3 (which has a linear negative relationship of $R^2 = 0.76$; Figure 4.11a) do not correlate with SiO_2. MgO and CaO show polynomial relationships with Al_2O_3 ($R^2 = 0.92$ and $R^2 = 0.93$; Figure 4.11b). A positive linear correlation of $R^2 = 0.70$ can be observed between H_2O+ and Al_2O_3 (Figure 4.11c).

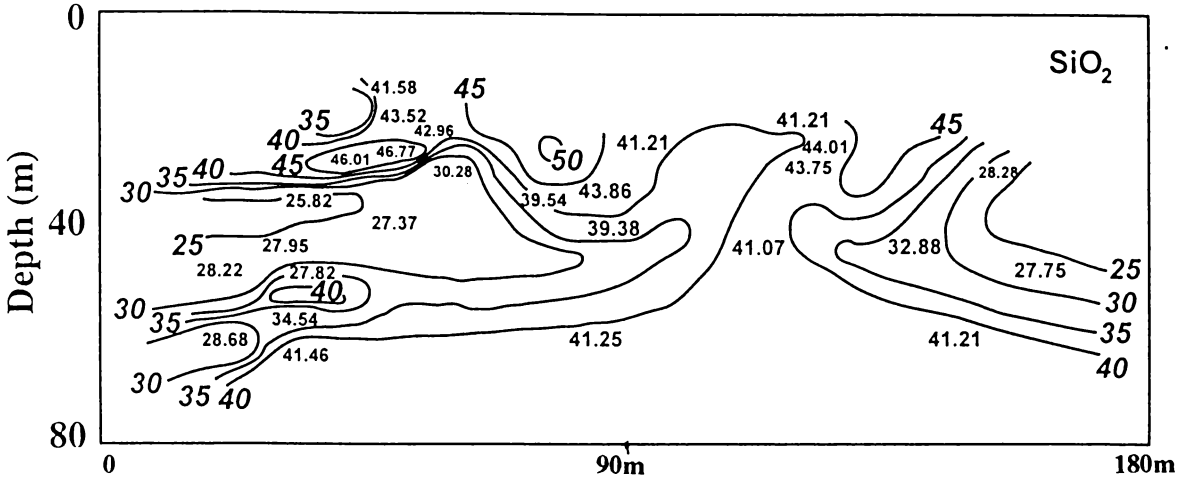

Figure 4.10g Iso-con Contour Cross Sections of SiO_2 in the Karamu Weathering Profile

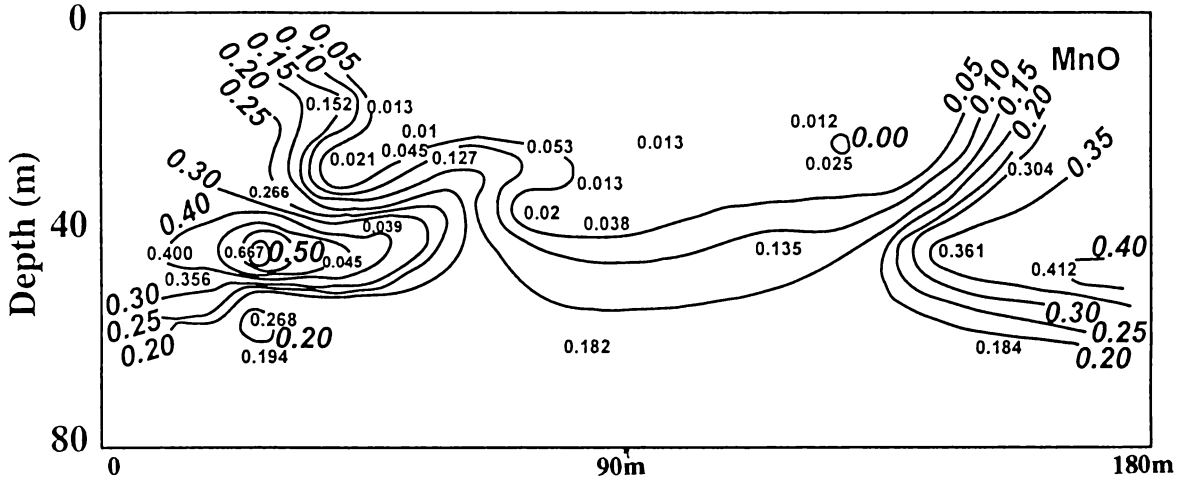

Figure 4.10h Iso-con Contour Cross Sections of MnO in the Karamu Weathering Profile

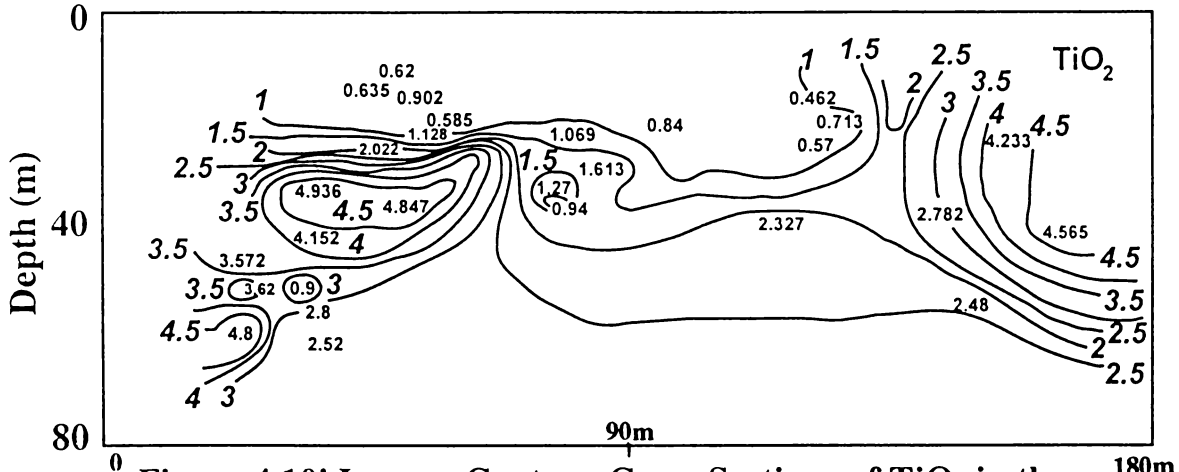

Figure 4.10i Iso-con Contour Cross Sections of TiO_2 in the Karamu Weathering Profile

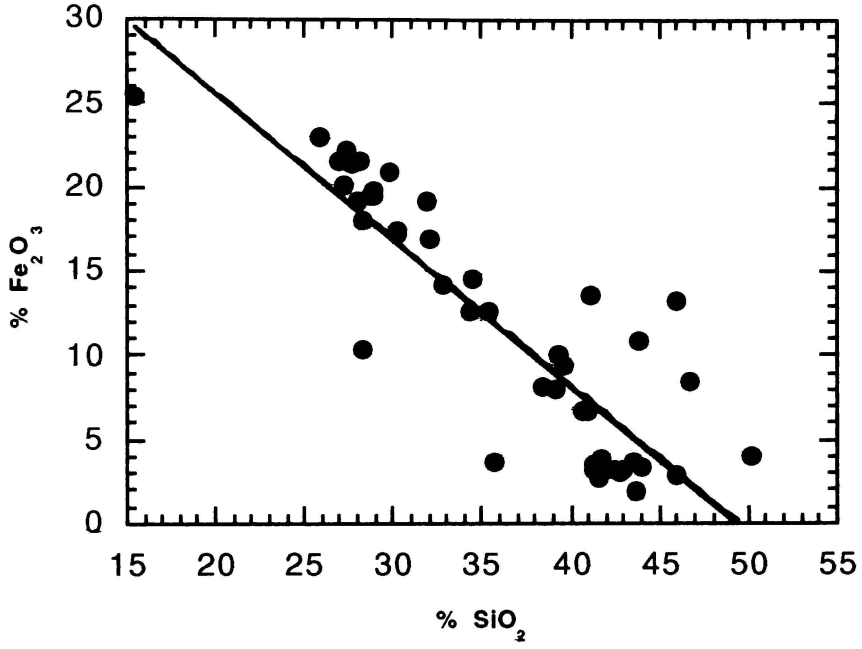

Figure 4.11a Plot of Fe_2O_3 vs SiO_2

$Y = M0 + M1*x + ... M8*x^8 + M9*x^9$	
M0	35
M1	-2.4
M2	0.041
R^2	0.92

$Y = M0 + M1*x + ... M8*x^8 + M9*x^9$	
M0	32
M1	-2.3
M2	0.041
R^2	0.93

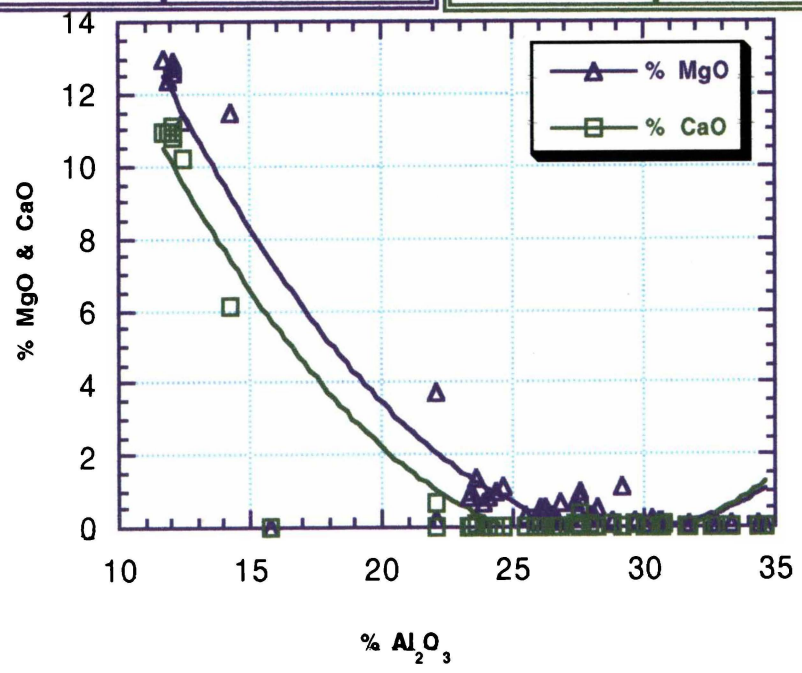

Figure 4.11b Plot of MgO and CaO vs Al_2O_3

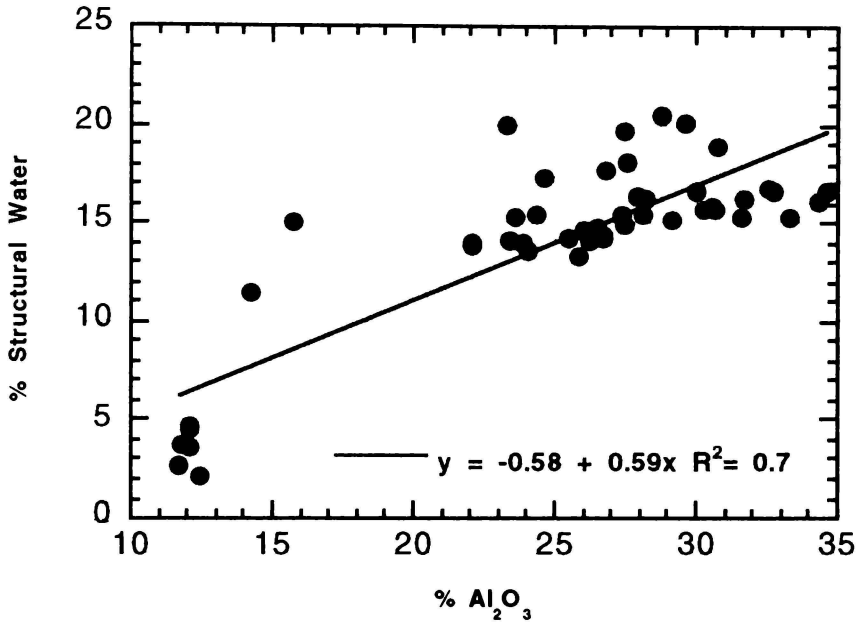

Figure 4.11c Plot of Structural Water vs Al_2O_3

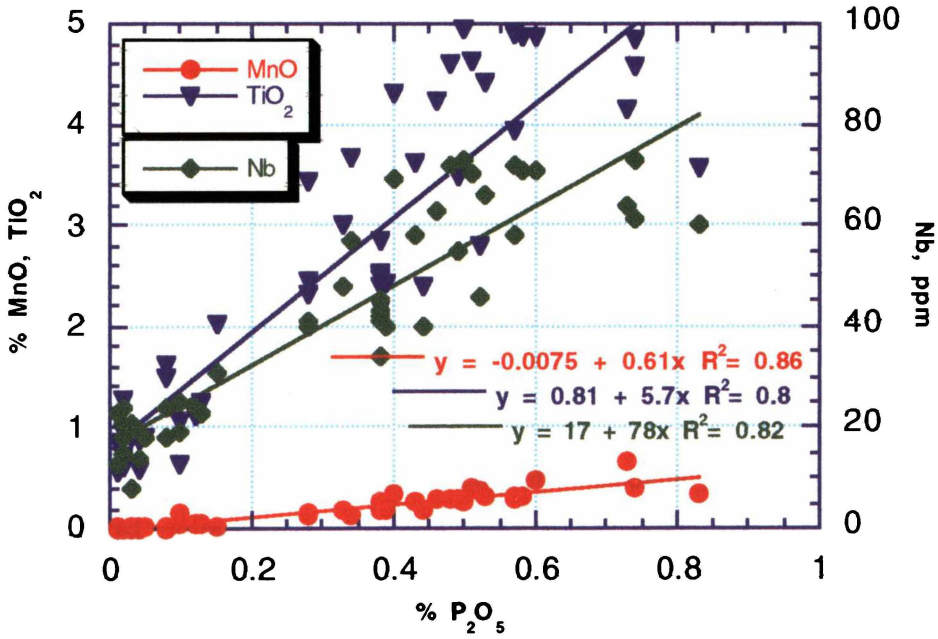

Figure 4.11d Plot of MnO, TiO_2 and Nb vs P_2O_5

MnO, TiO_2 and Nb show positive linear correlations with P_2O_5 (R^2 = 0.86, 0.80 and 0.82 respectively). V, Cr, Ni and Zn correlate linearly and positively with TiO_2 (R^2 = 0.72, 0.76, 0.68 and 0.70 respectively) and Nb (R^2 = 0.67, 0.75, 0.69 and 0.68 respectively). Cr and Ni correlate linearly and positively with MnO (R^2 = 0.69 and 0.68). Cr also correlates linearly and positively with P_2O_5 (R^2 = 0.64). According to Nesbitt and Wilson (1992), during chemical weathering of basalt, elements Ti, V, Cr and Nb are largely preserved while there is a decrease in MnO and P_2O_5 concentrations. In contrast, in the weathering profile of Karamu Basalt, these six elements appear to show little relative change in their abundance patterns (Figures 4.11 d-h).

Only Al_2O_3 showed a positive correlation with H_2O+. Al_2O_3 and H_2O+ are both major components of clay minerals and the percentage of clay increases along with weathering. Trends of changes in major and trace elements along the weathering profile are further discussed in Chapter 7.

4.3.3 Weathering Indices

The equations for calculating different weathering indices based on the chemical analysis results are given in Chapter 2. Accordingly, Ruxton's Ratio (RR), Reiche Product Index (PI), Reiche Weathering Potential Index (WPI), Miura Weathering Index (Wm) and Parker Weathering Index (W_p) were calculated and are included in Appendix 4.4. This Appendix also includes the values for a new weathering index proposed and explained in the next section. Some chemical predictors proposed in Chapter 6 are also included in Appendix 4.4.

Regression analysis was carried out on chemical composition versus depth (measured using the topmost point of the profile as the datum line). The R^2 values for 95% confidence level are included in Table 4.3. None of the individual major or trace element concentrations produced an acceptable correlation with depth. Trends of changes in major and trace elements along the weathering profile are further discussed in Chapter 7.

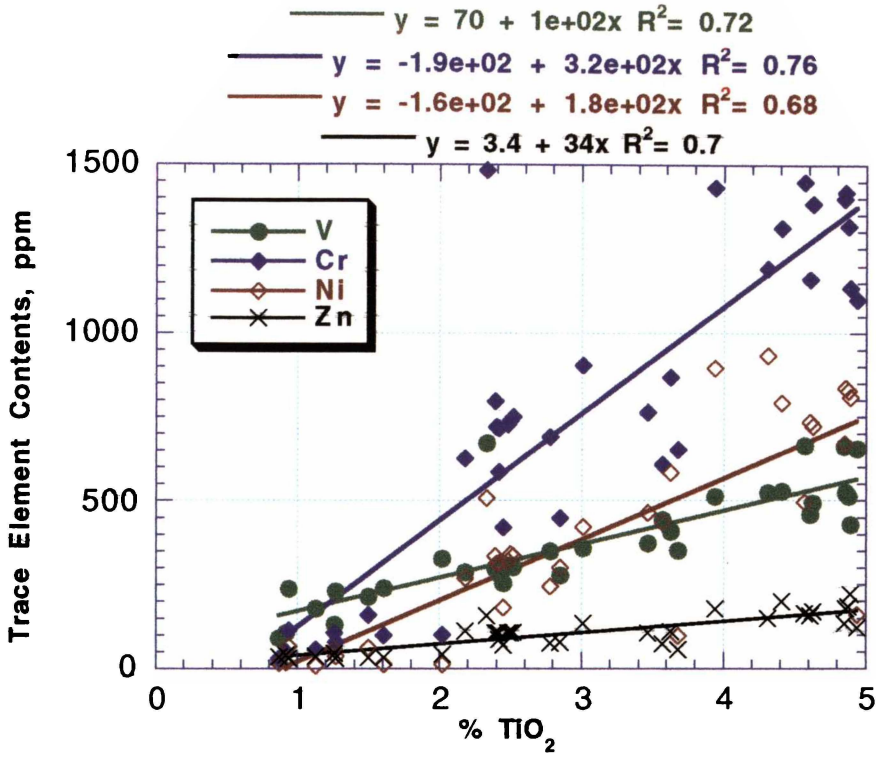

Figure 4.11e Plot of V, Cr, Ni and Zn vs TiO_2

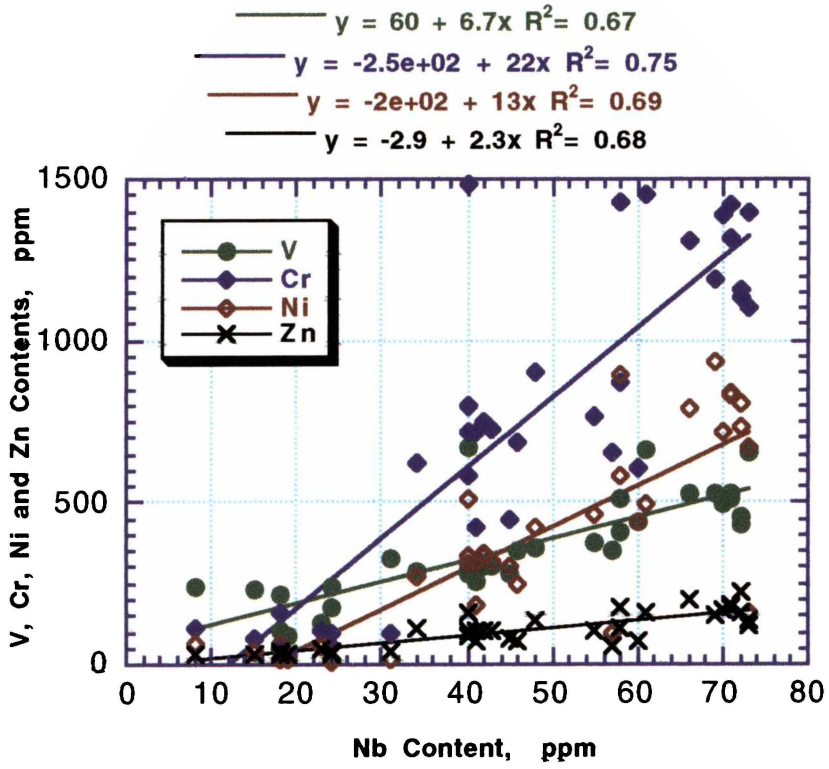

Figure 4.11f Plot of V, Cr, Ni and Zn vs Nb

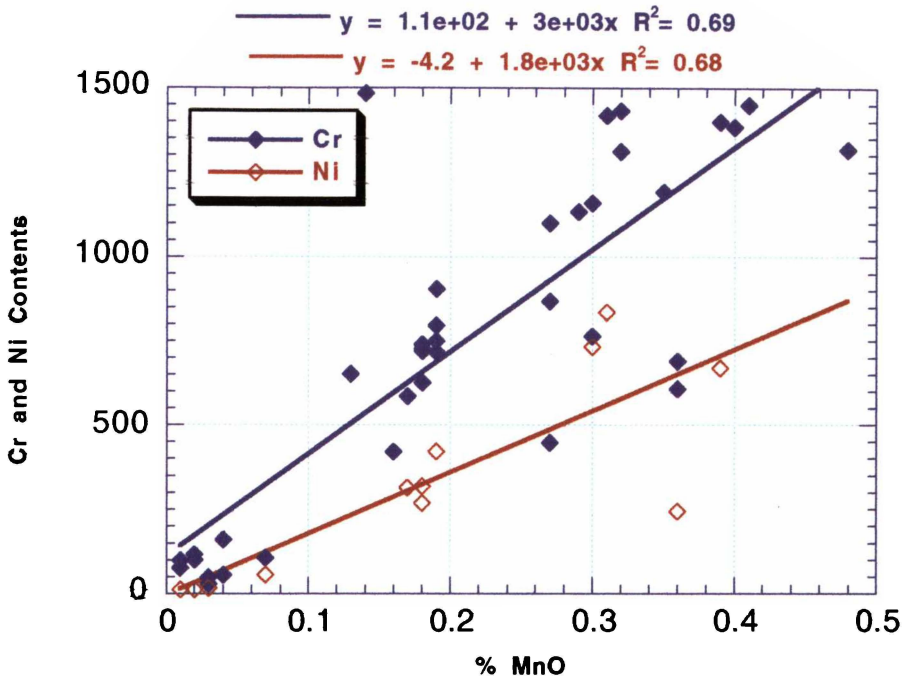

Figure 4.11g Plot of Cr and Ni vs MnO

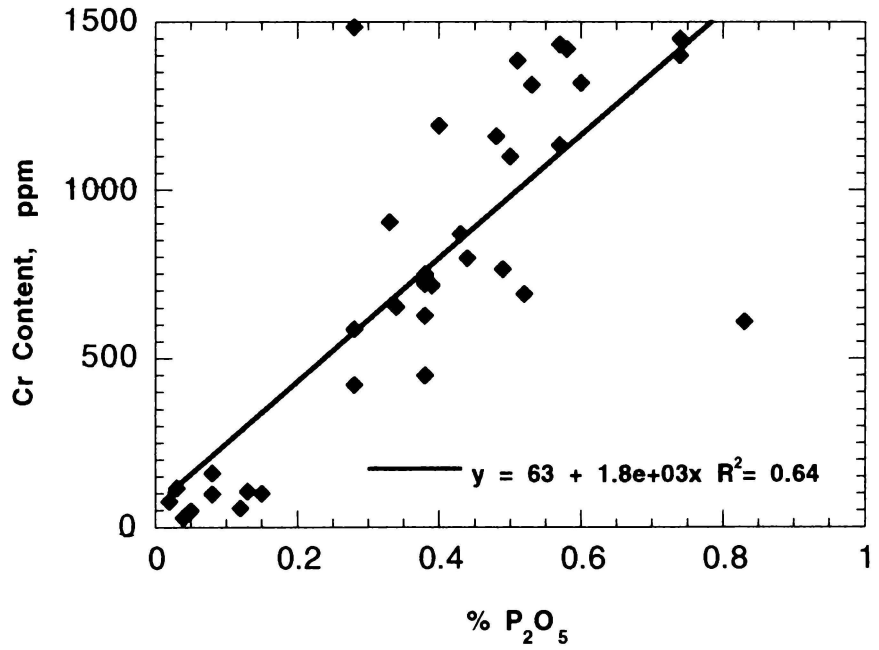

Figure 4.11h Plot of Cr vs P_2O_5

TABLE 4.3 REGRESSION COEFFICIENTS (R SQUARED VALUES AT 95% CONFIDENCE LIMIT) FOR ALL GEOCHEMICAL TEST RESULTS AND DEPTH

	Depth	SiO_2	Al_2O_3	MnO	MgO	CaO	Na_2O	K_2O	TiO_2	P_2O_5	Fe_2O_3	FeO	H_2O+	Th	Nb	Zr	Sr	Rb	Ba	V	Cr	Ni	Zn	La	Ce	Nd	Ga	Pb	Y	Ruxton	Reiche	Reiche	Miura	Parker	New	pH
	metres	%	%	%	%	%	%	%	%	%	%	%	%	ppm	ppm	ppm	ppm	ppm	ppm	ppm	ppm	ppm	ppm	ppm	ppm	ppm	ppm	ppm	ppm	Ratio	P.I.	W.P.I.	W.I.	W.I.	W.I.	
Depth, m																																					
% SiO_2	0.01																																				
% Al_2O_3	0.46	0.05																																			
% MnO	0.21	0.51	0.06																																		
% MgO	0.46	0.08	0.92	0.00																																	
% CaO	0.44	0.11	0.93	0.12	0.97																																
% Na_2O	0.37	0.13	0.82	0.10	0.83	0.91																															
% K_2O	0.25	0.23	0.46	0.08	0.48	0.54	0.66																														
% TiO_2	0.19	0.50	0.06	0.74	0.00	0.00	0.00	0.04																													
% P_2O_5	0.28	0.40	0.12	0.86	0.04	0.02	0.01	0.00	0.80																												
% Fe_2O_3	0.33	0.76	0.01	0.47	0.20	0.25	0.26	0.34	0.54	0.39																											
% FeO	0.54	0.01	0.50	0.00	0.38	0.38	0.31	0.16	0.02	0.08	0.05																										
% H_2O+	0.28	0.10	0.70	0.00	0.82	0.85	0.85	0.56	0.00	0.05	0.15	0.38																									
Th, ppm	0.42	0.28	0.40	0.37	0.41	0.23	0.19	0.04	0.39	0.40	0.12	0.28	0.42																								
Nb, ppm	0.17	0.50	0.07	0.76	0.32	0.00	0.00	0.04	0.96	0.82	0.51	0.01	0.00	0.34																							
Zr, ppm	0.23	0.03	0.37	0.14	0.33	0.30	0.27	0.10	0.04	0.08	0.00	0.25	0.28	0.54	0.02																						
Sr, ppm	0.42	0.11	0.88	0.10	0.90	0.96	0.93	0.59	0.28	0.19	0.22	0.35	0.87	0.32	0.27	0.43																					
Rb, ppm	0.00	0.48	0.05	0.19	0.11	0.15	0.22	0.35	0.28	0.11	0.31	0.02	0.20	0.11	0.21	0.00	0.18																			0.64 -	0.69
Ba, ppm	0.23	0.28	0.01	0.47	0.00	0.01	0.02	0.08	0.46	0.36	0.23	0.02	0.01	0.20	0.46	0.06	0.01	0.21																		0.70 -	0.79
V, ppm	0.00	0.48	0.00	0.56	0.03	0.05	0.05	0.07	0.72	0.58	0.54	0.01	0.00	0.02	0.67	0.00	0.04	0.13	0.24																	0.80 -	0.89
Cr, ppm	0.11	0.45	0.06	0.69	0.01	0.00	0.00	0.01	0.76	0.64	0.35	0.02	0.02	0.04	0.75	0.02	0.00	0.12	0.47	0.81																0.90 -	1.00
Ni, ppm	0.19	0.46	0.04	0.68	0.00	0.01	0.01	0.03	0.68	0.54	0.35	0.00	0.00	0.09	0.69	0.01	0.01	0.17	0.75	0.52	0.78															
Zn, ppm	0.21	0.35	0.11	0.61	0.01	0.00	0.00	0.00	0.70	0.54	0.26	0.04	0.03	0.13	0.68	0.02	0.00	0.09	0.61	0.59	0.87	0.84															
La, ppm	0.02	0.20	0.00	0.37	0.01	0.02	0.22	0.03	0.33	0.45	0.19	0.00	0.00	0.01	0.31	0.01	0.01	0.07	0.15	0.38	0.36	0.25	0.37														
Ce, ppm	0.00	0.19	0.04	0.31	0.11	0.11	0.08	0.07	0.18	0.36	0.26	0.09	0.06	0.01	0.23	0.16	0.08	0.02	0.07	0.23	0.13	0.16	0.08	0.28													
Nd, ppm	0.13	0.16	0.03	0.26	0.00	0.00	0.00	0.01	0.32	0.29	0.12	0.02	0.01	0.12	0.31	0.00	0.00	0.08	0.37	0.12	0.24	0.41	0.48	0.45	0.07												
Ga, ppm	0.42	0.03	0.40	0.00	0.62	0.61	0.54	0.37	0.01	0.01	0.32	0.61	0.45	0.43	0.00	0.71	0.56	0.01	0.00	0.04	..01	0.00	0.01	0.00	0.18	0.01											
Pb, ppm	0.38	0.00	0.47	0.17	0.32	0.27	0.22	0.19	0.10	0.22	0.01	0.35	0.36	0.29	0.12	0.15	0.25	0.05	0.12	0.08	0.27	0.34	0.32	0.09	0.02	0.17	0.12										
Y, ppm	0.67	0.06	0.02	0.07	0.00	0.00	0.00	0.01	0.15	0.08	0.05	0.02	0.00	0.09	0.14	0.00	0.00	0.03	0.23	0.03	0.10	0.21	0.32	0.26	0.00	0.87	0.01	0.08									
Ruxton's Ratio	0.30	0.41	0.83	0.12	0.88	0.93	0.92	0.59	0.12	0.20	0.80	0.80	0.84	0.33	0.35	0.37	0.89	0.48	0.08	0.08	0.01	0.03	0.00	0.03	0.13	0.00	0.44	0.26	0.01								
Reiche P.I.	0.06	0.89	0.32	0.44	0.42	0.49	0.50	0.72	0.62	0.36	0.92	0.37	0.39	0.02	0.54	0.11	0.47	0.67	0.35	0.27	0.44	0.57	0.47	0.19	0.10	0.23	0.02	0.03	0.10	0.82							
Reiche W.P.I.	0.37	0.21	0.88	0.09	0.96	0.97	0.94	0.68	0.26	0.19	0.45	0.89	0.94	0.41	0.28	0.62	0.96	0.30	0.02	0.02	0.00	0.00	0.01	0.00	0.09	0.00	0.56	0.32	0.00	0.93	0.48						
Miura W.I.	0.86	0.19	0.98	0.10	0.96	0.99	0.98	0.69	0.03	0.20	0.47	0.89	0.96	0.37	0.26	0.62	0.97	0.28	0.02	0.04	0.00	0.01	0.00	0.01	0.10	0.00	0.61	0.28	0.00	0.93	0.48	0.97					
Parker W.I.	0.84	0.20	0.93	0.10	0.97	1.00	0.98	0.68	0.04	0.20	0.49	0.38	0.85	0.35	0.28	0.47	0.96	0.26	0.03	0.05	0.00	0.01	0.00	0.02	0.11	0.00	0.61	0.27	0.00	0.92	0.49	0.99	0.99				
New W.I.	0.86	0.19	0.99	0.10	0.97	1.00	0.98	0.69	0.03	0.20	0.47	0.89	0.96	0.37	0.27	0.62	0.96	0.27	0.03	0.04	0.00	0.01	0.00	0.01	0.10	0.00	0.61	0.28	0.00	0.93	0.48	0.98	1.00	1.00			
pH Value	0.65	0.04	0.82	0.20	0.90	0.89	0.85	0.48	0.30	0.05	0.37	0.42	0.68	0.59	0.01	0.01	0.92	0.07	0.01	0.05	0.01	0.00	0.03	0.01	0.11	0.06	0.65	0.31	0.01	0.82	0.42	0.86	0.97	0.96	0.97		
El. Cond-ty	0.17	0.11	0.13	0.06	0.13	0.12	0.13	0.25	0.02	0.02	0.08	0.14	0.17	0.00	0.02	0.03	0.09	0.08	0.11	0.01	0.00	0.02	0.00	0.01	0.06	0.02	0.03	0.05	0.01	0.29	0.18	0.28	0.15	0.16	0.16	0.07	

Reiche Weathering Potential Index (WPI), Reiche product Index (PI), Ruxton's Ratio (RR), Parker Weathering Index (W_p), and Miura Weathering Index (Wm) values are plotted against depth and are given in Figures 4.12 a & b. The linear regression coefficients are given in Table 4.3. Reiche Weathering Potential Index, Reiche Product Index and Ruxton's Ratio do not show any correlation with depth ($R^2 < 0.40$) while Parker Weathering Index and Miura Weathering Index show good positive correlations with depth having $R^2 = 0.84$ and 0.86 respectively. However, plots of depth vs these weathering indices have one common feature: a sudden drop in value of the indices from the depth of around 70 m to depth of around 50 m. Thereafter, they maintain very low values. This indicates a sudden increase in the intensity of the weathering process between 50 – 70 m depths which is the range of slight to moderate stages of weathering in the Karamu Basalt profile. This phenomenon is also observed in the plots of depth versus MgO, CaO and FeO and is further discussed in Chapter 8.

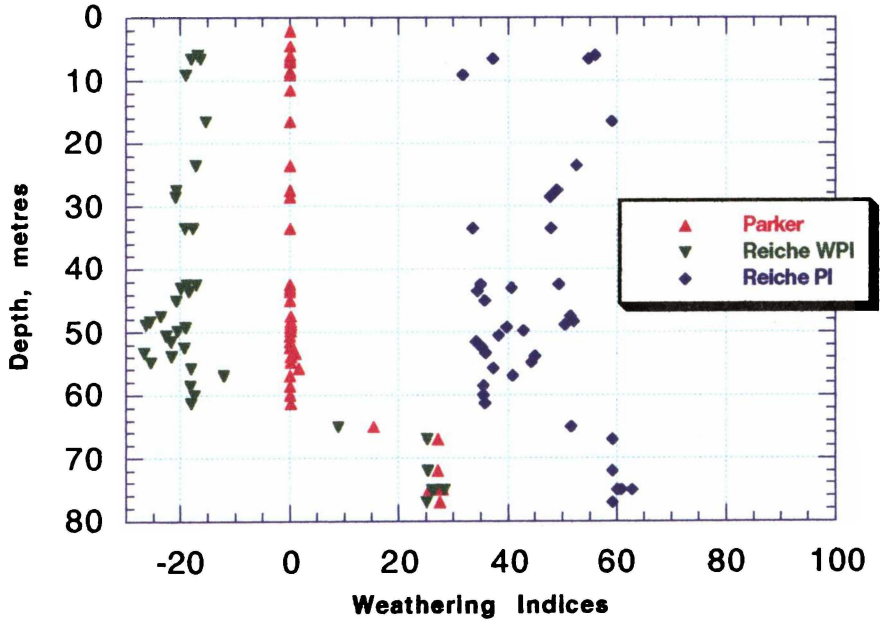

Figure 4.12a Plot of Weathering Indices (I) vs Depth

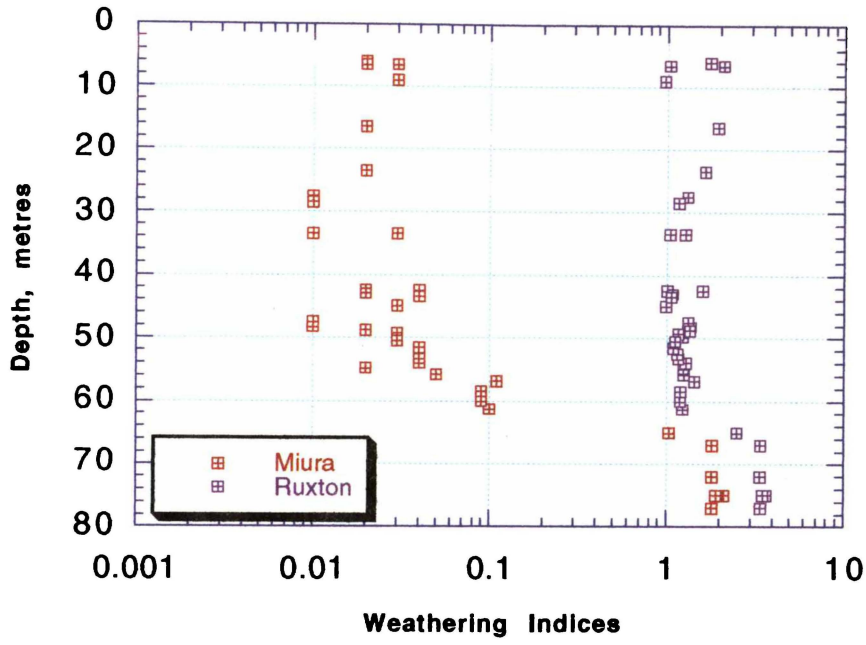

Figure 4.12b Plot of Weathering Indices (II) vs Depth

4.3.4 Chemical Concentrations Recalculated Assuming Al to be Constant

Values of Al_2O_3 increase from an average of 12.04 % in fresh basalt, to an average of 27.67 % in completely weathered material. Al_2O_3 is known to be retained in the weathering profile of basalts (Price *et al.*1991). Therefore, it was appropriate to re-evaluate the other chemical concentrations assuming a constant Al_2O_3 concentration along the weathering profile. TiO_2, another relatively immobile element, could have been considered too but its value did not vary significantly. Chemical concentrations, recalculated based on a constant Al_2O_3 concentration, are given in Appendix 4.6. Regression coefficients of these recalculated chemical concentrations versus depth did not vary significantly from the original values. The plots of new concentrations of SiO_2, TiO_2 and P_2O_5 versus depth were scattered. The plots of MgO, CaO and FeO versus depth show identical trends among themselves while Fe_2O_3 gave a somewhat mirror image of them (Figure 4.13a). The recalculated H_2O+ does not show a convincing plot with depth. It was mentioned in section 4.3.2 that H_2O+ correlates positively with Al_2O_3.

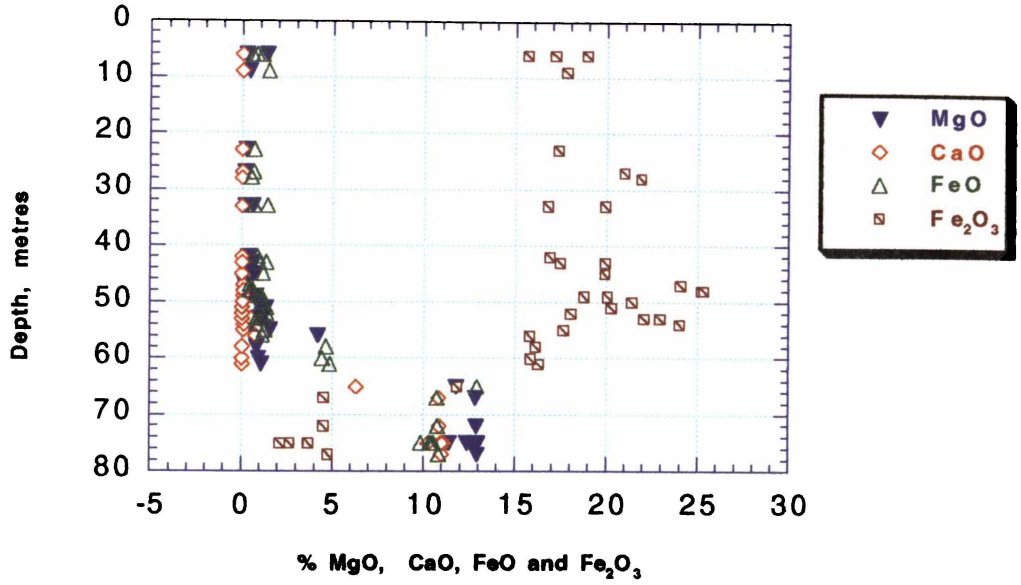

Figure 4.13a Plot of Depth vs % MgO, CaO, FeO and Fe_2O_3

It can be concluded that with the intensity of weathering, concentrations of MgO, CaO and FeO decrease and, as a result, there is an increase in the "apparent" concentration values of Al_2O_3, H_2O+ and Fe_2O_3.

4.3.5 A New Weathering Index

The elements and oxides taken into account in calculating the weathering indices discussed in section 4.3.3 do not include all the elements and oxides prevalent in Karamu Basalt. It should be noted that these indices were originally formulated for different kinds of rocks as mentioned in Chapter 2. Reiche Weathering Potential Index considers the bases, silica and trivalent cations but does not pay attention to FeO, which plays a major role in the weathering process of Karamu Basalt. Parker Weathering Index considers element to oxygen bond strength but is limited to the bases only. Miura Weathering Index considers all the elements changing in these processes but with additional elements such as Na, K and Mn, which are unavailable or in quantities below detection levels in many samples.

Therefore, an attempt was made to find a weathering index, which should include those elements, oxides of which give significant changes in value due to weathering of basalt. Chemical compositions of the samples show changes from fresh to weathered basalt.

The MgO, CaO and FeO concentrations decrease with the degree of weathering while the values of Al_2O_3, Fe_2O_3 and structural water concentrations increase. These oxides do not show lateral variation as per Figure 4.10.

Incorporating these changing oxides, a new weathering index could be written as follows:

$$\text{New W.I.} = \frac{FeO + CaO + MgO}{Fe_2O_3 + Al_2O_3 + H_2O^+} \qquad 4.4$$

Admittedly, this is a variation of the Miura Weathering Index. Figure 4.13b shows how this new weathering index varies with depth ($R^2 = 0.86$).

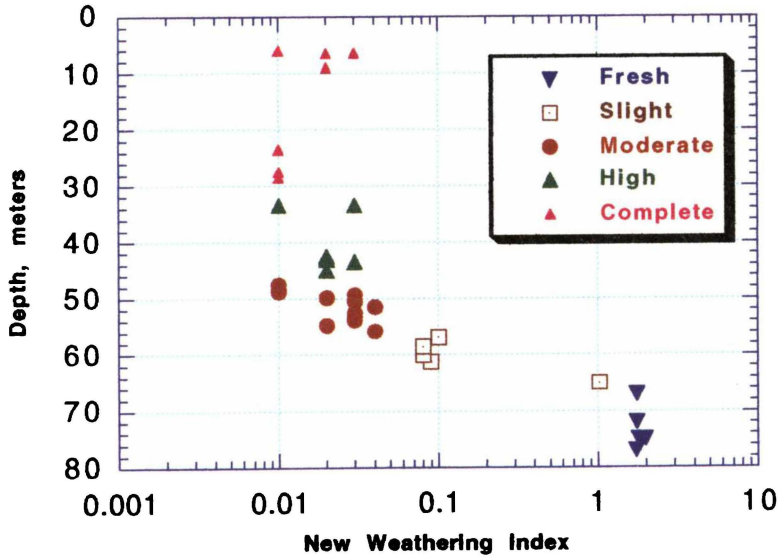

Figure 4.13b Plot of Depth vs New Weathering Index

4.4 Abrasion pH and Electrical Conductivity

The abrasion pH values were determined by dissolving powdered material in water. The method is detailed in Chapter 3. Electrical conductivity (which indirectly gives the percentage of soluble salts) was also determined (Table 4.4).

Grant (1969) used abrasion pH to determine the degree of weathering. The material was dissolved in water and the pH values of these solutions were measured. The proportion of soluble cations was also calculated. Ferrari and Magaldi (1983) too considered the abrasion pH useful in evaluating the degree of weathering.

Correlation of different elements with abrasion pH are as follows: Al_2O_3 shows a negative linear correlation of $R^2 = 0.82$ while MgO and CaO show positive linear correlations of $R^2 = 0.90$ and 0.89 (Figure 4.14a). Sr content shows a polynomial relationship $R^2 = 0.92$ with abrasion pH (Figure 4.14b).

Regression analysis gives an $R^2 = 0.65$ for depth versus abrasion pH (Figure 4.14c) but depth has a very low R^2 value versus electrical conductivity. The increase of abrasion pH with depth implies that with the intensity of weathering abrasion pH value decreases. The fresh basalt has basic abrasion pH values (around 8.5) and the completely weathered basalt has acidic values (around 4).

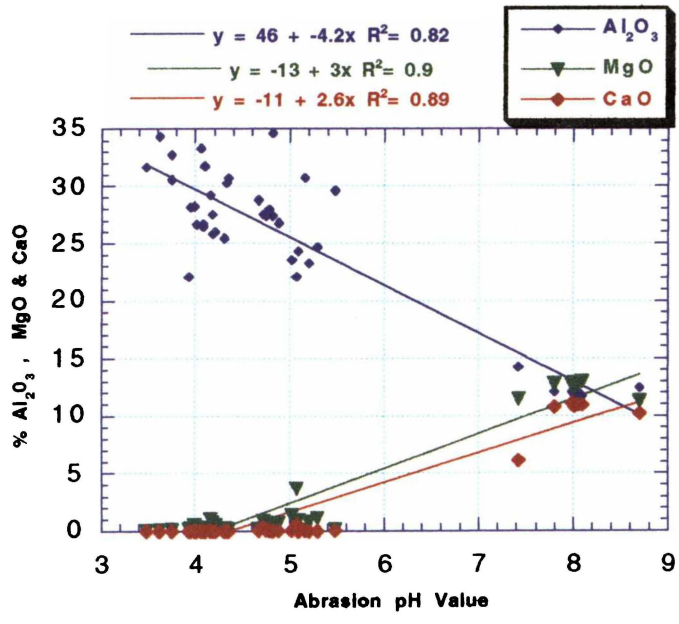

Figure 4.14 a Plot of % Al_2O_3, MgO & CaO vs Abrasion pH

Table 4.4 Electrical Conductivity and Abrasion pH Values					
Serial No.	**Descr-iption**	**Sample No.**	**El.Cond. microsiemen/cm**	**Abrasion pH**	**% Soluble Salts**
1	Fresh	MPJ 1	38.60	8.09	0.013
2	Basalt	MPJ 2	49.20	8.70	0.017
3		MPJ 3	18.30	8.05	0.006
4		MPJ 4	17.20	8.01	0.006
5		MPJ 5	26.00	7.80	0.009
6		MPJ 6	24.80	7.99	0.008
7		MPJ 7	31.50	8.01	0.011
Average			**29.37**	**8.09**	**0.01**
St. Dev			**11.44**	**0.28**	**0.00**
8	Slightly	MPJ 8	20.90	7.42	0.007
9	Weathered	MPJ 51	49.90	5.16	0.017
10	Basalt	MPJ 52	44.50	5.15	0.015
11		MPJ 53	43.80	5.11	0.015
12		MPJ 14	44.70	5.07	0.015
Average			**40.76**	**5.58**	**0.01**
St. Dev			**11.37**	**1.03**	**0.00**
13	Moderately	MPJ 9	53.90	5.48	0.018
14	Weathered	MPJ 10	49.90	5.16	0.017
15	Basalt	MPJ 11	111.30	4.78	0.038
16		MPJ 12	103.50	4.82	0.035
17		MPJ 13	74.20	4.67	0.025
18		MPJ 15	57.50	5.02	0.020
19		MPJ 16	57.40	4.75	0.020
20		MPJ 17	56.90	4.72	0.019
21		MPJ 18	43.70	5.20	0.015
22		MPJ 19	54.90	5.09	0.019
23		MPJ 20	43.50	5.29	0.015
24		MPJ 21	69.70	4.88	0.024
Average			**64.70**	**4.99**	**0.02**
St. Dev			**21.91**	**0.26**	**0.01**
25	Highly	MPJ 38	45.10	3.99	0.015
26	Weathered	MPJ 41	29.10	4.29	0.010
27	Basalt	MPJ 44	37.50	4.35	0.013
28		MPJ 47	30.34	4.31	0.010
29		MPJ 49	29.87	4.33	0.010
30		MPJ 50	30.18	4.21	0.010
Average			**33.68**	**4.25**	**0.01**
St. Dev			**6.39**	**0.13**	**0.00**
31	Completely	MPJ 31	30.30	4.01	0.010
32	Weathered	MPJ 32	27.60	3.93	0.009
33	Basalt	MPJ 33	33.40	4.08	0.011
34		MPJ 34	38.10	4.16	0.013
35		MPJ 36	20.60	4.08	0.007
36		MPJ 58	30.02	4.31	0.010
37		MPJ 60	29.91	4.28	0.010
Average			**29.99**	**4.12**	**0.01**
St. Dev			**5.34**	**0.14**	**0.00**
38	Rhyolitic	MPJ 22	97.30	4.82	0.331
39	Tephra	MPJ 23	40.60	3.75	0.138
40		MPJ 25	45.20	3.75	0.154
41		MPJ 26	16.20	4.10	0.055
42		MPJ 27	31.80	3.62	0.108
43		MPJ 28	40.00	3.48	0.136
44		MPJ 30	38.70	4.06	0.132
45		MPJ 35	23.80	4.19	0.081
Average			**41.70**	**3.97**	**0.14**
St. Dev			**24.45**	**0.42**	**0.08**
46	Paleosol	MPJ 29	52.60	3.95	0.018
47	MnO Incl	MPJ 39	75.20	4.18	0.026

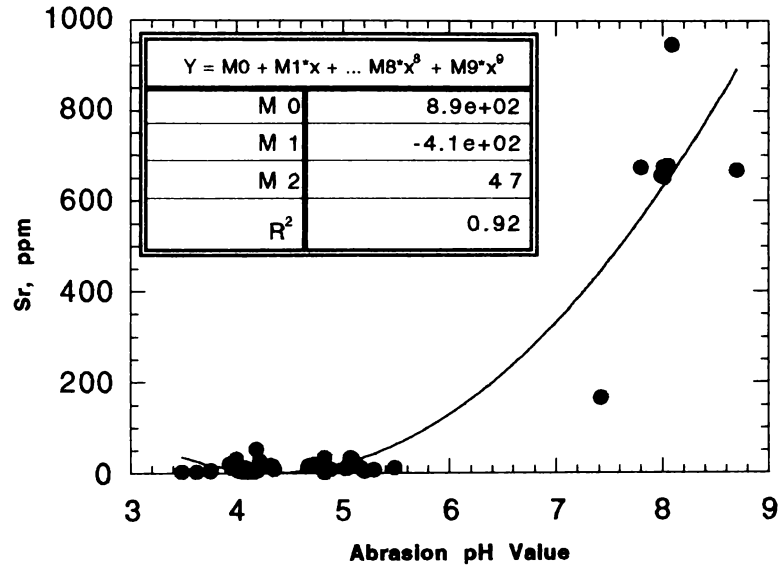

Figure 4.14b Plot of Sr vs Abrasion pH

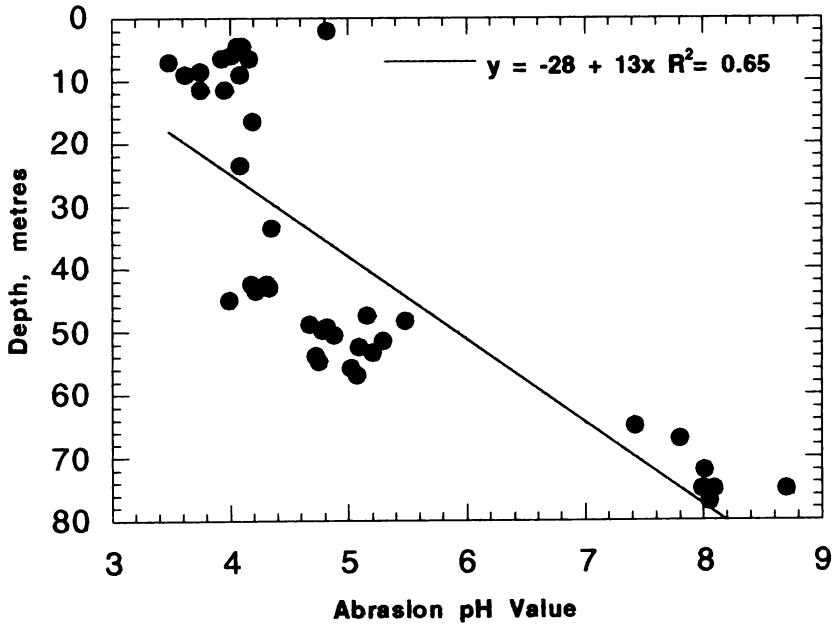

Figure 4.14c Plot of Depth vs Abrasion pH

In this study, using the conversion based on the theory of Rayment and Higginson (1992) explained in Chapter 3, the approximate percentages of soluble salts were calculated by multiplying the values of electrical conductivity (measured in microsiemens per centimetre) by 0.00034.

Electrical conductivity does not show a marked correlation with depth. Average values of electrical conductivity of fresh basalt and completely weathered basalt are similar (29.37 and 29.99 μS/cm respectively) but the average electrical conductivity value of moderately weathered basalt is the highest (64.7 μS/cm) while slightly weathered and highly weathered basalt maintain intermediate values (40.76 and 33.68 μS/cm respectively). Apparently soluble salts are produced more at the early stages of weathering and are washed away towards the latter stages. This again indicates the intensity of weathering was at a peak at slightly to moderately weathered stages.

4.5 Thickness of Iddingsite Rims in Weathered Olivine

The presence of iddingsite rims was a noticeable feature in the olivine crystals examined under the microscope. Iddingsite can apparently form without losing much of the major elements present but at latter stages of weathering it becomes redder and massive and forms clays and hematite and goethite (Colman, 1982). Comparison was made between the iddingsite rim thickness and the shore scleroscope hardness and Table 4.5 gives the values. Their correlation is discussed in Chapter 6.

4.6 Summary

The mineralogy and chemistry of materials at each stage of weathering of Karamu Basalt has been described. Primary minerals olivine, titanaugite and plagioclase weather into secondary minerals such as hematite, goethite, kaolinite and halloysite. Intermediate phases contain minerals such as smectites and illite.

TABLE 4.5 IDDINGSITE RIM THICKNESS & SHORE SCLEROSCOPE HARDNESS

Serial No.	Specimen No.	Degree of Weathering	Iddingsite Rim Thickness Average of 20 readings	Shore Scleroscope Hardness Average of 20 readings
1	12b	Fresh Basalt	16.21±4.64	22.3±2.51
2	17a	Fresh Basalt	12.68±3.29	32.4±4.24
3	18a	Fresh Basalt	11.44±5.94	28.5±4.66
4	22a	Fresh Basalt	5.75±8.51	54.2±6.21
		Average	11.52	34.35
		Standard Deviation	2.93	9.92
5	8a	Slightly Weathered	26.39±5.29	16.5±2.81
6	10a	Slightly Weathered	17.82±4.17	14.6±1.43
7	23a	Slightly Weathered	12.43±5.11	30.1±4.10
8	29a	Slightly Weathered	12.81±6.11	26.5±2.13
		Average	17.36	21.93
		Standard Deviation	4.74	6.38
9	3b	Moderately Weathered	24.02±6.22	8.7±0.91
10	6a	Moderately Weathered	35.14±7.65	12.3±2.52
11	13a	Moderately Weathered	26.35±3.59	12.0±1.11
12	20a	Moderately Weathered	24.53±3.66	12.2±0.92
		Average	30.17	9.04
		Standard Deviation	6.24	3.75
13	2a	Highly Weathered	45.32±6.80	0.0
14	4a	Highly Weathered	41.59±7.53	0.0
15	7a	Highly Weathered	39.40±7.10	0.0
16	14a	Highly Weathered	40.91±9.24	0.0
27	16a	Highly Weathered	29.11±3.88	7.5±1.65
18	19a	Highly Weathered	36.11±9.19	0.0
		Average	38.74	1.25
		Standard Deviation	4.09	2.08
19	11a	Completely Weathered	29.11±5.77	0.0
20	12a	Completely Weathered	35.97±4.94	2.5±0.88
21	17b	Completely Weathered	26.96±4.27	0.0
22	28a	Completely Weathered	34.29±3.42	0.0
		Average	31.58	0.63
		Standard Deviation	3.55	0.44

Major element chemistry shows that, even when the Al_2O_3 concentration is assumed to be constant, the CaO, MgO and FeO concentrations decrease with the intensity of weathering while the Fe_2O_3 concentration increases. Of the existing weathering indices considered, Parker and Miura weathering indices work well with Karamu Basalt. A new weathering index, which incorporates only those elements that seem to change in the weathering process, is proposed.

CHAPTER 5: GEOTECHNICAL INVESTIGATIONS AND OBSERVATIONS

5.1 Introduction

The field observations were made with the New Zealand Geomechanics Standards (1988) in mind. The weathering profile of Karamu Basalt was studied in detail and field tests were carried out. For laboratory geotechnical tests, specimens were prepared from the samples collected from each location. Depending on the nature and the amount of material required for each test, field and laboratory tests had to be at times limited to some weathering grades only. A description of the weathering profile, along with the results of geotechnical tests, are given in this chapter. Regression analysis was carried out among the geotechnical parameters and significant relationships as defined in Chapter 3 (p 57) are given as plots with corresponding regression equations.

5.2 Weathering Profile

The weathering profile on Karamu Basalt can be divided into 5 divisions following New Zealand Geomechanics Society (1988) weathering classification. They are fresh, slightly weathered, moderately weathered, highly weathered and completely weathered. A schematic diagram (Figure 5.1) gives an engineering description of the Karamu weathering profile.

5.2.1 Fresh Basalt

Dark-grey-coloured fresh basalt has vertical columnar jointing. Joints have aperture widths up to 10 mm and their spacing is 0.5 - 1 m. Fresh basalt shows no weathering effects such as discolouration or loss of strength. Columnar vertical jointing may have occurred at the time of formation of the rock, during solidification of lava. The uniaxial compressive strength is 194 - 332 MPa; point load strength index ($I_{S(50)}$) 3.4 – 7.7; and Schmidt rebound hardness 25 – 43.

Average depth (m)	Cross section	Degree of weathering	Sample numbers	Description of materials
0	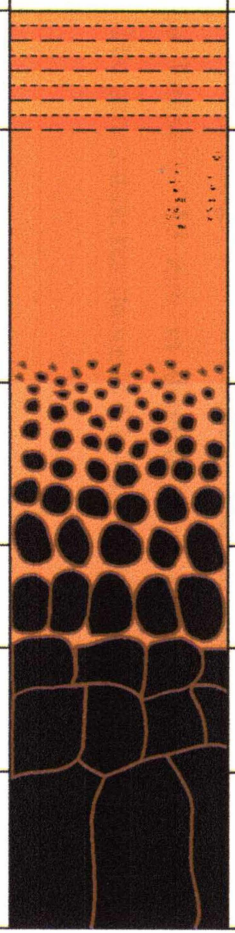	Alternating weathered tephra and paleosol layers	T: 22, 23, 25-28, 30, 35 P: 24 & 29	Alternating layers of : a) yellowish brown weathered tephra containing fragments of rhyolite with montmorillonite, kaolinite, halloysite and allophane. Plastic clayey soil material; b) reddish brown paleosol containing goethite and illite. More granular and less plastic soil compared to tephra.
6		Completely weathered basalt	31 - 34, 36, 58 - 60	Reddish brown soil with relict joints, but the original rock structure is preserved. Yellowish brown to orange soft clayey inclusions.
30		Highly weathered basalt	37 - 50	Small corestones (0.1-0.3 m) present . Majority of the material is soil, yet on close examination, corestones stand out. Original joint structure is still clear. Reddish brown hematite, black manganese oxide and white clays are present as distinct inclusions in the soil.
46		Moderately weathered basalt	9 - 13, 15 - 21, 54 - 57	Brown coloured rock blocks turn to less angular corestones of about 0.5 m dimension. Spaces are filled with clays and hematite.
56		Slightly weathered basalt	8, 14, 51 - 53	Rock is still dark grey but along the joint planes (apertures 20-30 mm) are discoloured to brown. Partly open joints with brownish clayey material as fillings. Near horizontal fractures appear.
66		Fresh basalt	1 - 7	Dark grey coloured fresh basalt with columnar jointing. Open joints of up to 10mm aperture width and 0.5 - I m vertical joint spacing.

Figure 5.1 Engineering Geological Description of the Weathering Profile at Karamu. Depths not to scale.

5.2.2 Slightly Weathered Basalt

In slightly weathered basalt, discolouration (to brown) can be observed on joint planes. The rest of the rock is dark grey in colour. Joint planes have apertures ranging from closed to 20 – 30 mm in width. Some joints are filled with brown material consisting mainly of clays and goethite. Near horizontal fractures at ~ 0.8 m spacing form prismatic to cubic rock blocks. The point load strength index ($I_{S(50)}$) is 0.24 – 0.73; and Schmidt rebound hardness 15 – 24.

5.2.3 Moderately Weathered Basalt

The brown discolouration on joints is more widespread in moderately weathered basalt compared to slightly weathered basalt. The rock mass is partly (~ 20 %) changed to soil. The rock blocks are brown in colour adjacent to joints due to weathering. The rock blocks turn into angular corestones of about 0.5 m in dimension. The penetration resistance is 3.5 – 4.5 MPa; and the vane shear strength is 95 – 183 kPa.

5.2.4 Highly Weathered Basalt

In highly weathered basalt, more than half the original rock mass has changed to dark brown soil. On close examination, rounded corestones of 0.1 – 0.3 m dimensions stand out. Original vertical joint structure and subsequent horizontal jointing are still clear. Reddish-brown hematite bands of up to 5 cm in thickness and several meters in length, black manganese oxide nodules up to a centimetre in diameter and white clayey inclusions are abundant in the soil. The penetration resistance is 3.7 – 4.6 MPa; and the vane shear strength is 113 – 147 kPa.

5.2.5 Completely Weathered Basalt

In completely weathered basalt, the original rock mass has completely changed to a reddish-brown soil with relict joints, and the original rock structure is preserved. Yellowish-brown to orange, soft inclusions of goethite and clay are present in the form of abundant lumps (~ 10 mm in diameter) and occasional bands (~100 mm in thickness). The penetration resistance is 4.1 – 4.5 MPa; and vane shear strength is 107 – 121 kPa.

5.2.6 Tephra and Paleosols

Further weathering forming residual soil (soil in which the relict rock structure is absent) has not taken place mainly due to the overlying alternating layers of yellowish-brown rhyolitic tephra and reddish-brown paleosols. The tephra is weathered and contains a high content of clays, mainly smectites, kaolinite, halloysite and allophane. The paleosols have a high content of goethite and illite. For tephra, the penetration resistance is 2.8 – 3.5 MPa; and the vane shear strength is 95 – 104 kPa. For paleosols, the penetration resistance is 2.8 – 3.6 MPa; and the vane shear strength is 102 – 121 kPa.

5.3 Other Geotechnical Features

Even though columnar jointing was present in the fresh basalt, the rock slopes were stable. Even the slightly weathered basalt slopes seemed to be in a stable condition. Evidence of small planar slides along the surfaces between rock and weathered material was observed in the case of slopes within moderately weathered basalt. The movement was not more than 0.2 m in height. Extensive examples of failure could be observed at different levels of weathering profile. Some of these slips were of a rotational nature and were about 1 - 2 m in height and about 0.5 - 1 m wide. The others were slab failures of about 6 m in height and about 3 m in width (Figures 4.4, 4.5 and 4.7).

Although weathering changes the mineralogy and chemistry, the outward appearance, in terms of structure, seems to remain unaltered throughout the observed weathering profile. This is evident from the relict features such as jointing and corestones. The joints are gradually filled with secondary minerals but even in the completely weathered material their orientation and even their size remain constant. The corestones, which become gradually smaller during the process of weathering, retain some fresh minerals.

Geotechnical parameters were obtained and regression analysis was carried out among them and with depth. Regression coefficient (R^2) values at 95% confidence level are given in Table 5.8. Depending on the availability of sampling facilities, accessibility and nature of testing equipment and materials required, some geotechnical tests were carried out on a limited number of samples.

5.4 Compressive Strength

In the field, the Schmidt rebound hardness values were obtained for 11 sample locations (7 of fresh and 4 of slightly weathered basalt) and 20 readings were taken at each location (Appendix 5.1). For the average values, corresponding compressive strength values were obtained using the conversion chart given by Miller in 1965, reproduced by Brown (1981) (Table 5.1a). Average Schmidt rebound hardness for fresh rock is 33 ± 7 (and the corresponding estimated compressive strength is 73 ± 28 MPa) and 19 ± 4 for slightly weathered (corresponding estimated compressive strength 32 ± 8 MPa). Fresh basalt locations were from roughly the same depths and locations as MPJ 3 - 5 in the central portion of the weathering profile of the north wall of the quarry. Samples MPJ 1 - 2 and 6 - 7 were from the two ends. There is a similarity among the values of compressive strength in the samples MPJ 3 - 5. The pair MPJ 1 - 2 has a higher value whilst the pair 6-7 has a lower value. The slightly weathered basalt samples show a change with depth: the deeper the sample, the higher is the value of compressive strength (Figure 5.2).

Uniaxial compressive strength determination of 10 fresh basalt specimens from the sample location MPJ 1 gave a range of values between 194 MPa to 332 MPa with an average value of 262 ± 47 MPa (Table 5.1b). This value is twice as high as the compressive strength estimated for sample MPJ 1 from the Schmidt rebound hardness test (i.e. 115 MPa).

Point load strength index $I_{S(50)}$ was calculated for 10 sample locations (7 from fresh and 3 from slightly weathered basalt). From each location 20 specimens were tested. The average point load strength index values are 5.6 ± 1.8 and 0.4 ± 0.3 for fresh and slightly weathered basalt and the corresponding compressive strength values are 123 ± 39 and 9 ± 6 MPa respectively (Table 5.1c). In the case of fresh basalt, these compressive strength values are higher than the corresponding values obtained by Schmidt rebound hardness method but the reverse is true for slightly weathered basalt.

Sample MPJ 8 is located closer to the fresh basalt than other slightly weathered basalt and shows intermediate values for most parameters. It can be considered a transition sample but from field classification it was definitely slightly weathered. For this sample,

TABLE 5.1 a SCHMIDT REBOUND HARDNESS (R) AND CORRESPONDING COMPRESSIVE STRENGTH

Serial No.	Sample No.	Degree of weathering	Hardness Average of 20 readings	Compressive* Strength, MPa
1	MPJ 1	Fresh Basalt	43.4 ± 4.74	115
2	MPJ 2	Fresh Basalt	41.5 ± 2.72	108
3	MPJ 3	Fresh Basalt	30.7 ± 4.81	60
4	MPJ 4	Fresh Basalt	32.4 ± 4.55	65
5	MPJ 5	Fresh Basalt	34.0 ± 5.70	70
6	MPJ 6	Fresh Basalt	26.7 ± 1.89	48
7	MPJ 7	Fresh Basalt	25.2 ± 2.04	45
	Average		**33**	**73**
	Standard Deviation		**7**	**28**
8	MPJ 8	Slightly Weathered	24.0 ± 4.57	41
9	MPJ 51	Slightly Weathered	19.0 ± 0.00	35
10	MPJ 52	Slightly Weathered	15.8 ± 0.42	26
11	MPJ 53	Slightly Weathered	15.4 ± 0.52	24
	Average		**19**	**32**
	Standard Deviation		**4**	**8**

* Compressive Strength estimated according to Brown (1981)

TABLE 5.1 b UNIAXIAL COMPRESSIVE STRENGTH OF SAMPLE MPJ 1

Serial No.	Specimen No.	Compressive Strength,MPa
1	MPJ 1. A	216.3
2	MPJ 1. B	298.8
3	MPJ 1. C	331.9
4	MPJ 1. D	270.8
5	MPJ 1. E	193.8
6	MPJ 1. F	237.8
7	MPJ 1. G	210.0
8	MPJ 1. H	297.9
9	MPJ 1. I	255.9
10	MPJ 1.J	306.8
	Average	**262.0**
	Standard Deviation	**46.8**

TABLE 5.1 c POINT LOAD INDEX Is(50) AND CORRESPONDING COMPRESSIVE STRENGTH

Serial No.	Degree of Weathering	Sample No.	Is(50) Average of 20 Readings	Compressive* Strength, MPa
1	Fresh	MPJ 1	7.72 ± 0.5	169.9
2	Fresh	MPJ 2	7.08 ± 0.2	155.9
3	Fresh	MPJ 3	3.42 ± 0.1	75.3
4	Fresh	MPJ 4	3.86 ± 0.2	84.9
5	Fresh	MPJ 5	3.94 ± 0.2	86.7
6	Fresh	MPJ 6	6.85 ± 0.3	150.7
7	Fresh	MPJ 7	6.27 ± 0.1	137.9
	Average		**5.59**	**123.04**
	Std. Dev.		**1.79**	**39.40**
8	Slight	MPJ 8	0.73 ± 0.1	16.1
9	Slight	MPJ 51	0.25 ± 0.2	5.6
10	Slight	MPJ 52	0.24 ±0.1	5.2
	Average		**0.41**	**8.98**
	Std. Dev.		**0.28**	**6.20**

* Compressive strength calculated according to Bieniawski (1975)

point load test values are much lower than those for fresh basalt and Schmidt hammer values are close to those for fresh basalt.

Point load test estimates of compressive strength show a significant (R^2 = 0.73) positive correlation with depth as against an insignificant (R^2 = 0.44) relationship between Schmidt hammer strength estimates and depth (Figure 5.2). It is suggested that the point load test depicts the degree of weathering better than the Schmidt hammer method. Uniaxial compressive strength test is the most reliable but the most expensive technique used. It also requires preparation of proper regular shaped samples (often cylindrical cores). Even though lower values are obtained by Schmidt hammer method (can be performed in the field without any sample preparation) and point load test (even irregular rock lumps can be used), these two tests may be still useful as relative indicators of compressive strength.

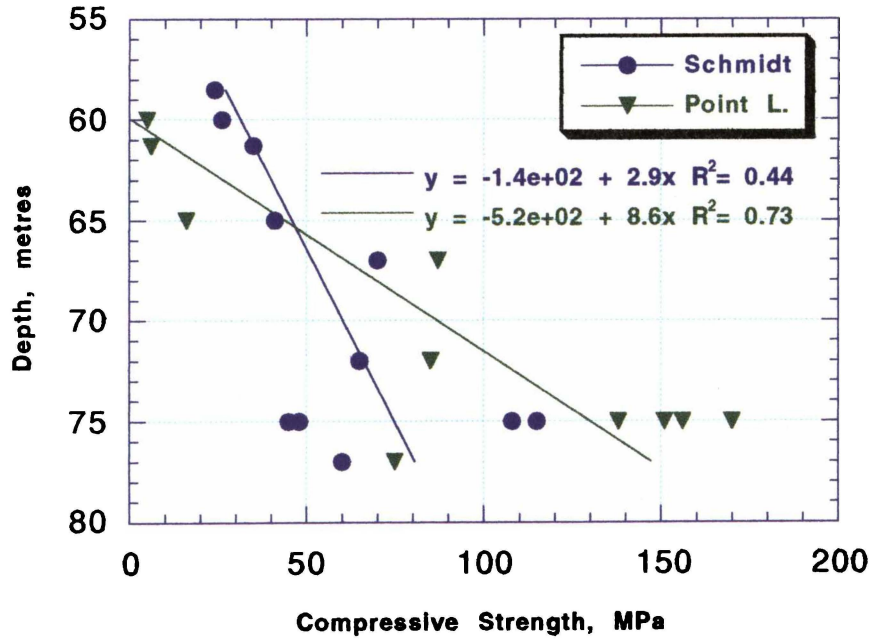

Figure 5.2 Plot of Depth vs Compressive Strength (Predicted by Schmidt Hardness and Point Load Index)

5.5 Penetration Resistance and Shear Strength

The penetration resistance for 27 sample locations and shear strength (using vane shear apparatus) for 28 sample locations were measured. These are for moderately, highly and completely weathered basalt plus some overlying tephra and paleosols (Table 5.2). Some locations had material suitable for only one of the two tests, which explains the gaps in the table.

The average penetration resistance values for moderately, highly and completely weathered basalt were 4.10 ± 0.22, 4.15 ± 0.13 and 4.37 ± 0.04 MPa respectively. There is little variation in the values. The penetrometer cannot penetrate hard rock so it can give a value only for weathered material. Therefore, the results obtained are for areas containing joint infill or weathered matrix.

The average shear strength values for moderately, highly and completely weathered basalt are 119 ± 32, 123 ± 13.5 and 115 ± 6 kPa respectively. In moderately weathered basalt individual readings as high as 200 kPa and as low as 82 kPa are observed. Hence, vane shear strength cannot be accepted as a measure of weathering.

Regression analysis between penetration resistance and shear strength shows no correlation. They are independent of each other. Neither of them show any correlation with depth.

5.6 Atterberg Limits & Particle Size Analysis

Penetrometer index and plastic limit were calculated for 34 samples using the cone penetrometer. The liquid limit and plastic limit values were obtained from them as per Allbrook (1980) and by a calibration method explained in Chapter 3. As per Lambe (1951), the plasticity index was calculated by subtracting the plastic limit from the liquid limit (Table 5.3). In the slightly weathered grade, most of the rock mass is still coherent material. Hence a quantity of fine particle fraction sufficient for these tests could be obtained only at sample location MPJ 14 where infill material was the most abundant within the slightly weathered rocks. The results of sample MPJ 14 reflect only the properties of infill material and not the bulk sample.

TABLE 5.2 PENETRATION RESISTANCE & VANE SHEAR STRENGTH				
Serial No.	Weathering Degree	Sample No.	Penetration Resistance, MPa Average of 20 readings	Shear Strength, kPa Average of 20 readings
1	Moderate	MPJ 9	3.89 ± 0.1	95 ± 6
2	Moderate	MPJ 10	3.89 ± 0.1	96 ± 2
3	Moderate	MPJ 11	3.86 ± 0.1	110 ± 7
4	Moderate	MPJ 12	3.89 ± 0.2	99 ± 6
5	Moderate	MPJ 13	3.87 ± 0.1	95 ± 2
6	Moderate	MPJ 16	4.39 ± 0.1	n/a
7	Moderate	MPJ 17	4.39 ± 0.1	n/a
8	Moderate	MPJ 18	4.23 ± 0.2	183 ± 9
9	Moderate	MPJ 19	4.25 ± 0.1	163 ± 7
10	Moderate	MPJ 20	4.26 ± 0.1	119 ± 2
11	Moderate	MPJ 21	4.21 ± 0.2	112 ± 6
	Average		**4.10**	**119**
	Std. Dev.		**0.22**	**32**
12	High	MPJ 38	4.38 ± 0.1	147 ± 7
13	High	MPJ 41	4.02 ± 0.1	n/a
14	High	MPJ 44	4.05 ± 0.1	117 ± 6
15	High	MPJ 47	4.11 ± 0.1	119 ± 2
16	High	MPJ 49	4.12 ± 0.1	113 ± 6
17	High	MPJ 50	4.21 ± 0.1	120 ± 7
	Average		**4.15**	**123**
	Std. Dev.		**0.13**	**14**
18	Complete	MPJ 31	n/a	121 ± 7
19	Complete	MPJ 32	n/a	107 ± 6
20	Complete	MPJ 33	n/a	110 ± 2
21	Complete	MPJ 34	n/a	113 ± 7
22	Complete	MPJ 36	n/a	121 ± 6
23	Complete	MPJ 58	4.39 ± 0.1	n/a
24	Complete	MPJ 60	4.34 ± 0.1	n/a
	Average		**4.37**	**115**
	Std. Dev.		**0.04**	**6**
25	Tephra	MPJ 22	3.01 ± 0.1	94.8 ± 2
26	Tephra	MPJ 23	3.02 ± 0.1	97.3 ± 5
27	Tephra	MPJ 25	3.13 ± 0.1	95 ± 2
28	Tephra	MPJ 26	3.17 ± 0.1	96 ± 3
29	Tephra	MPJ 27	3.11 ± 0.1	96 ± 4
30	Tephra	MPJ 35	n/a	104 ± 2
	Average		**3.09**	**97**
	Std. Dev.		**0.07**	**3**
31	Paleosol	MPJ 28	3.21 ± 0.1	121 ± 6
32	Paleosol	MPJ 29	3.21 ± 0.1	102 ± 4
	Average		**3.21**	**111**
33	MnO Incl.s	MPJ 39	4.38 ± 0.3	135

TABLE 5.3 ATTERBERG LIMITS; PERCENTAGE & ACTIVITY OF CLAY							
Serial no.	Weath. Degree	Sample no.	Liquid Limit,%	Plastic Limit,%	Plasticity Index,%	% Clay	Activity of Clay
1	Slight	MPJ 14	74.82	67.56	7.26	18.58	0.39
2	Moderate	MPJ 9	84.56	70.09	14.47	31.20	0.46
3	Moderate	MPJ 10	81.74	67.31	14.43	33.62	0.43
4	Moderate	MPJ 11	80.65	66.42	14.23	29.07	0.49
5	Moderate	MPJ 12	83.63	71.04	12.59	26.18	0.48
6	Moderate	MPJ 13	84.75	74.01	10.74	25.84	0.42
7	Moderate	MPJ 15	74.05	66.07	7.98	10.32	0.77
8	Moderate	MPJ 16	72.28	51.71	20.57	40.67	0.51
9	Moderate	MPJ 17	69.12	55.83	13.29	36.01	0.37
10	Moderate	MPJ 18	70.92	56.68	14.24	27.14	0.52
11	Moderate	MPJ 19	67.98	58.54	9.44	39.82	0.24
12	Moderate	MPJ 20	67.12	58.14	8.98	36.84	0.24
13	Moderate	MPJ 21	63.15	35.00	28.15	26.01	1.08
	Average		**75.00**	**60.90**	**14.09**	**30.23**	**0.50**
	Std. Dev.		**7.68**	**10.74**	**5.55**	**8.26**	**0.23**
14	High	MPJ 38	72.88	53.31	19.57	20.26	0.97
15	High	MPJ 41	58.87	53.22	5.65	33.68	0.17
16	High	MPJ 44	69.12	53.51	15.61	30.58	0.51
17	High	MPJ 47	70.68	50.91	19.77	37.39	0.53
18	High	MPJ 49	60.67	52.13	8.54	32.17	0.27
19	High	MPJ 50	52.61	42.58	10.03	37.10	0.27
	Average		**64.14**	**50.94**	**13.20**	**31.86**	**0.45**
	Std. Dev.		**7.96**	**4.21**	**5.97**	**6.29**	**0.29**
20	Complete	MPJ 31	76.01	56.23	19.78	10.14	1.95
21	Complete	MPJ 32	75.01	53.75	21.26	8.52	2.50
22	Complete	MPJ 33	64.01	51.92	12.09	25.78	0.47
23	Complete	MPJ 34	70.76	64.67	6.09	23.65	0.26
24	Complete	MPJ 36	81.72	67.01	14.71	19.33	0.76
25	Complete	MPJ 58	n/a	n/a	n/a	45.50	n/a
26	Complete	MPJ 60	n/a	n/a	n/a	41.96	n/a
	Average		**73.50**	**58.72**	**14.79**	**24.98**	**1.19**
	Std. Dev.		**6.59**	**6.73**	**6.12**	**14.35**	**0.98**
30	Tephra	MPJ 22	86.43	59.29	27.14	41.20	0.66
31	Tephra	MPJ 23	97.86	75.01	22.85	54.64	0.42
32	Tephra	MPJ 25	97.31	66.29	31.02	33.13	0.94
33	Tephra	MPJ 26	98.21	57.56	40.65	37.20	1.09
34	Tephra	MPJ 27	111.13	90.81	20.32	16.84	1.21
35	Tephra	MPJ 28	76.25	62.33	13.92	15.19	0.92
36	Tephra	MPJ 30	74.72	67.11	7.61	23.86	0.32
37	Tephra	MPJ 35	76.01	65.52	10.49	12.14	0.86
	Average		**89.74**	**67.99**	**21.75**	**29.28**	**0.80**
	Std. Dev.		**13.41**	**10.67**	**11.11**	**14.83**	**0.31**
38	Paleosol	MPJ 29	**64.12**	**50.28**	**13.84**	**16.10**	**0.86**
39	MnO inclusions	MPJ 39	**62.27**	**50.95**	**11.32**	**43.91**	**0.26**

Particle size distribution data were obtained for 44 samples (Appendix 5.2). The fraction smaller than 2 μm obtained from this method was considered as clay and its percentage by weight is included in Table 5.3. As per Lambe (1951), the activity of clay was calculated as % clay / plasticity index (Table 5.3).

Liquid Limit values for slightly, moderately, highly and completely weathered basalt are as follows: 75 %, 75 ± 8 %, 64 ± 8 %and 74 ± 7 %. Corresponding Plastic Limit values are 67.6 %, 61 ± 11 %, 51 ± 4 % and 59 ± 7 % and Plasticity Index values are 7 %, 14 ± 6 %, 13 ± 6 % and 15 ± 6 %. The clay percentage varies from 17.3 ± 2 %, for slightly weathered, 30 ± 8 % for moderately weathered through 32 ± 6 % for highly weathered to 25 ± 14 % for completely weathered basalt. Activity of clay has corresponding values of 0.4, 0.5 ± 0.2, 0.5 ± 0.3, and 1 ± 1.

These values show that the clays appear in the infill at the slight stage of weathering, and generally become more abundant through moderate to high stages of weathering. An interesting observation is that in the completely weathered material, the average clay content is reduced (however, the changes seem to fall within the error range) even though the plasticity index does not drop. In Chapter 4, it was ascertained by X-ray diffraction method that the clay mineral content was highest at the completely weathered stage. Samples MPJ 58 and 60, for which no Atterberg limit results could be obtained (as insufficient fine grained portion of sample was available due to the presence of many gritty inclusions), do indicate high percentages of clay.

Regression analysis shows that neither the Atterberg limits nor the percentage and activity of clay show any correlation with depth, but Plasticity Index shows a marked increase across the slight to moderate weathering grade boundary and then remains constant.

5.7 Water Content, Density and Porosity

Water content, dry density, particle density and porosity were calculated for 48 samples (Table 5.4). For each parameter, the values given for each sample represent averages of 5 replicates.

TABLE 5.4 WATER CONTENT, DENSITY AND POROSITY

Serial No.	Weathering Degree	Sample No.	Water Content, %	Dry Density kg/m^3	Particle Density, kg/m^3	Porosity %
1	Fresh	MPJ 1	0.00	2814	2821	0.25
2	Fresh	MPJ 2	0.00	2902	2911	0.31
3	Fresh	MPJ 3	0.00	2816	2821	0.18
4	Fresh	MPJ 4	0.00	2827	2834	0.25
5	Fresh	MPJ 5	0.00	2792	2805	0.46
6	Fresh	MPJ 6	0.00	2754	2769	0.54
7	Fresh	MPJ 7	0.00	2774	2782	0.29
	Average		**0.00**	**2811**	**2820**	**0.32**
	Std. Dev.		**0.00**	**48**	**46**	**0.13**
8	Slight	MPJ 8	12.04	2492	2568	2.96
9	Slight	MPJ 14	34.86	1845	2129	13.34
10	Slight	MPJ 51	33.87	2175	2327	6.53
11	Slight	MPJ 52	31.11	2059	2296	10.32
12	Slight	MPJ 53	30.62	2008	2151	6.65
	Average		**28.50**	**2116**	**2294**	**7.96**
	Std. Dev.		**9.37**	**241**	**176**	**3.98**
13	Moderate	MPJ 9	45.89	2066	2331	11.37
14	Moderate	MPJ 10	44.09	2066	2322	11.02
15	Moderate	MPJ 11	54.41	2031	2354	13.72
16	Moderate	MPJ 12	50.34	2045	2369	13.68
17	Moderate	MPJ 13	41.91	1832	2078	11.84
18	Moderate	MPJ 15	37.49	1845	2201	16.17
19	Moderate	MPJ 16	32.20	1841	2215	16.88
20	Moderate	MPJ 17	37.52	1842	2239	17.73
21	Moderate	MPJ 18	51.47	1887	2206	14.46
22	Moderate	MPJ 19	50.97	1867	2211	15.56
23	Moderate	MPJ 20	61.91	1868	2143	12.83
24	Moderate	MPJ 21	48.98	1706	2033	16.08
	Average		**46.43**	**1908**	**2225**	**14.28**
	Std. Dev.		**8.31**	**116**	**106**	**2.24**
25	High	MPJ 38	79.31	1787	2273	21.38
26	High	MPJ 44	34.00	1767	2063	14.35
27	High	MPJ 47	34.92	1754	2238	21.63
28	High	MPJ 49	35.00	1745	2247	22.34
29	High	MPJ 50	29.74	1735	2263	23.33
	Average		**42.59**	**1758**	**2217**	**20.61**
	Std. Dev.		**20.64**	**20**	**87**	**3.58**
30	Complete	MPJ 31	33.21	1554	2119	26.66
31	Complete	MPJ 32	42.51	1576	2128	25.94
32	Complete	MPJ 33	49.41	1502	2063	27.19
33	Complete	MPJ 34	42.54	1642	2213	25.80
34	Complete	MPJ 36	59.32	1591	2134	25.45
35	Complete	MPJ 58	35.25	1554	1985	21.71
36	Complete	MPJ 60	36.37	1556	2073	24.94
	Average		**42.66**	**1568**	**2102**	**25.39**
	Std. Dev.		**9.19**	**43**	**71**	**1.78**
37	Tephra	MPJ 22	47.86	1165	1942	40.01
38	Tephra	MPJ 23	55.19	1154	1948	40.76
39	Tephra	MPJ 25	54.80	1165	1913	39.10
40	Tephra	MPJ 26	55.34	1154	1952	40.88
41	Tephra	MPJ 27	90.92	1152	1942	40.68
45	Tephra	MPJ 28	55.69	1515	2134	29.01
42	Tephra	MPJ 30	60.68	1124	1946	42.24
43	Tephra	MPJ 35	45.73	1154	1945	40.67
	Average		**58.28**	**1198**	**1965**	**39.17**
	Std. Dev.		**14.01**	**129**	**69**	**4.20**
44	Paleosol	MPJ 24	16.37	1398	2104	33.56
46	Paleosol	MPJ 29	46.94	1502	2116	29.02
	Average		**31.66**	**1450**	**2110**	**31.29**
47	Inclusions	MPJ 39	58.65	1778	2275	21.85
48	Inclusions	MPJ 42	35.12	1787	2286	21.83
	Average		**46.89**	**1783**	**2281**	**21.84**

For fresh basalt the natural water content is zero and in slightly weathered basalt it has an average of 29 ± 9 %, in moderately weathered 46 ± 8 %, in highly weathered 43 ± 21 % and in completely weathered basalt, it is 43 ± 9 %. The corresponding average dry density values are 2811 ± 48 kg/m^3; 2116 ± 241 kg/m^3; 1908 ± 116 kg/m^3; 1758 ± 20 kg/m^3 and 1568 ± 43 kg/m^3. From fresh to completely weathered basalt, average porosity values are 0.3 ± 0.1 %; 8.0 ± 4 %; 14 ± 2 %; 20.6 ± 3.5 %, and 25.4 ± 2 % respectively.

With the intensity of weathering, the water content and porosity increase while the density decreases. Regression analysis shows that water content has no significant correlation with depth (R^2 = 0.37). Dry density has, at 95% confidence level, a positive linear correlation of R^2 = 0.69 with depth, while porosity has a negative linear correlation of R^2 = 0.81 with depth (Figures 5.3 a & b).

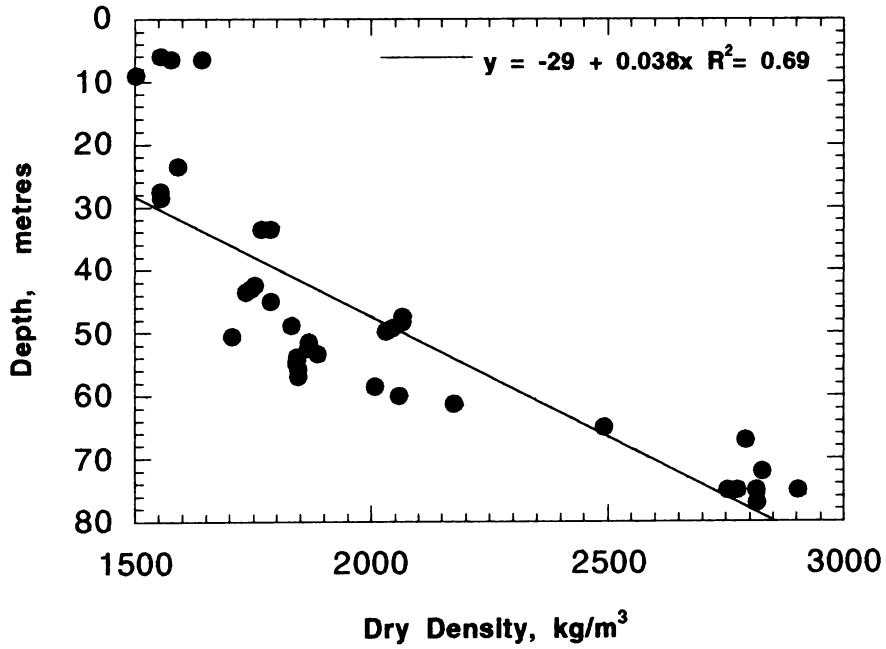

Figure 5.3a Plot of Depth vs Dry Density

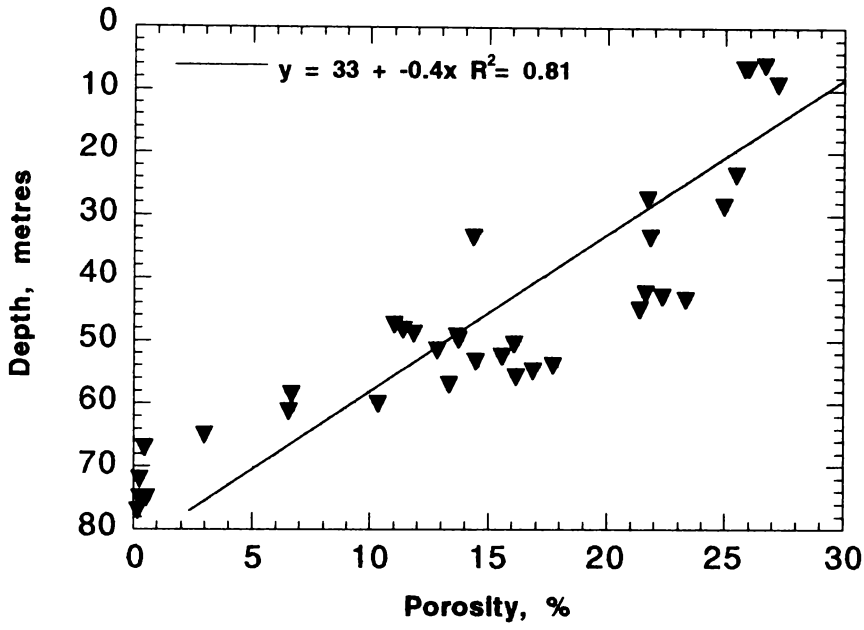

Figure 5.3b Plot of Depth vs Porosity

5.8 Cohesion and Angle of Internal Friction

Direct shear test results of 34 samples were generated (Table 5.5). Cohesion (c) and angle of internal friction (ϕ) values were calculated. The cohesion of the infill in slightly weathered material is zero and it gradually increases through moderately weathered (1 ± 1 kPa) and highly weathered (4 ± 2 kPa) to 5 ± 2 kPa in completely weathered basalt. The corresponding values of angle of internal friction are 36^0; 34 ± 1^0 ; 37 ± 1^0 and 35 ± 2^0 respectively. While cohesion shows, at 95% confidence level, a negative linear correlation of $R^2 = 0.77$ with depth (Figure 5.4a), the angle of internal friction shows no relationship at all with depth ($R^2 = 0.01$). The increase in cohesion with intensity of weathering is believed to be due to the formation of clay minerals. Clay minerals cause high cohesion in soils. The angle of internal friction may have been expected to decrease, but the results do not show this.

TABLE 5.5 DIRECT SHEAR TEST RESULTS

Serial No.	Weathering Grade	Sample No.	Cohesion(C) kPa	Phi Degrees
1	Slight	MPJ 14	0	36
2	Moderate	MPJ 9	1	33
3	Moderate	MPJ 10	1	34
4	Moderate	MPJ 11	2	33
5	Moderate	MPJ 12	1	33
6	Moderate	MPJ 13	1	32
7	Moderate	MPJ 15	0	34
8	Moderate	MPJ 16	0	35
9	Moderate	MPJ 17	0	36
10	Moderate	MPJ 18	0	35
11	Moderate	MPJ 19	0	33
12	Moderate	MPJ 20	0	34
13	Moderate	MPJ 21	0	36
	Average		**1**	**34**
	Std.Dev.		**1**	**1**
14	High	MPJ 38	7	36
15	High	MPJ 41	7	35
16	High	MPJ 44	2	36
17	High	MPJ 47	3	38
18	High	MPJ 49	3	38
19	High	MPJ 50	3	38
	Average		**4**	**37**
	Std.Dev.		**2**	**1**
20	Complete	MPJ 31	7	33
21	Complete	MPJ 32	7	33
22	Complete	MPJ 33	5	36
23	Complete	MPJ 34	4	35
24	Complete	MPJ 36	5	34
25	Complete	MPJ 58	2	36
26	Complete	MPJ 60	2	37
	Average		**5**	**35**
	Std.Dev.		**2**	**2**
27	Tephra	MPJ 22	9	31
28	Tephra	MPJ 23	9	31
29	Tephra	MPJ 25	9	31
30	Tephra	MPJ 26	9	31
31	Tephra	MPJ 27	9	31
32	Tephra	MPJ 28	9	31
	Average		**9**	**31**
	Std.Dev.		**0**	**0**
33	Paleosol	MPJ 29	**9**	**31**
34	MnO inclusions	MPJ 39	**8**	**35**

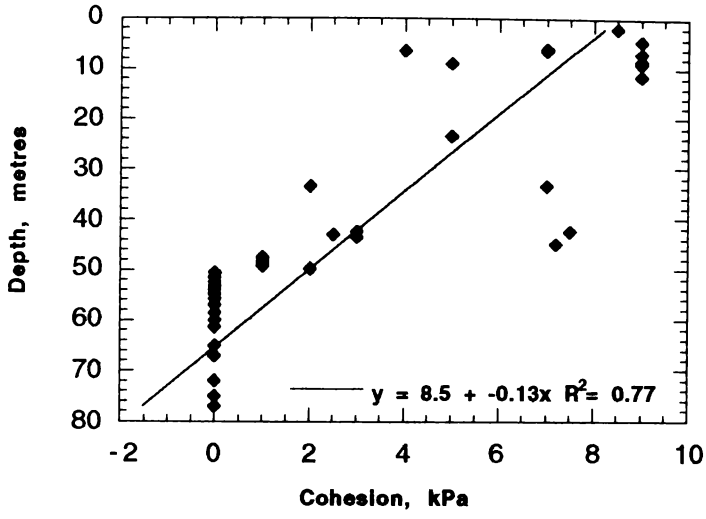

Figure 5.4a Plot of Depth vs Cohesion

5.9 Permeability

Permeability values for 34 samples were measured; each measurement represents a mean of 3 replicates (Table 5.6). Permeability could not be determined for fresh rock. Slightly weathered basalt has a low average permeability value of 0.1 x 10^{-4} m/s. It increases two-fold to 0.2 x 10^{-4} m/s in moderately weathered basalt. In highly weathered basalt, the value drastically increases to 7.7 x 10^{-4} m/s and in completely weathered basalt it is as high as 40 ± 9 x 10^{-4} m/s. It is clear that with increased weathering, permeability increases. The negative correlation (R^2 = 0.90) of permeability values with depth indicates this (Figure 5.4b).

5.10 The California Bearing Ratio

California Bearing Ratio values were obtained for 14 samples (Table 5.7). According to CBR test regulations, fresh rock samples have a CBR value of 100 %. It gradually decreases with the grade of weathering to values as low as 1 %. California Bearing Ratio correlates (R^2 = 0.75) positively with depth for a linear relationship with a higher regression coefficient of R^2 = 0.91 for a second order polynomial relationship (Figure 5.4c).

TABLE 5.6 PERMEABILITY VALUES OF SAMPLES			
Serial No.	Weathering Grade	Sample No.	Permeability x 10^{-4}, m/s
1	Slight	MPJ 14	0.1
2	Moderate	MPJ 9	0.2
3	Moderate	MPJ 10	0.2
4	Moderate	MPJ 11	0.2
5	Moderate	MPJ 12	0.2
6	Moderate	MPJ 13	0.2
7	Moderate	MPJ 15	0.1
8	Moderate	MPJ 16	0.2
9	Moderate	MPJ 17	0.2
10	Moderate	MPJ 18	0.2
11	Moderate	MPJ 19	0.2
12	Moderate	MPJ 20	0.2
13	Moderate	MPJ 21	0.2
	Average		**0.2**
	Std. Dev.		**0.05**
14	High	MPJ 38	7.7
15	High	MPJ 41	7.7
16	High	MPJ 44	7.7
17	High	MPJ 47	7.7
18	High	MPJ 49	7.8
19	High	MPJ 50	7.7
	Average		**7.7**
	Std. Dev.		**0.04**
20	Complete	MPJ 31	45.5
21	Complete	MPJ 32	43.3
22	Complete	MPJ 33	42.7
23	Complete	MPJ 34	45.7
24	Complete	MPJ 36	50.0
25	Complete	MPJ 58	26.8
26	Complete	MPJ 60	27.9
	Average		**40.3**
	Std. Dev.		**9.1**
27	Tephra	MPJ 22	25.0
28	Tephra	MPJ 23	25.0
29	Tephra	MPJ 25	25.0
30	Tephra	MPJ 26	25.0
31	Tephra	MPJ 27	25.0
32	Tephra	MPJ 28	25.0
	Average		**25.0**
	Std. Dev.		**0.0**
33	Paleosol	MPJ 29	**25.0**
34	MnO Inclusions	MPJ 39	**7.7**

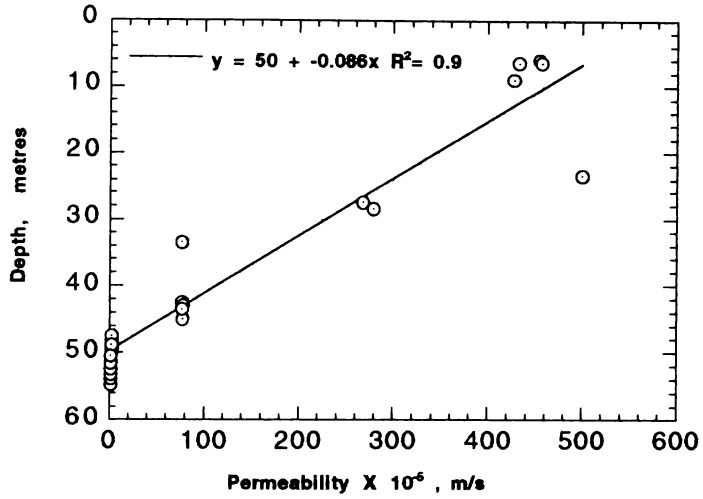

Figure 5.4b Plot of Depth vs Permeability

TABLE 5.7 CALIFORNIA BEARING RATIO VALUES

Serial No.	Weathering Grade	Sample No.	CBR %
1	Fresh	MPJ 1	100
2	Fresh	MPJ 4	100
3	Slight	MPJ 14	40
4	Slight	MPJ 51	45
5	Moderate	MPJ 10	25
6	Moderate	MPJ 18	30
7	High	MPJ 44	15
8	High	MPJ 50	15
9	Complete	MPJ 31	1
10	Complete	MPJ 34	4.5
11	Complete	MPJ 36	1
12	Complete	MPJ 60	3.5
13	Tephra	MPJ 22	4
14	Paleosol	MPJ 29	1

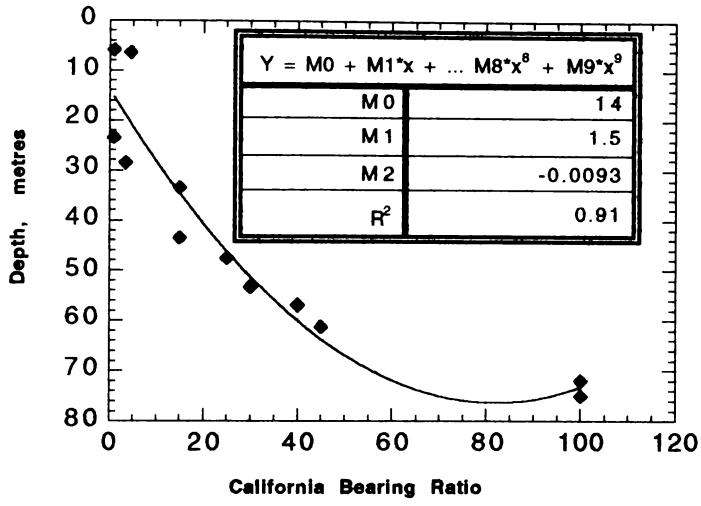

Figure 5.4c Plot of Depth vs California Bearing Ratio

5.11 All Geotechnical Parameters

All geotechnical and index parameters obtained and discussed so far are summarised in Appendix 5.3. Correlation matrix for these parameters and depth is given as Table 5.8. Within this matrix there are some gaps where certain tests demanded incompatible material characteristics (e.g. Schmidt hammer results could not be correlated with vane shear strength because they were tested on materials from different weathering grades). Of all these parameters, correlations of $R^2 \geq 0.64$ at 95% confidence level with depth were shown by UCS (point load), dry density, porosity, cohesion, permeability and CBR only (Table 5.8).

Regression analysis gives relationships between the following parameters:

a) Compressive strength (Point Load) with dry density (R^2: linear – 0.67; polynomial - 0.9)

(b) California Bearing Ratio with dry density (linear; $R^2 = 0.96$)

(c) California Bearing Ratio with porosity (linear; $R^2 = 0.85$)

(d) California Bearing Ratio with permeability (linear; $R^2 = 0.84$)

(e) California Bearing Ratio with cohesion (linear; $R^2 = 0.71$)

Plots of these relationships are given in Figures 5.5 a-c.

TABLE 5.8 LINEAR REGRESSION COEFFICIENTS (R SQUARED VALUES AT 95% CONFIDENCE LIMIT) FOR ALL GEOTECHNICAL TEST RESULTS AND DEPTH

	Depth metres	Water content %	CS Schm. MPa	CS P.Load MPa	Penetr resist MPa	Vane Sh. Str. kPa	Clay %	LL %	PL %	PI %	Activ. of Clay	C kPa	Phi degree	Density kg/m^3	Poros %	Perm m/s
Depth, m																
Water Content, %	0.37															
Comp. Strength (Schmidt), MPa	0.44	**0.74**														
Comp. Strength (Point Load), MPa	**0.73**	**0.86**	0.58													
Penetration Resistance, MPa	0.01	0.00	_	_												
Vane Shear Strength, kPa	0.17	0.00	_	_	0.07											
% Clay	0.15	0.04	_	_	0.19	0.00										
Liquid Limit, %	0.00	0.02	_	_	0.31	0.12	0.16									
Plastic Limit, %	0.01	0.01	_	_	0.42	0.09	0.07	**0.68**								
Plasticity Index, %	0.01	0.01	_	_	0.06	0.00	0.02	0.01	0.25							
Activity of Clay	0.27	0.00	_	_	0.04	0.00	0.52	0.04	0.03	0.39						
Cohesion, kPa	**0.77**	0.38	_	_	0.00	0.09	0.00	0.01	0.04	0.00	0.25					
Angle of Intern. Friction, Degrees	0.01	0.21	_	_	0.26	0.15	0.01	0.54	0.42	0.04	0.08	0.27				
Dry Density, kg/m^3	**0.69**	**0.65**	0.55	**0.67**	0.13	0.01	0.03	0.17	0.22	0.09	0.21	0.30	0.11			
Porosity, %	**0.81**	0.50	0.45	0.59	0.31	0.14	0.02	0.15	0.17	0.02	0.16	0.56	0.28	**0.88**		
Permeability, m/s	**0.90**	0.03	_	_	0.16	0.05	0.01	0.00	0.00	0.00	0.27	0.42	0.08	0.34	0.31	
California Bearing Ratio	**0.75**	0.08	_	_	0.24	0.14	0.02	0.00	0.02	0.11	0.22	**0.71**	0.20	**0.96**	**0.85**	**0.84**

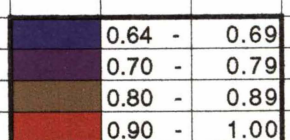

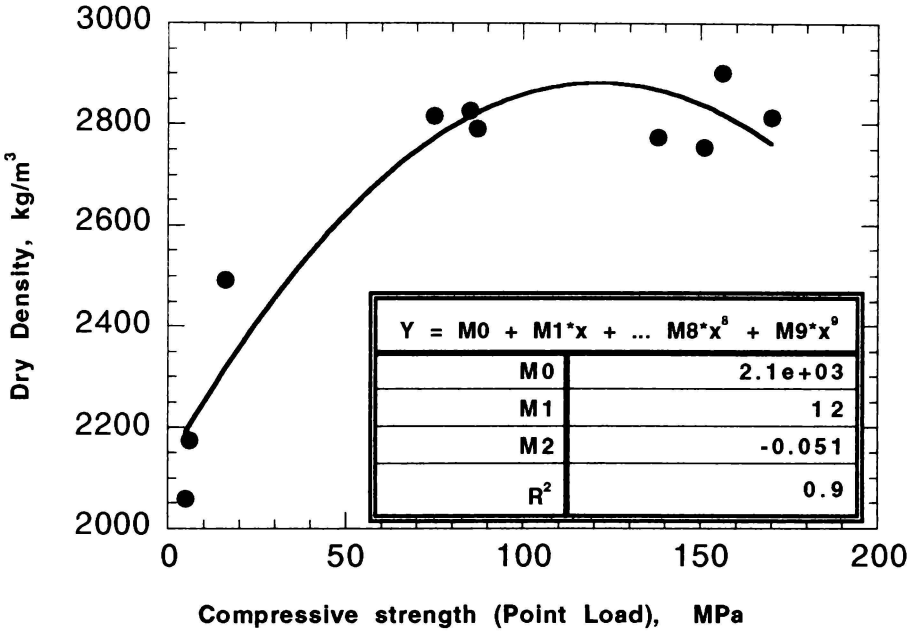

Figure 5.5a Dry Density vs Compressive Strength (Predicted by Point Load Index)

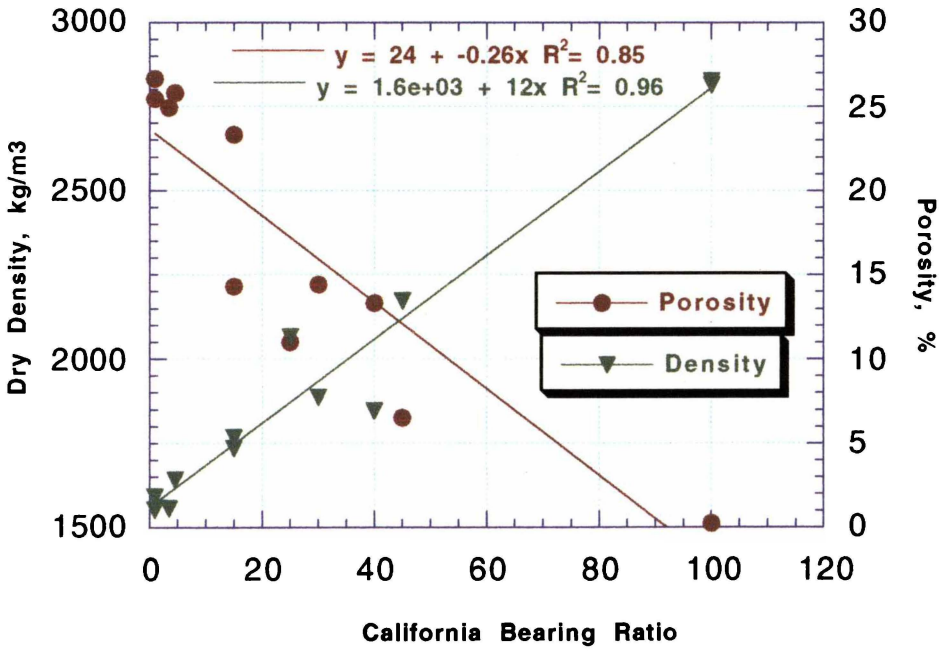

Figure 5.5b Plot of Density & Porosity vs CBR

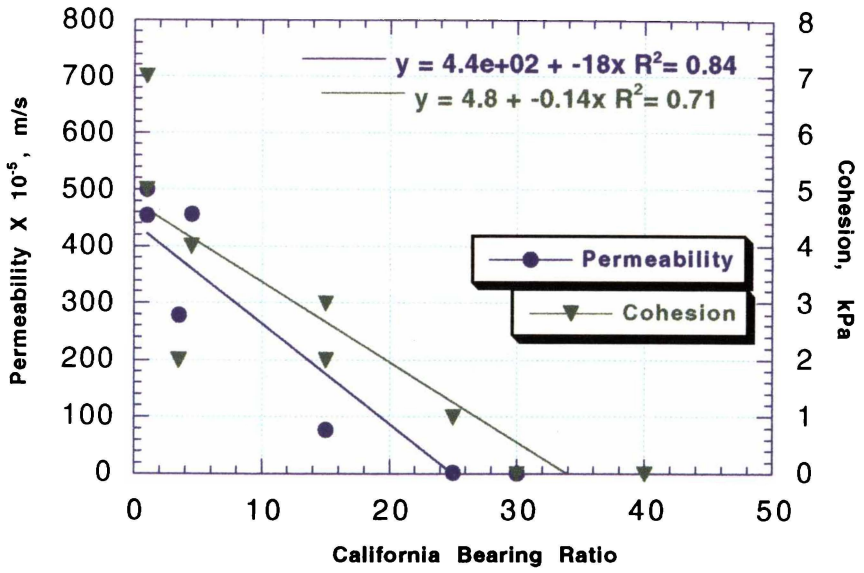

Figure 5.5c Plot of Permeability and Cohesion vs CBR

Most variations of geotechnical parameters with depth can be related to a general increase in rock weathering up-profile. Weathering of basalt causes the rock to gradually breakdown into smaller particles which are more loosely held together and clay minerals are formed in increasing quantities. These parameters can be grouped into two:

(a) Parameters that decrease from depth to surface i.e. dry density, compressive strength and California Bearing Ratio; and

(b) Parameters that increase from depth to surface i.e. porosity, permeability, cohesion and water content.

Parameters within each group show positive correlation with each other. Each parameter from one group shows negative correlation with every parameter in the other group. So the explanation of the geotechnical aspects of the process of weathering is simplified. Due to weathering:

(a) From fresh rock to slightly weathered stage, porosity increases; and consequently permeability increases. An increase in the porosity values does not necessarily mean that there must be a corresponding increase in permeability, but in Karamu

weathering profile, inter-connectability of pores seems to be maintained in weathered material. Due to increase in porosity the density decreases causing the compressive strength as well as CBR values to decrease.

(b) At the moderately weathered stage, there is a marked increase in the abundance of clay-sized particles within associated increase in cohesion and plasticity. More water is retained in clay-rich material.

(c) With increased intensity of weathering, these trends are maintained but the changes become less pronounced.

5.12 Summary

The Karamu weathering profile consists of five stages of weathering: Fresh; slight; moderate; high and complete weathering. Residual soil (weathered material without the relict rock structure) is not formed because of overlying rhyolitic tephra and paleosols. Jointing is present in fresh rocks and their traces can be seen even in completely weathered rocks. Highly and completely weathered material form unstable slopes where rotational and slab failure easily occurs.

Unconfined compressive strength can best be determined using core samples on a loading machine with parallel plates. If large samples cannot be obtained for coring, point load testing is recommended on regular shapes or irregular lumps. Schmidt rebound hammer should be used only in the extreme case when samples cannot be collected but can be tested *in situ*. Atterberg limits and angle of internal friction do not show relationships with other parameters. With weathering porosity, permeability, cohesion and water content increase, whereas density, strength and CBR values decrease.

CHAPTER 6: RELATIONSHIPS BETWEEN GEOCHEMICAL AND GEOTECHNICAL PROPERTIES AND COMPARISON WITH OTHER LITHOLOGIES

6.1 Introduction

The geochemical and geotechnical results and observations obtained were used to explore possible relationships and trends that indicate geochemical influences on the geotechnical properties. The aims were: a) to identify the geochemical parameters which show statistically acceptable relationships with geotechnical parameters, and b) to determine which combinations of the geochemical parameters could serve as predictors of geotechnical parameters.

Values of some important geochemical and geotechnical parameters show that they sometimes overlap in adjoining grades of weathering. Therefore, relationships were sought for all available values without grouping them into weathering grades. The data for samples of rhyolitic tephra, paleosols and inclusions were not included in this analysis.

Initially linear, semi-logarithmic and second order polynomial regression analyses were used to identify these relationships. The regression coefficient values (R^2) at 95% confidence level for all available geochemical and geotechnical data and depth were determined (Table 6.1). Fr those parameters which had zero values, logarithmic relationships could not be determined. Those geotechnical parameters which showed acceptable correlations ($R^2 \geq 0.64$, as defined in Chapter 3) with geochemical parameters are given as plots in this chapter. However, plots with high R^2 values that did not produce convincing plots, in terms of spread of data points or clusters, were excluded. Principal component analysis was carried out with all geochemical data. Best subsets regression analysis was carried out and some groups of geochemical parameters were identified as predictors of geotechnical values. The value of these predictors for different lithologies was examined using independent datasets.

TABLE 6.1 REGRESSION COEFFICIENTS (R SQUARED VALUES AT 95% CONFIDENCE LIMIT) FOR ALL GEOTECHNICAL TEST RESULTS VS GEOCHEMICAL TEST RESULTS AND DEPTH

		Depth	SiO2	Al2O3	MnO	MgO	CaO	Na2O	K2O	TiO2	P2O5	Fe2O3	FeO	StrWat	Th	Nb	Zr	Sr	Rb	Ba	V	Cr	Ni	Zn	La	Ce	Nd	Ga	Pb	Y	Ruxton	Reiche	Reiche	Miura	Parker	New	pH	EC
		metres	%	%	%	%	%	%	%	%	%	%	%	%	ppm	ppm	ppm	ppm	ppm	ppm	ppm	ppm	ppm	ppm	ppm	ppm	ppm	ppm	ppm	ppm	Ratio	P.I.	W.P.I.	W.I.	W.I.	W.I.		
Water	linear	0.37	0.25	0.65	0.02	0.74	0.75	0.66	0.59	0.04	0.00	0.47	0.73	0.70	0.30	0.04	0.47	0.70	0.22	0.01	0.03	0.00	0.01	0.01	0.00	0.24	0.00	0.60	0.23	0.01	0.74	0.02	0.76	0.75	0.75	0.75	0.69	0.19
Content	log	0.14	0.26	0.70	0.01	0.53				0.01	0.01	0.62	0.62	0.70	0.51	0.01	0.50	**0.62**	0.20	0.00	0.01	0.03	0.02	0.03	0.02	0.14	0.02	0.69	0.55	0.07	0.72	0.06		0.68		0.71	0.66	0.23
%	polyn	0.68	0.26	0.76	0.15	0.74	0.75	0.72	0.65	0.13	0.19	0.67	0.73	0.73	0.55	0.20	0.54	0.73	0.22	0.03	0.05	0.11	0.14	0.11	0.05	0.25	0.01	0.74	0.36	0.07	0.74	0.23	0.76	0.76	0.75	0.76	0.72	0.23
UCS	linear	0.44	0.60	0.43	0.32	0.39	0.44	0.72	0.81	0.49	0.22	0.41	0.27	0.59	0.00	0.52	0.52	0.63	0.89	0.42	0.47	0.46	0.46	0.38	0.29	0.24	0.19	0.51	0.30	0.11	0.53	0.44	0.49	0.54	0.44	0.52	0.52	0.00
Schmidt	log	0.45	0.57	0.44	0.36	0.40				0.52	0.19	0.43	0.32	0.70	0.11	0.56	0.56	0.51	0.71	0.39	0.49	0.48	0.49	0.40	0.48	0.21	0.33	0.54	0.33	0.21	0.49	0.46		0.46		0.45	0.50	0.00
MPa	polyn	0.47	0.46	0.46	0.40	0.39	0.44	0.77	0.85	0.63	0.57	0.58	0.57	0.71	0.10	0.66	0.66	0.71	0.90	0.52	0.51	0.48	0.52	0.45	0.61	0.30	0.50	0.61	0.34	0.44	0.86	0.81	0.85	0.85	0.85	0.85	0.67	0.00
UCS	linear	0.73	0.78	0.57	0.38	0.49	0.66	0.92	0.91	0.64	0.24	0.50	0.26	0.86	0.09	0.67	0.63	0.79	0.83	0.67	0.64	0.62	0.61	0.58	0.58	0.18	0.31	0.57	0.47	0.28	0.74	0.69	0.69	0.77	0.66	0.74	0.64	0.00
Pt. Load	log	0.74	0.76	0.60	0.42	0.48				0.69	0.19	0.54	0.34	0.92	0.07	0.71	0.66	0.66	0.83	0.64	0.69	0.65	0.67	0.62	0.80	0.12	0.33	0.59	0.43	0.43	0.67	0.70		0.60		0.59	0.61	0.00
MPa	polyn	0.75	0.83	0.74	0.48	0.49	0.72	0.92	0.94	0.87	0.77	0.84	0.83	0.93	0.10	0.80	0.81	0.79	0.89	0.68	0.82	0.68	0.79	0.70	0.91	0.41	0.37	0.63	0.47	0.64	0.92	0.98	0.90	0.93	0.92	0.92	0.72	0.18
Penetr.	linear	0.01	0.09	0.02	0.00	0.14	0.02	0.30	0.21	0.05	0.03	0.06	0.06	0.01	0.16	0.03	0.23	0.03	0.33	0.00	0.06	0.03	0.05	0.03	0.01	0.01	0.04	0.01	0.08	0.02	0.08	0.00	0.00	0.06	0.02	0.06	0.09	0.23
Resist.	log	0.02	0.09	0.03	0.00	0.09				0.06	0.01	0.09	0.08	0.00	0.11	0.01	0.20	0.08	0.37	0.00	0.15	0.08	0.09	0.02	0.00	0.00	0.06	0.00	0.06	0.01	0.08	0.01		0.04		0.07	0.09	0.18
MPa	polyn	0.31	0.10	0.08	0.02	0.14	0.33	0.35	0.21	0.06	0.03	0.11	0.10	0.15	0.30	0.05	0.27	0.10	0.43	0.04	0.28	0.08	0.05	0.03	0.10	0.13	0.07	0.12	0.13	0.04	0.09	0.09	0.09	0.13	0.33	0.07	0.10	0.28
Shear	linear	0.04	0.20	0.25	0.29	0.25	0.23	0.18	0.17	0.27	0.18	0.28	0.08	0.00	0.07	0.30	0.15	0.00	0.20	0.30	0.22	0.26	0.49	0.27	0.00	0.20	0.33	0.00	0.28	0.39	0.05	0.10	0.01	0.37	0.21	0.16	0.01	0.04
Strength	log	0.03	0.22	0.25	0.18	0.29				0.26	0.20	0.28	0.08	0.00	0.08	0.26	0.15	0.01	0.17	0.15	0.26	0.24	0.26	0.23	0.03	0.16	0.34	0.00	0.36	0.32	0.05	0.23		0.30		0.17	0.01	0.02
kPa	polyn	0.10	0.33	0.25	0.36	0.33	0.31	0.18	0.36	0.27	0.19	0.28	0.08	0.01	0.09	0.32	0.15	0.12	0.26	0.59	0.32	0.26	0.63	0.30	0.12	0.20	0.37	0.04	0.41	0.39	0.06	0.45	0.02	0.41	0.31	0.18	0.01	0.08
% Clay	linear	0.15	0.04	0.17	0.01	0.01	0.02	0.01	0.01	0.01	0.00	0.00	0.01	0.01	0.08	0.01	0.18	0.00	0.27	0.02	0.00	0.02	0.06	0.01	0.01	0.03	0.03	0.23	0.01	0.07	0.19	0.11	0.12	0.03	0.00	0.00	0.07	0.00
	log	0.24	0.03	0.17	0.00	0.02				0.01	0.03	0.00	0.01	0.01	0.06	0.03	0.17	0.00	0.19	0.06	0.00	0.02	0.06	0.01	0.01	0.03	0.01	0.19	0.01	0.06	0.15	0.05		0.06		0.00	0.08	0.00
	polyn	0.36	0.32	0.17	0.01	0.04	0.02	0.01	0.01	0.02	0.01	0.02	0.01	0.22	0.10	0.07	0.18	0.00	0.37	0.19	0.03	0.03	0.07	0.01	0.01	0.03	0.19	0.28	0.01	0.09	0.33	0.29	0.34	0.05	0.01	0.01	0.22	0.01
Liquid	linear	0.00	0.32	0.02	0.35	0.01	0.02	0.27	0.18	0.39	0.36	0.37	0.37	0.09	0.23	0.32	0.11	0.02	0.22	0.02	0.46	0.38	0.14	0.23	0.13	0.04	0.02	0.03	0.07	0.00	0.21	0.38	0.03	0.04	0.02	0.03	0.08	0.12
Limit	log	0.00	0.30	0.02	0.32	0.01				0.35	0.36	0.36	0.37	0.07	0.21	0.32	0.11	0.02	0.22	0.02	0.46	0.38	0.14	0.23	0.13	0.04	0.02	0.03	0.07	0.00	0.21	0.38		0.04		0.03	0.08	0.12
	polyn	0.04	0.32	0.02	0.35	0.01	0.02	0.27	0.18	0.39	0.36	0.37	0.37	0.09	0.23	0.32	0.11	0.02	0.22	0.02	0.46	0.38	0.14	0.23	0.13	0.04	0.02	0.03	0.07	0.00	0.21	0.38	0.03	0.04	0.02	0.03	0.08	0.18
Plastic	linear	0.01	0.07	0.01	0.11	0.02	0.06	0.18	0.17	0.11	0.13	0.12	0.12	0.03	0.01	0.09	0.00	0.00	0.02	0.00	0.21	0.11	0.03	0.05	0.05	0.11	0.00	0.01	0.04	0.03	0.03	0.10	0.00	0.01	0.07	0.01	0.08	0.09
Limit	log	0.01	0.07	0.01	0.11	0.02				0.11	0.12	0.11	0.12	0.02	0.00	0.08	0.01	0.00	0.02	0.00	0.21	0.11	0.03	0.05	0.05	0.11	0.00	0.01	0.04	0.03	0.03	0.10		0.01		0.01	0.08	0.10
	polyn	0.04	0.07	0.01	0.11	0.02	0.06	0.18	0.17	0.13	0.15	0.14	0.16	0.05	0.02	0.10	0.02	0.03	0.02	0.00	0.21	0.11	0.03	0.05	0.05	0.11	0.00	0.01	0.04	0.03	0.03	0.10	0.00	0.01	0.07	0.01	0.08	0.12
PLasticity	linear	0.01	0.16	0.00	0.11	0.18	0.06	0.00	0.05	0.14	0.08	0.11	0.11	0.02	0.21	0.11	0.11	0.02	0.20	0.11	0.07	0.15	0.08	0.13	0.02	0.06	0.07	0.20	0.01	0.08	0.03	0.10	0.04	0.18	0.06	0.17	0.04	0.00
Index	log	0.01	0.16	0.00	0.11	0.18				0.11	0.06	0.12	0.11	0.01	0.30	0.10	0.10	0.01	0.20	0.11	0.07	0.15	0.06	0.11	0.02	0.04	0.05	0.21	0.00	0.07	0.03	0.08		0.17		0.15	0.03	0.00
	polyn	0.01	0.16	0.00	0.11	0.18	0.06	0.00	0.05	0.18	0.16	0.12	0.13	0.04	0.32	0.14	0.15	0.03	0.27	0.15	0.09	0.19	0.14	0.13	0.02	0.06	0.07	0.20	0.01	0.08	0.03	0.10	0.04	0.18	0.06	0.17	0.04	0.00
Activity	linear	0.18	0.21	0.09	0.17	0.04	0.03	0.00	0.17	0.11	0.09	0.07	0.07	0.07	0.03	0.10	0.25	0.01	0.58	0.15	0.02	0.08	0.04	0.04	0.02	0.05	0.00	0.47	0.02	0.01	0.50	0.32	0.05	0.04	0.03	0.04	0.17	0.03
of	log	0.28	0.17	0.09	0.17	0.04				0.11	0.10	0.05	0.06	0.06	0.02	0.10	0.22	0.00	0.42	0.13	0.01	0.09	0.04	0.03	0.02	0.04	0.02	0.42	0.00	0.00	0.41	0.30		0.03		0.03	0.18	0.02
Clay	polyn	0.35	0.56	0.09	0.17	0.04	0.03	0.00	0.17	0.17	0.11	0.07	0.09	0.06	0.05	0.12	0.27	0.02	0.78	0.16	0.03	0.10	0.04	0.05	0.05	0.06	0.03	0.51	0.03	0.02	0.72	0.32	0.05	0.04	0.03	0.04	0.17	0.03
Cohesion	linear	0.57	0.09	0.00	0.00	0.36	0.19	0.11	0.11	0.22	0.15	0.05	0.09	0.08	0.07	0.19	0.31	0.17	0.03	0.16	0.11	0.02	0.03	0.13	0.10	0.04	0.11	0.03	0.20	0.00	0.11	0.04	0.11	0.23	0.22	0.23	0.68	0.00
kPa	log	0.49	0.09	0.00	0.00	0.36				0.21	0.15	0.03	0.08	0.06	0.06	0.20	0.30	0.15	0.03	0.15	0.11	0.02	0.02	0.14	0.11	0.02	0.11	0.02	0.23	0.00	0.10	0.03		0.21		0.21	0.71	0.00
	polyn	0.60	0.09	0.00	0.00	0.36	0.19	0.11	0.11	0.28	0.15	0.06	0.12	0.10	0.09	0.21	0.32	0.18	0.03	0.17	0.15	0.04	0.05	0.13	0.13	0.05	0.11	0.04	0.21	0.00	0.16	0.08	0.15	0.27	0.25	0.25	0.84	0.01
Angle of	linear	0.01	0.07	0.03	0.03	0.12	0.05	0.03	0.03	0.04	0.04	0.05	0.41	0.02	0.17	0.33	0.15	0.18	0.13	0.02	0.04	0.22	0.14	0.03	0.05	0.12	0.01	0.00	0.05	0.01	0.10	0.12	0.05	0.03	0.07	0.03	0.05	0.03
Int. Fr.	log	0.02	0.07	0.03	0.03	0.12				0.03	0.03	0.04	0.40	0.01	0.15	0.32	0.16	0.16	0.12	0.02	0.04	0.22	0.14	0.03	0.05	0.12	0.01	0.00	0.04	0.00	0.08	0.10		0.01		0.01	0.03	0.02
Degrees	polyn	0.13	0.07	0.03	0.03	0.12	0.05	0.03	0.03	0.04	0.04	0.05	0.43	0.04	0.18	0.35	0.17	0.20	0.13	0.02	0.04	0.22	0.14	0.03	0.05	0.12	0.01	0.00	0.05	0.01	0.10	0.12	0.05	0.03	0.07	0.03	0.05	0.03
Dry	linear	0.69	0.14	0.78	0.05	0.85	0.86	0.78	0.65	0.01	0.08	0.42	0.86	0.70	0.38	0.00	0.42	0.82	0.12	0.00	0.02	0.01	0.01	0.01	0.04	0.00	0.06	0.63	0.33	0.02	0.78	0.00	0.82	0.86	0.86	0.87	0.95	0.02
Density	log	0.41	0.15	0.83	0.07	0.73				0.00	0.07	0.63	0.77	0.76	0.60	0.01	0.43	**0.85**	0.17	0.03	0.01	0.06	0.09	0.10	0.04	0.02	0.11	0.72	0.69	0.15	0.72	0.00		0.85		**0.86**	0.94	0.05
kg/m^3	polyn	0.90	0.15	0.86	0.25	0.85	0.86	0.84	0.67	0.18	0.21	0.74	0.86	0.81	0.58	0.24	0.44	0.86	0.18	0.11	0.13	0.31	0.24	0.23	0.04	0.06	0.08	0.76	0.48	0.11	0.82	0.18	0.85	0.88	0.86	0.88	0.95	0.07
Porosity,	linear	0.81	0.07	0.62	0.01	0.65	0.63	0.54	0.43	0.00	0.09	0.30	0.70	0.45	0.36	0.00	0.36	0.58	0.07	0.08	0.05	0.02	0.05	0.09	0.00	0.07	0.08	0.55	0.31	0.06	0.55	0.05	0.57	0.63	0.63	0.64	0.83	0.00
%	log	0.57	0.07	0.64	0.08	0.60				0.00	0.06	0.46	0.66	0.51	0.52	0.02	0.34	0.62	0.07	0.14	0.02	0.06	0.14	0.13	0.03	0.02	0.15	0.58	0.59	0.24	0.52	0.02		0.69		0.71	0.87	0.00
	polyn	0.88	0.11	0.65	0.22	0.66	0.64	0.60	0.45	0.08	0.21	0.56	0.72	0.58	0.47	0.12	0.36	0.61	0.07	0.17	0.14	0.22	0.15	0.17	0.02	0.09	0.12	0.58	0.41	0.18	0.57	0.18	0.62	0.67	0.64	0.67	0.92	0.01
Perm-	linear	0.90	0.13	0.00	0.20	0.06	0.12	0.03	0.06	0.03	0.08	0.01	0.01	0.33	0.06	0.04	0.00	0.14	0.18	0.53	0.00	0.09	0.28	0.16	0.06	0.08	0.21	0.10	0.07	0.12	0.18	0.59	0.35	0.07	0.13	0.10	0.51	0.32
eability	log	0.82	0.10	0.00	0.26	0.07				0.03	0.08	0.01	0.01	0.34	0.01	0.05	0.01	0.17	0.08	0.67	0.00	0.09	0.34	0.19	0.07	0.15	0.22	0.05	0.08	0.18	0.13	0.49		0.03		0.09	0.54	0.42
m/s	polyn	0.90	0.41	0.03	0.22	0.12	0.34	0.06	0.39	0.04	0.09	0.01	0.01	0.37	0.05	0.06	0.20	0.17	0.37	0.71	0.01	0.11	0.32	0.19	0.05	0.15	0.25	0.42	0.08	0.16	0.33	0.62	0.44	0.16	0.36	0.10	0.66	0.50
Californ.	linear	0.75	0.01	0.85	0.10	0.88	0.84	0.94	0.64	0.03	0.16	0.16	0.90	0.68	0.36	0.07	0.23	0.81	0.16	0.18	0.04	0.13	0.13	0.16	0.03	0.00	0.05	0.46	0.45	0.04	0.74	0.12	0.79	0.84	0.84	0.85	0.96	0.00
Bearing	log	0.46	0.01	0.90	0.24	0.74				0.08	0.23	0.37	0.83	0.76	0.53	0.12	0.19	0.86	0.14	0.18	0.03	0.21	0.28	0.26	0.17	0.01	0.16	0.55	0.83	0.20	0.67	0.09		0.89		0.92	0.97	0.01
Ratio	polyn	0.97	0.05	0.91	0.57	0.88	0.87	0.82	0.64	0.28	0.39	0.80	0.90	0.82	0.55	0.27	0.25	0.85	0.17	0.27	0.13	0.45	0.49	0.41	0.22	0.33	0.17	0.59	0.86	0.38	0.80	0.18	0.83	0.88	0.87	0.89	0.97	0.15

6.2 Influences of Individual Geochemical Factors on Geotechnical Parameters

6.2.1 Compressive Strength vs Geochemical Parameters

Only fresh and slightly weathered basalt could be tested for determination of compressive strength with the Schmidt hammer and point load methods. Penetration resistance was tried for the moderately, highly and completely weathered basalt.

6.2.1.1 Schmidt Rebound Hammer Method

Compressive strength values obtained by this method show, at 95% confidence level, positive linear correlations with Na_2O ($R^2 = 0.72$), K_2O ($R^2 = 0.81$) and Rb ($R^2 = 0.89$) concentration patterns. Na_2O and K_2O are below the detection levels in other weathering grades but in fresh and slightly weathered basalt the compressive strength (Schmidt) correlates positively with them. The plot of compressive strength (Schmidt) versus Rb is similar to the plots versus Na_2O and K_2O. Compressive Strength (Schmidt) shows polynomial correlations with the six weathering indices (Figures 6.1 a-d).

6.2.1.2 Point Load Test

Compressive strength values obtained by this method show polynomial correlations with SiO_2 ($R^2 = 0.83$), CaO ($R^2 = 0.72$), Zn ($R^2 = 0.70$), V ($R^2 = 0.82$) and Cr ($R^2 = 0.68$); linear correlations with Na_2O ($R^2 = 0.92$), K_2O ($R^2 = 0.91$), Rb ($R^2 = 0.83$) and Sr ($R^2 = 0.79$) concentration patterns. Compressive Strength (point load) shows polynomial correlations with the six weathering indices (Figures 6.2 a-j).

6.2.1.3 Penetration Resistance

Penetration resistance determination could be carried out only for weathered material. Penetration resistance values do not show any significant relationships with the geochemical parameters.

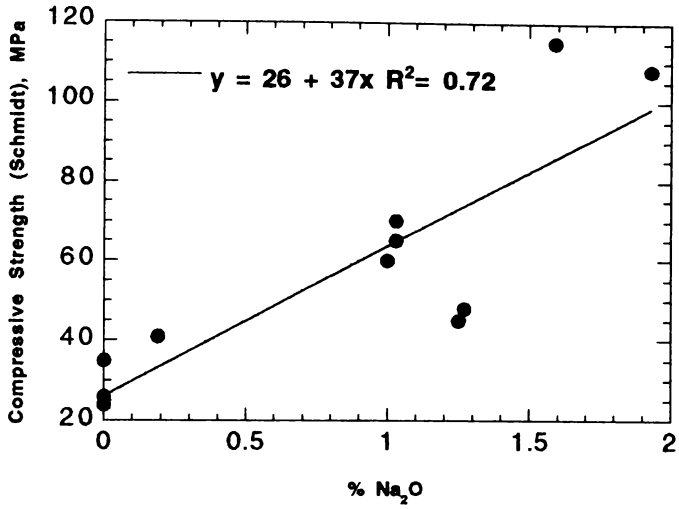

Figure 6.1a Plot of Compressive Strength (Predicted from Schmidt Hardness) vs % Na_2O

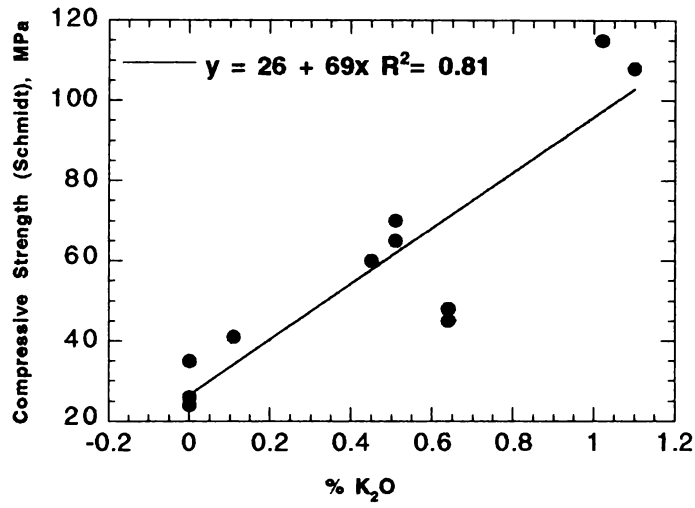

Figure 6.1b Plot of Compressive Strength (Predicted from Schmidt Hardness) vs % K_2O

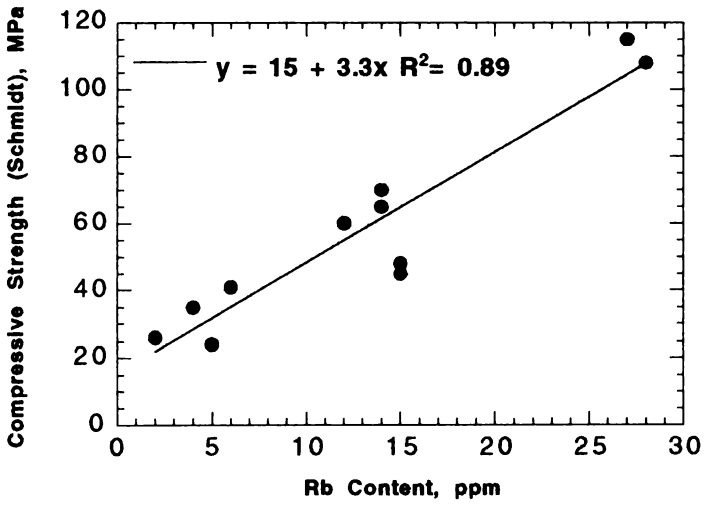

Figure 6.1c Plot of Compressive Strength (Predicted from Schmidt Hardness) vs Rb

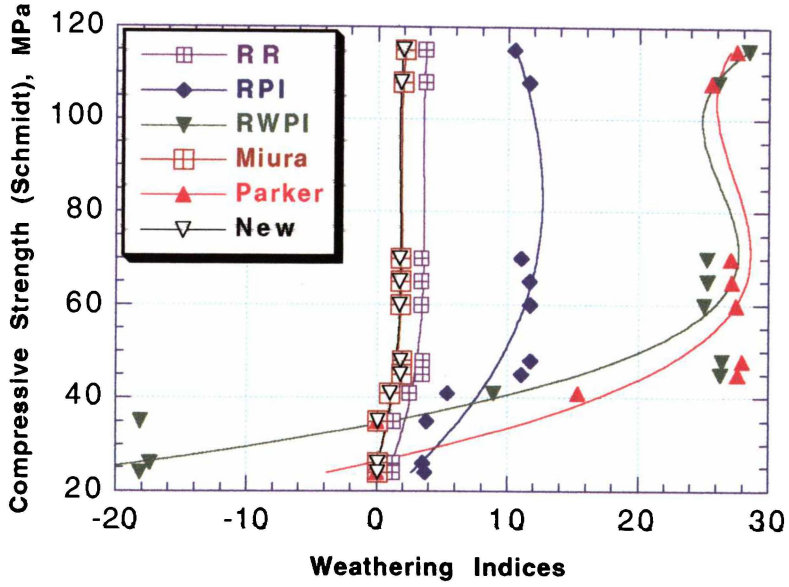

Figure 6.1d Plot of Compressive Strength (Predicted from Schmidt Hardness) vs Weathering Indices

$Y = M0 + M1*x + \ldots M8*x^8 + M9*x^9$	
M0	-3.9
M1	0.27
M2	-0.0032
M3	1.2e-05
R^2	0.86

$Y = M0 + M1*x + \ldots M8*x^8 + M9*x^9$	
M0	-8.6
M1	0.58
M2	-0.0047
M3	9.4e-06
R^2	0.81

$Y = M0 + M1*x + \ldots M8*x^8 + M9*x^9$	
M0	-1.2e+02
M1	5.4
M2	-0.065
M3	0.00025
R^2	0.85

$Y = M0 + M1*x + \ldots M8*x^8 + M9*x^9$	
M0	-4.1
M1	0.22
M2	-0.0027
M3	1.1e-05
R^2	0.85

$Y = M0 + M1*x + \ldots M8*x^8 + M9*x^9$	
M0	-63
M1	3.3
M2	-0.039
M3	0.00015
R^2	0.85

$Y = M0 + M1*x + \ldots M8*x^8 + M9*x^9$	
M0	-3.9
M1	0.21
M2	-0.0026
M3	1e-05
R^2	0.85

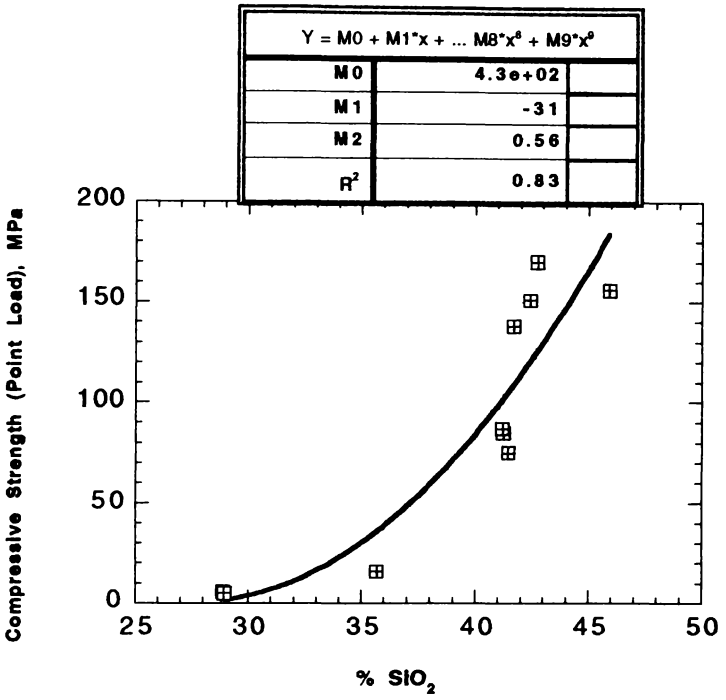

Figure 6.2a Plot of Compressive Strength (Predicted from Point Load Index) vs % SiO_2

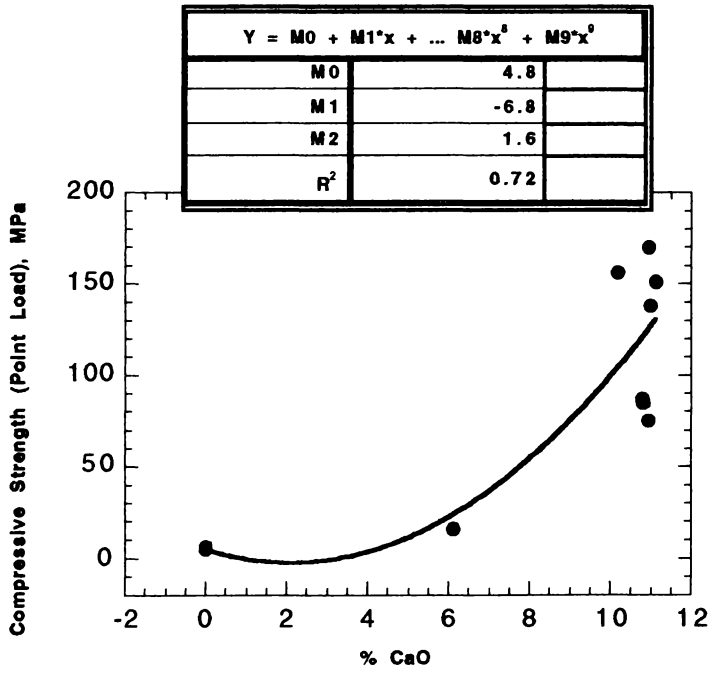

Figure 6.2b Plot of Compressive Strength (predicted by Point Load Index) vs % CaO

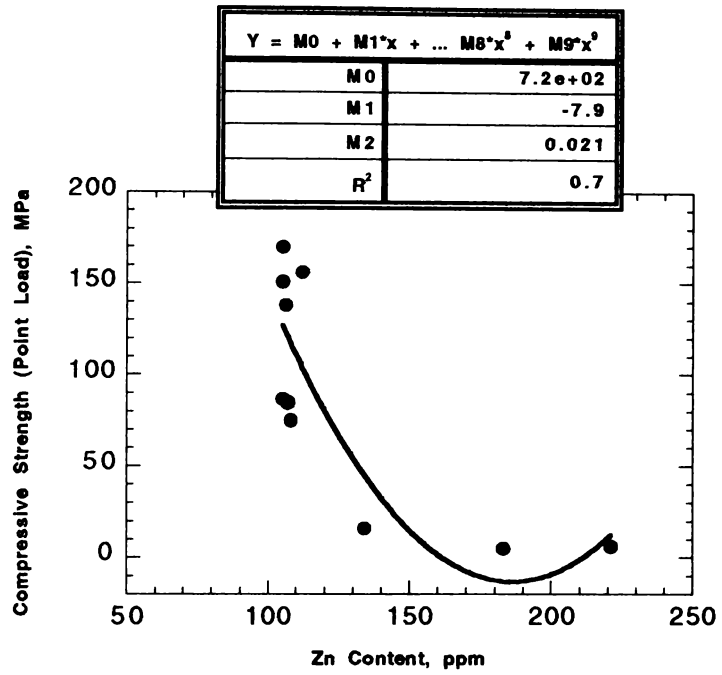

Figure 6.2 c Plot of Compressive Strength (Predicted by Point Load Index) vs Zn

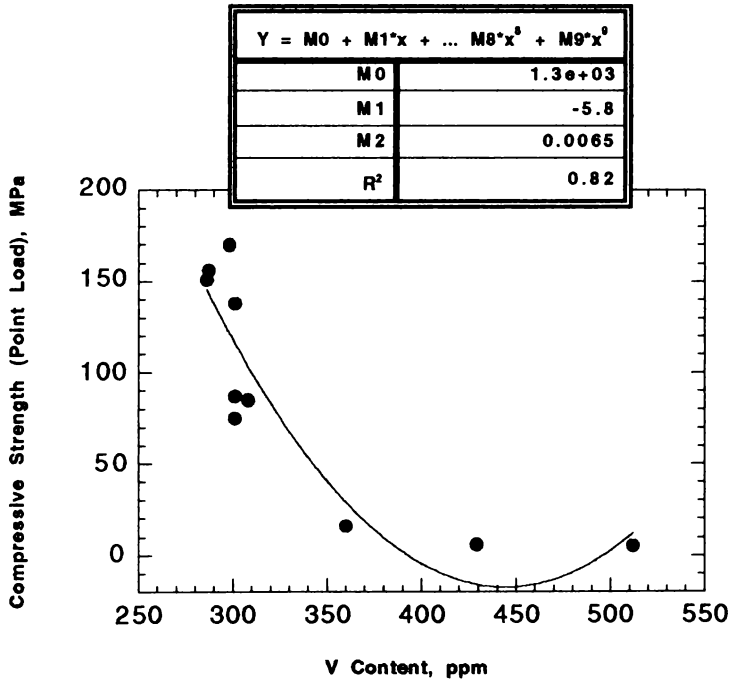

Figure 6.2d Plot of Compressive Strength (Predicted by Point Load Index) vs V

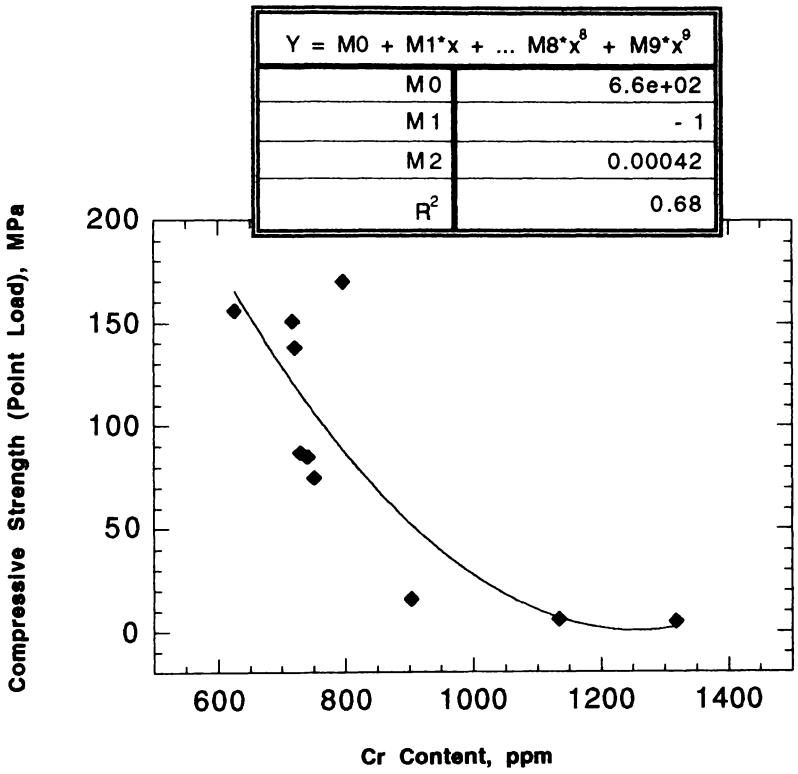

Figure 6.2e Plot of Compressive Strength (Predicted by Point Load Index) vs Cr

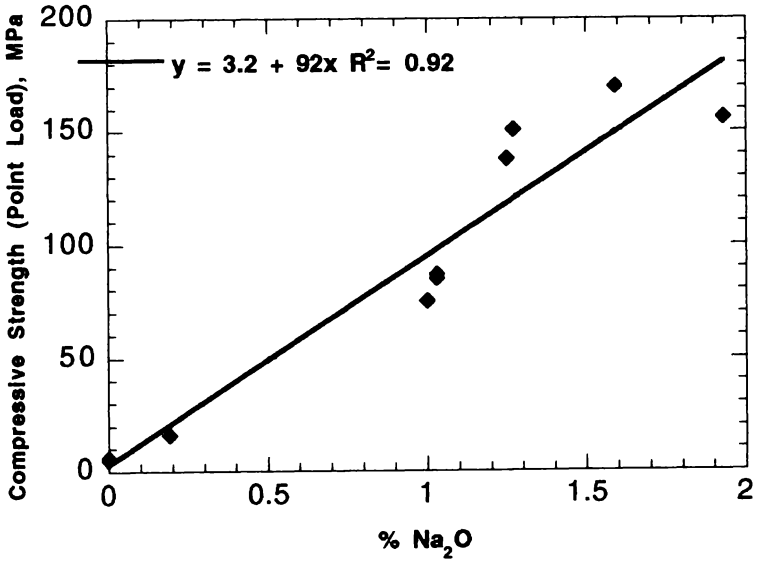

Figure 6.2f Plot of Compressive Strength (Predicted from Point Load Index) vs % Na_2O

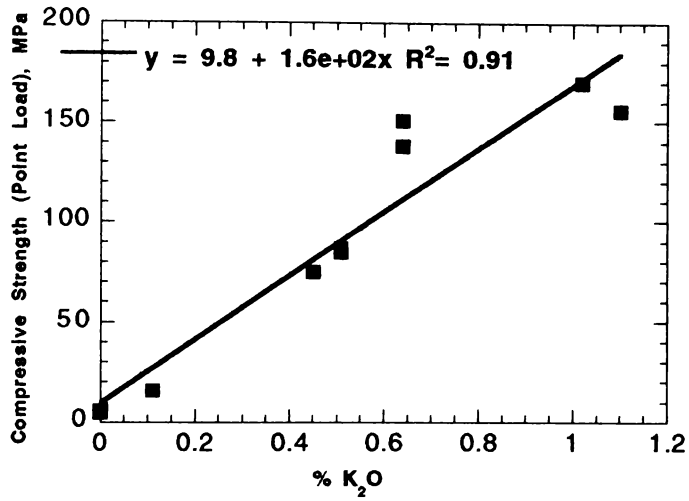

Figure 6.2g Plot of Compressive Strength (Predicted from Point Load Index) vs % K_2O

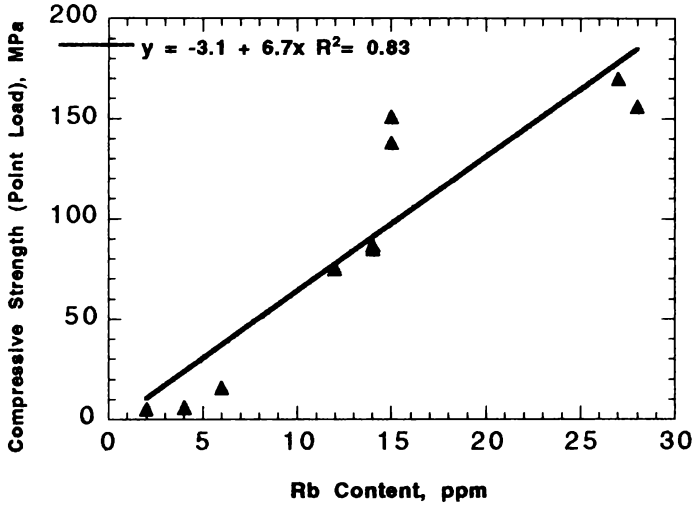

Figure 6.2h Plot of Compressive Strength (Predicted from Point Load Index) vs Rb

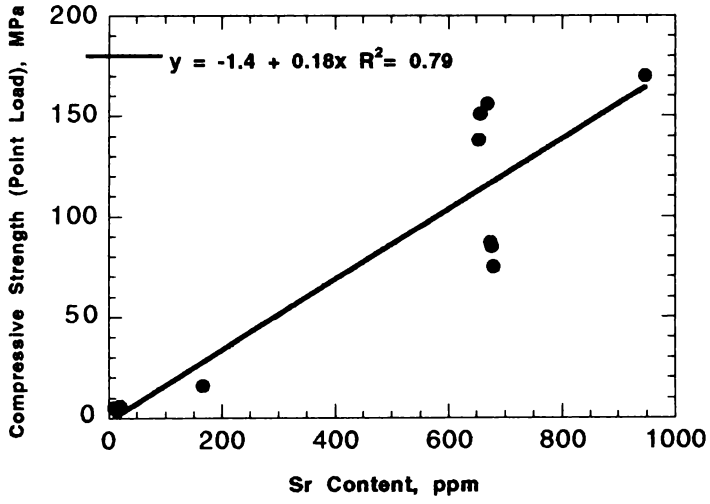

Figure 6.2i Plot of Compressive Strength (Predicted from Point Load Index) vs Sr

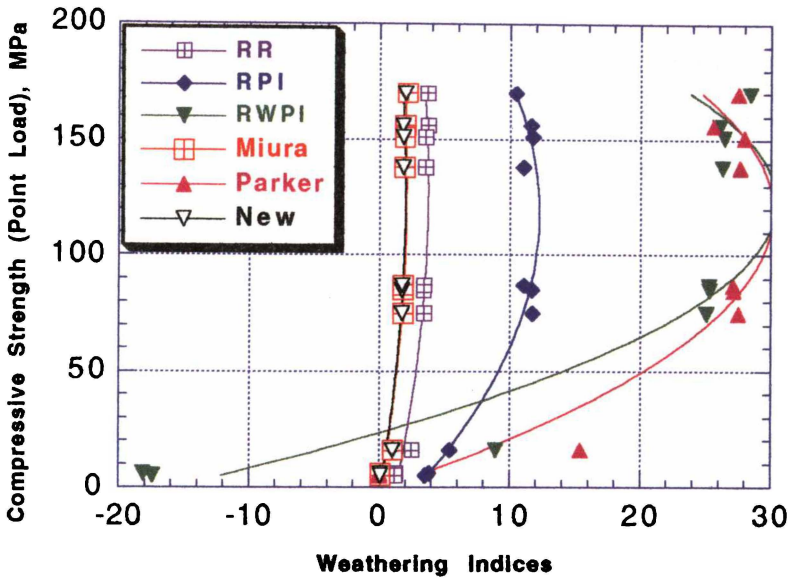

Figure 6.2 j Plot of Compressive Strength (Predicted from Point Load Index) vs Weathering Indices

$Y = M0 + M1*x + \ldots M8*x^8 + M9*x^9$	
M0	1.3
M1	0.038
M2	-0.00015
R^2	0.92

$Y = M0 + M1*x + \ldots M8*x^8 + M9*x^9$	
M0	2.9
M1	0.16
M2	-0.00067
R^2	0.98

$Y = M0 + M1*x + \ldots M8*x^8 + M9*x^9$	
M0	-16
M1	0.75
M2	-0.003
R^2	0.9

$Y = M0 + M1*x + \ldots M8*x^8 + M9*x^9$	
M0	0.14
M1	0.029
M2	-0.00011
R^2	0.93

$Y = M0 + M1*x + \ldots M8*x^8 + M9*x^9$	
M0	0.58
M1	0.5
M2	-0.0021
R^2	0.92

$Y = M0 + M1*x + \ldots M8*x^8 + M9*x^9$	
M0	0.14
M1	0.029
M2	-0.00011
R^2	0.92

6.2.2 Correlation between Shore Scleroscope Hardness and Olivine Rim Thickness

The presence of iddingsite rims was a noticeable feature in the olivine crystals examined under the microscope. Their presence points to the oxidation of olivine that causes Fe^{2+} to oxidise and turn into Fe^{3+} and precipitate as hematite, together with processes of clay mineral formation occurring at the same time. These rims become thicker with the intensity of weathering. Shore scleroscope measures the surface hardness that indicates the strength of material. Comparison of the iddingsite rim thickness (measured in thin sections under the microscope) and the Shore scleroscope hardness (measured on polished samples prepared from the same specimens), shows a significant negative linear correlation of $R^2 = 0.83$ between them. With increasing thickness of the rims, the surface hardness decreases (Figure 6.3). This relationship is possible because rim thickness and surface hardness are both related to the degree of rock weathering.

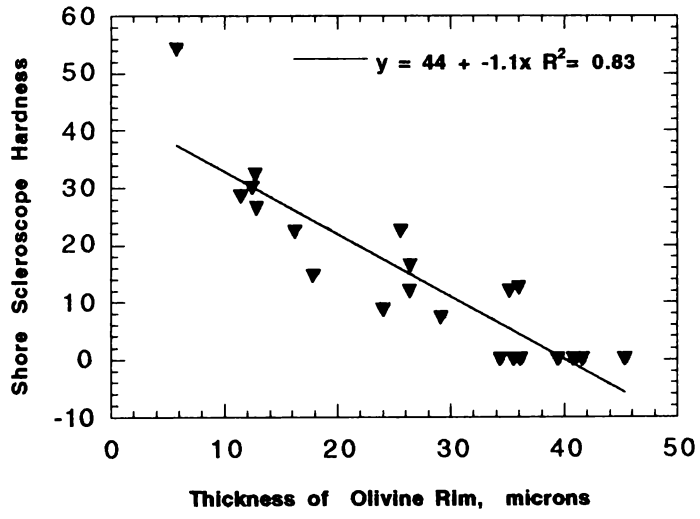

Figure 6.3 Plot of Shore Scleroscope Hardness vs Olivine Rim Thickness

The following equation can be written:

Shore Scleroscope Hardness = 44 - 1.1 x Rim Thickness (microns) ... 6.1

This equation enables us to estimate the possible hardness from thin sections of weathered basalt. The procedure would be to measure, under the microscope, the thickness of the iddingsite rims in microns. Using the above formula Shore scleroscope hardness can be obtained.

6.2.3. Shear Strength

6.2.3.1 Field Shear Vane

Shear strength values, obtained from field vane shear apparatus, do not show significant relationships with any of the geochemical parameters. It must be noted that these results are similar to penetration test results, and it is possible that these tests are not accurate enough to recognise subtle changes at later stages of weathering.

6.2.3.2 Cohesion and Angle of Internal Friction

Cohesion shows a significant negative linear correlation (R^2 = 0.68) with abrasion pH value, and a better (R^2 = 0.84) second order polynomial correlation (Figure 6.4). Angle of internal friction shows no significant relationship with geochemical parameters.

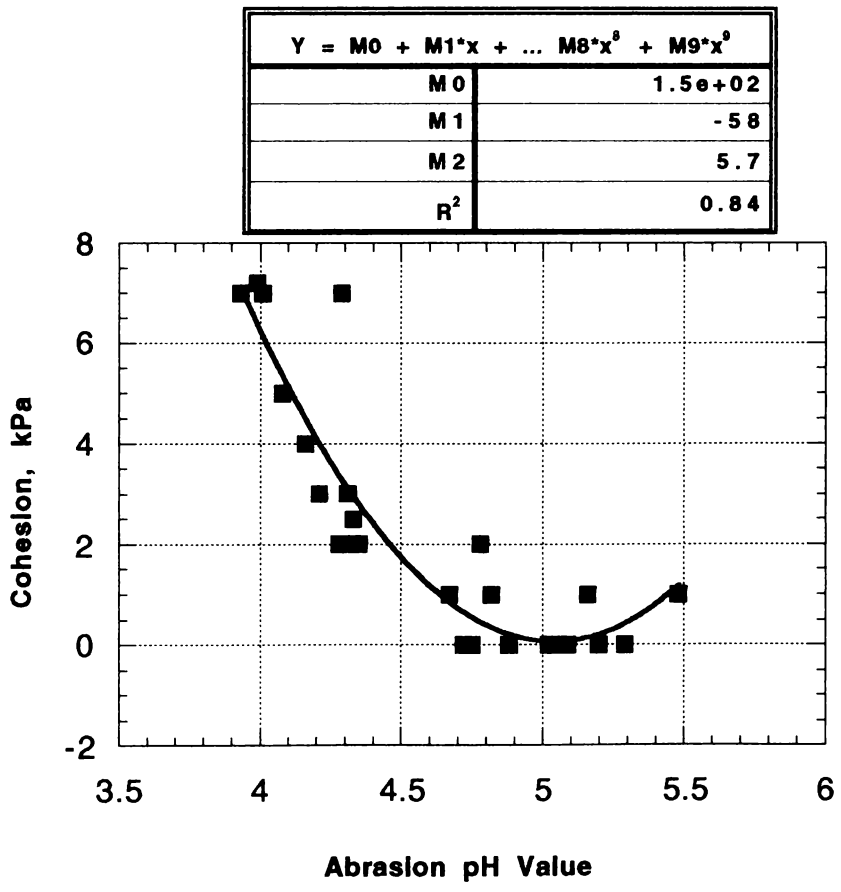

Figure 6.4 Plot of Cohesion vs Abrasion pH

6.2.4 Clay Content

Percentage of clay-sized material was determined by the particle size distribution analysis. These values do not show any relationship with the geochemical parameters.

6.2.5 Atterberg Limits and Activity of Clay

Atterberg limits and activity of clay do not demonstrate any correlation with geochemical parameters.

6.2.6 Water Content, Density and Porosity

Water content shows a positive linear relationship with structural water ($R^2 = 0.70$) and a negative linear relationship ($R^2 = 0.74$) with Ruxton's Ratio (Figures 6.5a and b).

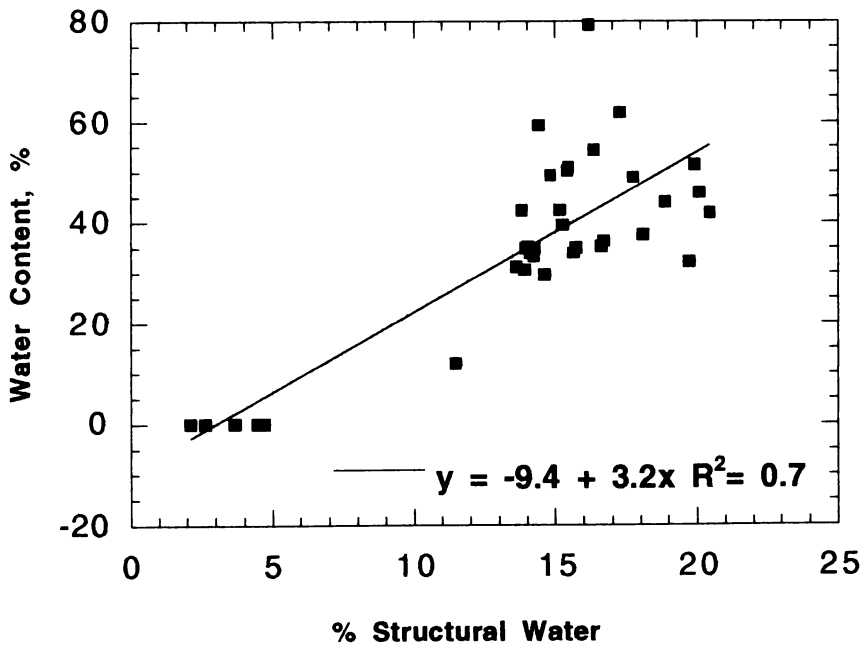

Figure 6.5a Plot of Water Content vs % Structural Water

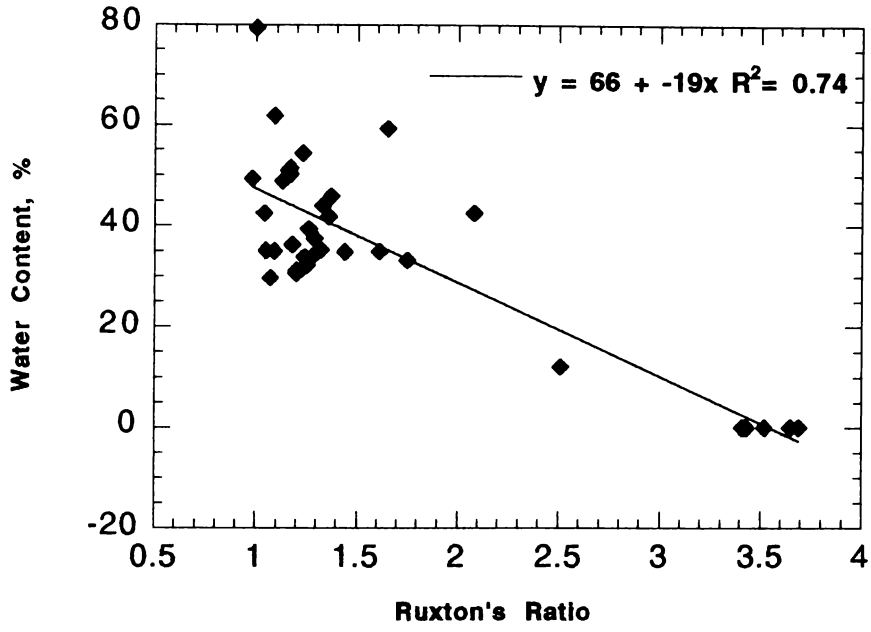

Figure 6.5b Plot of Water Content vs Ruxton's Ratio

Dry density shows a significant positive linear correlation with CaO (R^2 = 0.86), and FeO (R^2 = 0.86) and a negative linear correlation with Al_2O_3 (R^2 = 0.78) concentration patterns. It shows polynomial relationships with trace elements Sr (R^2 = 0.86) and Ga (R^2 = 0.76). A log-normal negative relationship is shown with Pb (R^2 = 0.69). Dry density shows a positive linear correlation of R^2 = 0.95 with abrasion pH values. It also correlates polynomially with Ruxton's Ratio (R^2 = 0.94); Miura (R^2 = 0.98) and New (R^2 = 0.98) weathering indices (Figures 6.6 a-h).

Porosity demonstrates an increase from depth to surface. During weathering, fracturing occurs and mineral grains are moved away from each other and the matrix becomes looser. The porosity is therefore expected to increase. Porosity shows polynomial correlations of R^2 = 0.92 with abrasion pH and of R^2 = 0.72 with FeO (Figures 6.7a and b).

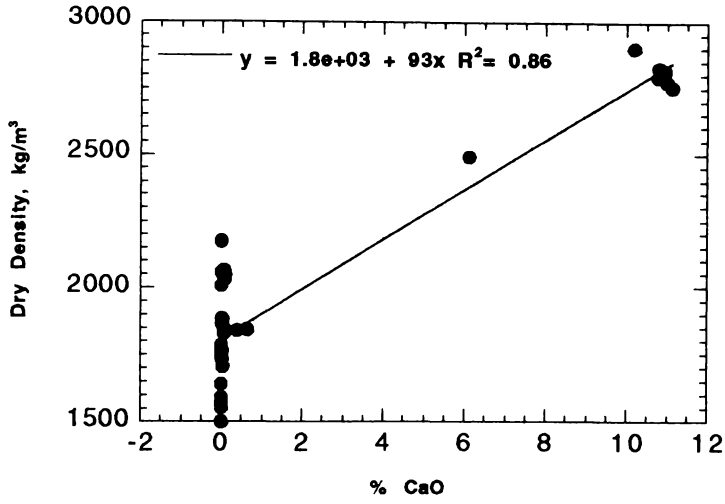

Figure 6.6a Plot of Dry Density vs % CaO

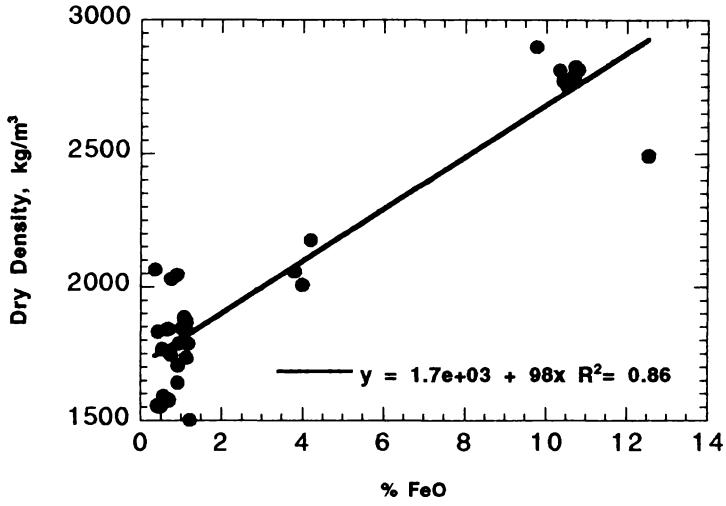

Figure 6.6b Plot of Dry Density vs FeO

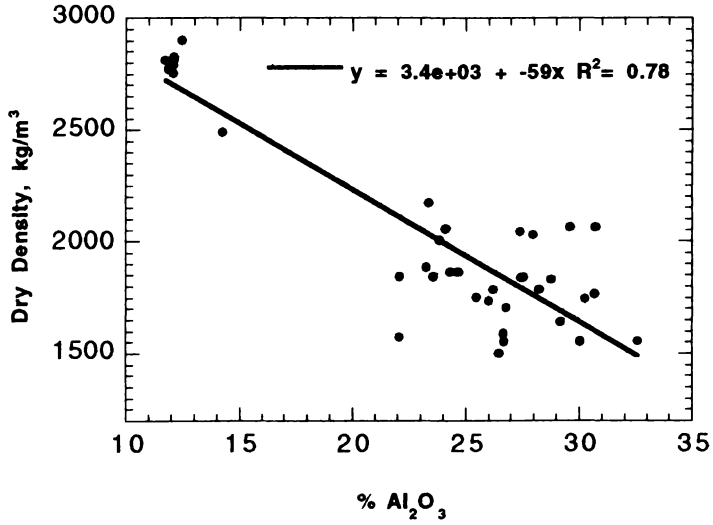

Figure 6.6c Plot of Dry Density vs % Al_2O_3

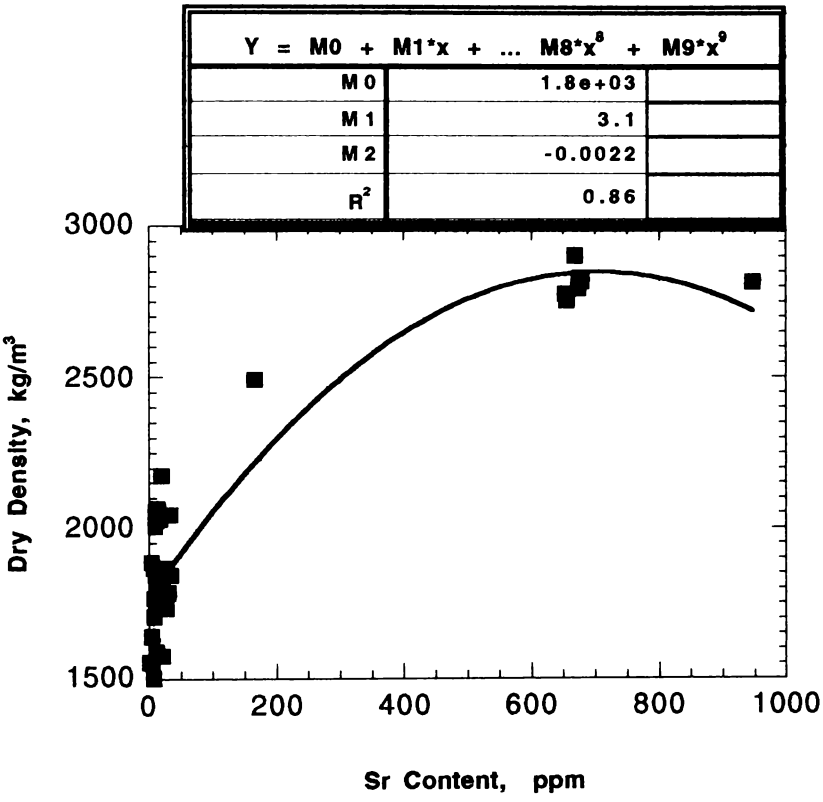

Figure 6.6d Plot of Dry Density vs Sr

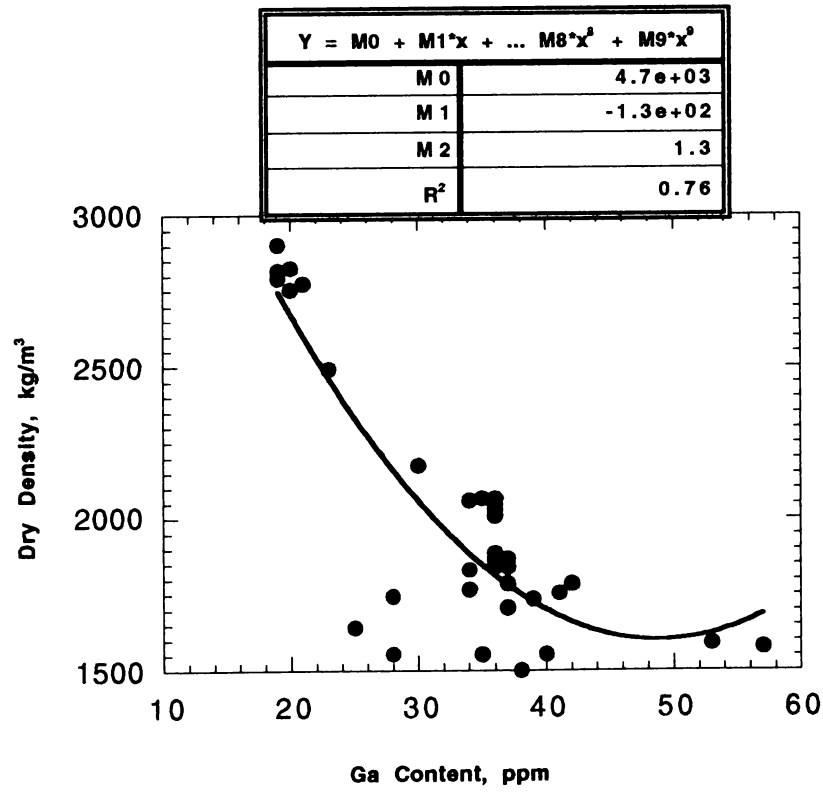

Figure 6.6e Plot of Dry Density vs Ga

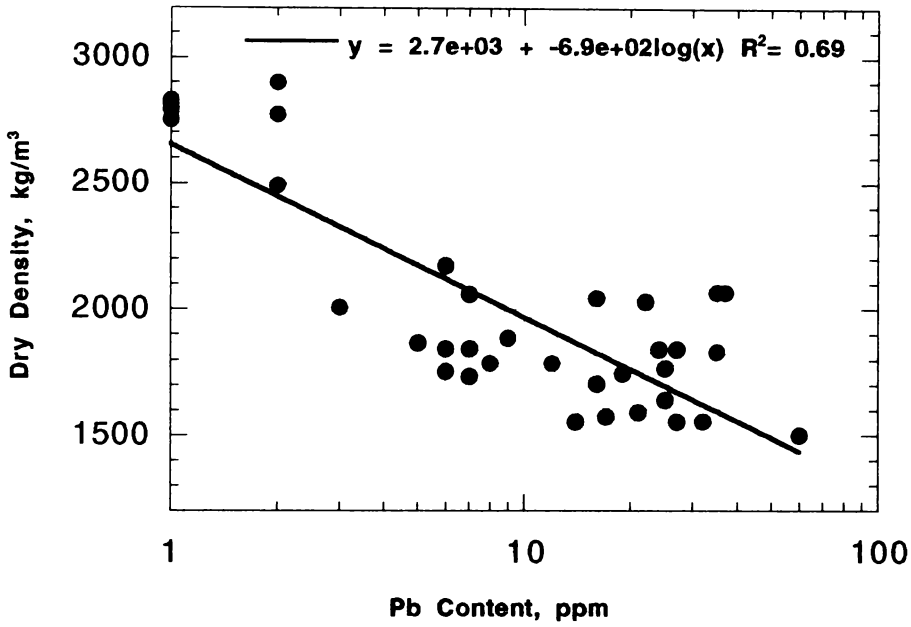

Figure 6.6 f Plot of Dry Density vs Pb

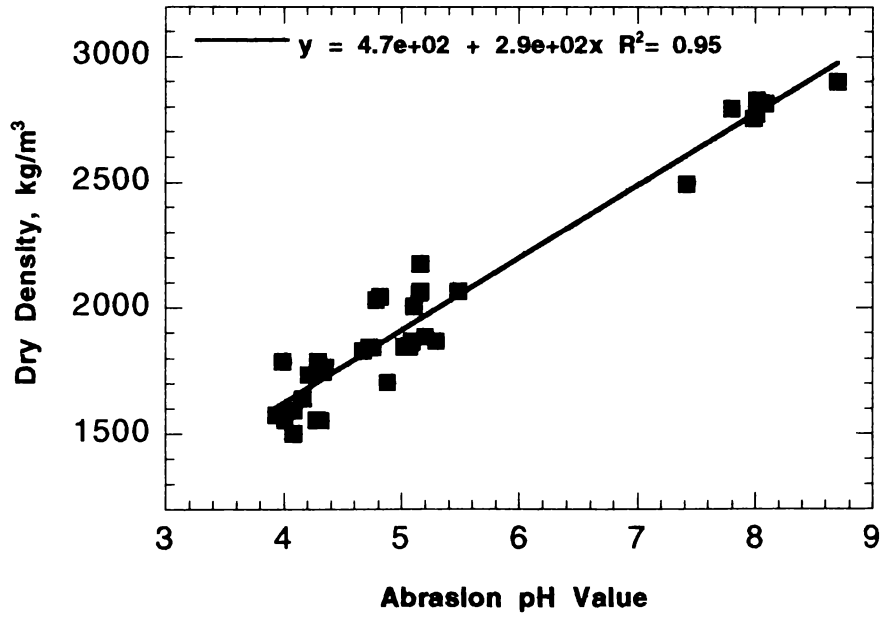

Figure 6.6g Plot of Dry Density vs Abrasion pH

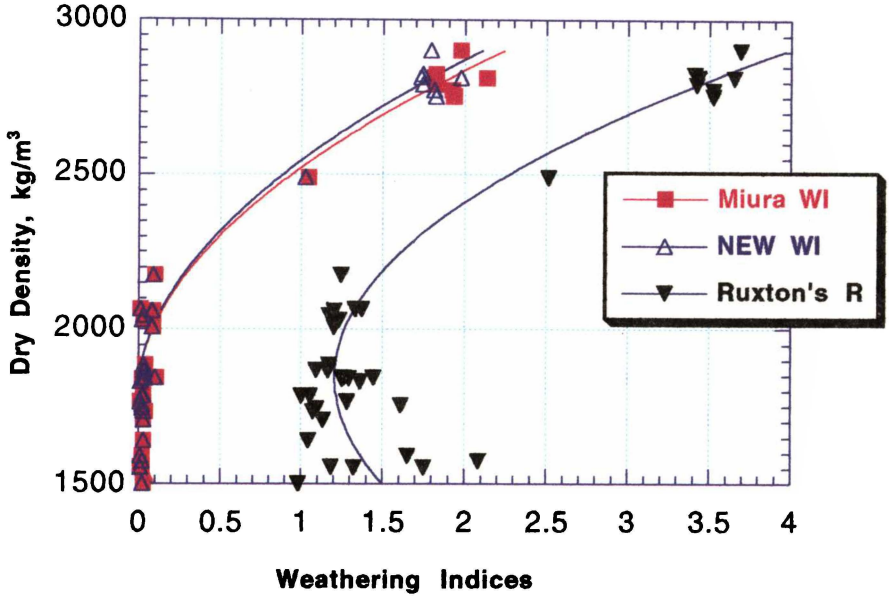

Y = M0 + M1*x + ... M8*x^8 + M9*x^9	
M0	5.3
M1	-0.006
M2	1.7e-06
R^2	0.98

Y = M0 + M1*x + ... M8*x^8 + M9*x^9	
M0	4.9
M1	-0.0056
M2	1.6e-06
R^2	0.98

Y = M0 + M1*x + ... M8*x^8 + M9*x^9	
M0	9.6
M1	-0.0091
M2	2.5e-06
R^2	0.94

Figure 6.6h Plot of Dry Density versus Weathering Indices

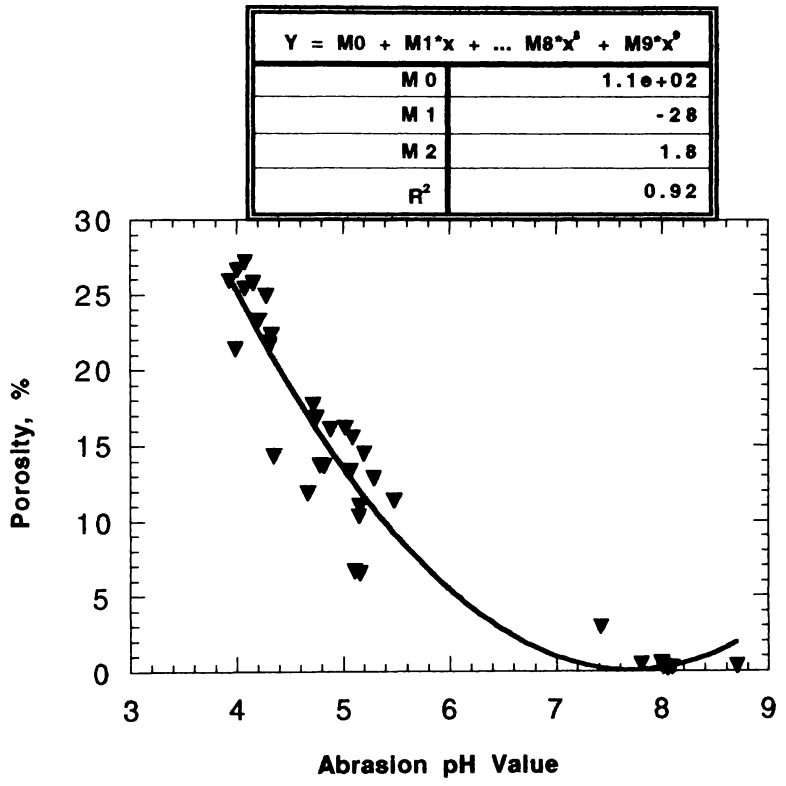

Figure 6.7a Plot of Porosity vs Abrasion pH

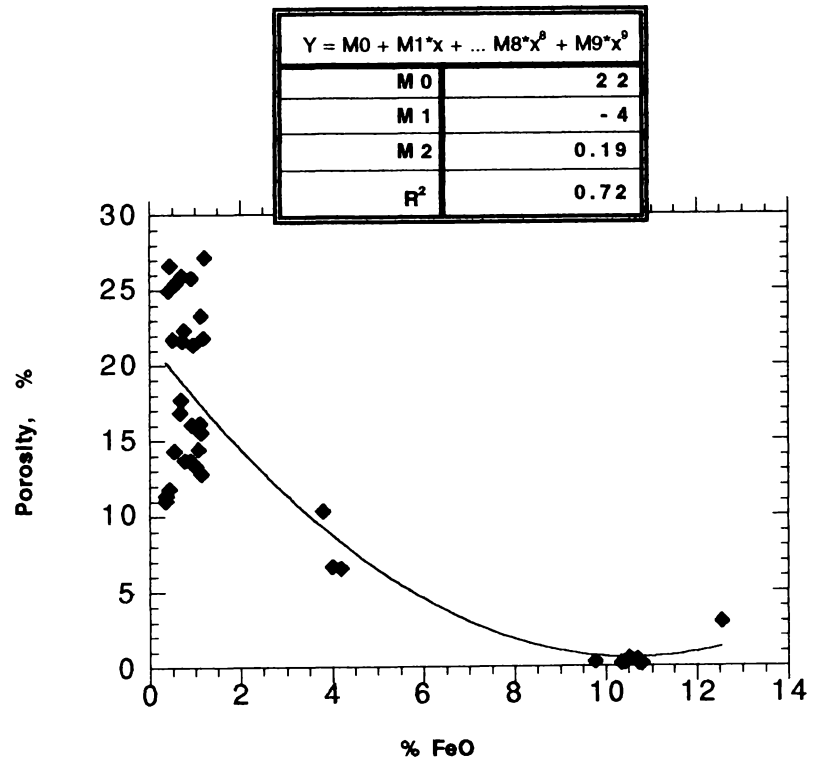

Figure 6.7b Plot of Porosity vs FeO

6.2.7 Permeability

Permeability does demonstrate significant polynomial relationships with the chemical parameters Ba content ($R^2 = 0.71$) and abrasion pH value ($R^2 = 0.66$) (Figures 6.8 a and b).

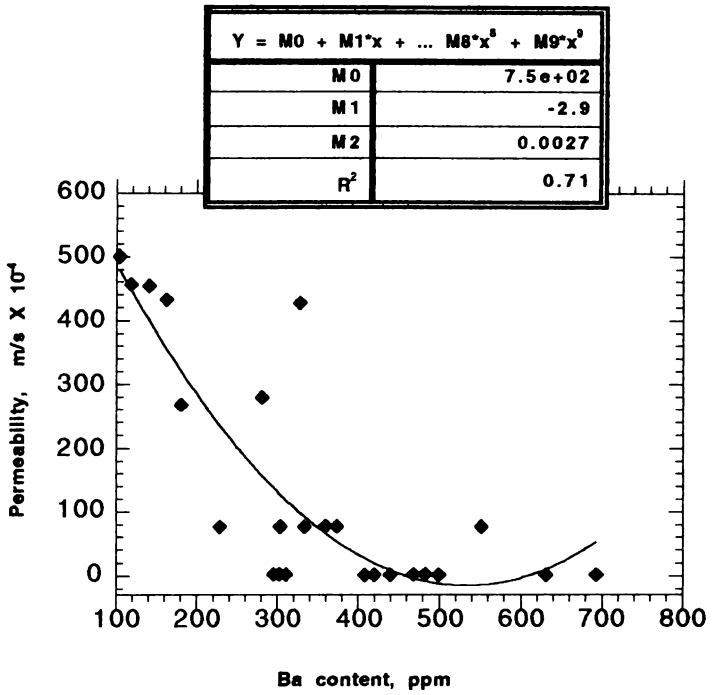

Figure 6.8a Plot of Permeability vs Ba

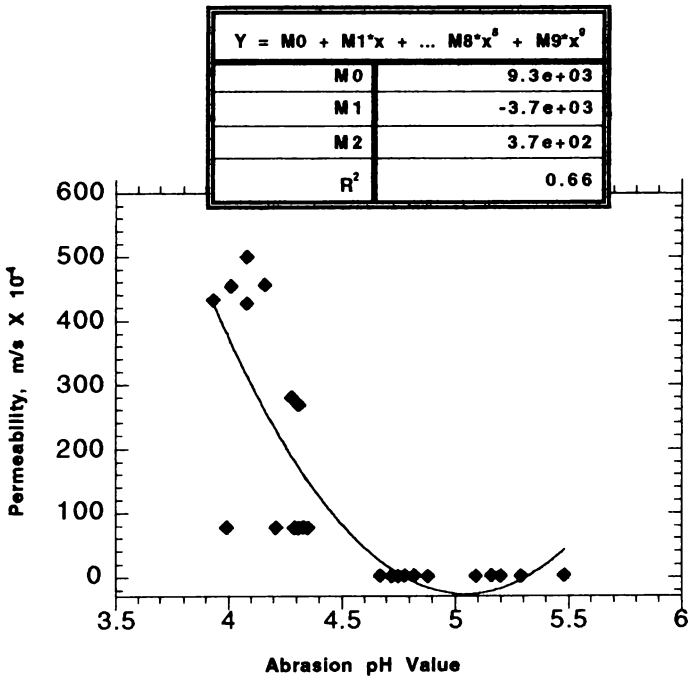

Figure 6.8b Plot of Permeability vs Abrasion pH

6.2.8 California Bearing Ratio

California Bearing Ratio shows positive linear relationships with MgO ($R^2 = 0.88$) and FeO ($R^2 = 0.90$) and a negative linear correlation with Al_2O_3 ($R^2 = 0.85$) concentration patterns. It shows a polynomial correlation ($R^2 = 0.86$) with Pb content and a positive linear correlation of $R^2 = 0.96$ with abrasion pH (Figures 6.9 a-e).

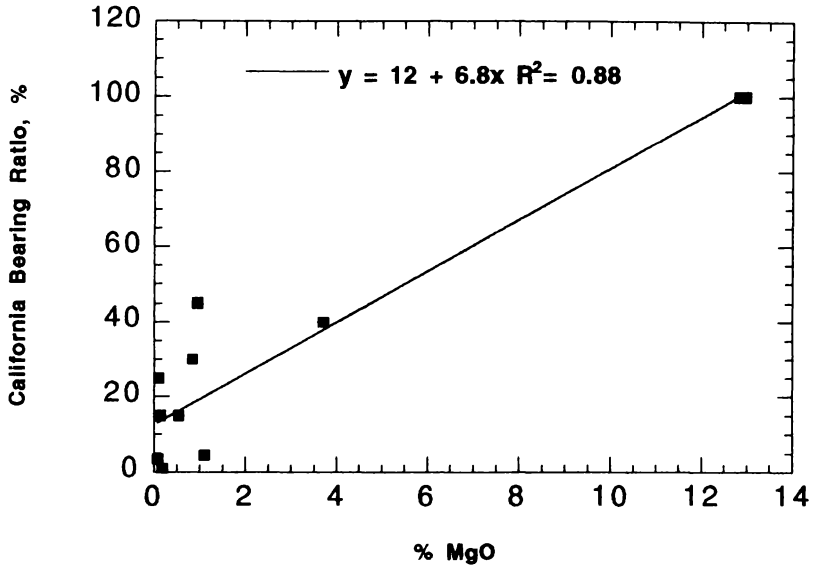

Figure 6.9 a Plot of California Bearing Ratio vs % MgO

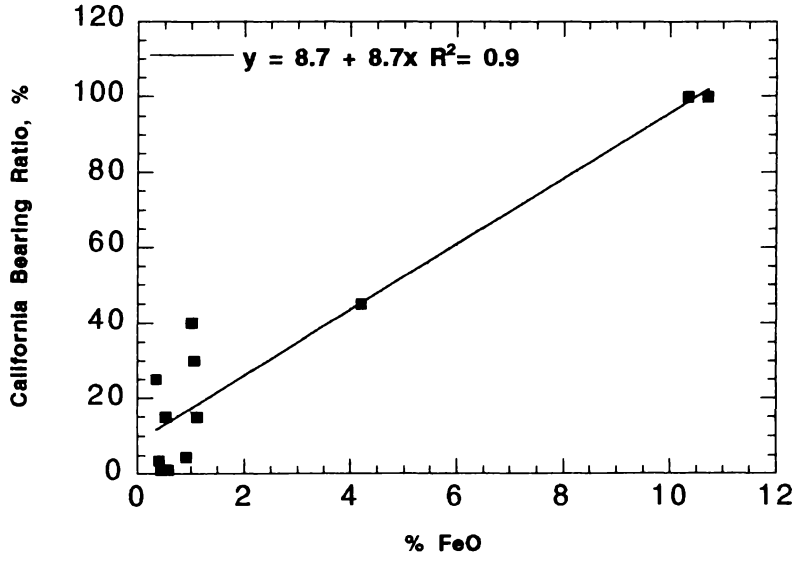

Figure 6.9b Plot of California Bearing Ratio vs % FeO

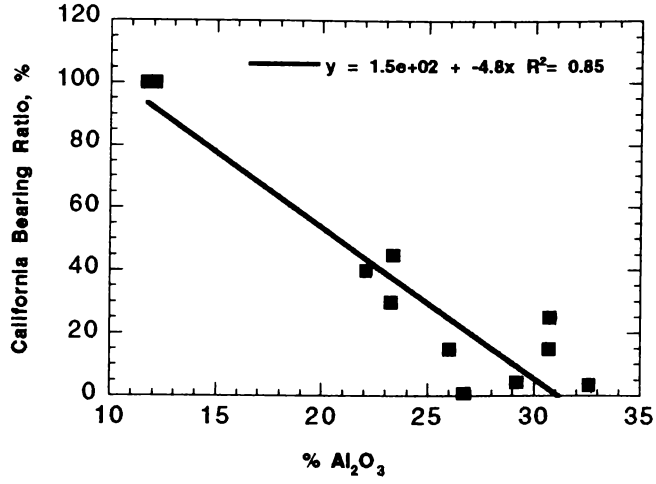

Figure 6.9 c Plot of California Bearing Ratio vs % Al_2O_3

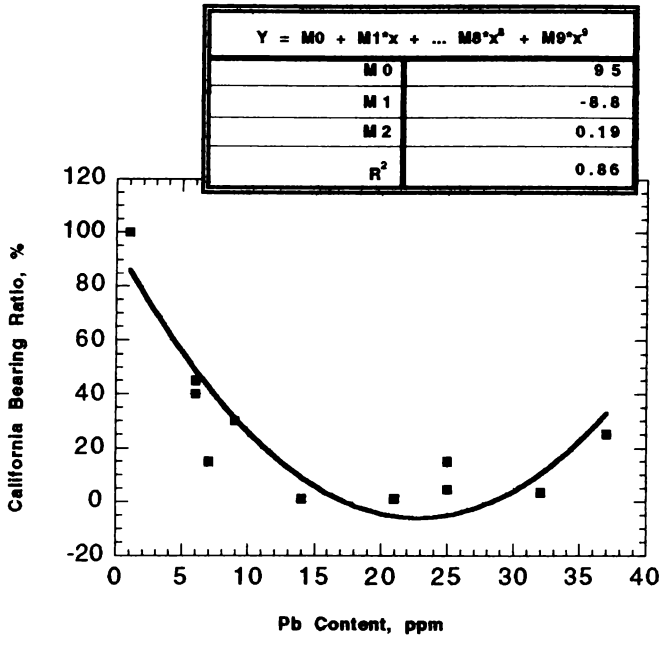

Figure 6.9d Plot of California Bearing Ratio vs Pb

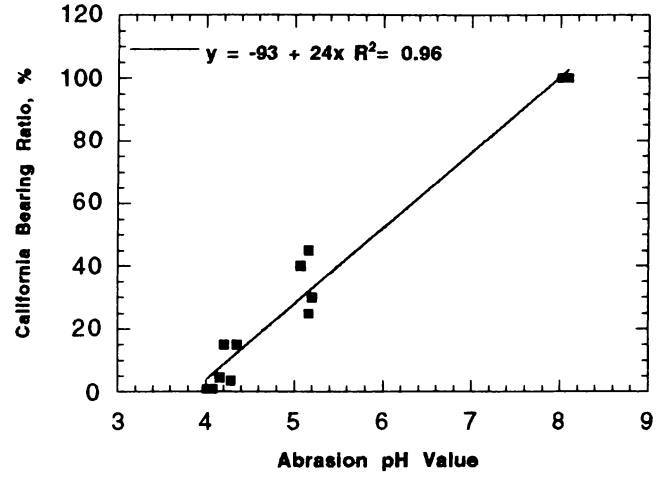

Figure 6.9e Plot of California Bearing Ratio vs Abrasion pH

6.2.9 General Trends Recognised by Simple Regression of Geotechnical Parameters versus Geochemical Parameters

The following trends can be identified from the regression analysis presented:

(a) California Bearing Ratio and other strength parameters consistently correlate with cation concentration patterns.
(b) Dry density too shows good correlations with a number of cation concentration patterns.
(c) Abrasion pH correlates significantly with all bulk material properties (density, porosity and permeability) and California Bearing Ratio.
(d) None of the soil engineering parameters shows any acceptable relationship with chemical parameters except for cohesion versus abrasion pH.
(e) Strength parameters and dry density produce significant regression coefficients with weathering indices, but their plots indicate complex relationships. Weathering indices reduce their value rapidly at the early stages of weathering with subsequent minor changes.

6.3 Influences of Groups of Geochemical Factors on Geotechnical Parameters

Statistical analysis, namely principal component analysis and best subsets regression analysis, was carried out using the software Minitab 13, on the geochemical and geotechnical data obtained.

6.3.1 Principal Component Analysis

Principal component analysis (Chapter 3) on all major and trace element concentrations, pH and electrical conductivity was undertaken in order to identify the geochemical parameters which best explain the variations in their values. This way, the repetitive presence of highly correlated geochemical parameters in the structure of a possible predictor could be avoided. Six principal components, in varying proportions of factor loadings of the chemical concentrations, were distinguished. A principal component here is a linear combination of chemical variables (some results given as Appendix 6.1).

Extensive regression analysis of these chemical data identified that most variations could be explained by the combination of following ten chemical parameters: Al_2O_3, MnO, MgO, CaO, Na_2O, K_2O, P_2O_5, Nb, Ba and H_2O+ contents. These chemical components are highly correlated with each other. When regression analysis was carried out with each principal component against each chemical parameter, it was found that the first principal component very strongly relates to CaO (R^2 = 0.95) which means CaO concentration explains 95% of the variations.

Further, CaO delineates the fresh rock from the other basalt and can be used to discriminate fresh basalt. This is evident from Figure 6.10a, which is a plot of depth versus CaO. Fresh basalt samples are grouped together having high CaO values. All other weathering grades have low CaO values. MgO, which highly correlates with CaO (R^2 = 0.97), follows a similar pattern (Figure 6.10b). Most variations of geochemical data can be explained by the variations of either CaO or MgO concentrations. "An analysis of principal components often reveals relationships that were not previously suspected and thereby allows interpretations that would not ordinarily result" (Johnson & Wichern, 2001, p 426). This analysis suggests that CaO or MgO are important geochemical parameters within the early stages of weathering of Karamu Basalt.

6.5.1 Best Subsets Regression Analysis

Best subsets regression analysis (Chapter 3) was used to search for small sets of geochemical parameters, which might give good predictions of geotechnical parameters. In cases where the value of a certain geochemical parameter repetitively equals to zero or when the number of samples tested was small, it was not possible to carry out this analysis successfully. The problem in most cases was the insufficient coverage of all weathering grades. This is controlled mostly by the nature of the test and its material requirements. Only water content, California Bearing Ratio, dry density and porosity covered the whole range of weathering grades. Of them, California Bearing Ratio, the most expensive of the tests, had the problem of having a limited specimen number, therefore was not included. Even though cohesion could be determined only for weathered material, it was also used in this analysis due to the high number of available test results. The unavailability of a geotechnical testing method, that covers the whole range of weathering grades, can be considered an important reason to try to determine some geochemical predictor. This aspect of the study was an attempt at that.

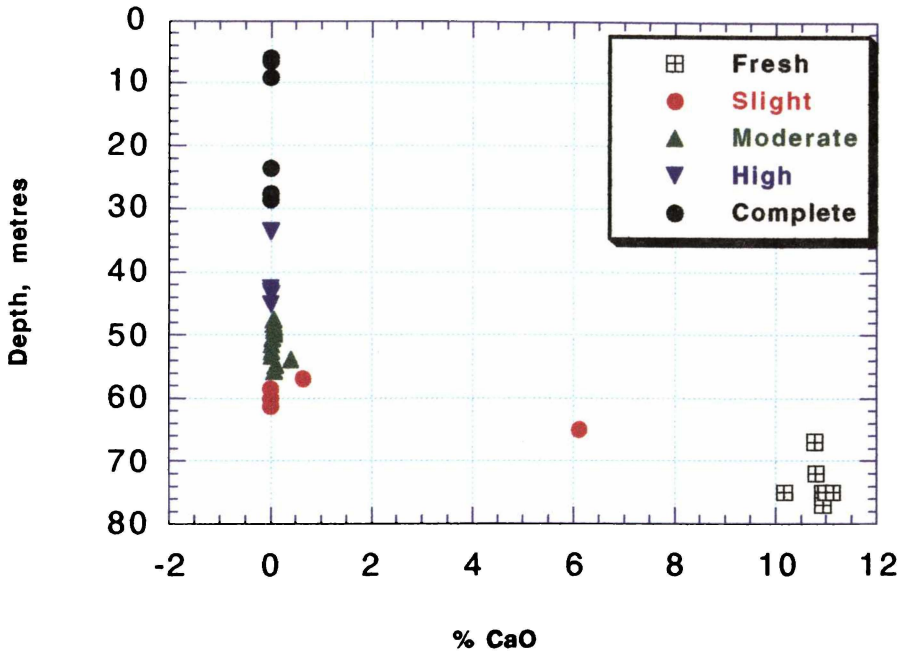

Figure 6.10a Plot of Depth vs % CaO

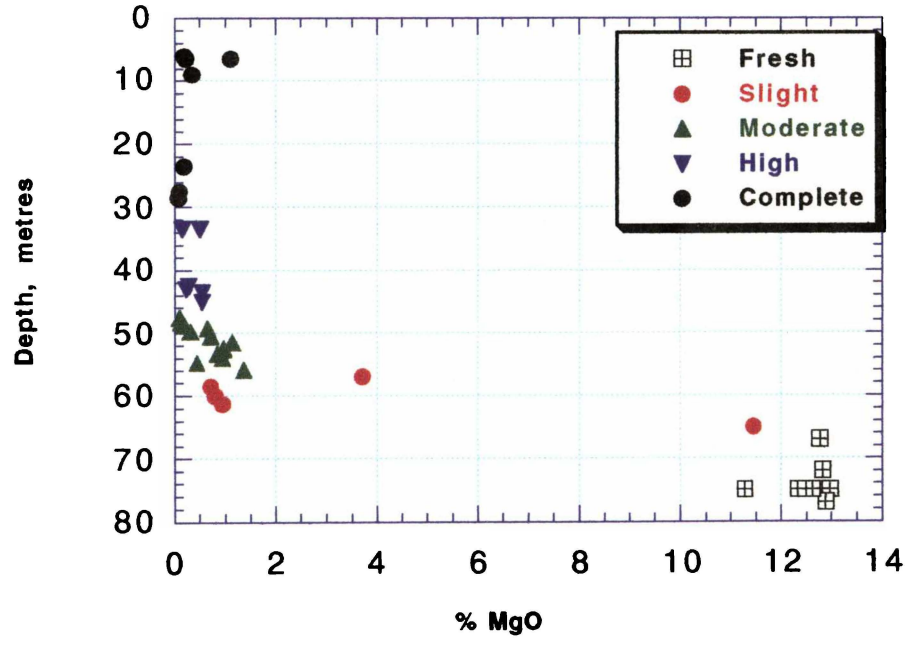

Fig 6.10b Plot of Depth vs % MgO

The best subsets regression was carried out using separately water content, cohesion, dry density and porosity as the geotechnical parameter to be predicted by the chemical parameters. Several promising combinations of geochemical variables which may provide reliable predictions for each of the 4 geotechnical parameters were obtained. Each geotechnical parameter generated a number of individual geochemical predictors or combinations of geochemical predictors. The higher the coefficient of correlation, the larger was the number of components in the combination. Best candidates as predictors were small sets with no more than three or four subsets (singles being the best, doubles next best and so on) as beyond this level a predictor would become cumbersome and of limited practical value. A compromise was then sought between maintaining goodness of fit between the predictor and the observations, and penalising predictors with too many components.

The software (Minitab 13) automatically checked the reliability and repeatability of each subset in terms of the strength of the relationship, ensuring the correlations were the results of normal relationships. Subsets satisfying Minitab acceptance criteria were produced in table form (for example, Appendix 6.2). The four best subsets to predict each of the four geotechnical parameters (a total of sixteen subsets) were selected from the resulting tables (Table 6.2). The squared correlation coefficients (R^2) at 95% confidence level are given within brackets. It is interesting to note that CaO, MgO and abrasion pH came up as possible chemical predictors for most of the geotechnical parameters considered.

Within the software, weightings were assigned to each component of the geochemical subsets chosen, and the resulting predictive equations were correlated with all geotechnical parameters. Minitab picked the predictor that was the most highly correlated with a range of geotechnical parameters.

TABLE 6.2 RESULTS OF BEST SUBSETS REGRESSION ANALYSIS

Geotechnical Parameter	Set 1	Set 2	Set 3	Set 4
Water Content	MgO	CaO	CaO; El. Cond-vity	SiO_2 ; Th
	(R^2 =0.79)	(R^2 =0.80)	(R^2 =0.81)	(R^2 =0.83)
Cohesion	MnO; CaO; P_2O_5	MnO; MgO; P_2O_5	MnO; CaO; P_2O_5; H_2O	MnO; MgO; P_2O_5; H_2O
	(R^2 =0.64)	(R^2 =0.65)	(R^2 =0.74)	(R^2 =0.78)
Dry Density	pH: Ti; Sr; Fe_2O_3	CaO	pH	pH; Al_2O_3 ; El. Cond-vity
	(R^2 =0.86)	(R^2 =0.91)	(R^2 =0.96)	(R^2 =0.97)
Porosity	pH	MgO	pH; H_2O	pH; Ba; Ti
	(R^2 =0.70)	(R^2 =0.75)	(R^2 =0.93)	(R^2 =0.95)

It was found that the linear combination of TiO_2, Sr, Fe_2O_3 and abrasion pH (given below as "Predictor x") suggested by the dry density regression (Figure 6.10c), also provides the best predictions for other geotechnical parameters.

$$\text{Predictor x} = 225\ pH + 283\ TiO_2 + 7.4\ Sr - 80\ Fe_2O_3 \quad \ldots 6.2$$

where Sr values are in parts per million and TiO_2 and Fe_2O_3 are given as percentages by weight.

6.4 Applicability of Chemical Predictors to Other Rock Types

It was appropriate to test the applicability of the chemical Predictor x and the new weathering index discussed in chapter 4, to other rock types from New Zealand and overseas. Publications which record both chemical and engineering analyses are rare. Those with geochemical analyses, rarely have engineering parameters, and similarly, publications which have engineering parameters rarely have geochemical analysis results. However, some publications and graduate degree theses were obtained where both chemical and geotechnical data were available. From New Zealand, Bassett (1998) on andesite; Hetherington (1989) on greywacke; Hind (1986) on ignimbrite; Moon (1989) on ignimbrite and Stevenson (1986) on rhyolite were available. From Japan, Oyama and Chigira (1999) on mudstone and tuff; from France, Veldkamp *et al.* (1990) on basalt, and from India, Sahasrabudhe and Vaidyanath (1981) on laterite were obtained. Data on rhyolitic tephras from Karamu conducted additionally in this study were also taken for consideration. All chemical and geotechnical data are given in Table 6.3.

Predictor x and its modifications together with another predictor (Predictor 2) and the New Weathering Index were tested for their suitability as predictors of geotechnical parameters of Karamu Basalt and other lithologies. The regression coefficients of these relationships are given in Table 6.4. Acceptable plots are given in the following sections, and a complete list of the derived predictor equations is given in section 6.6.

Regression Analysis: Dry versus pH, TiO2, Sr, Fe2O3

The regression equation is
Dry = 1015 + 225 pH + 283 TiO2 + 7.38 Sr - 80.2 Fe2O3

Predictor	Coef	SE Coef	T	P
Constant	1014.5	216.3	4.69	0.000
pH	225.05	36.84	6.11	0.000
TiO2	282.79	63.19	4.48	0.000
Sr	7.384	1.586	4.66	0.000
Fe2O3	-80.17	17.45	-4.59	0.000

S = 73.98 R-Sq = 86.0% R-Sq(adj) = 83.6%

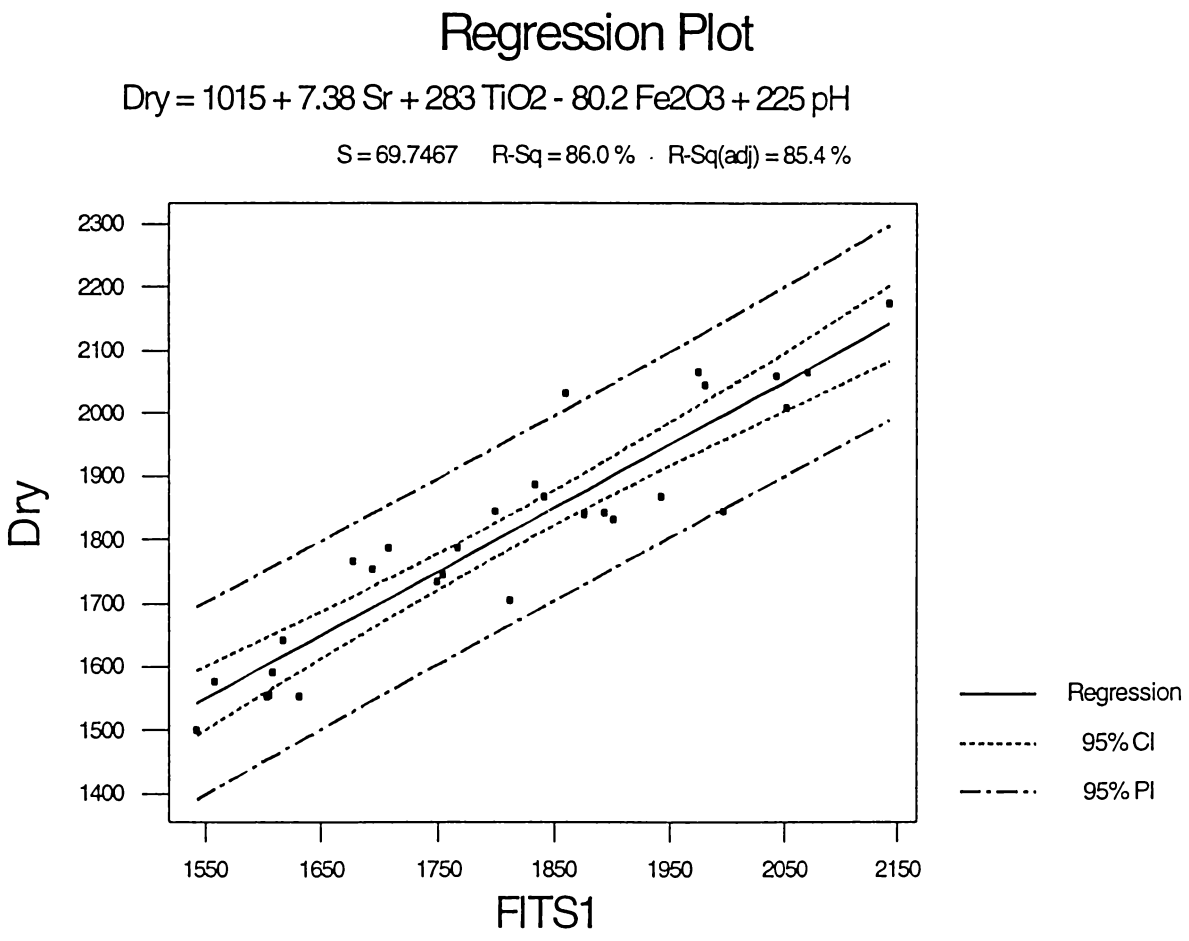

Figure 6.10 c Regression Plot of Dry Density versus Best Subset of Chemical Parameters "Fits 1"

TABLE 6.3 GEOCHEMICAL AND GEOTECHNICAL DATA FOR OTHER NEW ZEALAND AND OVERSEAS ROCK MATERIALS

	Sample	SiO_2	Al_2O_3	MgO	CaO	MnO	P_2O_5	TiO_2	Fe_2O_3	FeO	H_2O	Sr	pH	Water Content	Density	Porosity	CBR	Cohesion	Int. Fr. Angle	Is(50)	Shore	UCS	Permeability	Liquid Limit	Plastic Limit	Plastic. Index	Schmidt Hardn.	Predict.	Predict.	Predict.	Predict.	Predict.	New Weath.
	Name	%	%	%	%	%	%	%	%	%	%	ppm	Value	%	kg/m^3	%	Value	kPa	degrees		Hardness	MPa	10^{-4}xm/s	%	%	%	R	x	No. 1	No. 1a	No. 1b	No. 2	Index
Coromandel	CW.AN	55.16	19.75	1.73	0.10	0.18	0.00	0.78	3.82	3.82	11.99		5.14	27.90	1141	57.30	15												-1.09	14.33		-2.13	0.16
Andesite, NZ	HW.AN	56.22	19.42	1.62	0.54	0.10	0.00	0.66	3.05	3.05	10.84		5.00	22.60	1669	36.30	20												-0.74	14.27		0.68	0.16
(Bassett, 1998)	MW.AN	61.41	16.28	1.26	4.40	0.08	0.04	0.61	3.04	3.04	4.19		5.72	4.60	2365	11.40	45			2.20									-0.90	16.26		5.97	0.37
	SW. AN	60.61	16.12	1.39	5.08	0.10	0.04	0.63	3.13	3.13	3.37		7.12	2.80	2443	8.40	55			3.60									-0.92	20.44		5.70	0.42
	UW. AN	61.43	15.92	2.01	5.33	0.11	0.04	0.60	3.15	3.15	2.94		7.25	3.20	2496	7.60				5.10									-1.05	20.70		4.68	0.48
Whitehall	F-a	63.21	16.49	2.04	2.58	0.08	0.19	0.77	1.68	3.78	2.41			0.21	2690	1.61				9.53	85.6								1.02			8.11	0.41
Greywacke, NZ	SW-a	64.12	16.41	2.22	1.51	0.10	0.19	0.76	0.96	4.37	2.30			0.62	2610	2.58				7.23	63.3								1.70			7.37	0.41
(Hetherington,	MW-a	65.57	16.05	1.39	0.91	0.08	0.15	0.67	4.56	0.76	3.56			1.45	2530	4.71				2.75	36.8								-2.22			7.88	0.13
1989)	HW-a	65.77	16.82	1.20	0.70	0.05	0.09	0.82	5.07	0.32	4.20			9.23	1780	28.97				2.41	12.1								-2.20			7.63	0.09
	HW-b	63.71	18.09	1.36	1.59	0.06	0.08	0.81	5.02	0.00	3.88										18.2								-2.19			7.13	0.11
	HW-c	64.84	17.73	1.11	0.63	0.03	0.06	0.73	3.67	0.39	5.82			7.95															-1.12			6.92	0.08
	CW-a	67.11	14.90	1.07	0.25	0.06	0.11	0.88	6.75	0.27	5.38			14.57	1500	42.26					5.0								-3.67			7.27	0.06
	CW-d	62.12	18.15	0.97	0.19	0.03	0.08	0.88	5.77	0.31	8.45			17.37	1510	42.38													-2.69			6.06	0.05
	CW-f	63.58	16.04	1.81	3.02	0.15	0.17	0.67	1.71	3.80	3.24			0.22	2750	1.15					85.8								0.64			5.94	0.41
Tauranga	WAIM 1	71.30	15.16	0.26	2.36	0.04	0.08	0.38	1.69	0.98	0.74							8.8	36	1.76		79.4							-0.36			11.08	0.20
Ignimbrite, NZ	WAIM 2	73.09	14.29	0.15	1.36	0.08	0.03	0.29	1.50	0.77	1.29							1.1	36	0.48		5.4							-0.49			9.14	0.13
(Hind, 1986)	WAIM 3	71.96	13.85	0.25	1.39	0.06	0.02	0.26	1.13	1.05	2.65											2.4							-0.22			8.59	0.15
	GREY 1	68.00	14.70	0.44	1.73	0.05	0.04	0.40	2.31	1.32	3.45							4.7	30	1.43		30.4							-0.91			8.43	0.17
	GREY 2	62.40	23.64	0.14	0.12	0.02	0.02	0.72	2.41	0.63	9.37											4.5							0.11			6.17	0.03
	WAIT	65.56	17.58	0.35	2.57	0.09	0.07	0.55	3.66	1.25	2.83							4.7	33	1.45		40.8							-1.74			8.39	0.17
Whakamaru	Whaka/u	70.81	15.66	0.23	1.55	0.07	0.02	0.33	1.33	1.33	3.04	145			1212			0.06	35								20		-0.17		14.33	8.16	0.16
Ongatiti & Owharoa	Whaka/l	72.97	14.15	0.49	2.30	0.06	0.06	0.29	1.19	1.19	0.28	183			2124			9	34								28		-0.18		18.13	10.13	0.25
Ignimbrites, NZ	Ong/1	68.42	15.77	0.25	2.59	0.02	0.01	0.41	1.31	1.31	3.07	201			1300			0.19	38								17		0.13		20.23	9.21	0.21
(Moon, 1989)	Ong/2	66.65	15.95	0.63	2.69	0.11	0.05	0.41	2.04	2.04	3.11	204			1580			0.4	33								24		-0.61		19.80	6.96	0.25
	Ong/3	68.80	14.90	0.70	2.62	0.07	0.10	0.36	1.73	1.73	1.70	193			1911			3.4	33								36		-0.47		18.84	9.42	0.28
	Owh/m	73.63	12.96	0.13	1.10	0.02	0.02	0.12	0.75	0.75	4.19	78			1580														-0.33		7.47	8.97	0.11
	Owh/l	73.67	13.00	0.14	1.13	0.02	0.02	0.11	0.78	0.78	3.94	82			1928			0.8	34								36		-0.40		7.81	9.08	0.12
	P1b	72.16	14.11	0.03	1.84	0.04	0.45	0.38	1.46	1.46	0.80				2440	2.16				5.09	128								-0.13			17.41	0.20
Minden	P3a	73.32	14.21	0.25	1.80	0.08	0.06	0.36	1.28	1.28	0.40				2330	2.31				2.27	182								-0.02			9.94	0.21
Rhyolite, NZ	P3b	72.92	14.23	0.25	1.72	0.04	0.05	0.36	1.31	1.31	0.92									2.17	71								-0.05			10.51	0.20
(Stevenson, 1986)	P4b_0	72.96	14.15	0.17	1.95	0.09	0.08	0.36	1.27	1.27	0.50				2460	0.57				5.46									0.00			10.09	0.21
	P4b_6	72.73	14.05	0.22	1.96	0.06	0.08	0.35	1.16	1.16	0.79				2490	0.35				7.96	187								0.06			10.61	0.21
	P5c	73.04	14.07	0.33	1.99	0.07	0.09	0.35	1.26	1.26	0.09				2500	0.15				6.30	224								-0.03			10.72	0.23
	O1	76.57	12.77	0.10	0.80	0.03	0.02	0.14	0.73	0.73	0.07				2050	5.07				1.73	17.6								-0.24			10.97	0.12
	Lw3b	73.54	13.24	0.15	1.18	0.05	0.03	0.23	1.07	1.07	1.30				2130	4.73				1.19	15.9								-0.26			9.89	0.15
	MPJ 22	41.58	34.64	0.02	0.00	0.00	0.02	0.62	2.69	2.69	16.68	2	4.82	47.86	1165	40.01		9	31				25.000	86.43	59.29	27.14	768	-0.52	13.94	-0.32	2.95	0.05
Rhyolitic Tephra,	MPJ 23	43.52	30.56	0.14	0.00	0.01	0.03	0.90	3.63	3.63	15.83	7	3.75	55.19	1154	40.76		9	31				25.000	97.86	75.01	22.85	358	-0.48	10.78	0.23	3.13	0.08
Karamu, NZ	MPJ 25	41.21	32.73	0.07	0.02	0.01	0.01	0.84	3.48	3.48	16.63	5	3.75	54.80	1165	39.10		9	31				25.000	97.31	66.29	31.02	387	-0.54	10.72	-0.04	2.48	0.07
	MPJ 27	41.72	31.73	0.11	0.00	0.01	0.02	0.96	3.82	3.82	16.20	5	4.10	55.34	1154	40.88		9	31				25.000	98.21	57.56	40.65	410	-0.46	11.85	0.04	2.81	0.08
	MPJ 27	43.75	34.34	0.07	0.00	0.03	0.01	0.57	1.94	1.94	16.12	5	3.62	90.92	1152	40.68		9	31				25.000	111.1	90.81	20.32	554	0.06	10.92	0.56	2.25	0.04
	MPJ 28	44.01	31.65	0.04	0.00	0.00	0.02	0.71	3.30	3.30	15.35	5	3.48	55.69	1515	29.01		9	31				25.000	76.25	62.33	13.92	373	-0.81	9.63	-0.31	3.63	0.07
Kakinokidai	M3-O	61.26	14.62	2.10	3.92	0.08	0.15	0.59	3.54	2.04	2.94		8.20			7.00							0.00007					-1.48	23.13		7.08	0.38
Mudstone, Japan	M3-R	61.17	14.57	2.08	4.21	0.08	0.15	0.59	3.09	2.40	2.80		8.50			8.00							0.00010					-1.03	24.48		7.19	0.42
(Oyama and Chigira,	M4-O	61.05	15.16	2.03	3.35	0.07	0.12	0.61	4.01	1.56	3.26		8.10			7.00							0.00004					-1.88	22.43		6.78	0.31
2000)	M4-R	60.60	14.99	1.95	3.83	0.07	0.13	0.62	3.25	2.26	2.84		8.50			9.00							0.00003					-1.08	24.42		7.30	0.38
Fukuda Tuff, Japan	T1-O	64.85	9.89	0.43	1.12	0.05	0.04	0.15	0.90	0.72	3.08		4.00			8.00							0.00100					-0.38	11.63		8.65	0.16
(Oyama and Chigira,	T1-R	61.60	10.50	0.92	1.15	0.06	0.04	0.15	1.13	0.75	4.89		9.00			2.00							0.00025					-0.61	26.40		6.64	0.17
2000)	T2-O	62.13	9.80	0.37	0.97	0.05	0.04	0.14	1.11	0.60	4.47		7.00			4.00							0.00200					-0.62	20.38		8.00	0.13
	T2-R	64.92	10.33	0.48	1.07	0.05	0.05	0.14	0.90	0.92	5.08		9.00			5.00							0.00050					-0.41	26.59		7.66	0.15
Limagne Basalt,	Fz	45.80	14.10	8.40	10.40	0.20	0.70	2.70	6.00	6.00	1.00				3000														3.45			3.92	1.18
France	Fx	45.10	15.00	7.00	10.70	0.20	1.00	3.00	5.80	5.80	1.60				2900														4.70			10.70	1.05
Veldkamp et al,1990	Fw	44.50	15.40	8.00	10.60	0.20	0.90	2.60	6.05	6.05	2.20				2700														3.05			7.16	1.04
	Fv	44.70	14.60	9.00	10.60	0.20	0.80	2.70	6.25	6.25	1.40				2700														3.20			4.37	1.16
Guna Laterite, India	347RM	50.51	25.88	0.00	0.00	0.00	0.00	3.06	4.90	4.90	10.96				2350									34.00	18.90	15.10			5.81			5.73	0.12
(Sahasrabudhe and	348RM	50.67	25.88	0.00	0.00	0.00	0.00	3.36	4.10	4.10	11.66				2320									33.60	15.64	17.96			7.66			5.35	0.10
Vaidyanath, 1981)	349RM	35.71	25.63	0.00	0.00	0.00	0.00	2.67	10.70	10.70	13.75				2580									29.31	18.29	11.52			-1.36			4.23	0.21
	350RM	41.13	30.24	0.00	0.00	0.00	0.00	3.06	5.40	5.40	14.42				2500									42.80	19.48	23.32			5.31			3.87	0.11

6.4.1 Geotechnical Properties vs Chemical Predictor x

The Predictor x (x = 225 pH + 283 TiO_2 + 7.4 Sr - 80 Fe_2O_3) was taken as an independent variable and geotechnical parameters of Karamu Basalt as dependant variables and regression analysis was carried out (Table 6.4). The following parameters gave good log-normal correlations (R^2 values are at 95% confidence level are given in brackets): California Bearing Ratio (0.91); dry density (0.92); porosity (0.73); compressive strength, determined by point load index (0.72); water content (0.74); permeability (0.64) as given in Figures 6.11 a-e. The predictor showed a two-stage increase with depth (Figure 6.11f) with the point of inflection around 50 – 60 m depth. Cohesion, angle of internal friction, penetration resistance, percent clay, Atterberg limits, penetration resistance, and shear strength gave very weak correlations with the Predictor x.

It can be concluded that with chemical analysis results along with abrasion pH values, some geotechnical parameters can be predicted for Karamu Basalt (section 6.6). The next step was to check whether this chemical predictor could be used for predicting geotechnical parameters of other lithologies.

6.4.2 Modifications of Predictor x

Abrasion pH values were available for only andesites (Bassett, 1998), mudstone and tuff (Oyama and Chigira, 1999) and rhyolitic tephra from the study location. Trace element strontium values were available for only ignimbrite (Moon, 1989) and rhyolitic tephra. Due to unavailability of information on abrasion pH values and trace element analysis on strontium for other rock types, suitability of Predictor x to other lithologies could not be tested. In order to overcome this shortcoming, several modifications to the Predictor x were considered.

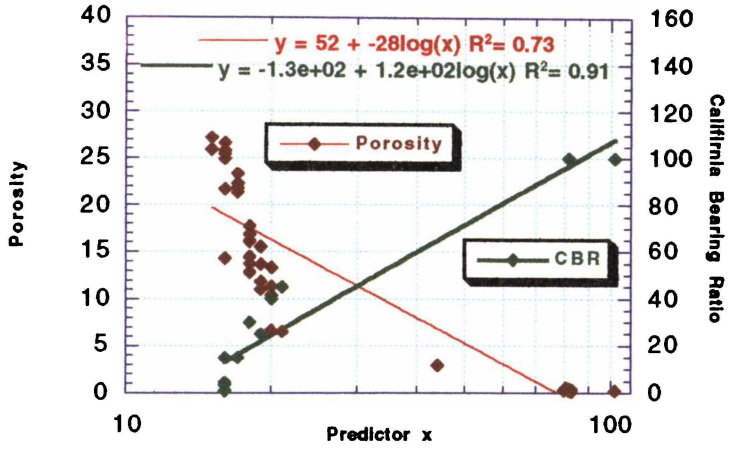

Figure 6.11a Plots of Porosity and CBR vs Predictor x for Karamu Basalt

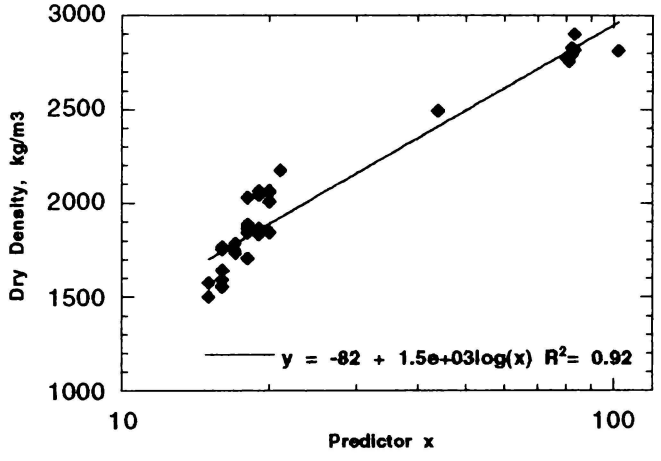

Figure 6.11b Plot of Dry Density vs Predictor x for Karamu Basalt

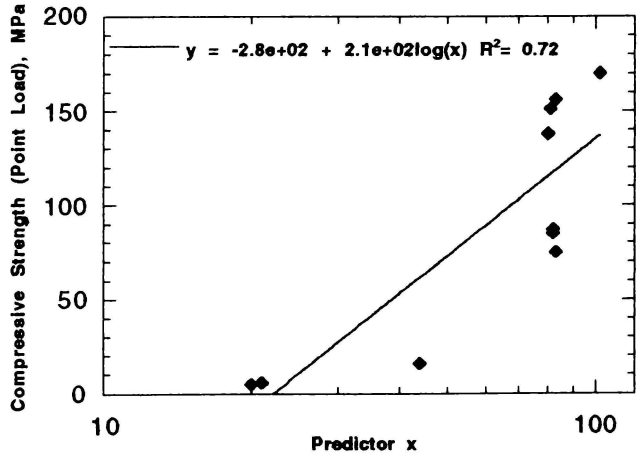

Figure 6.11c Plot of Compressive Strength (Determined by Point Load Index) vs Predictor x for Karamu Basalt

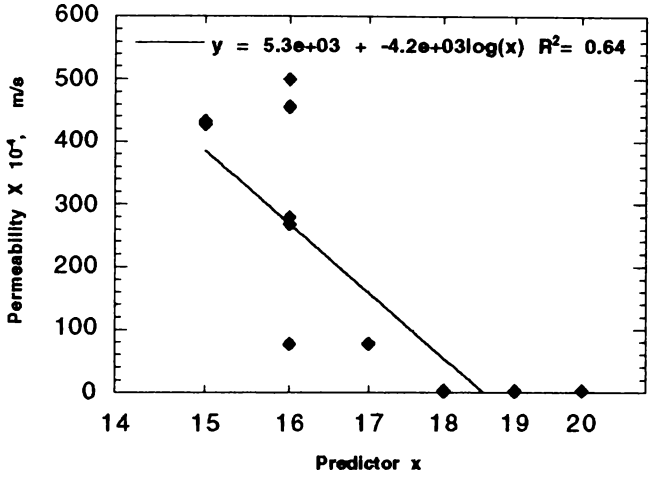

Figure 6.11d Plot of Permeability vs Predictor x for Karamu Basalt

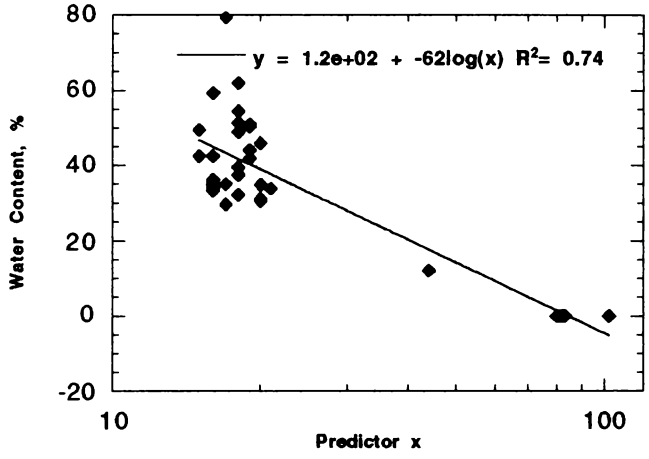

Figure 6.11 e Plot of Water Content vs Predictor x for Karamu Basalt

It seemed appropriate to remove the pH and Sr from the formula and reduce the formula of the Predictor x to [283 TiO_2 - 80 Fe_2O_3] which could be further simplified in order to obtain a more feasible formula, giving:

Predictor No. 1 = 3.5 TiO_2 - Fe_2O_3 ... 6.3

With this revised predictor, i.e. Chemical Predictor No.1, Karamu Basalt shows significant relationships for water content, dry density, porosity and California Bearing Ratio (Table 6.4). Using the chemical analyses, Chemical Predictor No. 1 was calculated for other rock types. Since some values of Predictor No. 1 for other rock types were negative, their logarithms could not be used in the regression analysis. Regression coefficients R^2, at 95% confidence level, for relationships between the geotechnical parameters and the modified predictors are given in Table 6.4. The coefficients, calculated for the whole data set, are also presented in the table.

The Predictor x could be further modified to Chemical Predictor No.1a to include the pH values, where pH values were available but no strontium values were available:

Predictor No. 1a = 2.8 pH + 3.5 TiO_2 - Fe_2O_3 ... 6.4

It could also be modified to Chemical Predictor No.1b to include strontium values instead of pH values for data sets where trace element results were available but no pH values were available:

Predictor No. 1b = 0.1Sr + 3.5 TiO_2 - Fe_2O_3 ... 6.5

Regression coefficients (R^2), at 95% confidence level, for relationships of geotechnical parameters (of Karamu Basalt and other lithologies) against the predictors are given in Table 6.4.

Chemical Predictor No.1 has $R^2 \geq 0.64$ for the following parameters:

1. Water content of greywacke (Hetherington, 1989) (Figure 6.12a)
2. Porosity of greywacke (Hetherington, 1989), rhyolite (Stevenson, 1986) and mudstone (Oyama and Chigira, 1999) (Figures 6.12 b and c)
3. Angle of internal friction of ignimbrite (Moon, 1989) (Figure 6.12d)
4. Shore hardness of greywacke (Hetherington, 1989) (Figure 6.12e)
5. Unconfined compressive strength of rhyolite (Stevenson, 1986) (Figure 6.12f)
6. Liquid limit of rhyolitic tephra (Figure 6.12g)

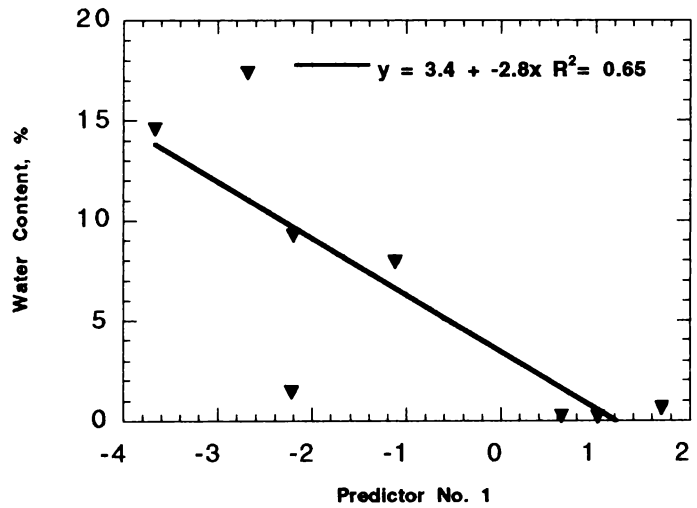

Figure 6.12a Plot of Water Content vs Predictor No. 1 for Greywacke (Hetherington)

TABLE 6.4 REGRESSION COEFFICIENTS (R^2) OF GEOTECHNICAL DATA FROM DIFFERENT LITHOLOGIES AGAINST CHEMICAL PREDICTORS

	Water Content %	Dry Density kg/m^3	Porosity %	CBR	Cohesion kPa	Angle of Int. Fr. degrees	Point Load Index	Shore Hardness	Uniaxial Comp. Str Mpa	Permea-bility m/s	Liquid Limit %	Plastic Limit %	Plastic. Index %	Schmidt Hardn.
VERSUS CHEMICAL PREDICTOR x i.e. 225pH + 283TiO_2 + 7.4Sr - 80Fe_2O_3														
RHYOLITIC TEPHRA	0.00	0.09	0.09		0.00	0.00				0.00	0.00	0.00	0.00	
KARAMU BASALT	0.74	0.92	0.73	0.91	0.48	0.09	0.78			0.72	0.11	0.18	0.04	0.62
VERSUS CHEMICAL PREDICTOR No.1 i.e. 3.5TiO_2 - Fe_2O_3														
ANDESITE (Bassett,1998)	0.00	0.01	0.02	0.76			0.86							
GREYWACKE (Hetherington,1989)	0.65	0.71	0.69				0.84	0.82						
IGNIMBRITE (Hind,1986)					0.02	0.27	0.04		0.11					
IGNIMBRITE (Moon, 1989)		0.16			0.01	0.85								0.38
RHYOLITE, (Stevenson,1986)		0.75	0.85				0.51		0.72					
RHYOLITIC TEPHRA	0.73	0.40	0.42		0.00	0.00				0.00	0.81	0.65	0.01	
MUDSTONE (Oyama & Chigira, 2000)			0.64							0.14				
TUFF (Oyama & Chigira, 2000)			0.71							0.09				
BASALT (Veldkamp, 1990)		0.27												
LATERITE (Sahasrabudhe & Vaidyanath		0.76									0.26	0.11	0.41	
ALL ABOVE DATA	0.20	0.20	0.16	0.76	0.06	0.13	0.34	0.82	0.03	0.25	0.43	0.47	0.06	0.38
KARAMU BASALT	0.76	0.89	0.73	0.86	0.15	0.07	0.34			0.13	0.19	0.15	0.00	0.31
VERSUS CHEMICAL PREDICTOR No. 1a i.e. 2.8pH + 3.5TiO_2 - Fe_2O_3														
ANDESITE (Bassett,1998)	0.75	0.71	0.32	0.95			0.78							
RHYOLITIC TEPHRA	0.09	0.29	0.30		0.00	0.00				0.00	0.00	0.11	0.22	
MUDSTONE (Oyama & Chigira, 2000)			0.74							0.09				
TUFF (Oyama & Chigira, 2000)			0.72							0.21				
KARAMU BASALT	0.74	0.94	0.80	0.93	0.63	0.13	0.50			0.47	0.15	0.18	0.02	0.43
VERSUS CHEMICAL PREDICTOR No. 1b i.e. 0.1Sr + 3.5TiO_2 - Fe_2O_3														
IGNIMBRITE (Moon, 1989)		0.01			0.04	0.03								0.21
RHYOLITIC TEPHRA	0.69	0.27	0.30		0.00	0.00				0.00	0.72	0.55	0.00	
KARAMU BASALT	0.72	0.84	0.61	0.82	0.03	0.02	0.78			0.35	0.07	0.11	0.02	0.62
VERSUS CHEMICAL PREDICTOR No. 2 i.e. 25.2MnO - 1.6MgO + 16.2P_2O_5 - 0.5H_2O+														
ANDESITE (Bassett,1998)	0.96	0.96	0.96	0.24			0.91							
GREYWACKE (Hetherington,1989)	0.12	0.29	0.07				0.06	0.05						
IGNIMBRITE (Hind,1986)					0.44	0.49	0.11		0.50					
IGNIMBRITE (Moon, 1989)		0.04			0.46	0.04								0.12
RHYOLITE, (Stevenson,1986)		0.25	0.00				0.05		0.00					
RHYOLITIC TEPHRA	0.35	0.58	0.53		0.00	0.00				0.00	0.27	0.28	0.17	
MUDSTONE (Oyama & Chigira, 2000)			0.03							0.03				
TUFF (Oyama & Chigira, 2000)			0.33							0.33				
BASALT (Veldkamp, 1990)		0.00												
LATERITE (Sahasrabudhe & Vaidyanath		0.76									0.14	0.20	0.09	
ALL ABOVE DATA	0.39	0.17	0.55	0.24	0.33	0.44	0.00	0.05	0.03	0.24	0.21	0.23	0.35	0.12
KARAMU BASALT	0.62	0.77	0.69	0.81	0.78	0.04	0.20			0.34	0.04	0.07	0.02	0.20
VERSUS NEW WEATHERING INDEX i.e. (FeO + CaO + MgO) / (Fe_2O_3 + Al_2O_3 + H_2O+)														
ANDESITE (Bassett,1998)	0.96	0.89	0.88	0.62			1.00							
GREYWACKE (Hetherington,1989)	0.82	0.87	0.85				0.91	0.94						
IGNIMBRITE (Hind,1986)					0.95	0.01	0.97		0.29					
IGNIMBRITE (Moon, 1989)		0.14			0.35	0.09								0.00
RHYOLITE, (Stevenson,1986)		0.88	0.83				0.41		0.74					
RHYOLITIC TEPHRA	0.44	0.02	0.02		0.00	0.00				0.00	0.09	0.31	0.14	
MUDSTONE (Oyama & Chigira, 2000)			0.22							0.23				
TUFF (Oyama & Chigira, 2000)			0.03							0.77				
BASALT (Veldkamp, 1990)		0.08												
LATERITE (Sahasrabudhe & Vaidyanath,1981)		0.59									0.42	0.04	0.57	
ALL ABOVE DATA	0.42	0.36	0.36	0.72	0.23	0.28	0.30	0.89	0.46	0.56	0.60	0.55	0.23	0.00
KARAMU BASALT	0.71	0.86	0.71	0.92	0.23	0.03	0.59			0.10	0.03	0.01	0.17	0.45

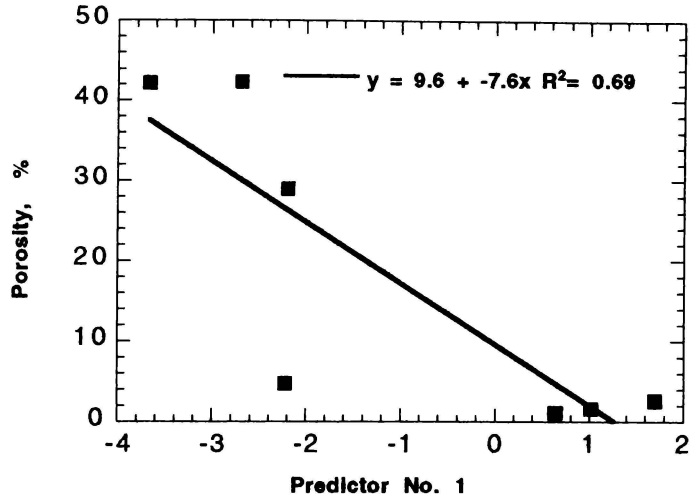

Figure 6.12b Plot of Porosity vs Predictor No. 1 for Greywacke (Hetherington)

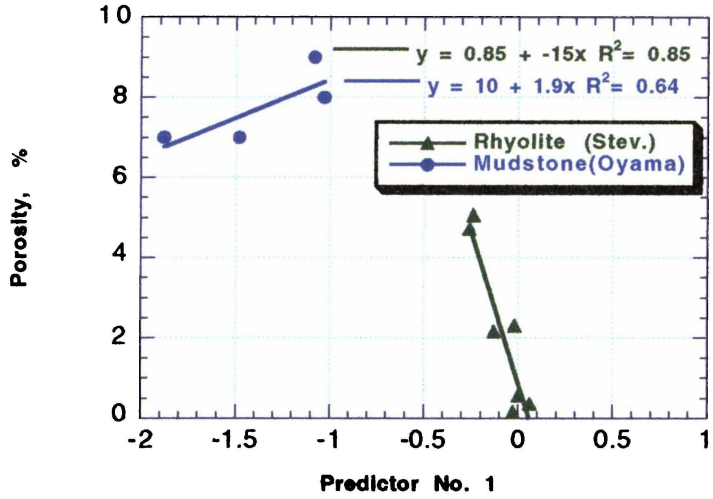

Figure 6.12c Plot of Porosity vs Predictor No. 1 for Rhyolite (Stevenson) and Mudstone (Oyama & Chigira)

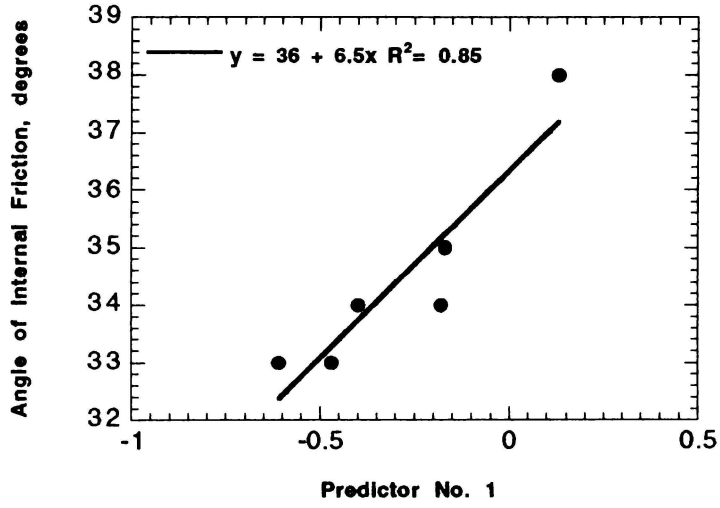

Figure 6.12d Plot of Angle of Internal Friction vs Predictor No. 1 for Ignimbrite (Moon)

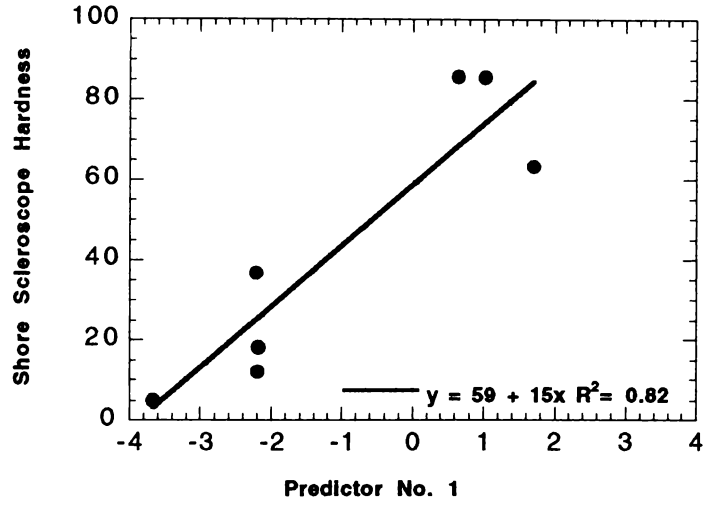

Figure 6.12e Plot of Shore Scleroscope Hardness vs Predictor No.1 for Greywacke (Hetherington)

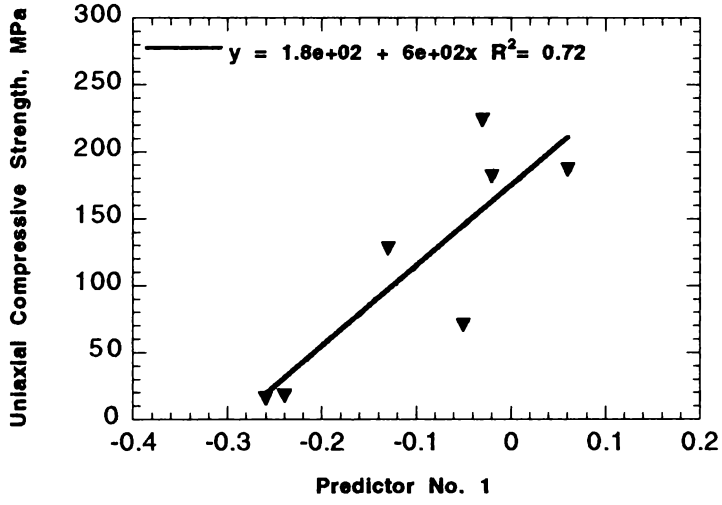

Figure 6.12 f Plot of Compressive Strength vs Predictor No.1 for Rhyolite (Stevenson)

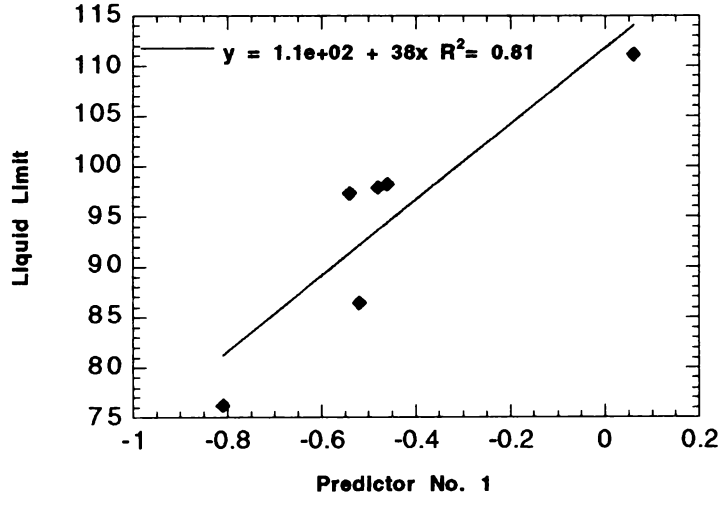

Figure 6.12g Plot of Liquid Limit vs Predictor No. 1 for Rhyolitic Tephra

The difference between titanium and ferric iron oxide concentrations is incorporated in the Predictor No. 1. Titanium is not a mobile element; ferric iron concentration increases with the intensity of weathering by oxidation of ferrous iron. Therefore the values of this predictor must decrease with the intensity of weathering.

The plots of porosity vs Predictor No. 1 show similar trends for greywacke and rhyolite, i.e. with decreasing predictor values, porosity increases. Like in Karamu Basalt, in greywacke and rhyolite, porosity increases with the intensity of weathering. An opposite trend is shown by mudstone. Here the porosity decreases with decreasing predictor values. Mudstone is not a lithology comparable with volcanic rocks and it consists mainly of secondary minerals that are products of weathering and alteration of primary minerals. This stresses the importance of applying mathematically derived equations with caution.

Water content in greywacke increases with decreasing predictor values indicating a confirmation of an increase in porosity and clay content due to weathering. Angle of internal friction in ignimbrite (Moon, 1989) decreases with decreasing predictor values. Shore scleroscope hardness of greywacke also decreases with decreasing predictor values, and so does the uniaxial compressive strength of rhyolite. Even though the Predictor No. 1 does not give any relationship for Karamu Basalt, it can be used for some other lithologies.

Predictor No. 1a incorporates titanium, ferric oxide concentrations and the pH values. The pH value is positive here. The pH decreases with the intensity of weathering in Karamu Basalt. Decrease in the predictor values will indicate increased weathering.

Karamu Basalt does not show good relationships with Predictor No.1a. Chemical Predictor No 1a was tested on the other data with pH values and there were good relationships for the following parameters:

1. Water content and dry density of andesite (Bassett, 1998) (Figure 6.12h)
2. Porosity of tuff (Oyama and Chigira, 1999) (Figure 6.12i)

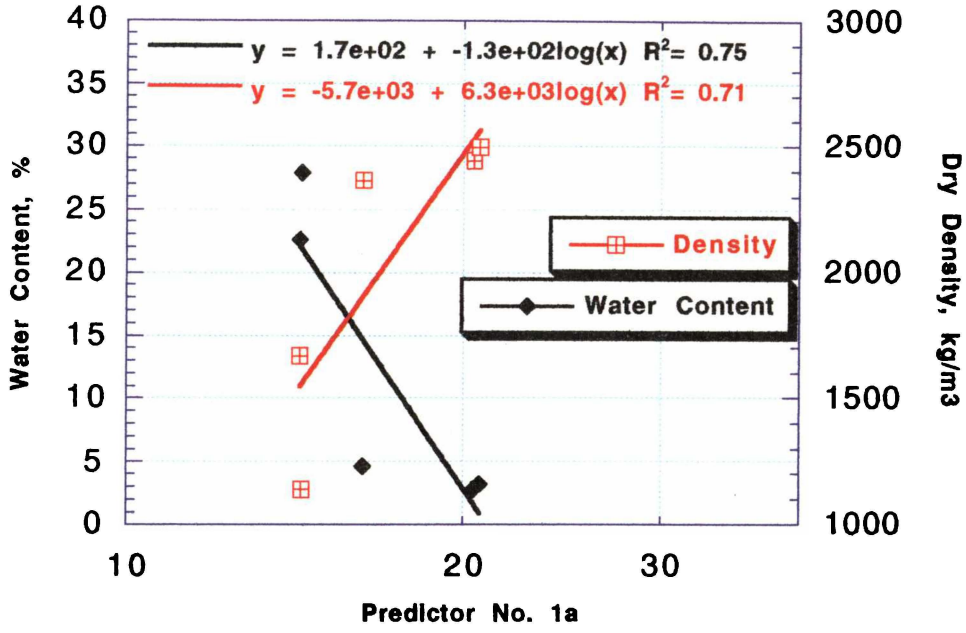

Figure 6.12h Plot of Water Content & Dry Density vs Predictor No.1a for Andesite (Bassett)

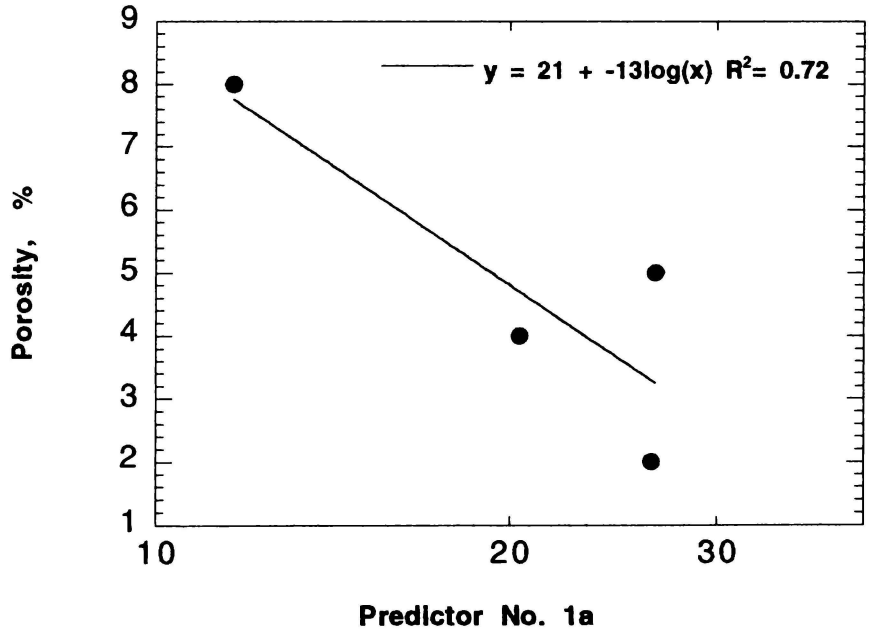

Figure 6.12 I Plot of Porosity vs Predictor No. 1a for Tuff (Oyama & Chigira)

In andesite, plots of water content and dry density vs Predictor No. 1a have opposing trends. With the intensity of weathering, the density decreases while the water content increases. Porosity also increases with the intensity of weathering. This is also true for tuff which shows a linear relationship between porosity and Predictor No. 1a.

With Predictor No.1b Karamu basalt shows good relationships for water content, dry density and point load index (Figures 6.12 j - 1). Chemical Predictor No 1b, which incorporates titanium and ferric oxides plus strontium was tested on the ignimbrite (Moon, 1989) data, the only data set of other authors with strontium values and geotechnical parameters together. There was no significant relationship. With rhyolitic tephra it gave a relationship for liquid limit (Figure 6.12 m). Strontium values seem to have no meaning for ignimbrites but seem meaningful in the case of Karamu Basalt. It was earlier mentioned that strontium, following the pattern of calcium, shows a positive correlation with compressive strength.

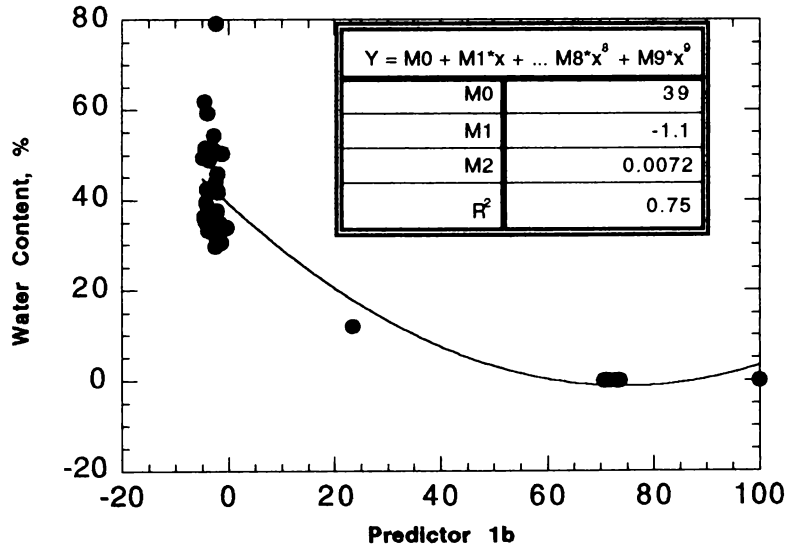

Figure 6.12j Plot of Water Content vs Predictor 1b for Karamu Basalt

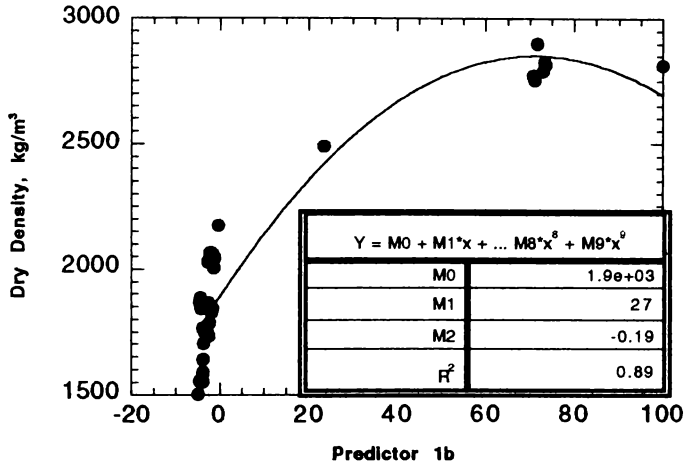

Figure 6.12k Plot of Dry Density vs Predictor 1b for Karamu Basalt

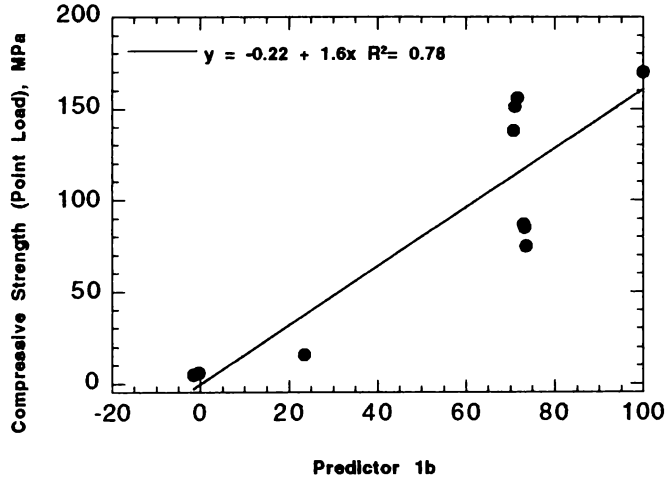

Figure 6.12 l Plot of Compressive Strength (estimated by Point Load Index) vs Predictor 1b

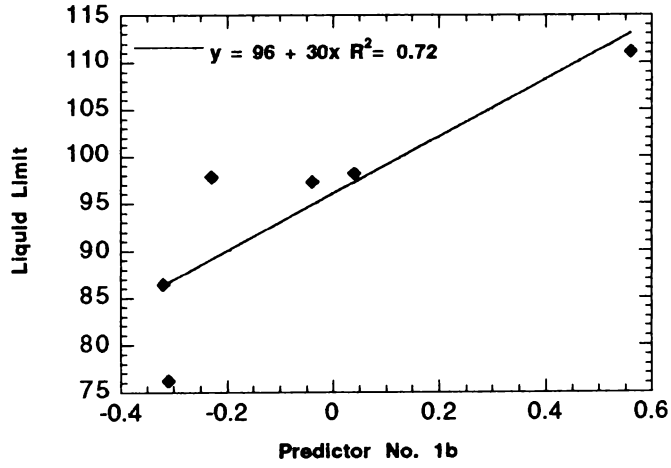

Figure 6.12 m Plot of Liquid Limit vs Predictor No. 1b for Rhyolitic Tephra

Chemical Predictor x was the most suitable for predicting the geotechnical parameters of Karamu Basalt. Yet, it cannot be used, as a whole, for tests against available data on other lithologies due to incompleteness of the data. Most of those researchers cited have carried out only major element chemical analysis on their samples whereas this study has the chemical investigation extended to trace elements, pH and electrical conductivity.

6.4.3 Chemical Predictor No. 2

Since most information available on other lithologies was limited only to major chemical analyses, it seemed appropriate to determine a chemical predictor which did not contain abrasion pH values or trace element analyses. Based on the best subsets regression analysis results given in Table 6.2, the subsets containing only major element contents were reconsidered. The best subset that involved only major elements was obtained by the best subsets analysis (R^2 = 0.78) based on the cohesion values of Karamu Basalt. It was found that the linear combination "Predictor No. 2" (equation 6.6) containing MnO, MgO, P_2O_5 and H_2O+, suggested by cohesion also provides reasonable predictions for other geotechnical parameters (Figure 6.13a).

$$\text{Predictor No. 2} = P_2O_5 - 25.2\ MnO - 1.6\ MgO - 0.5\ H_2O+ \quad \ldots 6.6$$

Even though statistical analysis indicated this subset, from the aspect of changes in chemistry due to weathering of Karamu Basalt, this does not make much sense. With the intensity of weathering, MgO decreases while structural water increases. In Predictor No. 2, both those parameters are given negative values in place of opposing signs. MnO is in small quantities but the multplication by 25.2, probably makes it significant. Recognising that this statistically-derived equation may not have a physical or chemical basis, its validity as a purely mathematical predictor was tested using regression analysis.

The Predictor No. 2 shows a general decrease from surface to depth in the Karamu Basalt profile. However this decrease is most prominent only after the moderate stage of weathering (~ 50 – 60 m in depth) (Figure 6.13b). Among geotechnical parameters of Karamu basalt, cohesion (R^2 = 0.78), porosity (R^2 = 0.69) and California Bearing Ratio (R^2 = 0.81) show correlations with Predictor No. 2 (Figures 6.13 c & d).

Regression Analysis: Cohesion versus MnO, MgO, P2O5, LOI

The regression equation is
Cohesion = 11.6 - 25.2 MnO - 1.60 MgO + 16.2 P2O5 - 0.536 LOI

26 cases used 11 cases contain missing values

Predictor	Coef	SE Coef	T	P
Constant	11.572	2.531	4.57	0.000
MnO	-25.188	5.716	-4.41	0.000
MgO	-1.5975	0.3971	-4.02	0.001
P2O5	16.181	3.574	4.53	0.000
LOI	-0.5358	0.1434	-3.74	0.001

S = 1.290 R-Sq = 77.9% R-Sq(adj) = 73.7%

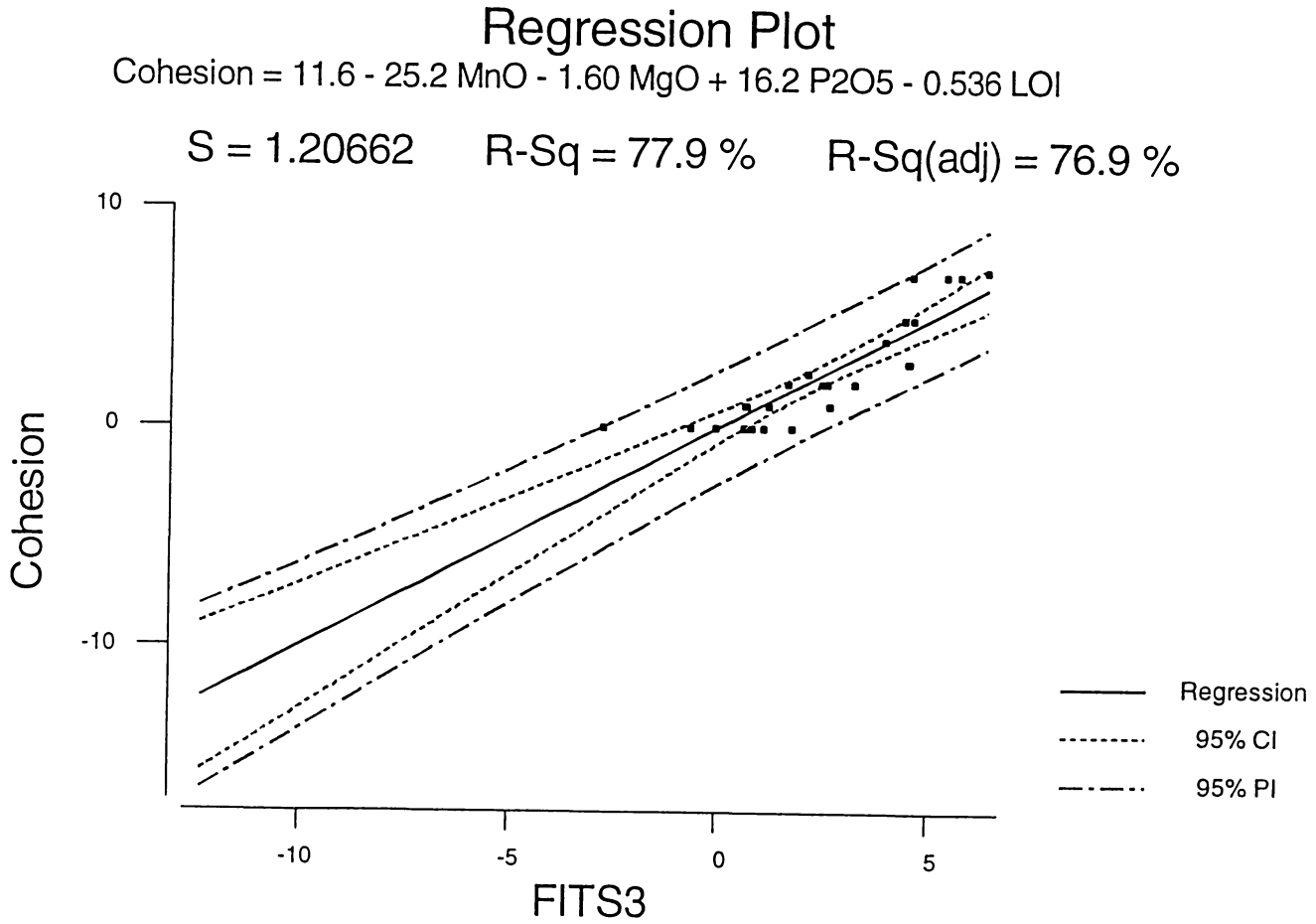

Figure 6.13 a Regression Plot of Cohesion versus Best Subset (Major Elements Only) "Fits 3"

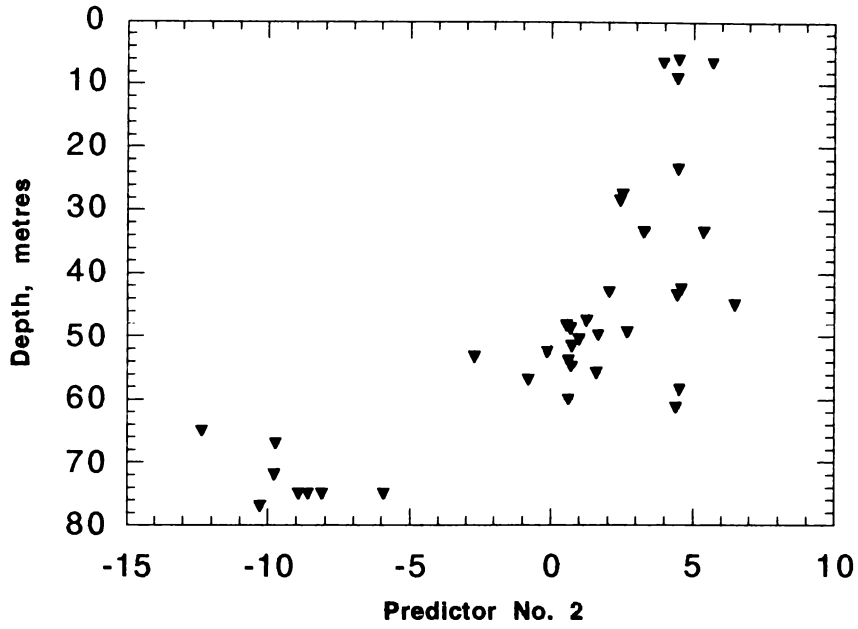

Figure 6.13b Plot of Depth vs Predictor No. 2 for Karamu Basalt

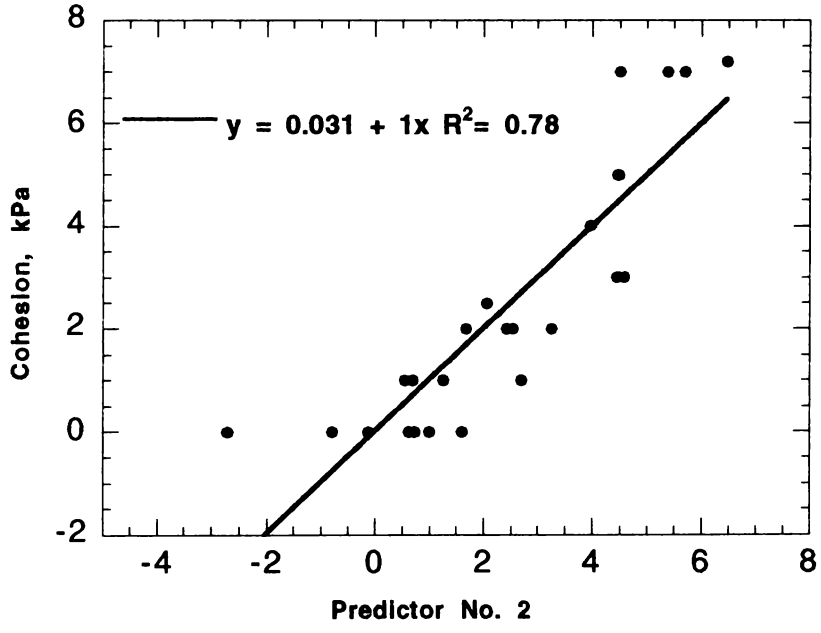

Figure 6.13c Plot of Cohesion vs Predictor No. 2 for Karamu Basalt

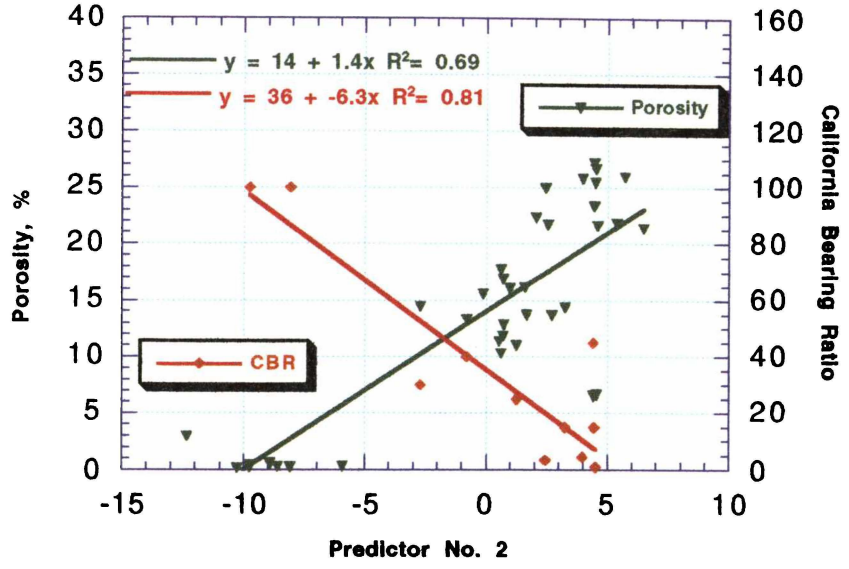

Figure 6.13d Plot of Porosity & CBR vs Predictor No. 2 for Karamu Basalt

Using the available results of chemical analyses, Predictor No. 2 was calculated for different rock types. Relationships between the Predictor No. 2 and the geotechnical parameters are given in Table 6.4 as linear regression coefficient values (R^2). This table also contains R^2 values for the total data set and Karamu Basalt.

The following parameters for andesite (Bassett, 1998) maintain, at 95% confidence level, R^2 values of 0.96 with the Predictor No. 2:

1. Water content (Figure 6.13e)
2. Dry density (Figure 6.13f)
3. Porosity (Figure 6.13g)

Even though good correlations are shown by the geotechnical parameters of andesite versus Predictor No. 2, they are exact opposite relationships to those of Karamu Basalt. With increasing predictor values, in Karamu Basalt the porosity increases whereas it decreases in andesite. Andesite (Bassett, 1998) contains negligible quantities of P_2O_5, so the predictor relies predominantly on MnO, MgO and structural water.

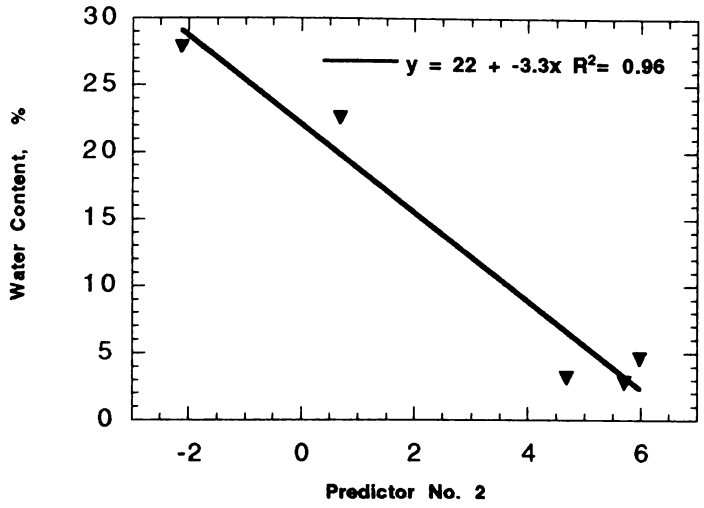

Figure 6.13e Plot of Water Content vs Predictor No. 2 for Andesite (Bassett)

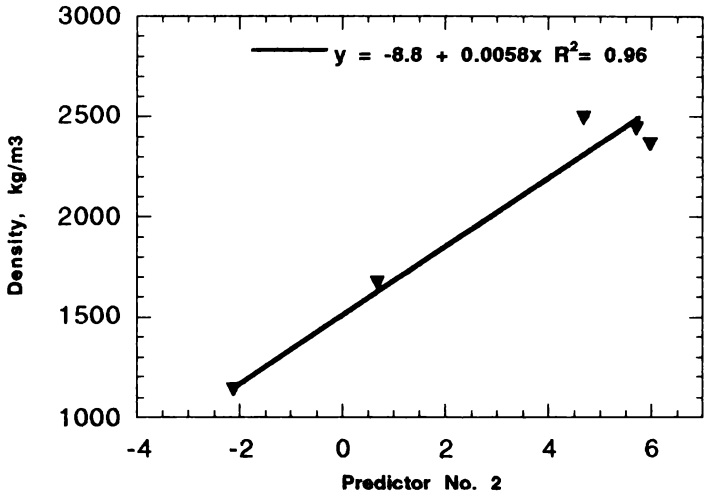

Figure 6.13f Plot of Dry Density vs Predictor No. 2 for Andesite (Bassett)

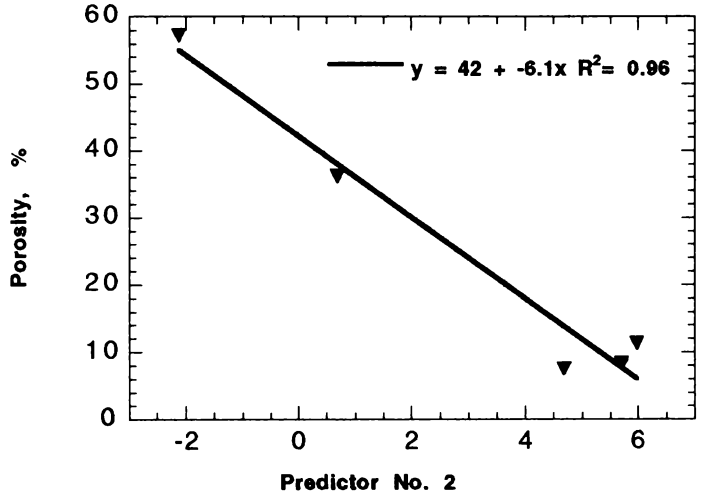

Figure 6.13g Plot of Porosity vs Predictor No. 2 for Andesite (Bassett)

The Predictor No. 2 seems less indicative of geotechnical parameters compared to the Predictor x. It contains only the results of major element analyses and the components are combined in an unacceptable manner from the aspect of chemical weathering. The predictors containing the abrasion pH values seem suitable for a larger number of lithologies. This makes us realise the importance of obtaining abrasion pH values for samples tested in a similar study. Abrasion pH is an indicator of the changes taking place in mineral chemistry and it can be inferred that mineral chemistry plays an important role in geotechnical properties.

6.5 New Weathering Index as a Predictor of Geotechnical Parameters

New Weathering Index which is equal to $(CaO + MgO + FeO) / (Al_2O_3 + Fe_2O_3 + H_2O+)$ was tested as a predictor of geotechnical parameters. The water in the formula is structural water as determined by chemical analysis. Of all geotechnical parameters of Karamu Basalt, the following show log-normal relationships with the New Weathering Index: dry density ($R^2 = 0.86$), water content ($R^2 = 0.71$), porosity ($R^2 = 0.71$) and California Bearing Ratio ($R^2 = 0.92$) (Figures 6.14 a and b). The new weathering index can be used in the prediction of some geotechnical parameters for Karamu Basalt.

Chemical weathering index is akin to an equilibrium constant and is indicative of a weathering reaction that affects physical properties. Equilibrium constants are logarithmically related to free energy. Physical properties (all geotechnical properties are physical) are related to the free energy change (A.P.W. Hodder, pers. comm., 2001). The logarithms of New Weathering Index values have linear relationships with geotechnical parameters.

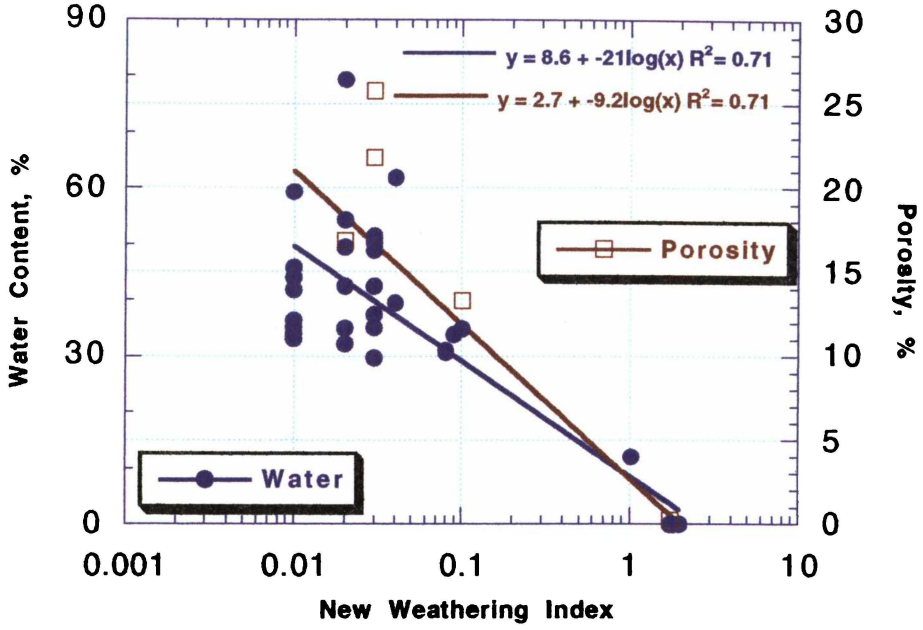

Figure 6.14a Plot of Water Content & Porosity vs New Weathering Index for Karamu Basalt

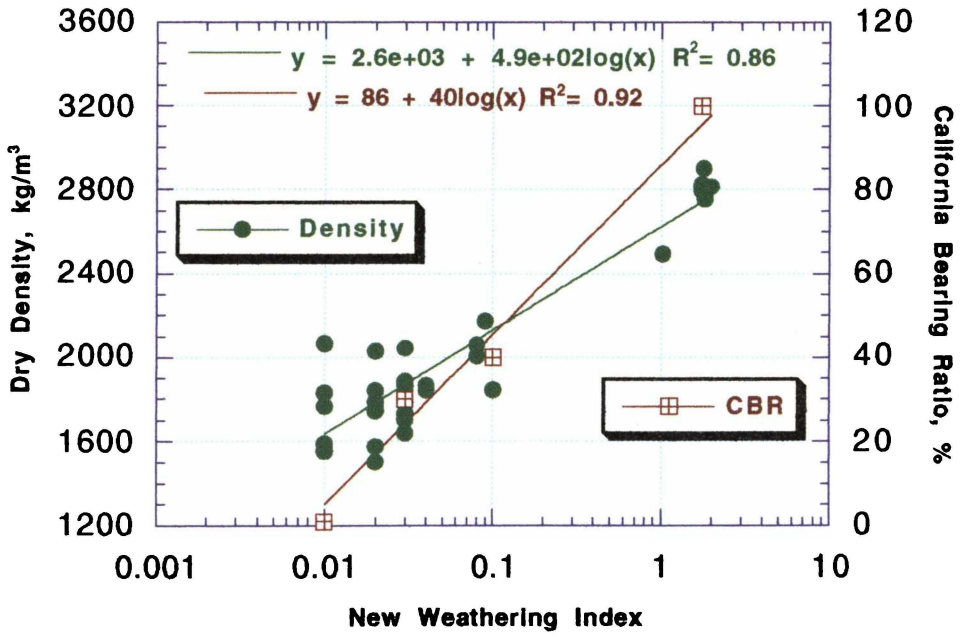

Figure 6.14b Plot of Dry Density & CBR vs New Weathering Index for Karamu Basalt

The new weathering index was calculated for the rock types: andesite, greywacke, ignimbrite, rhyolite, rhyolitic tephra, basalt, tuff and mudstone. Relationships between the new weathering index and the geotechnical parameters for these rock types are given in Table 6.4 as log-normal regression coefficients R^2. For comparison purposes the regression coefficients obtained for the total data set and for Karamu Basalt are also included in the table.

These relationships indicate that new weathering index is good (R^2 >0.64) for the prediction of the following:

1. Water content of andesite (Bassett, 1998) and greywacke (Hetherington, 1989) (Figure 6.14c)
2. Dry density of andesite (Bassett, 1998), greywacke (Hetherington, 1989) and rhyolite (Stevenson, 1986) (Figure 6.14d)
3. Porosity of andesite (Bassett, 1998), greywacke (Hetherington, 1989) and rhyolite (Stevenson, 1986) (Figure 6.14e)
4. Cohesion of ignimbrite (Hind, 1986) (Figure 6.14f)
5. Shore hardness of greywacke (Hetherington, 1989) (Figure 6.14g)
6. Point load index of andesite (Bassett, 1998), greywacke (Hetherington, 1989) and of ignimbrite (Hind, 1986) (Figure 6.14h)
7. Unconfined compressive strength of rhyolite (Stevenson, 1986) (Figure 6.14i)
8. Permeability of tuff (Oyama and Chigira, 1999) (Figure 6.14j)

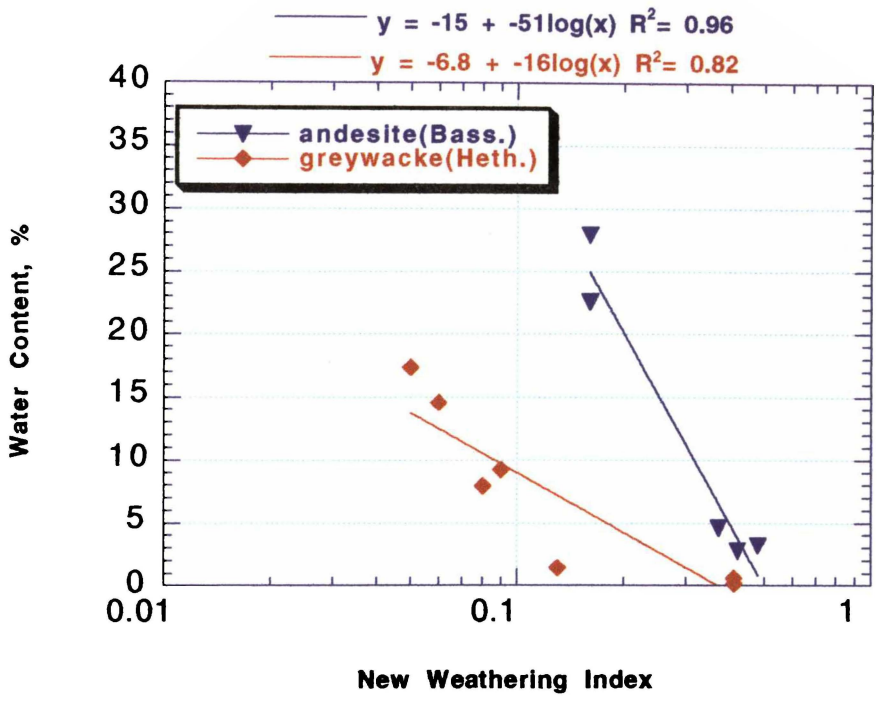

Figure 6.14c Plot of Water Content vs New Weathering Index

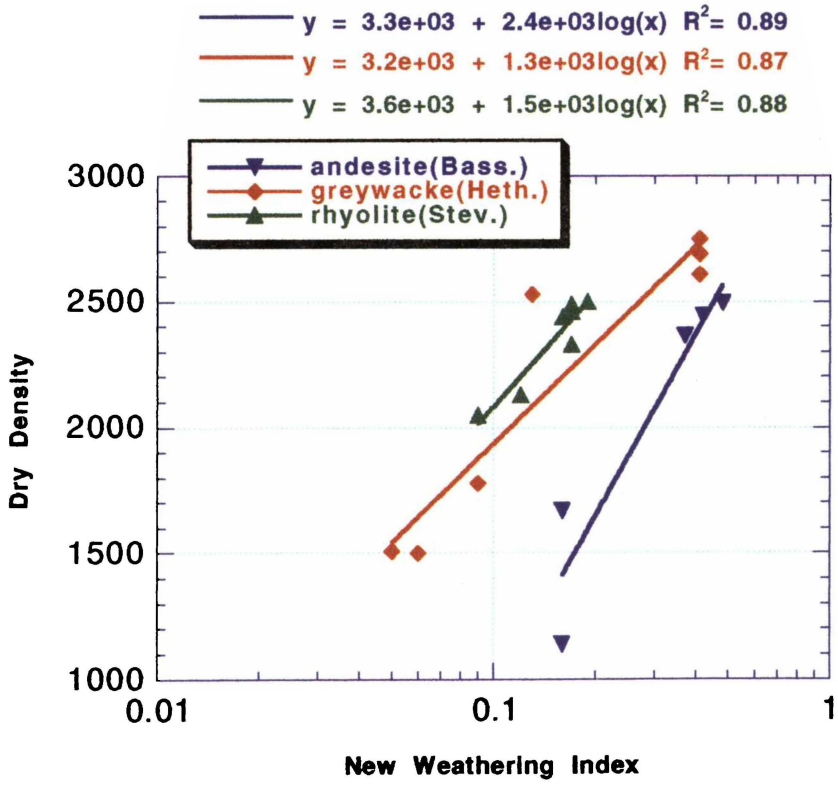

Figure 6.14d Plot of Dry Density vs New Weathering Index

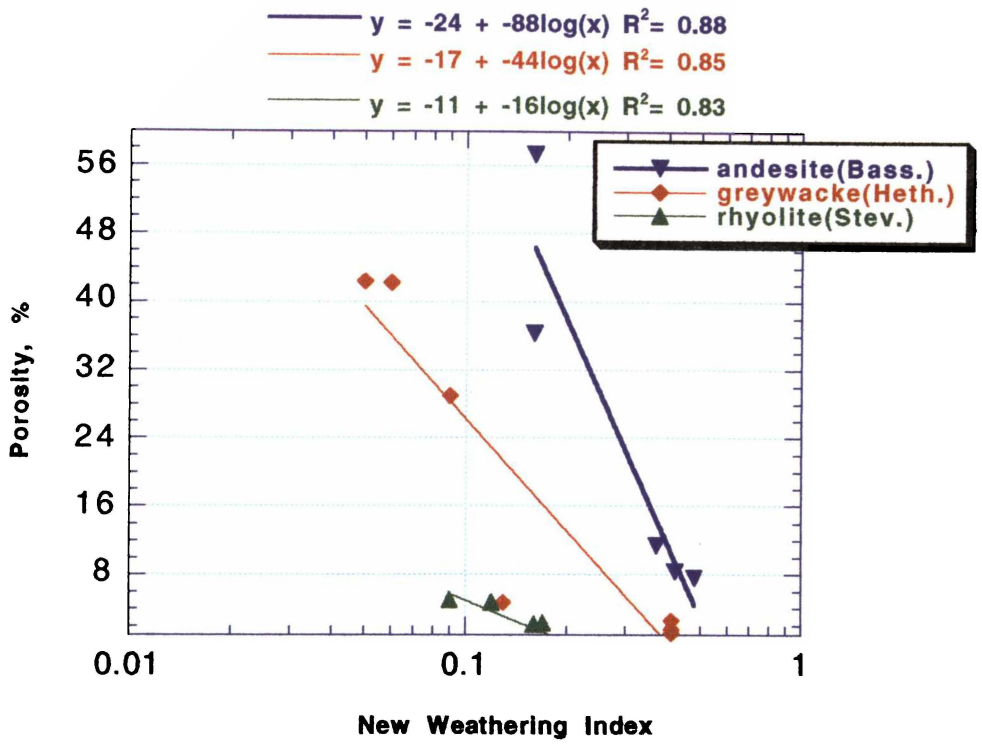

Figure 6.14e Plot of Porosity vs New Weathering Index

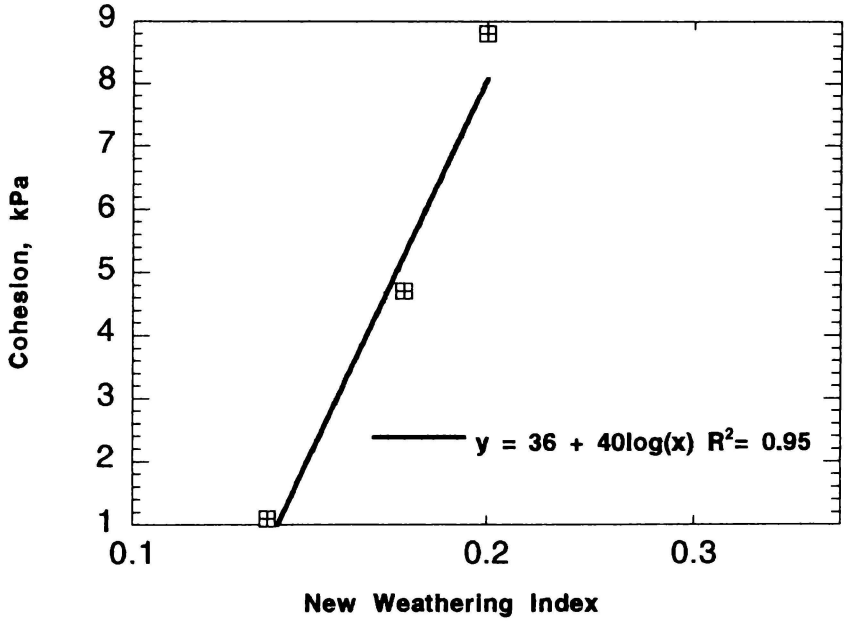

Figure 6.14f Plot of Cohesion vs New Weathering Index for Ignimbrite (Hind)

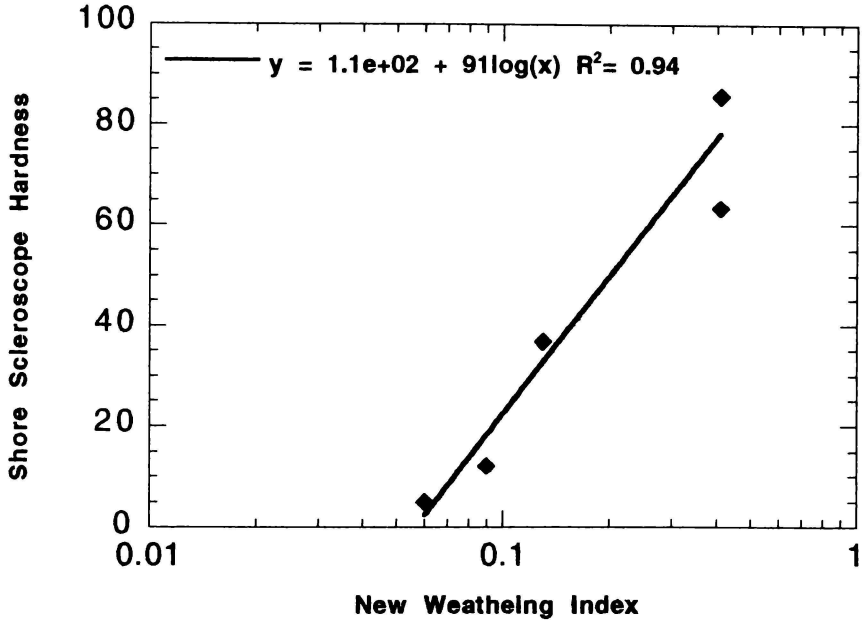

Figure 6.14g Plot of Shore Scleroscope Hardness vs New Weathering Index for Greywacke (Hetherington)

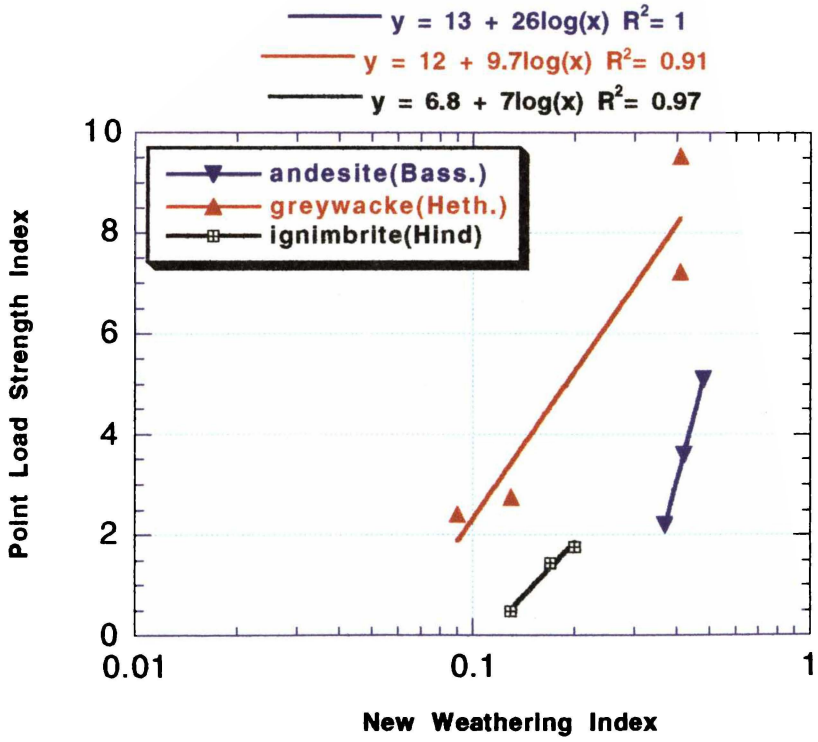

Figure 6.14h Plot of Point Load Index vs New Weathering Index

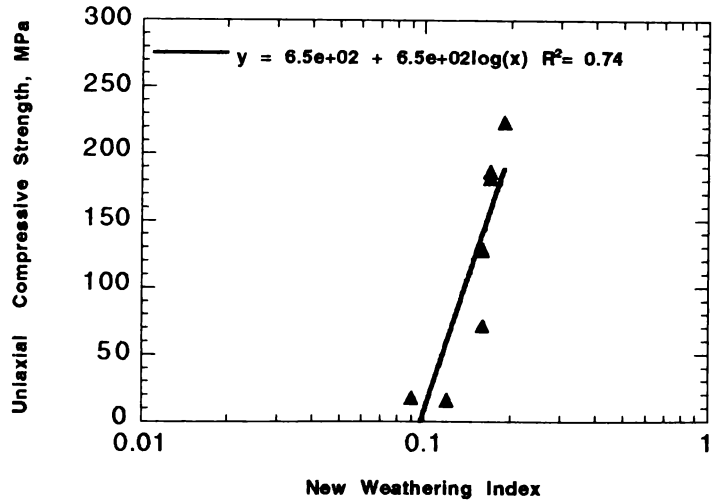

Figure 6.14i Plot of Uniaxial Compressive Strength vs New Weathering Index for Rhyolite (Stevenson)

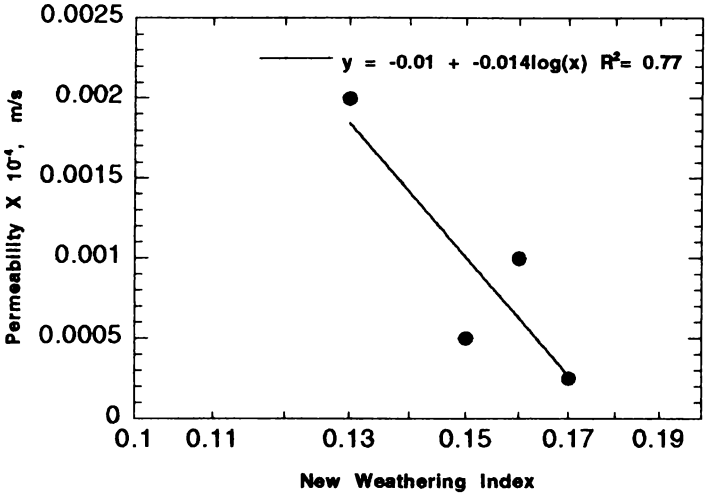

Figure 6.14j Plot of Permeability vs New Weathering Index for Tuff (Oyama & Chigira)

In most cases, geotechnical parameters of andesite samples give good relationships with logarithms of the New Weathering Index. Andesite is an intermediate extrusive rock while basalt is a basic extrusive rock. They often have compatible lithologies, their main difference being in the silica content. The New Weathering Index does not take into account silica content. Similarities of their relationships between geotechnical properties and New Weathering Index are not surprising. This indicates that the New Weathering Index is suitable for andesite also.

Geotechnical properties of rhyolite, which is a silicic volcanic rock, do respond to the New Weathering Index in a similar pattern but to a lesser degree than andesite. In rhyolites there are higher contents of sodium, potassium and silicon than basalt. The New Weathering Index does not incorporate any of those three elements. Therefore, in rhyolites, the geotechnical properties may not relate exceptionally well with the New Weathering Index. However, the geotechnical properties of rhyolite (Stevenson, 1986) do demonstrate significant relationships with the New Weathering Index.

Tuff and ignimbrite do not relate well with the New Weathering Index. They are both formed by pyroclastic flows or falls, and often have a rhyolitic composition. They therefore need not relate exceptionally well with the New Weathering Index as stated above for rhyolite.

In the case of greywacke of North Island, New Zealand, the geotechnical properties showed good relationships with the New Weathering Index. Often greywacke is composed largely of weathered and redeposited igneous material. Hence, greywacke may demonstrate similarities with basalt and andesite.

Even though individual data sets show good relationships with the New Weathering Index, when taken as a whole the total data set (excluding Karamu Basalt) does not show any relationship. Different lithologies mixed haphazardly would not give relationships, which some lithologies individually maintain. The New Weathering Index is suitable for Karamu Basalt and a few other related lithologies, but it cannot be used as a universal and versatile chemical predictor of geotechnical parameters for all rock types.

6.6 Predictive Equations Proposed

Based on the preceding discussion, the following equations (R^2 values obtained at 95% confidence level are given within brackets) can be proposed in order to predict the geotechnical properties of different lithologies. These equations have been developed using limited datasets and represent the best which could be derived within the scope of available data, but they cannot be considered robust predictors at this stage.

(a) For Karamu Basalt

California Bearing Ratio = 130 + 120 log Predictor x (R^2 = 0.91) ... 6.7

Dry Density, kg/m^3 = -82 + 1500 log Predictor x (R^2 = 0.92) ... 6.8

Porosity, % = 52 – 28 log Predictor x (R^2 = 0.73) ... 6.9

Comp. Strength (P.L), MPa = - 280 + 210 log Predictor x (R^2 =0.72) ... 6.10

Water content, % = 120 – 62 log Predictor x(R^2 = 0.74) ... 6.11

Permeability, m/s = 5300 – 4200 log Predictor x (R^2 = 0.64) ... 6.12

Water content, % = 39 – 1.1 Predictor 1b + 0.0072 (Predictor 1b)^2
(R^2 = 0.75) ... 6.13

Dry Density, kg/m^3 = 1900 + 27 Predictor 1b – 0.19 (Predictor 1b)^2
(R^2 = 0.89) ... 6.14

Comp. Strength (P.L), MPa = - 0.22 + 1.6 Predictor 1b (R^2 =0.78) ... 6.15

Cohesion, kPa = 0.03 + 1*Predictor 2 (R^2 = 0.78) ... 6.16

California Bearing Ratio = 36 – 6.3 * Predictor 2 (R^2 = 0.81) ... 6.17

Porosity, % = 14 + 1.4 * Predictor 2 (R^2 = 0.69) ... 6.18

Water Content (%) = 8.6 - 21 log (NWI) (R^2 = 0.71) ... 6.19

Dry Density (kg m^{-3}) = 2600 + 490 log (NWI) (R^2 = 0.86) ... 6.20

Porosity (%) = 2.7 + 9.2 log (NWI) (R^2 = 0.71) ... 6.21

California Bearing Ratio (%) = 86 + 40 log (NWI) (R^2 = 0.92) ... 6.22

(b) **For greywacke (Hetherington, 1989)**

Water Content, % = 3.4 – 2.8 * Predictor 1 (R^2 = 0.65) ... 6.23

Porosity, % = 9.6 – 7.6 * Predictor 1 (R^2 = 0.69) ... 6.24

Shore Hardness = 59 + 15 * Predictor 1 (R^2 = 0.82) ... 6.25

Water Content, % = - 6.8 – 16 log NWI (R^2 = 0.82) ... 6.26

Dry Density, kg/m^3 = 3200 + 1300 log NWI (R^2 = 0.87) ... 6.27

Porosity (%) = - 17 - 44 log (NWI) (R^2 = 0.85) ... 6.28

Shore Hardness = 110 + 91 log NWI (R^2 = 0.94) ... 6.29

Point Load Index = 12 + 9.7 log NWI (R^2 = 0.91) ... 6.30

(c) For rhyolite (Stevenson, 1986)

Porosity, % = 85 - 15 * Predictor 1 (R^2 = 0.85) ... 6.31

UCS, MPa = 180 + 600 * Predictor 1 (R^2 = 0.65) ... 6.32

Dry Density, kg/m^3 = 3600 + 1500 log NWI(R^2 = 0.88) ... 9.33

Porosity (%) = -11 - 16 log NWI (R^2 = 0.83) ... 9.34

UCS, MPa = 650 + 650 log NWI (R^2 = 0.74) ... 9.35

(d) For ignimbrite (Hind, 1986)

Cohesion, kPa = 36 + 40 log NWI (R^2 = 0.95) ... 9.36

Point Load Index = 6.8 + 7 log NWI (R^2 = 0.97) ... 9.37

(e) **For ignimbrite (Moon, 1989)**

Angle of Int. Fr., degrees = 36 + 6.5 * Predictor 1 (R^2 = 0.85) ... 9.38

(f) **For rhyolitic tephra from Karamu**

Liquid Limit = 110 + 38 * Predictor 1 (R^2 = 0.81) ... 9.39

Liquid Limit = 96 + 30 * Predictor 1 b (R^2 = 0.72) ... 9.40

(g) For andesite (Bassett, 1998)

Water Content, % = 170 – 130 log Predictor 1a (R^2 = 0.75) ... 9.41

Dry Density, kg/m^3 = -5700 + 6300 log Predictor 1a (R^2 = 0.71) ... 9.42

Water content, % = 22 – 33 * Predictor 2 (R^2 = 0.96) ... 9.43

Dry Density, kg/m^3 = -8.8 + 0.0058 * Predictor 2 (R^2 = 0.96) ... 9.44

Porosity, % = 42 – 6.1 * Predictor 2 (R^2 = 0.96) ... 9.45

Water Content, % = - 15 – 51 log NWI (R^2 = 0.96) ... 9.46

Dry Density, kg/m^3 = 3300 + 2400 log NWI (R^2 = 0.89) ... 9.47

Porosity (%) = - 24 - 88 log NWI (R^2 = 0.88) ... 9.48

Point Load Index = 13 + 26 log NWI (R^2 = 1.00) ... 9.49

(h) For tuff (Oyama and Chigira, 1999)

Porosity, % = 21 – 13 log Predictor 1a (R^2 = 0.72) ... 9.50

Permeability X 10^{-4}, m/s = - 0.01 – 0.014 log NWI (R^2 = 0.77) ... 9.51

6.7 Summary

Several significant relationships between geochemical and geotechnical parameters could be established. Most strength parameters, as well as density, show positive relationships with MgO, CaO, FeO, pH and weathering indices, while showing negative relationships with Al_2O_3, Fe_2O_3 and H_2O+. Negative correlations are also shown by porosity with the abrasion pH value and permeability with depth. Compressive strength and density also show negative relationships with TiO_2 and positive relationships with Sr. A linear relationship between the Shore scleroscope hardness and olivine rim thickness was established.

Principal component analysis indicated that most variations of the chemical parameters could be explained by the subset of the following ten chemical parameters: Al_2O_3, MnO, MgO, CaO, Na_2O, K_2O, P_2O_5, Nb, Ba and H_2O+ concentrations. It was also determined that CaO explains 95 % of variations in other chemical concentrations. CaO and MgO concentrations could be used as discriminators of fresh Karamu Basalt.

Best subsets regression analysis produced several chemical predictors of geotechnical parameters. CaO, MgO and abrasion pH values were repeatedly appearing either as single predictors or as components in combinations.

The chemical Predictor x which includes abrasion pH value, TiO_2, Sr, and Fe_2O_3 concentration values, seems good in estimating geotechnical parameters such as California Bearing Ratio, dry density, porosity, permeability, compressive strength (P.L.) and water content for Karamu Basalt. Its applicability cannot be tested for other rock types excepting rhyolitic tephra due to incompleteness of data. It does not show good relationships with the geotechnical parameters of tephra. Modifications of the Predictor x, i.e. Predictor 1, Predictor 1a and Predictor 1b are suitable for a few lithologies but only Predictor 1b is suitable for Karamu Basalt. Predictor No. 2 is not versatile. The New Weathering Index formulated in Chapter 4 can be used for predicting geotechnical properties, not only of Karamu Basalt but of other rocks such as andesite, greywacke, and rhyolite. All statistically acceptable predictive equations are presented.

CHAPTER 7: SUMMARY OF WEATHERING OF KARAMU BASALT

7.1 Introduction

As evident from the previous chapters, the weathering of basalt is not a simple process where one can pinpoint a single factor or parameter that differentiates effectively and quantitatively between grades of weathered material. It is a complicated process involving chemical reactions which create a set of new minerals and physical changes within and between each stage of weathering. This chapter provides a synthesis of the data discussed previously as a basis for postulating a theory for weathering as given in Chapter 8.

It must be reiterated that, at the initial stages of this study, the different qualitative grades of weathering, viz. fresh, slightly weathered, moderately weathered, highly weathered and completely weathered were identified in the field based on the New Zealand Geomechanics Standards classification. The parameters which show a gradual change vertically along the weathering profile are depicted in Figure 7.1. With the help of the information accumulated, an attempt was made to clarify the complete weathering process of Karamu Basalt from points of view such as mineralogy, environment, chemistry, weathering indices and geomechanics.

7.2 Mineralogy

Chemical weathering of rocks is partly a change in mineralogy. The primary minerals olivine, titanaugite and plagioclase gradually disappear and a new set of secondary minerals take their place. These secondary minerals are the result of degradational processes and not strictly formative processes. Formation of iddingsite rims takes place at the initial stages of weathering but olivine does not disappear until the latter stages. Iddingsite, as previously observed by Colman (1982), can form without losing much of the major elements present and contains primarily Si, Mg and Fe. As weathering

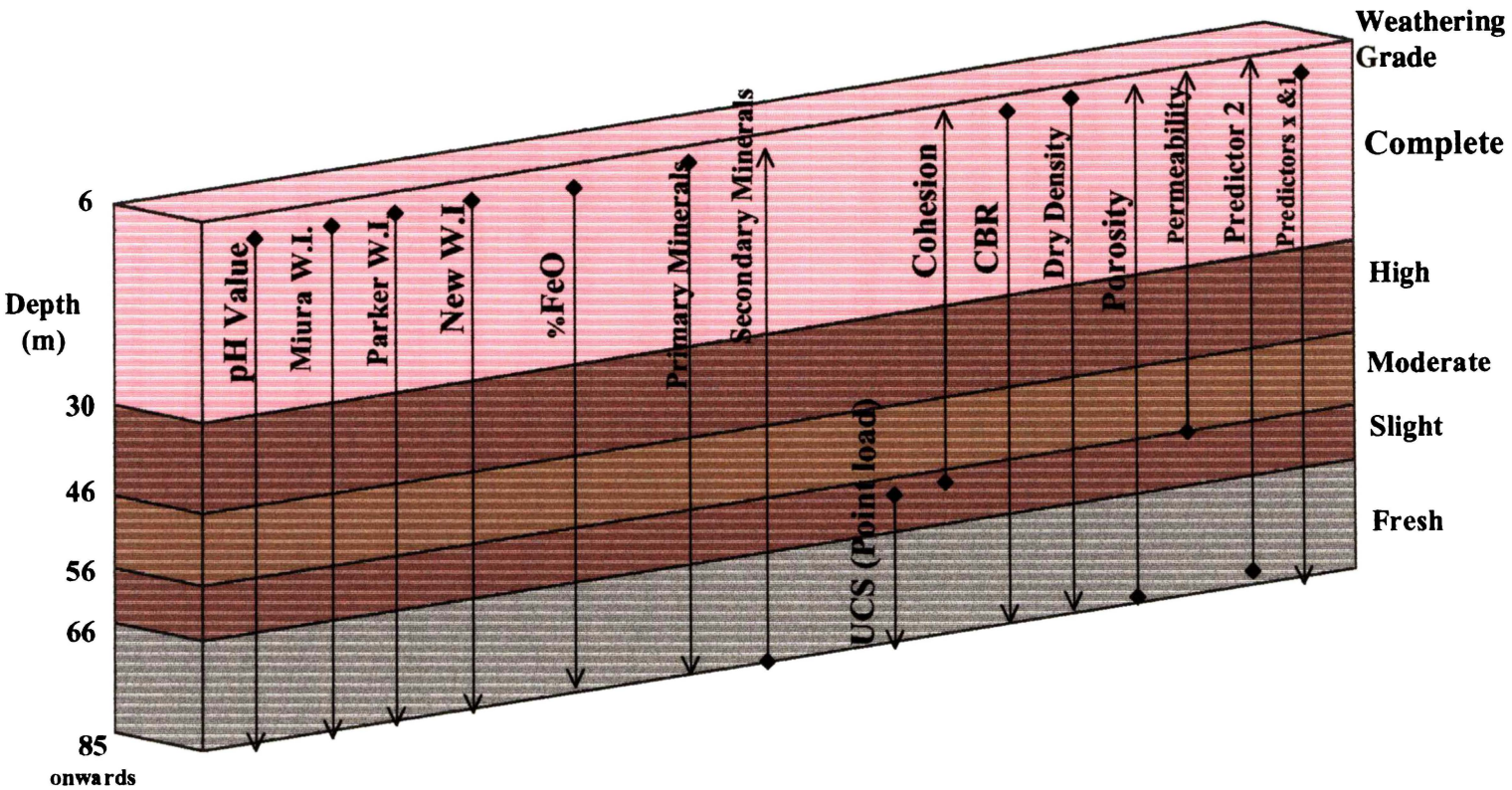

Figure 7.1 Significant Changes in Parameters with Depth

increases, the pale yellow iddingsite rims turn to redder hues and increase in thickness while the cores weather to clays. The end products are leached of Mg and consist mainly of iron oxides and oxyhydroxides.

Weathering of titanaugite takes place first at the grain edges and fractures. Titanaugite first develops cracks along cleavage planes and then alters to hematite. The end products of titanaugite are iron oxides, oxyhydroxides and some clay. Plagioclase phenocrysts first show a mottled appearance indicating sericitisation. Plagioclase laths first alter along grain fractures and grain boundaries and then disappear, turning completely to clay.

Titanomagnetite, which is scattered over the matrix, remains unaltered throughout the weathering process. Glass shows changes to smectite at the slightly weathered stage and later disappears completely. Eggleton and Keller (1982; in Moore, 1996) concluded that volcanic glass is the component most susceptible to weathering. The accessory minerals apatite and chromite disappear completely, probably forming soluble phosphates and chromates.

The order of commencement of dissolution as given by Moore (1996), i.e. glass > olivine > plagioclase > pyroxene > opaque oxides, has also been, to a certain extent, true for Karamu Basalt. However titanomagnetite, the opaque oxide present in Karamu Basalt, does not alter at any stage of weathering. The starting order of mineral disintegration for Karamu Basalt is glass > olivine > plagioclase > pyroxene while the finishing order (order of disappearance) is glass > plagioclase > pyroxene > olivine.

The minerals present in the completely weathered material are: titanomagnetite, goethite, hematite, manganosite, montmorillonite, illite, halloysite, kaolinite, beidellite, saponite and vermiculite. Considering grades of weathering in the light of mineralogical differences, based on petrographic studies, the pattern of Figure 7.2 was obtained.

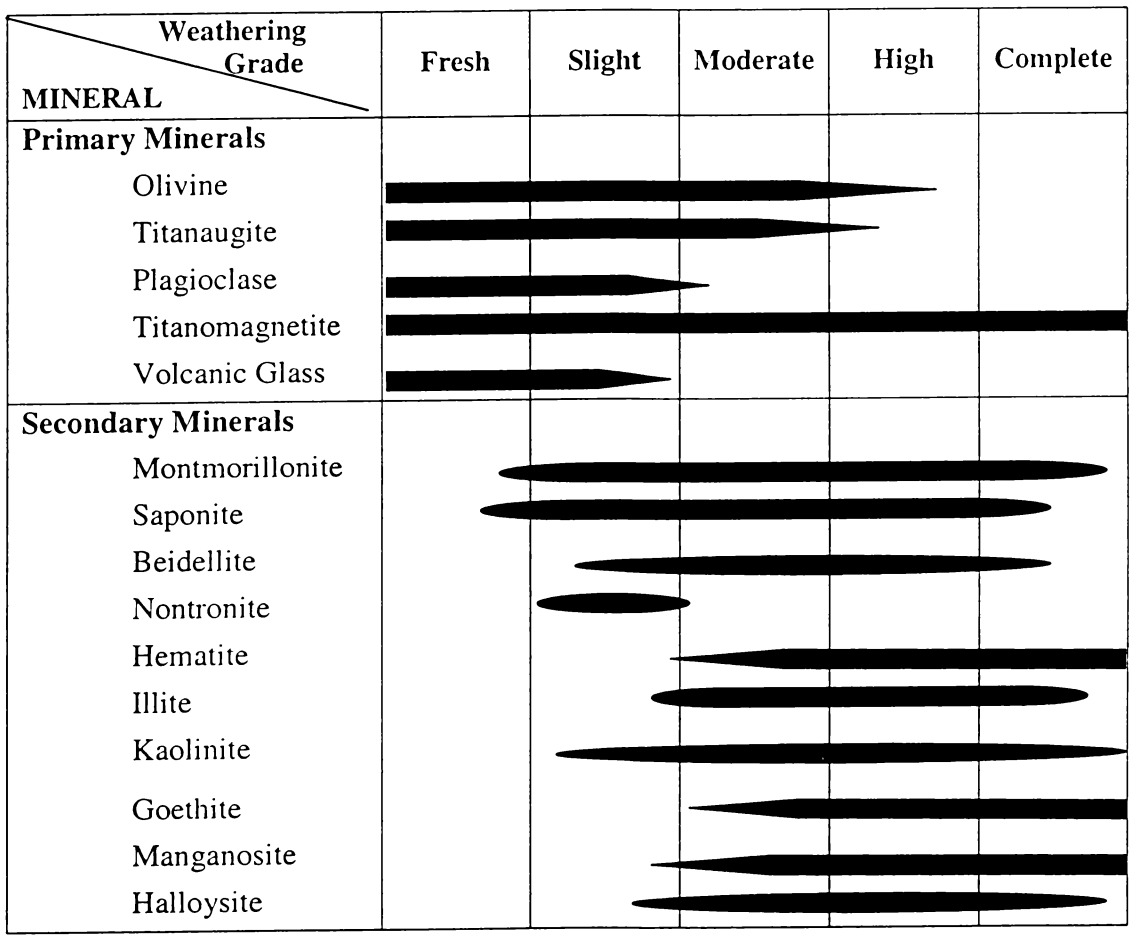

Figure 7.2 Changes in Mineralogy at Each Stage of Weathering of Karamu Basalt

7.3 Weathering Environments

Changes in environment can be important in understanding the processes of weathering. The reduction of the abrasion pH value from 8.5 in fresh rock to 4 in completely weathered rocks indicates an increase in acidity due to weathering. The increase in acidity is possibly caused by the release of hydrogen ions from water and incorporation into the weathering minerals. It can be assumed that the weathering started in a water- and oxygen-rich environment. When a mineral, which originally contained lower-valency cations, finds itself in oxidising environments, lower-valency cations such as Fe^{2+} will turn into higher-valency cations (Fe^{3+}) causing a decrease in size and a charge imbalance that could subsequently change the crystal structure. Fine cracks may have been present in primary minerals before the formation of secondary minerals but they noticeably widen the cracks while filling them. Outer dimensions of the primary mineral grains do not show a change, yet the strength could be affected negatively.

Further, moderate weathering causes olivine to alter to montmorillonite and saponite; and plagioclase to beidellite, kaolinite and illite. Titanaugite alters to montmorillonite and hematite. These new minerals have less dense structures, therefore the density of rocks can be affected. The formation of smectite indicates that at this stage the microenvironment may have been that of restricted drainage conditions as described by Glassman (1982). During intense weathering, smectites and illite undergo further changes. Smectites and illite are both partly replaced by kaolinite and halloysite (leaching out of other cations leaving aluminium and silicon). It is possible that the weathering profile was at well drained at latter stages.

7.4 Chemical Composition

As discussed in Chapter 4, major elements were recalculated assuming a constant Al concentration. The average percentages (Appendix 4.6) of all samples for each grade of weathering were plotted against depth (Figure 7.3a). SiO_2 shows no systematic trends of change in concentration throughout the complete weathering process. At the slightly weathered stage, the contents of the MgO, CaO and FeO drop markedly while Fe_2O_3 and H_2O+ concentrations increase significantly. By the moderately weathered stage, MgO, CaO and FeO concentrations drop to almost zero.

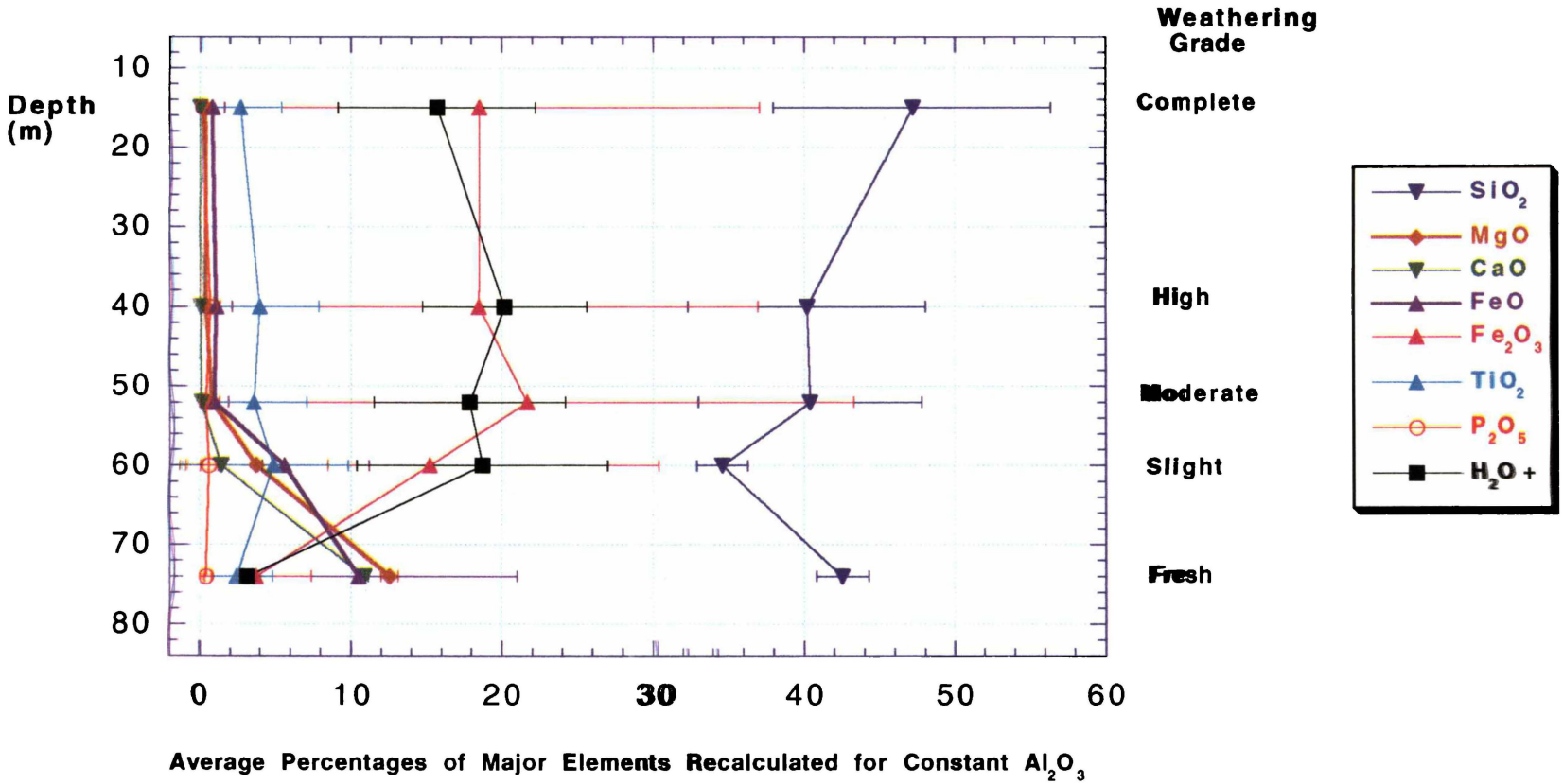

Figure 7.3a Changes in Recalculated Major Element Concentrations in Different Weathering Grades (error bars represent ± 1 standard deviation)

At moderately weathered stage, Fe_2O_3 experiences a further increase in concentration. At the highly weathered stage, no further changes are incurred except for the slight increase in H_2O+ and the slight decrease in Fe_2O_3, which drops noticeably at the latter stages of weathering. When the weathering is complete, SiO_2, H_2O+ and Fe_2O_3 show increased concentrations compared to the fresh rock. H_2O+ concentrations increase significantly. By the moderately weathered stage, MgO, CaO and FeO concentrations drop to almost zero.

TiO_2 and P_2O_5 concentrations remain more or less constant throughout the weathering stage. Therefore the elements Ti and P can be considered immobile.

Apparently loss of Mg and Ca takes place between fresh and moderate stages of weathering. The drop in Fe^{2+} is complete at the moderate stage of weathering, which gives an indication that the oxidation of iron is carried out in the first portion of the weathering process. Judging by the changes in major element concentrations, weathering has reached its most intense stage at the "moderate" stage itself. Ti, which is found mostly in titanomagnetite, remains in the profile since titanomagnetite does not alter in the weathering profile of Karamu Basalt.

Average compositions of trace elements (Appendix 4.4) of all samples from each stage of weathering were plotted against depth (Fig 7.3b -1 and 2). At the slightly weathered stage, a significant increase is shown by Cr, Ni, Ga, Y, Nb, Ba, La and Nd and a noticeable increase by V, Zn, Zr, Ce, Pb and Th. There is a decrease in Rb and Sr. At the moderately weathered stage, most of the trace element concentrations decrease, namely V, Cr, Ni, Zn, Y, Nb, Ba, La and Nd while Ga, Zr, Ce, Pb and Th continue to increase. Sr continues to decrease while Rb increases slightly. At the highly weathered stage, V, Cr, Ga, Nb, La, Ce and Nd increase while Ni, Y, Ba, Pb and Th decrease. Zn, Rb, Sr and Zr remain the same. When the weathering is complete, a drop in the concentrations compared to fresh rock is observed for Cr, Ni, Zn, Rb, Sr, Y, Nb, Ba and Nd. An increase in abundance is shown by Ga, Zr, Pb and Th. However, La, V and Ce remain more or less the same.

The differences from fresh to completely weathered basalt in V, Zn, Zr, Nb, La and Ce concentrations are small because they are relatively immobile.

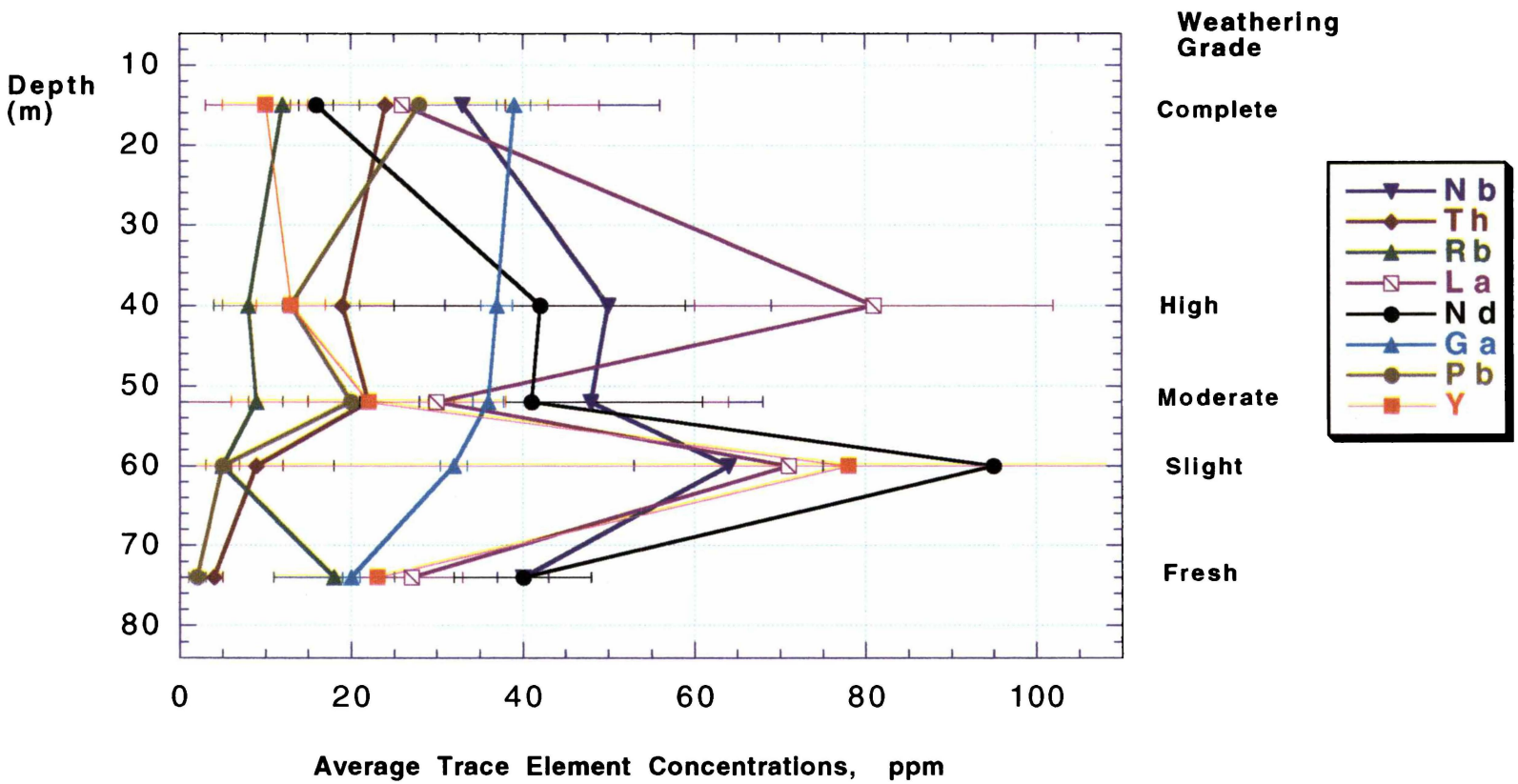

Figure 7.3b-1 Changes in Trace Element Concentrations in Different Weathering Grades (error bars represent ± 1 standard deviation)

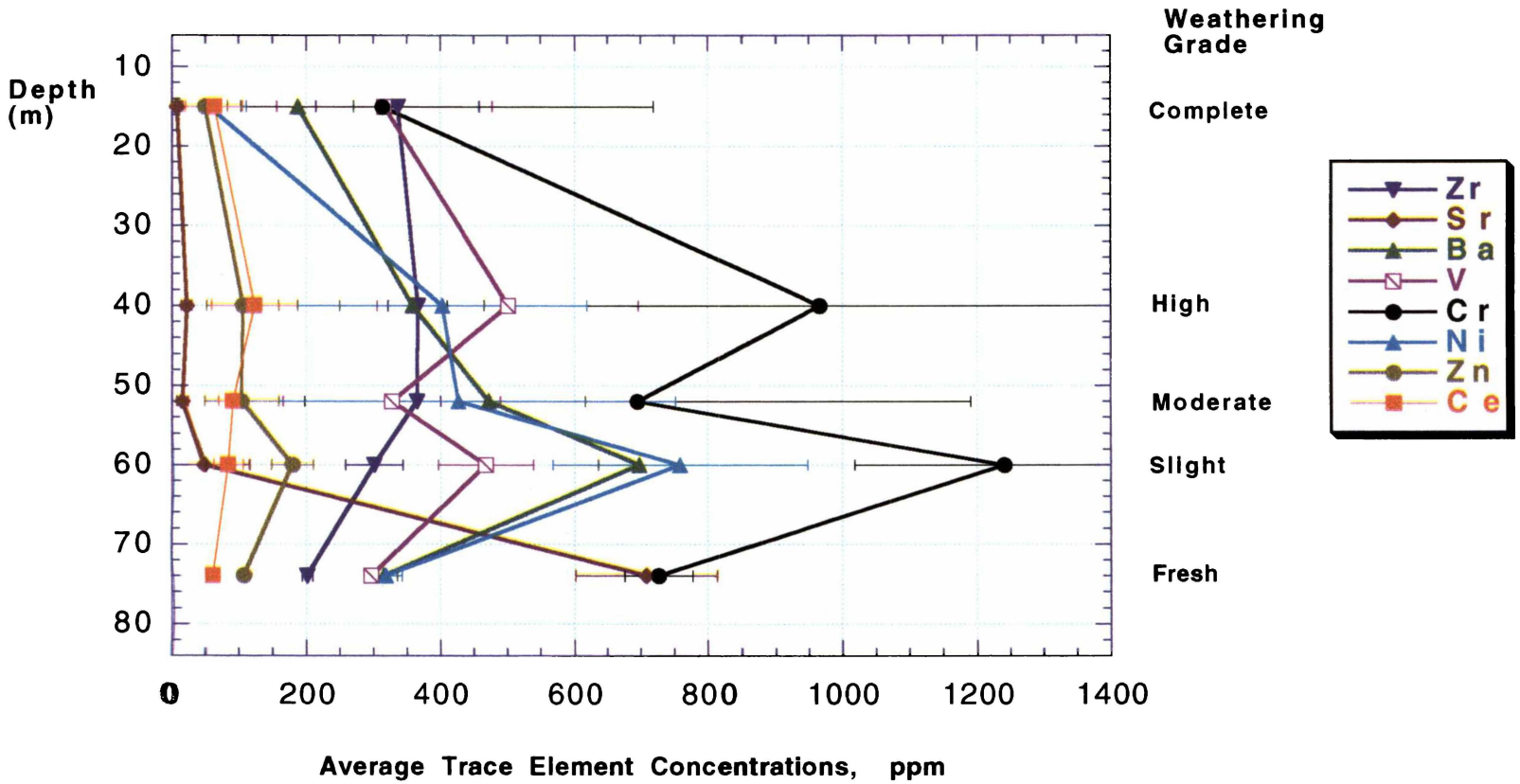

Figure 7.3b-2 Changes in Trace Element Concentrations in Different Weathering Grades (error bars represent ± 1 standard deviation)

Based on studies of some Australian basalts, Price *et al.* (1991, p 245) state "relatively slight alteration at the earliest stages of weathering can produce drastic changes in the concentrations of REE, Y and Ba, and petrographic assessment of the freshness of samples is not precise enough to eliminate, prior to analysis, cases where these effects may be manifested". In Karamu Basalt, the rare earth elements La, Ce and Nd as well as Y and Ba show a similar tendency (increase at the slightly weathered stage) to that described by Price *et al.* (1991). In this study, this phenomenon is also shown by a few more trace elements such as V, Cr, Ni, Zn, Ga, Zr, Nb, Pb and Th. At this stage of weathering, petrography does not indicate drastic changes in mineralogy.

According to the table of mineral/melt partition coefficients for basaltic rocks (Rollinson, 1993) Sr and Rb are present in plagioclase; Ni in olivine, augite and magnetite; V in magnetite and augite; Cr in magnetite and augite; rare earth elements in glass and magnetite. According to Nesbitt and Wilson (1992), Zn, Zr, Nb, Th, Ga and Y are found in glass.

Sr and to a lesser extent Rb have followed the pattern of Ca to which they have an affinity according to their ionic radii. Ba too decreases similarly, except for an increase at the slight weathering stage. Due to its large size, it may be affected by sorption. Th increases in concentration similar to Si which has the same tetravalent charge. Nb and Zr, which have charges and radii similar to Ti, follow Ti with its variability but recover their original concentrations at the end of weathering. The variations of trace element concentrations are taking place throughout the weathering process.

7.5 Weathering Indices

Weathering indices calculated for Karamu Basalt, except for the Reiche Product Index, are consistent in their patterns of change during weathering (Figures 7.3c- 1 and 2). They have a gradual decrease to moderate weathering and then remain low. Reiche Product and Weathering Product Indices (formulated for sedimentary rocks) decrease at slight weathering and then increase erratically. Both of these indices show considerable scatter in the averages calculated for each weathering grade, and are thus not considered

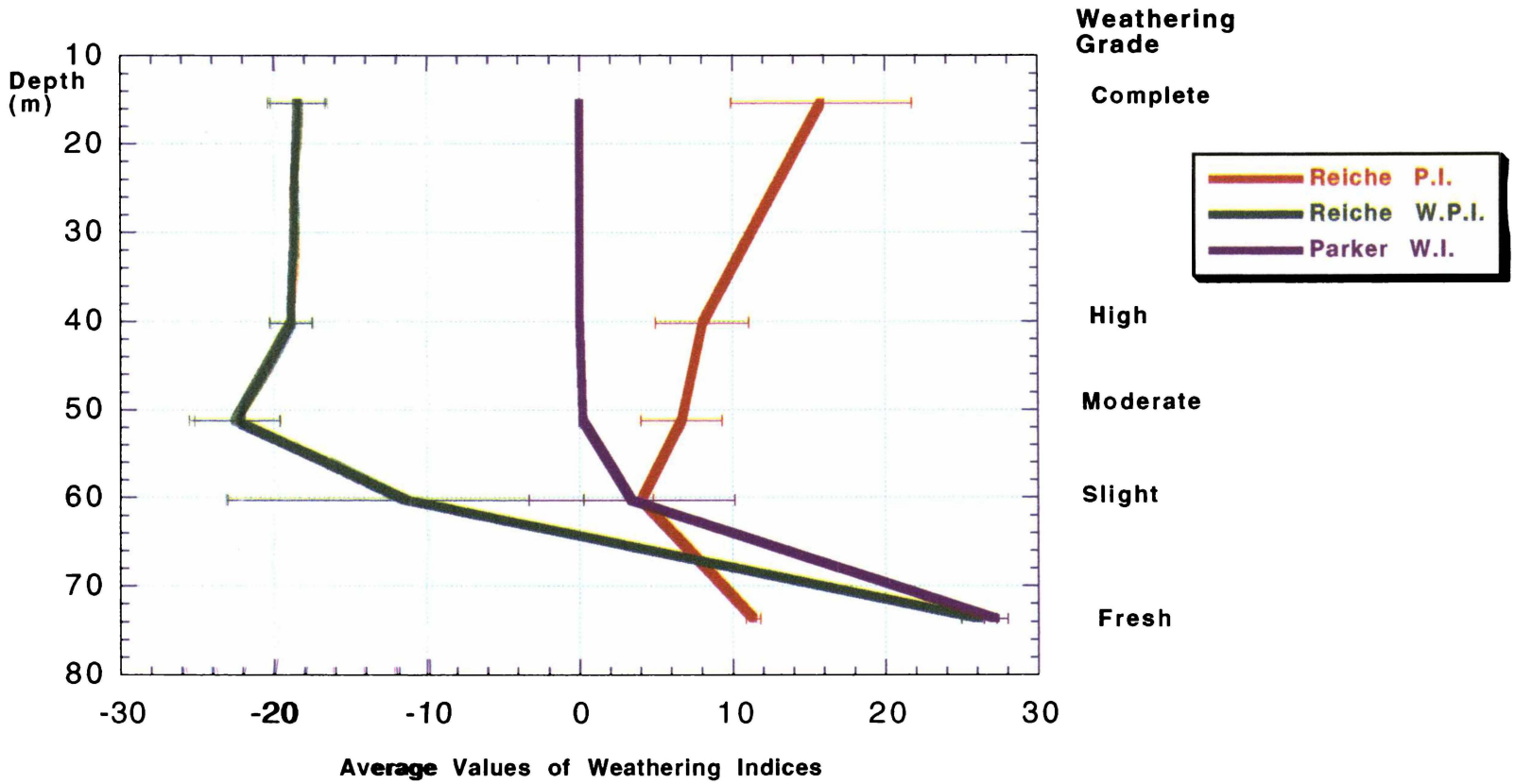

Figure 7.3c-1 Changes in Weathering Indices in Different Weathering Grades (error bars represent ± 1 standard deviation)

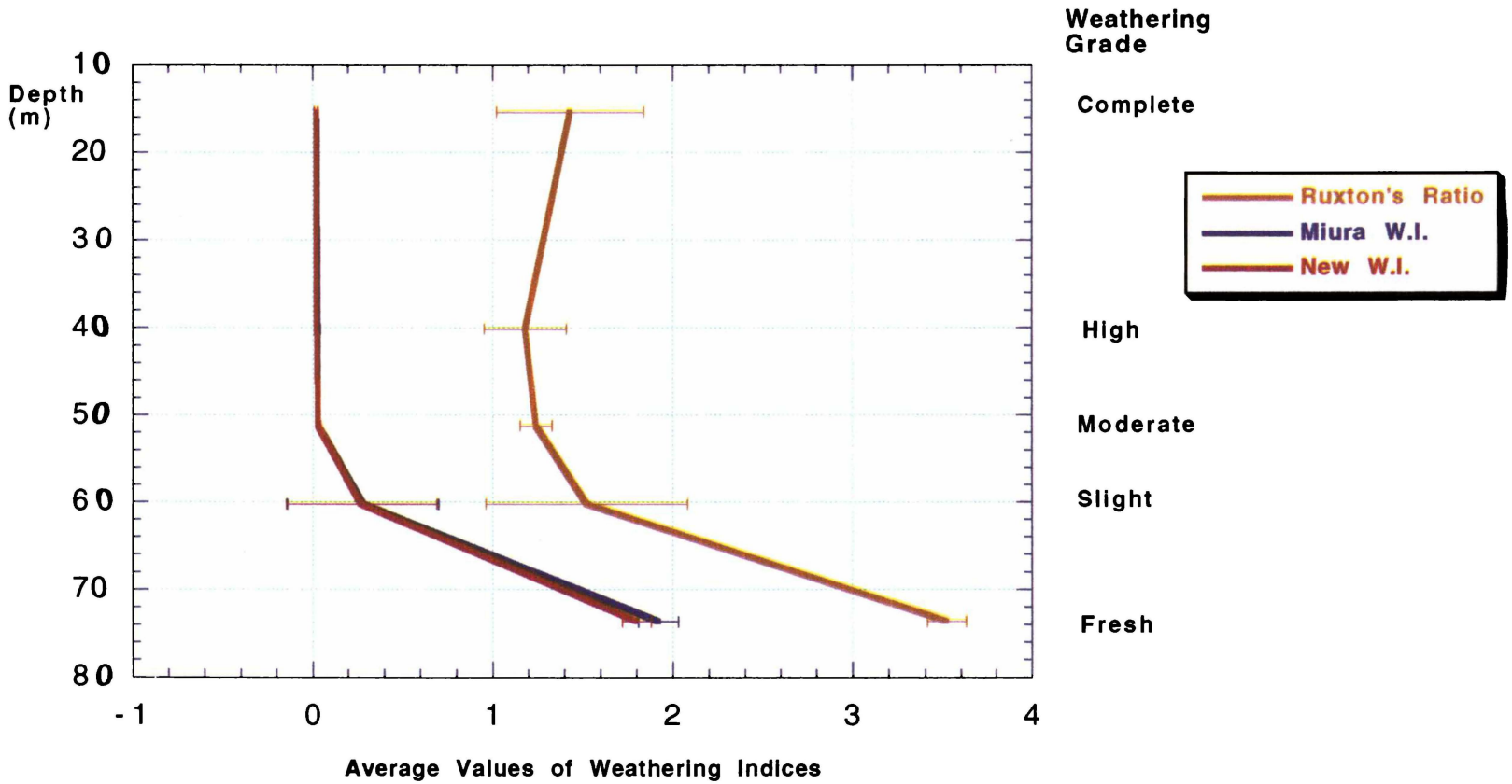

Figure 7.3c-2 Changes in Weathering Indices in Different Weathering Grades (error bars represent ± 1 standard deviation)

suitable for Karamu Basalt. Parker Weathering Index shows a general decrease with weathering, however the variation in the averages is large, and again cannot be considered suitable for Karamu Basalt. Ruxton's Ratio (formulated for granites), is restricted to SiO_2. Al_2O_3 and SiO_2 concentration in Karamu Basalt (Figure 7.3a) shows an erratic abundance pattern. This is reflected in the graph of Ruxton's Ratio (Figure 7.3c-2) that shows an increase from high to completely weathered basalt. A weathering index should not show a non-systematic change. Therefore, this is not considered a suitable weathering index for these mafic rocks.

The remaining two weathering indices are suitable descriptors of the weathering process. Miura Weathering Index (formulated for plutonic rocks) is comprehensive but gives equal weighting to elements such as Mn, Na and K, which are not important consitituents of Karamu Basalt, as to elements such as Mg, Ca, and Fe which statistical analysis indicated were the key elements in the weathering process. As described in Chapter 4, vertical changes with no lateral variation, were shown by the concentration patterns of MgO, CaO, FeO, Fe_2O_3, Al_2O_3 and H_2O+. The New Weathering Index is a variation of the Miura Index designed to simplify the calculation when dealing with mafic materials. It is formulated as the ratio of concentrations of MgO, CaO and FeO (which are reducing with the intensity of weathering), to the concentrations of Fe_2O_3, Al_2O_3 and H_2O+ (which are increasing with the intensity of weathering). Therefore, New Weathering Index can be considered most indicative of the weathering process of Karamu Basalt and other low-silica igneous rocks, because it better assesses the actual changes taking place during the weathering process of this material.

7.6 Geotechnical Features

Geotechnical features change at each stage of weathering and they are observed in the field in exposures, the most outstanding being the presence of joints. Fresh basalt has columnar jointing, presumably formed at the stage of solidification of lava. In fresh basalt, the columnar joints have an average spacing of 0.8 m and the joint apertures are open up to 10 mm wide. When slightly weathered, the joint apertures gradually increase to a maximum of 30 mm. Along the joint planes discolouration takes place. Brown earthy material, containing clay minerals, iron oxides and oxyhydroxides, partially fills

the apertures. Near horizontal fractures appear at ~ 0.8 m spacing on the columns, turning the rock mass into neat blocks. In moderately weathered basalt, these rock blocks convert into less angular corestones of 0.5 m or so in dimension. The space between them is filled with loose soil-like material, consisting of clay minerals, iron oxides and oxyhydroxides, formed during disintegration of the original rock. In highly weathered material, the rock blocks convert to corestones of smaller (0.1 – 0.3 m) dimensions. The vast majority of the material is soil, yet the relict structure reveals weathered corestones on close visual examination.

Completely weathered material does not contain any relicts from the rock but the original rock fabric remains preserved if undisturbed. Faint outlines of original joint planes can be traced. A significant feature of this weathering profile, which makes it rather unusual, is the absence of a layer of residual soil with no relict rock texture. The reason for this could be that before a substantial residual soil layer could be formed, rhyolitic tephra has been deposited several times over the weathering profile since 0.35 Ma.

7.7 Geotechnical Parameters

Except for the determination of California Bearing Ratio and some index properties such as density, porosity, and water content, the same geotechnical tests could not be applied to material throughout the weathering profile as the individual techniques are limited to narrow ranges of material characteristics. Most tests cover only some grades of weathering. Nevertheless, their average values are depicted on Figure 7.3d. Throughout the complete weathering profile, density and porosity complement each other, i.e. when porosity increases, density decreases and vice versa. Water content and permeability increase with weathering, following the pattern of porosity. California Bearing Ratio decreases following the pattern set by density. Reduction in density makes the material less strong, hence the decrease in California Bearing Ratio.

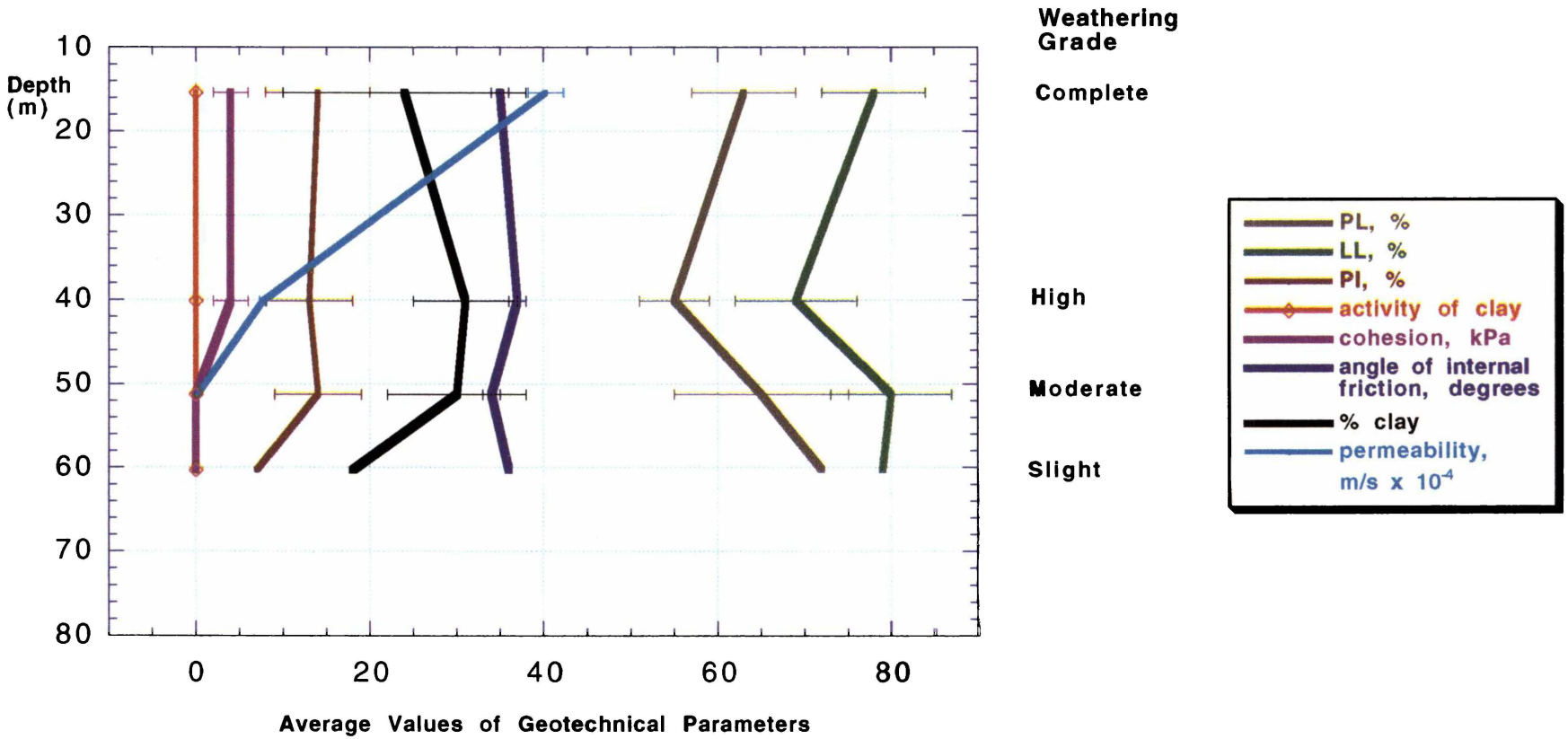

Figure 7.3d-1 Changes in Geotechnical Parameters in Different Weathering Grades (error bars represent ± 1 standard deviation)

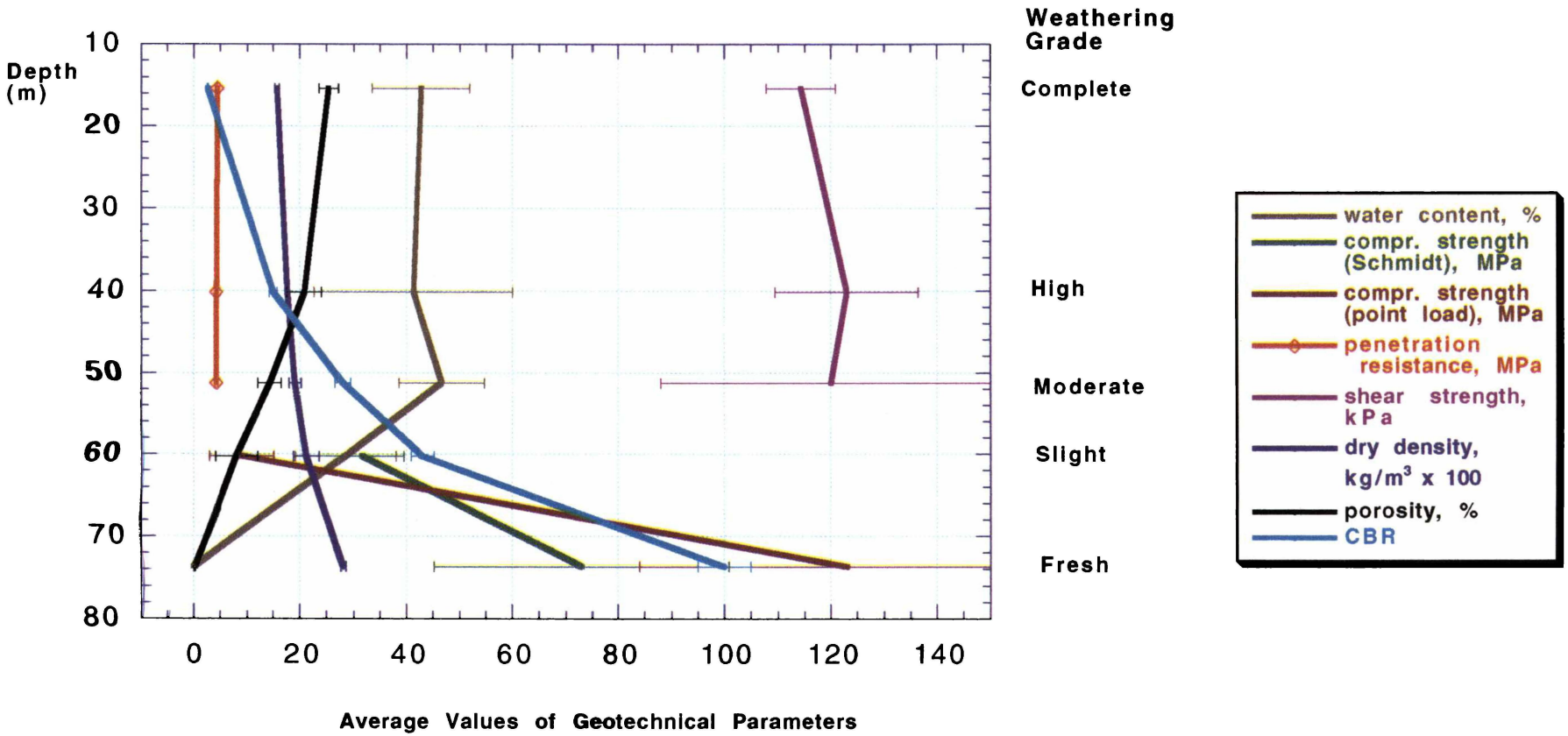

Figure 7.3d-2 Changes in Geotechnical Parameters in Different Weathering Grades (error bars represent ± 1 standard deviation)

Compressive strength values determined by Schmidt hammer and point load test are restricted to fresh and slightly weathered basalt, yet show a marked decrease in strength from fresh to weathered basalt. From slight to moderately weathered stage, there is an increase in cohesion, and plasticity. From moderate to highly weathered stages, average Atterberg limits, and shear strength parameters show no systematic changes with increased weathering, and the variation is less the measured standard deviations for each weathering grade. Therefore, beyond the moderately weathered stage, the weathering is characterized by an increase in the proportion of clay minerals (and changes in mineralogy as described above) within the weathering profile as the corestones continue to decay, but the influence of these changes on the measurable geotechnical parameters is negligible.

7.8 An Overview of the Weathering Process

The weathering process of the Karamu Basalt is complex, involving both chemical and physical changes. An attempt is made in Chapter 8 to postulate a hypothesis to explain the weathering sequence. To facilitate this, a conceptual model for the weathering process based on the measured changes is given in Figure 7.4. The following sections summarise the nature of the overall changes from one stage of weathering to the next.

7.9.1 From Fresh to Slightly Weathered

Fresh Karamu Basalt possesses inherent columnar jointing which facilitates vertical movement of water and air, which could aid the chemical weathering of constituent minerals. At the slightly weathered stage, titanaugite shows development of microfractures and olivine develops orange-coloured iddingsite rims. Oxidation of Fe^{2+} takes place, as evident from the reduction of FeO concentration and the increase in Fe_2O_3 concentration. This may also be the cause of discolouration of rock along joint planes. Mg^{2+} and Ca^{2+}, which are constituent cations of the three major primary minerals olivine, titanaugite and plagioclase, drop in content. This loss of major cations is petrographically connected to the mottled appearance in plagioclase, development of cracks in titanaugite and cryptocrystalline substances present in cracks. From the fresh to slight stages, intact rock loses ~50 % of its strength and a sudden occurrence of microfracturing is apparent.

Weathering Grade	GEOCHEMICAL ASPECTS OF WEATHERING PROCESS		GEOTECHNICAL ASPECTS OF WEATHERING PROCESS	
Fresh	Porphyritic texture Primary minerals only: olivine, titanaugite, plagioclase, titanomagnetite and glass Pale iddingsite rims in olivine	Presence of high concentrations of: SiO_2, Al_2O_3, MgO, CaO and FeO Highest abrasion pH value	Columnar jointing: spacing 0.8 m apertures 10 mm Very strong	High density Low porosity
Slight	Olivine: thicker iddingsite rims (17μm) Titanaugite: microfractures Plagioclase: turbid and speckly appearance Titanomagnetite unaltered Glass → smectites	Decrease in: SiO_2, MgO, CaO and FeO Increase in: Al_2O_3, Fe_2O_3 and H_2O^+	Joint apertures widen (20-30 mm) Discolouration on joint planes Strength medium	Less dense More porous
Moderate	Olivine: further thickening of iddingsite rims (30μm) Olivine and titanaugite → clays, hematite and goethite Plagioclase → clays Titanomagnetite unaltered	Increase in: Al_2O_3, Fe_2O_3 and SiO_2	Joints filled with brown clayey material Large core stones (~0.5 m) Low strength	Cohesive; plastic Medium density and porosity
High	Relict porphyritic texture Primary minerals altered but relict phenocrysts of olivine Clays abundant Titanomagnetite unaltered	Constant: Al_2O_3, Fe_2O_3 and SiO_2	Core stones smaller (0.1 – 0.3 m) More soil than rock	Higher cohesion and clay content Higher shear strength
Complete	Relict outlines of olivine and augite identifiable Secondary minerals (clays, hematite, goethite) and titanomagnetite constitute the material	Constant: H_2O^+ High Al_2O_3 and SiO_2 Decrease in: Fe_2O_3 Lowest abrasion pH value	Joint outlines still traceable Material completely soil Original structure retained Very weak	Highest porosity Lowest density High permeability High plasticity index

Figure 7.4 Proposed Conceptual Model for the Complex Weathering Process of Karamu Basalt

On a macro scale, fracture apertures widen and horizontal fracturing appears. Density of the rock decreases, while porosity and water content increase. Titanaugite shows development of cracks and olivine develops orange coloured iddingsite rims. At the slightly weathered stage, the abrasion pH values have dropped from an average of 8 to an average of 5.6.

7.9.2 From Slightly to Moderately Weathered

From the slight to moderate weathering stages, olivine, and titanaugite crystals decompose into minerals such as montmorillonite, saponite, goethite and hematite while plagioclase alters to kaolinite and illite. MgO and CaO now reach very low values but Al_2O_3 and Fe_2O_3 increase. Abrasion pH decreases from 5.6 to 5. Formation of clays changes the rock texture, turning the rock blocks into corestones in a matrix. Clay content creates cohesion. Porosity increases; density and intact strength reduce. Weathering indices gain very low values indicating that the geochemical changes of weathering are almost complete.

7.9.3 From Moderately to Highly Weathered

From moderate to high weathering stages, major element changes are more or less subdued, except for the decrease in abrasion pH value. Trace elements such as La, Cr and V show an increase. Primary minerals olivine, titanaugite and plagioclase change to secondary minerals goethite, hematite, kaolinite, illite, halloysite and beidellite. Corestones become more rounded and smaller (0.1 - 0.3 m) and the matrix is plastic, reflecting the presence of clay minerals. Most changes are within the matrix except for the reduction in size of corestones, indicating progressive weathering.

7.9.4 From Highly to Completely Weathered

From highly to completely weathered stages, weathering reaches its maximum extent. Porosity reaches its highest value and density its lowest value. Permeability values increase, while abrasion pH values are at their lowest. Al_2O_3 concentration increases and only secondary minerals are present. Material is all plastic soil, yet the original structure is retained, which prohibits classifying it as residual soil according to the NZ Geomechanics Standards (1988).

CHAPTER 8: INTERPLAY OF CHEMISTRY, MINERAL STRUCTURE AND ENGINEERING PROPERTIES

8.1 Introduction

The summary of weathering, as given in the previous chapter, suggests that there is a reasonable basis to postulate a new theory on the interplay of chemistry, mineral structure and engineering properties during early stages of rock weathering. This chapter proposes a hypothesis, and describes supporting evidence. A summary of the main conclusions from its evaluation together with a suggestion of a simplified engineering classification of weathering is presented at the end of the chapter.

8.2 Hypothesis

The plots of MgO, CaO and FeO versus depth and geotechnical parameters for which a full range of weathering grades is represented (California Bearing Ratio, dry density and porosity, and water content) versus depth show a striking resemblance. They all have a similar relationship to depth, most notably a "break" in slope. These similarities still exist when the oxide concentrations are recalculated assuming a constant Al_2O_3 content throughout the weathering process (these recalculated values are given in Appendix 4.6). A simplified view of these relationships sees both strength, density and oxide concentrations decreasing in a two-stage fashion (Figures 8.1 a-e): a rapid decrease occurs from fresh to moderately weathered, followed by only slight changes beyond this point (note that the lines shown on these plots are mere best-fit by eye estimates to highlight the general trends). Porosity and water content show mirror images of these trends (Figures 8.1 f and g). A concurrence between these trends is supported by the statistical analysis presented in chapter 6:

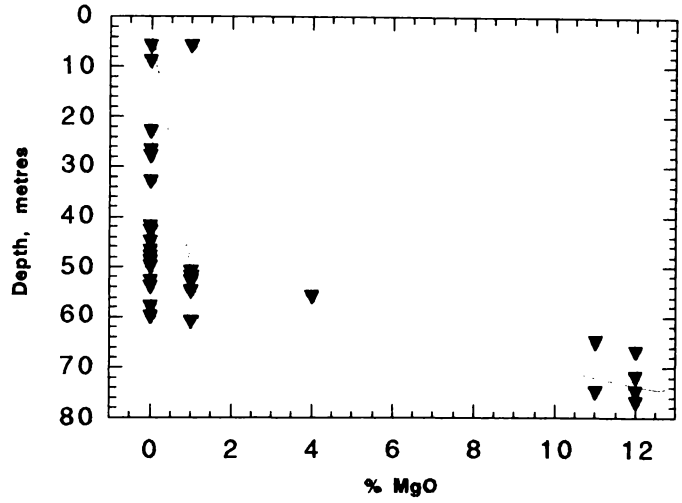

Figure 8.1a Plot of Depth vs %MgO (Recalculated for Constant Al)

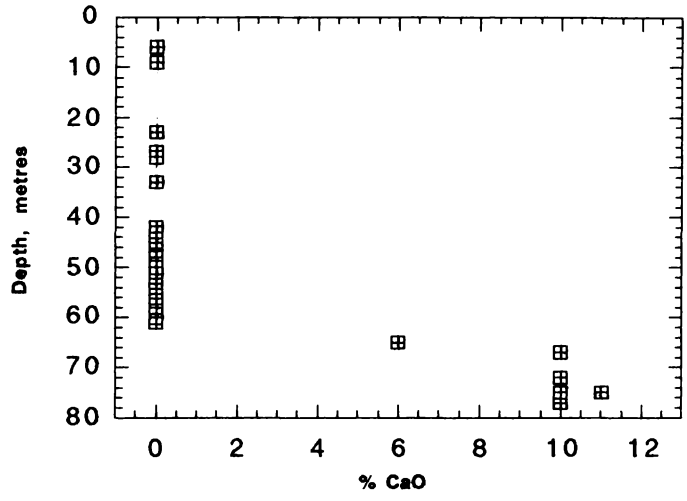

Figure 8.1b Plot of Depth vs %CaO (Recalculated for Constant Al)

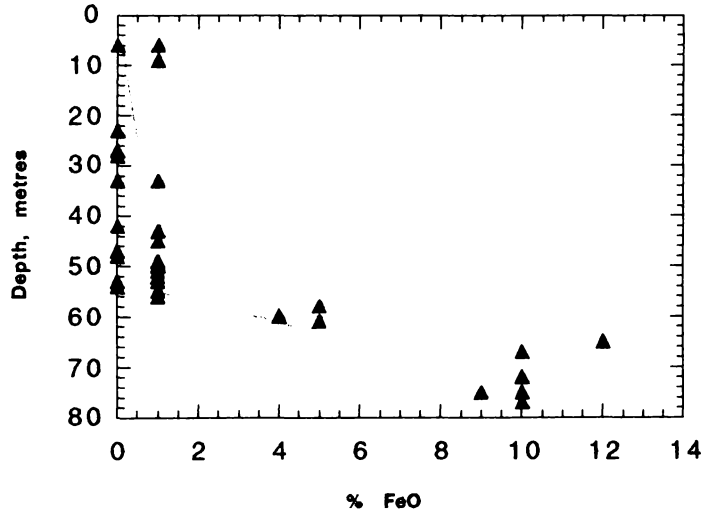

Figure 8.1c Plot of Depth vs % FeO (Recalculated for Constant Al)

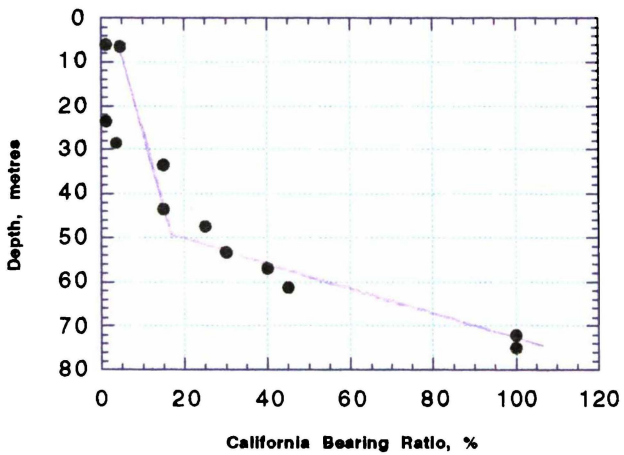

Figure 8.1d Plot of Depth vs California Bearing Ratio

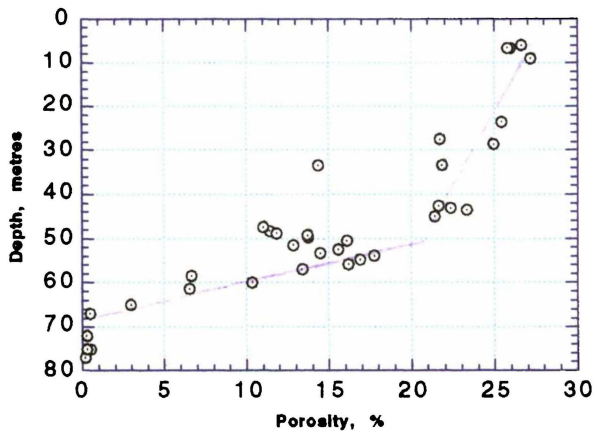

Figure 8.1f Plot of Depth vs Porosity

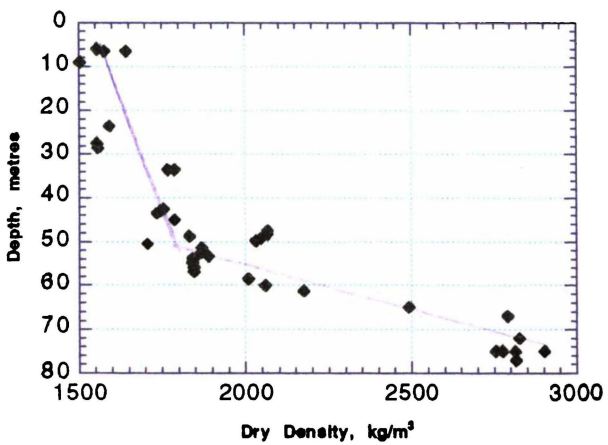

Figure 8.1e Plot of Depth vs Dry Density

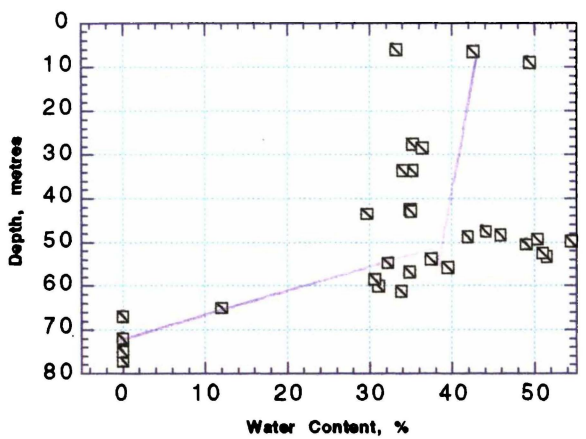

Figure 8.1g Plot of Depth vs Water Content

(a) Regression analysis indicated significant relationships between dry density versus the concentrations of CaO and FeO, porosity versus FeO, and CBR versus MgO and FeO concentrations

(b) The principal component analysis indicated that changes in CaO and MgO accounted for 95 % of the variation within geochemical parameters, and provided precise discriminators between fresh and weathered basalt

(c) Best subsets regression consistently recognised CaO and MgO as components of best subsets that could be used as predictors of geotechnical parameters

(1) It is suggested that there is a causal relationship between these trends: i.e. a decrease in the absolute quantities of the cations Mg^{2+}, Ca^{2+} and Fe^{2+} leads to a loss of strength of the rocks in the fresh to moderately weathered phase of weathering.

It is notable that of the observed chemical and mineralogical changes, measurable mineralogical changes appear to lag behind the chemical changes, and hence the slightly weathered rock still has an identifiable mineralogical suite similar to the fresh rock (Figure 7.4). Also, the rock mass shows little field evidence of the weathering process beyond some discoloration along fracture surfaces. This is despite a dramatic fall in the intact strength of the rock (Chapter 5). In a similar way, Price *et al.* (1991), working on basalts of Australia, observed a dramatic mobilisation of Ba and REE in the early stages of weathering with no associated discernable mineralogical changes. Similar trace element behaviour was reported in Chapter 4; it can be assumed that this mobilisation of trace elements may have been triggered by the removal of cations as documented here. Anomalous chemical concentrations in early grades of weathering without immediately recognisable mineralogical change have thus been documented previously.

(2) It is thus suggested that the chemical changes discussed above do not reflect a major change in the mineralogy of the material (although it is acknowledged that some minor changes have occurred), but indicate subtle changes in the structure of the minerals within the rock caused by the removal of Ca^{2+}, Mg^{2+} and Fe^{2+} ions from the crystal lattice, and by their replacement by H^{+} and possibly Al^{3+} ions. This causes a loss of stability and strength of the individual minerals, and hence a decrease in the intact strength of the rock.

By the slightly weathered stage, the microstructure of the material is significantly more fractured than in the fresh rock, but initially this is not apparent at a macroscopic scale. Towards the end of the slightly weathered stage, horizontal fractures become evident in the field expression of the rock.

(3a) The microscopic fracturing is hypothesised as an immediate response to replacement of Ca^{2+}, Mg^{2+} and Fe^{2+} with H^{+} (also Al^{3+}). Disruption of the crystal lattice is due to charge and ionic size differences of the original and substituting cations. Thus, the microfracturing is attributed to a "chemical" cause.

(3b) Larger macroscopic fractures, however, develop horizontally, and are believed to be the result of relaxation of the weakened rock mass towards the ground surface. A loss of intact rock strength will result in "locked in" stresses being greater than the tensile strength of the material, which will fracture in the direction perpendicular to the maximum tensile stress (vertical in this case). This breaks the rock mass into discrete prismatic units. Thus, the macrofracturing is attributed to a "physical" cause.

Once the available Ca^{2+}, Mg^{2+} and Fe^{2+} ions are essentially removed from the lattice, at the moderately weathered stage, the fracturing process ceases. However, the material has effectively lost all of its intact rock strength at this stage, and has an interlocked network of discontinuities. A large proportion of clay minerals now characterises the observed mineralogy. No further major strength loss is noted, but with further weathering the rock mass becomes more typically plastic, presumably as a consequence of the increasing proportion of clay minerals. The "rock" is now behaving as a soil for all practical engineering purposes, although hard corestones of intact material still remain.

(4) Following the exhaustion of the available, readily removed cations, weathering largely takes the form of conversion of primary minerals to secondary clay mineral species. This process is believed to happen largely by hydrolysis and is concentrated along the discontinuity surfaces. Further weathering decreases the

size of core-stones and increases the proportion of clay minerals, and the clay mineral species evolve following previously well described trends.

The four paragraphs in italics effectively develop a hypothesis for the weathering process. The following sections will consider these aspects in more detail, and present supporting evidence for these ideas.

8.3 Loss of Cations and Their Replacement with Other Cations

The initial loss of cations occurs in the very early stages of weathering, when the rock is still competent, though broken by a series of columnar joints.

8.3.1 Presence of Cations

The potential sources of the cations to be removed from the rock are given in Table 8.1. Since Karamu Basalt consists mainly of olivine, augite and plagioclase phenocrysts embedded in a groundmass of plagioclase microlites and glass, the presence of cations in them was considered.

TABLE 8.1 SOURCES OF CATIONS

Mineral	Ca	Fe^{2+}	Mg
olivine		♦	♦
titanaugite	♦	♦	♦
plagioclase	♦		
glass	♦	♦	♦

8.3.2 Process of Removal of Ca, Mg, Fe Cations

Several processes may be responsible for removing the cations from the material, each of which have been previously described by various authors:

(a) diffusion (Stegena, 1983; Colman and Dethier, 1986; Hochella and Banfield, 1995);

(b) hydrolysis (Loughnan, 1969; Selby, 1993; Bland and Rolls, 1998);
(c) dissolution (Fredericksen, 1951; Loughnan, 1969; Stegena, 1983; Schott and Berner, 1984; Wollast and Chou, 1984; Hochella and Banfield, 1995);
(d) leaching (Bland and Rolls, 1998).

8.3.2.1 Diffusion

Colman and Dethier (1986) note that optical examinations show that weathering can invade uncracked and uncleaved regions of silicate minerals via submicroscopic diffusion avenues. Diffusion is the process by which the cations can move within the crystal, without the help of a separate medium, from areas of higher concentration to lower. Stegena (1983) defines a diffusion process as one wherein the medium in which diffusion takes place does not move, only the unequally distributed materials move, owing to the concentration gradients to open joint surfaces. In this way Ca^{2+}, Mg^{2+} and Fe^{2+} and other ions can be transported out of crystals, and indeed the intact rock itself, without requiring pathways for water entry. Equally, any ion of low concentration within the intact rock can be transported inwards, allowing exchange.

The evidence to be expected for a diffusion process is:

(a) maintenance of euhedral crystal form despite chemical changes taking place;
(b) zonation from edge to centre of crystal reflecting concentration gradient of cations – this zonation likely to be equal around edges, also perhaps along cracks / cleavage areas;
(c) areas in the crystals without cracking or cleavage show evidence of alteration;
(d) concentration gradient across the mineral from centre to edge (after weathering).

The most convincing evidence for a diffusion process in the rocks in this study is the development of iddingsite rims around olivine crystals. These retain the outer form of the original olivine crystals, and gradually increase in thickness with further weathering. Thin yellow linings of the crystals' outer surfaces are already apparent in the fresh rock; this has been interpreted as being due to interaction with magmatic water during solidification (Colman, 1982). Once the rock is considered slightly weathered thick iddingsite rims are ubiquitous throughout the rock. The original rims in the material classified as fresh rock are thus believed to be the first indication of rock alteration via diffusion-controlled processes. Development of thick iddingsite rims in the slightly

weathered stage reflects the onset of weathering as the rocks are near to the surface and concentration gradients develop towards open joint surfaces.

8.3.2.2 Hydrolysis

Generically, hydrolysis is the process in which H^+ and OH^- of water react with ions of the minerals. The OH^- of the water becomes attached to the cations, available because of the diffusion process, to form hydroxides, thus releasing H^+, which later can occupy the positions where the cations were in the lattice. The formation of clay minerals is generally seen as the result of a hydrolysis process (Selby, 1993).

The evidence expected for a hydrolysis process is discoloration; change from original smooth crystal faces in areas where the mineral is in contact with water (fractures, cracks, cleavage planes) giving irregularities; widening of fractures and cracks; maybe some empty spaces due to removal of material (minor pitting) and secondary mineral formation.

In this study, possible evidence for hydrolysis is:

(a) sericitation (speckly appearance) in some plagioclase crystals along principal cleavage planes at the slightly weathered stage;
(b) microfractures in titanaugite in slightly weathered rock;
(c) thickening of iddingsite rims in olivine crystals in slightly weathered material;
(d) alteration of glass to smectites
(e) extensive development of secondary clay minerals from moderately to completely weathered basalt.

Some hydrolysis may occur in the early stages of weathering, but indications of intense hydrolysis are only shown at or after the moderately weathered stage when smectites and goethite are formed in large quantities.

8.3.2.3 Dissolution (Hydration)

Chemical dissolution of ionic compounds involves (Chang, 1998) the destruction of the three-dimensional networks in the solid, and separation of cations and anions from each other by hydration, which is the process of surrounding the separated charged ions by

polar water molecules. Hydration serves to stabilise the ions in solution and prevent cations from combining with anions (Chang, 1998).

Silicate minerals contain covalent bonds; these bonds are not readily broken down in water, requiring initial reactions to separate the cations from the anionic groups. The term "dissolution" as used in a mineral sense is thus a rather looser term referring to two processes:

(a) the cations are initially separated from the anionic group (possibly by hydrolysis as described above); and
(b) the cations and anionic groups are then hydrated to disperse them within the water phase.

A common equation describing dissolution of olivine (forsterite) is as follows:

$$Mg_2SiO_4 + 4H_2O \rightarrow 2Mg^{2+}(aq) + 4OH^-(aq) + H_4SiO_4(aq) \quad \ldots 8.1$$

In this case, the Mg^{2+} and OH^- ions and the H_4SiO_4 are hydrated individually, and dispersed within the water. In this way, material is removed from where the water can come into contact with the material, such as along outer surfaces, cracks, pores, or open cleavages (Baynes and Dearman, 1978).

Ca in ferromagnesian minerals behaves in the same chemical manner as it does in the weathering of feldspars. Althaus and Tirtadinata (1989) state that feldspar dissolution takes place as a first step forming a thin layer of hydroxonium feldspar $(H_3O)[AlSi_3O_8]$ via ion exchange of H_3O^+ for K^+ or Na^+. A hydration front moves into the feldspar matrix ahead of a leaching front. The subsequent steps of feldspar dissolution can be hydrolysis of the hydrogenated feldspar.

A diffusion model and a surface reaction model for mineral dissolution are proposed by Eggleston and Hellmann (1989) who stated that in albite, Na-O, Al-O and Si-O bonds have different strengths and therefore the rupture will be differential.

In Karamu Basalt, evidence for dissolution includes (see section 4.2):

(a) a few pits filled with smectite in crystals of olivine at the moderately weathered stage;

(b) titanaugite crystals have diminished in size in thin-section, replaced by hematite and goethite, and show occasional evidence of surface pitting (etch-pits) and blunted edges under SEM from the slightly weathered stage ; and

(c) disappearance of plagioclase crystals, and replacement by clay minerals, mainly smectites, at and beyond moderately weathered

(d) alteration of glass to smectites.

As for hydrolysis, evidence of minor dissolution is apparent early in the weathering process, but substantial changes appear only after the moderately weathered stage.

8.3.2.4 Redox (oxidation-reduction reactions)

Some elements can exist in several oxidation states. The stability in any oxidation state depends on the energy change involved in adding or removing electrons (Ollier, 1984). Oxidation of minerals by gaseous oxygen occurs probably entirely by the intermediary of water, present in quantity ranging from films of moisture to complete immersion (Carrol, 1970).

According to Frye, (1974), the Fe^{2+} in the ferromagnesian minerals is unstable in the presence of free O_2. The two following separate reactions may take place:

(a) Under reducing conditions, Fe^{2+} may be taken into solution as a soluble cation, its ionic potential being between that of Mg^{2+} and Ca^{2+}.

(b) Under oxidising conditions, Fe^{2+} is a hydrolysate element (helps hydrolysis).

The following oxidising reaction equation can be written:

$$2Fe^{2+}(aq) + 1.5O_2 \rightarrow Fe_2O_3 \qquad \ldots 8.2$$

The oxidation product can be partially goethite α.FeO(OH) plus lepidocrocite γ.FeO(OH).

Bland and Rolls (1998) stated that FeO formed by the hydrolysis of olivine oxides to form goethite as follows:

$$2FeO + 0.5O_2 + H_2O \rightarrow 2FeO(OH) \quad \ldots 8.3$$

In Karamu Basalt, the evidence for Redox could be observed as:

(a) brown outlines in olivine in early stages of weathering and in later stages brown colouring of olivine and augite grains
(b) in thin sections iron staining can be seen in space between mineral grains
(c) brown colour in the weathered material

8.3.2.5 Leaching

Leaching is the removal of soluble elements from rocks by percolating water (Whitten and Brooks, 1972). Leaching thus provides a transport mechanism for components of weathered primary minerals, but even though it does not provide a ready mechanism for separation of the cations from the crystal lattice, it can be considered to effectively enhance diffusion. Hydrolysis and dissolution thus separate the components from the solid; leaching serves to move these materials once in the aqueous medium.

In the rocks of this study, there is no evidence for leaching preserved in the slightly and moderately weathered specimens. However, at later stages of weathering (highly and completely weathered) the following features are apparent (as mentioned in Chapter 4) which may be indicative of leaching (among other processes):

(a) discoloration from black to shades of brown in the matrix, and yellow and white clays along fracture planes;
(b) bands and lenses of hematite and goethite;
(c) clay concentrations in the matrix; and
(d) manganese oxide nodules.

8.3.2.6 Synthesis

From the evidence above, it can be concluded that diffusion is the most important mechanism for removal of cations in the very early stages of the weathering process. At latter stages, the evidence indicates that hydrolysis, dissolution, Redox and finally leaching become the controlling factors. However, it must be recognised that none of these mechanisms act in isolation, and some evidence is apparent for each process at all stages of weathering.

8.3.3 Replacement

Removing the cations from their lattice positions creates a charge imbalance within the crystal lattice. This can be remedied by the influx of other cations, such as H^+ and Al^{3+}. H^+ is available in water and is mobile; it is therefore assumed that the H^+ is the important replacement cation owing to its availability and mobility. Both H^+ and Al^{3+} cations are present in the slightly and moderately weathered samples based on the chemical analysis (Al^{3+}), and abrasion pH measurements (H^+). Al^{3+} cations are found by Eggleton (1984) to be present in the iddingsite rims of olivine at markedly higher concentrations than in the associated olivine crystals themselves (3.28 % cf. 0.05 %).

In fresh Karamu Basalt, the abrasion pH value is 8.5 indicating that alkaline earths (Ca, Mg) are still present. At the slightly weathered stage, an abrasion pH of 5.6 suggests that alkaline earths have been removed and there is more H^+ in the system; at moderately weathered level, abrasion pH decreases further to 5, which means more H^+ ions are in the system, taking the place of alkaline earths. From this, it is inferred that H^+ is playing an active role in the diffusion mechanism, and this is in keeping with the recognition of abrasion pH as an important indicator of weathering grade.

Comparison of sizes based on ionic radii of elements for coordination number 6 (Aylward and Findlay, 1998) is possible using Table 8.2.

TABLE 8.2 IONIC RADII FOR DIFFERENT CATIONS IN COORDINATION 6
(after Aylward and Findlay, 1998)

ELEMENT	IONIC RADIUS picometres (10^{-12} m)
Magnesium (Mg^{2+})	72
Calcium (Ca^{2+})	100
Iron (Fe^{2+})	78
Iron (Fe^{3+})	64
Aluminium (Al^{3+})	53
Oxygen (O^{2-})	140
Hydrogen (H^{+})	negligible

It is suggested that replacement of Mg^{2+}, Ca^{2+}, or Fe^{2+} with H^{+} or Al^{3+}, involves a weakening of the crystal structure which leads to a loss of strength in the crystals because:

(a) they have different valencies which cause a charge imbalance;

(b) the reduction in size disrupts the bond angles and interionic spacings and thus reduces bond strength.

Iddingsite is a complex of goethite and layer silicates. Its formation indicates loss of Mg from olivine and increase of Al. When considering the ionic radius ratio, if H^{+} and Al^{3+} substitute for Mg^{2+} and Fe^{2+}, the crystal lattice might become metastable and thus be disrupted by the applied stress. This might be achieved as an initial diffusion controlled reaction, simplistically represented here as:

$$Mg_2SiO_4 + 2H^{+} \rightarrow MgH_2SiO_4 + Mg^{2+} \qquad 8.4$$

Followed by the hydrolysis of the displaced cation

$$Mg^{2+} + 2H_2O \rightarrow Mg(OH)_2 + 2H^{+} \qquad 8.5$$

There is insufficient published information available to allow genuine calculation of bond strength changes associated with these possible changes to primary minerals. However, by analogy of the changes in crystal strength within the olivine group as the proportions of Mg and Fe vary along the solid solution between forsterite and fayalite, the importance of lattice dimensions and charge imbalance on mechanical properties can be appreciated. In the olivine series, replacement of magnesium by iron increases the lattice parameters by a few percent. Deer *et al.* (1962) have given the cell parameter and ionic radius data (Table 8.3).

TABLE 8.3 CELL PARAMETERS, IONIC RADII (after Deer *et al.* 1962) AND BULK MODULUS (after Carmichael, 1982)

Mineral	Cell Parameter a, Å	Cell Parameter b, Å	Cell Parameter c, Å	Major Cation Radius, (10^{-12} m)	Bulk Modulus MPa
Forsterite	4.76	10.20	5.99	66	127930
Fayalite	4.81	10.48	6.10	74	136570

A change from fayalite (Fe_2SiO_4) to forsterite (Mg_2SiO_4) would mean that bivalent iron is being replaced by magnesium. In this case, there is a decrease of 1 % in the lattice parameters and a decrease of 11 % in ionic radius. When comparing the isothermal bulk modulus (incompressibility) as given by Carmichael (1982) and included in Table 8.3, a decrease of 6.3 % from fayalite to forsterite is apparent. It is therefore interpreted that there is a direct relationship between ionic radius changes and strength changes. Without substantial evidence, it is assumed that this relationship is linear, as this is the simplest form of relationship possible when no physical evidence exists to suggest that a more complex model should be employed.

According to the above mentioned analogy a replacement of Mg^{2+} with Al^{3+} represents a 23 % decrease in radius, therefore, at least a 2 % decrease in the lattice dimensions might be expected. However, this replacement also reduces the radius to charge ratio by nearly 50 %, which will significantly enhance the difference, so lattice parameters may be reduced by as much as 4 %. Therefore, if magnesium were replaced with aluminium

in the primary minerals of Karamu Basalt, the decrease in lattice dimensions will be expected to cause a decrease in the bulk modulus of > 12 %. It is thus inferred that intact strength will be similarly decreased.

8.4 Development of Stress Release Fractures in Karamu Basalt

Most of the fractures observed in Karamu Basalt are vertical columnar joints with an average spacing of ~ 0.8 m. These are the result of tensile fracture during cooling of the lava. They are present in the fresh basalt rock mass and are thus not part of the weathering sequence examined in this study. However, their presence facilitates the weathering process as they allow for water and air movement.

There is an increase in fracturing on a macroscopic scale in the slightly weathered rock, particularly the appearance of near-horizontal fractures (section 5.2.2 and Figure 5.1). These fractures divide the rock into discrete blocks of ~ 0.8 m size. At the moderately weathered stage, these fractures increase in frequency and form corestones of ~ 0.5 m dimension. The space between them becomes filled with clays (illite and smectite) and hematite. This section considers the mechanism of horizontal fracture development.

In the case of the rocks in this study, the maximum tensile stress is developed towards the ground surface, as lateral confining stresses have been little affected by erosion until the very recent development of the quarry (1970s). As the density of the overlying material decreases with later stages of weathering owing to the alteration of primary minerals to lower density secondary clay minerals and sesquioxides, the overburden stress decreases. The rock body attempts to expand vertically through relaxation of the residual stresses, which remain from both cooling stresses (Bock, 1979) and previously higher overburden stresses.

The imbalance in the crystal lattice induced by the removal of cations results in a considerable loss of compressive strength in the slightly weathered basalts of this study (the average compressive strength values estimated from point load tests were for fresh basalt: 123 MPa; slightly weathered basalt: 9 MPa). Whilst tensile stresses were not determined, it is assumed that an analogous loss of tensile strength would have taken

place. A loss of tensile strength means that cracks can propagate by extension through tensile fracture at their tips much more readily.

It is suggested that the strength drop observed in Karamu Basalt is sufficient to allow crack extension in response to locked-in stresses alone. The compressive strength of slightly weathered Karamu Basalt is of the same order of magnitude as the residual stresses measured by Bock (1979) in basalt columns (15 MPa). Therefore, residual tensile stresses are inferred to be adequate to allow the development of macrofractures in the slightly and moderately weathered basalts. Initial horizontal fractures develop at the slightly weathered stage. These become more frequent and open thereafter.

8.5 Further Weathering and Development of Secondary Minerals

Observations of increased clay abundance, increased plasticity, decrease in density, and appearance of secondary minerals as seen from XRD results all indicate a dramatic increase in clay content beyond the moderately weathered stage. This section briefly reviews the "back end" of the weathering process. The development of clay minerals during weathering is well accepted and detailed in many texts (Nahon *et al.*, 1982; Wollast and Chou, 1984; Ollier, 1991; Velde, 1992). Only a brief indication of the relevance to the rocks in this study is given here.

Velde (1992) notes that high-temperature silicate minerals become unstable under atmospheric conditions, particularly in response to the water forming mineral structures containing crystalline water that is hydrogen bonded in the form of OH units. These structures are recognised as clay minerals.

Colman (1982) gives the following as an idealised sequence for the alteration of olivine and pyroxene to clays:
fresh mineral → montmorillonite → halloysite → kaolinite → gibbsite
but notes that not all stages are seen in any single sequence, with the full sequence being most common in the weathering of ferromagnesian minerals.

In basaltic rocks, Haskins and Bell (1995) observed the formation of expansive clays, predominantly montmorillonite, due to deuteric alteration of glass, olivine, pyroxene and plagioclase. They see the formation of montmorillonite from volcanic glass as being

in two stages: the development of palagonite, a hydrated mafic volcanic glass, associated with the release of iron oxides; followed by crystallisation to form montmorillonite. They observe the montmorillonite to be concentrated in small (0.5 – 1.2 mm), disseminated clay spots.

Fresh Karamu Basalt consists of 33 % olivine, 28 % titanaugite, 34 % plagioclase and 2 % glass. Considering the chemical composition of the above, it is possible that they all turn into smectite, at least partially, during weathering. Montmorillonite and saponite are the earliest formed smectites, followed by nontronite and beidellite. After smectites, illite is formed, followed by kaolinite and then halloysite.

8.6 Comparison with Other Rock Types

Returning to the similarities mentioned earlier in the case of Karamu Basalt, between the distribution of California Bearing Ratio, dry density and the three ions of Ca^{2+}, Mg^{2+} and Fe^{2+}, an attempt was made to compare these for other rock types. Bassett (1998) has determined California Bearing Ratio for greywacke and andesite in Coromandel, New Zealand (data given in Appendix 8.1). Information regarding the depths of the greywacke and andesite samples is not available since they have been collected from several different locations along a road. However, Bassett (1998) has followed the same classification system as used in this study enabling a comparison within the corresponding weathering grades. In order to check the changes in the weathering profile, samples were numbered in the descending order from fresh to completely weathered basalt as follows: fresh – 5; slightly weathered – 4; moderately weathered – 3; highly weathered - 2 and completely weathered – 1.

California Bearing Ratio, dry density, porosity and water content values were plotted against these ranks for greywacke, andesite and Karamu Basalt (Figures 8.2 a -d). A similarity of trends can be observed. Plots of normalised (percent current / percent initial) MgO and CaO values against the weathering grade for greywacke (Bassett, 1998 had determined only total Fe concentrations hence FeO could not be plotted) and Karamu Basalt were made (Figures 8.3 a & b). In both cases, greywacke follows the trend of basalt. It has been postulated that due to weathering of basalt, the strength is

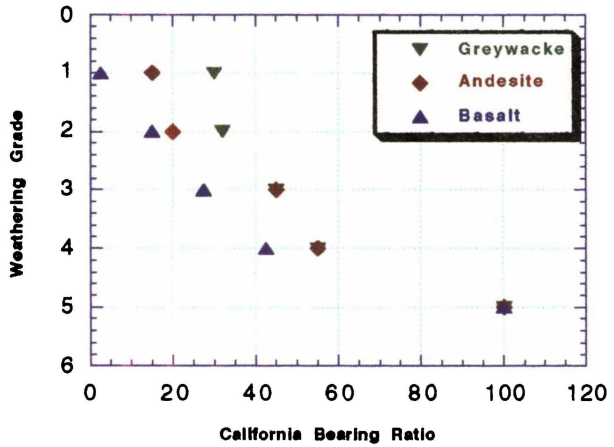

Figure 8.2a Plot of Weathering Grade vs California Bearing Ratio

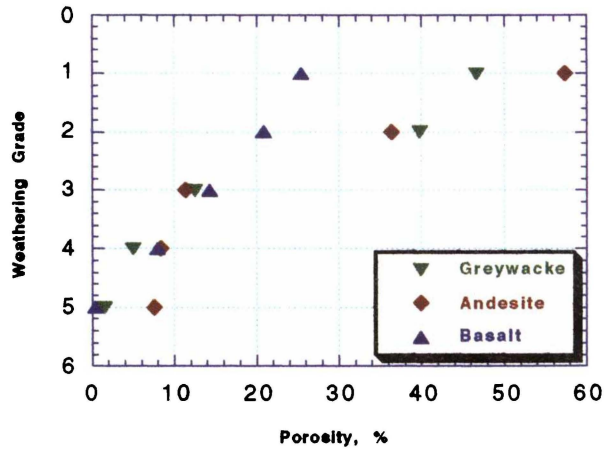

Figure 8.2c Plot of Weathering Grade vs Porosity

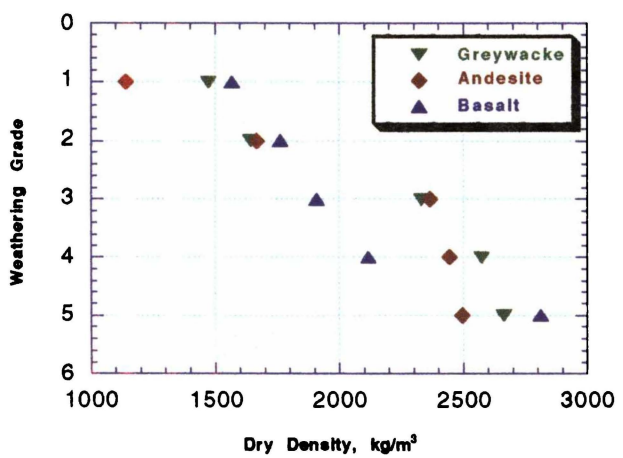

Figure 8.2b Plot of Weathering Grade vs Dry Density

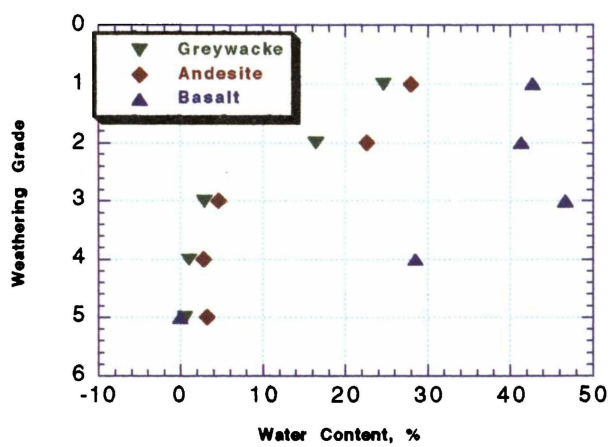

Figure 8.2d Plot of Weathering Grade vs Water Content

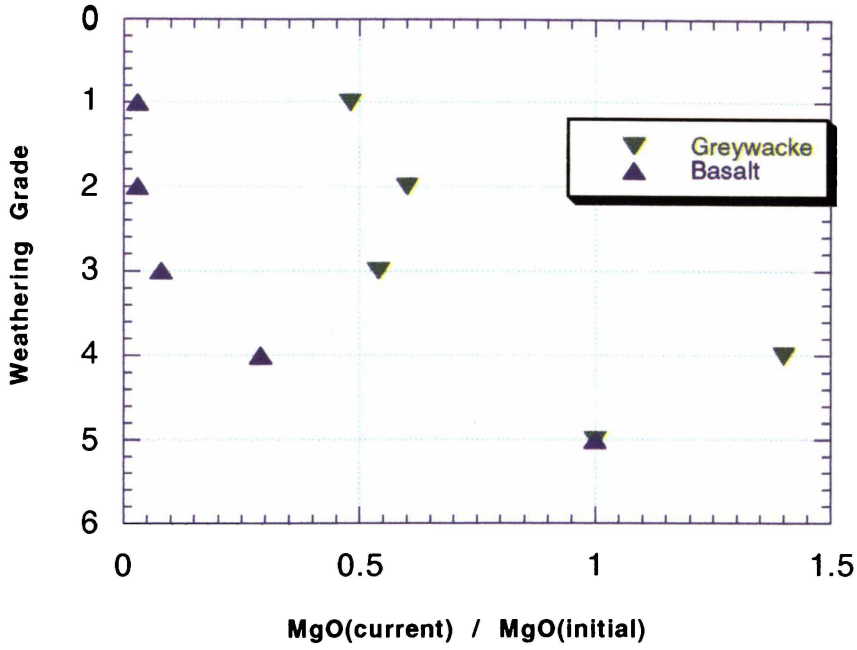

Figure 8.3a Plot of Weathering Grade vs Normalised MgO

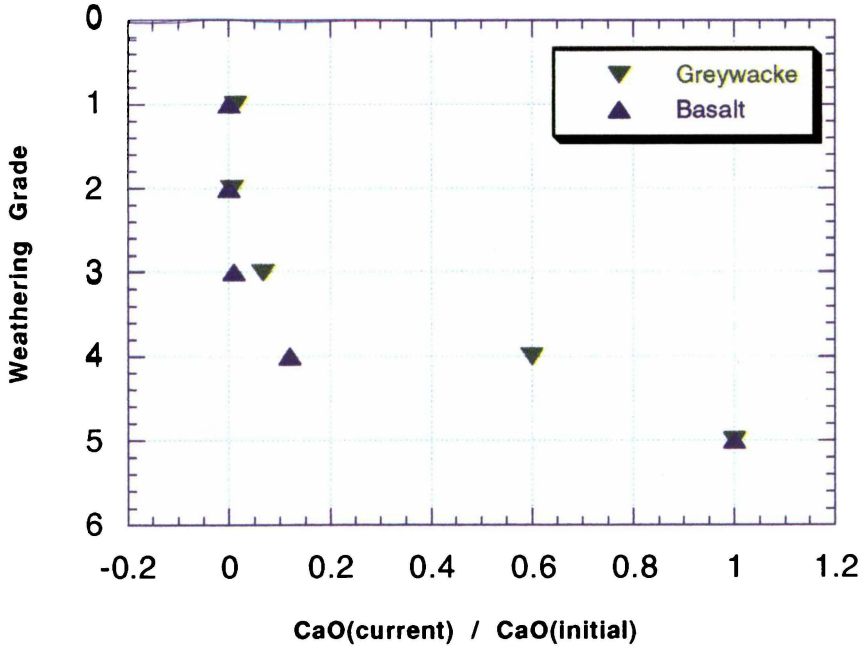

Figure 8.3b Plot of Weathering Grade vs Normalised CaO

reduced by the removal of Ca and Mg. These data suggest that it may be true for other rock types too, especially greywacke.

8.7 Implications for the Classification of Weathering Profiles

The NZ Geomechanics Society Standards (1988) for weathering profile descriptions divides a weathering profile into 6 grades based largely on the field expression of the rock, noting in particular colour changes and the ratio of corestones to matrix. On the basis of the measurements made here, it is clear that a 6-fold classification of the Karamu Basalt weathering profile is of unnecessary detail for engineering purposes, as it does not reflect the changes in the mechanical properties of the material adequately. In particular, a rock described as "slightly weathered" may be assumed intuitively to be a reasonably competent material, yet in reality it has lost most of its strength. Thus, a simpler 3-fold classification is proposed here, which is believed to better describe the likely geotechnical behaviour of the materials constituting the Karamu Basalt weathering profile.

"Fresh" rock shows no obvious effects of weathering, and the classification of "fresh" rock remains the same in this new scheme. However, according to the New Zealand Geomechanics Society (1988) standards, slight discoloration on joint surfaces may occur in fresh rock. The measurements in this study indicate that any obvious discolouration may indicate a substantial loss in intact strength.

"Slightly" weathered material characteristically shows discoloured surfaces and little other apparent alteration, yet it may have undergone a dramatic loss in strength, which is unable to be fully detected without laboratory testing. From the weathering model presented here, the processes of degradation in the slightly to moderately weathered materials are associated with diffusional processes and the development of fractures. At this stage the material is still acting as a rock mass in the engineering sense, albeit significantly weakened. It is thus suggested that these two grades be combined, and called "weathered rock". The fact that it displays a rock mass behaviour, rather than considerations of intact strength, provides the important characteristic defining this weathering grade. "Weathered rock" as defined here can be expected to have a much-reduced intact strength compared with fresh rock.

Average depth (m)	Cross section	Degree of weathering	Sample numbers	Description of materials
0	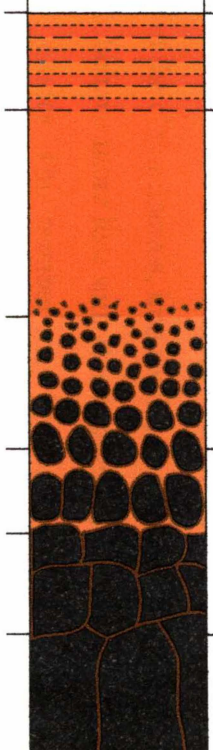	Alternating weathered tephra and paleosol layers	T: 22, 23, 25-28, 30, 35 P: 24 & 29	Alternating layers of : a) yellowish brown weathered tephra containing fragments of rhyolite with montmorillonite, kaolinite, halloysite and allophane. Plastic clayey soil material; b) reddish brown paleosol containing goethite and illite. More granular and less plastic soil compared to tephra.
6		Saprolitic Soil	31 - 34, 36 - 50 58 - 60	Rock mass is changed to a reddish brown soil with relic joints and corestones up to 0.3 m dimension. The original rock structure is preserved. Yellowish brown to orange soft clayey inclusions are present.
30				
46		Weathered Rock	8 - 21, 51 - 57	Material ranges from discoloured rock blocks of 0.8 m average dimension and apertures of 20 - 30 mm width to rounded core stones of about 0.5 m dimension with joint infill consisting of iron oxides and hydroxides and clays. Original joint structure is preserved.
56				
66		Fresh Rock	1 - 7	Dark grey coloured fresh basalt with columnar jointing. Open joints of upto 10mm aperture width and 0.5 - lm vertical joint spacing.

Figure 8.4 Description of the Weathering Profile at Karamu (according to the proposed classification). Depths not to scale.

In contrast, the weathering processes beyond the moderately weathered stage are characterised by the formation of clays, leading to development of soil–type behaviour in the material. This distinction, with its ramifications of plastic deformation and softening with changes in moisture content, is critical for engineering projects. It is therefore suggested that highly weathered, completely weathered and residual soil grades are combined and called simply "saprolitic soil".

A description of the weathering profile of Karamu Basalt according to the proposed classification is given as Figure 8.4. Whilst this three-fold classification is derived for Karamu Basalt, it is interesting to speculate its expandability to other lithologies. At present there is insufficient data to confirm this speculation.

8.8 Summary

The process of weathering of Karamu Basalt seems to be an initially diffusion controlled action. The loss of cations Ca^{2+} and Mg^{2+} is being compensated for by an influx of H^{+} and Al^{3+}. This replacement creates an imbalance in the charge to radius ratio and subsequently reduces the strength of the constituent minerals. Residual stresses within the rock are large enough to fracture the weakened intact rock, developing a network of cracks. These allow pathways for water movement, and facilitate hydrolysis, dissolution, redox and leaching, leading to secondary mineral formation. Initial indications are that the same process may be acting in other rock types such as greywacke and andesite.

Slightly weathered rock is not necessarily a competent material and it is much weaker than its external appearance indicates. However, slightly and moderately weathered rocks exhibit rock mass behaviour. Alterations after the moderately weathered stage are mainly changes in the clay minerals, iron oxides and hydroxides. Highly and completely weathered basalt behave more like soil. It is suggested that basaltic weathering profiles need not have 6 grades. This number may be conveniently reduced to 3: fresh rock, weathered rock and saprolitic soil.

CHAPTER 9: SUMMARY AND CONCLUSIONS

9.1 Objectives of Study

The objectives of this project were a) to evaluate the geochemical and geotechnical parameters of the Karamu Basalt at different stages of weathering; b) to determine possible relationships between the two sets of parameters; c) to quantify these relationships and formulate models based on statistical analysis; and d) to formulate a hypothesis to explain the weathering processes.

9.2 Findings and Conclusions

9.2.1 Mineral Assemblage

Constituent mineral assemblage can be considered as an indicator of the degree of weathering. Fresh rock has predominantly three primary minerals; olivine, titanaugite and plagioclase, which disappear when the weathering is complete and are replaced by secondary minerals hematite, goethite, kaolinite, montmorillonite, illite and halloysite. At intermediate stages, minerals such as saponite, nontronite and beidellite are formed, and later, decomposed. Figure 7.2 indicates the mineral assemblage observed at each stage of weathering.

9.2.2 Chemistry

From a chemical perspective, the weathering of Karamu basalt can be considered as loss of bases, oxidation of Fe^{2+}, accumulation of Al_2O_3, and incorporation of water. In other words, weathering is the reduction in MgO, CaO and FeO concentrations and the increase in Al_2O_3, Fe_2O_3 and H_2O+ concentrations. These chemical changes play major roles in influencing geotechnical parameters as evident from the following trends identified from regression analysis:

(a) Strength parameters consistently correlate with cation concentration patterns.

(b) Dry density shows good correlations with a number of cation concentration patterns.
(c) Abrasion pH correlates significantly with all bulk material properties (density, porosity and permeability) and California Bearing Ratio.

9.2.2.1 New Weathering Index

A number of previously published chemical weathering indices (Miura, Parker, Reiche, and Ruxton's Ratio) considered were derived for different lithologies. Hence, a "new weathering index" (NWI) that includes only important changing oxides in Karamu Basalt is proposed:

$$NWI = (MgO+CaO+FeO) / (Al_2O_3+Fe_2O_3+H_2O+) \quad \ldots 9.1$$

As discussed in Chapter 6, the New Weathering Index correlates well with some index and geotechnical parameters for Karamu Basalt such as water content, dry density, porosity and California Bearing Ratio. Equations enabling the New Weathering Index to be used as a predictor of geotechnical properties are given below:

$$\text{Water Content (\%)} = 8.6 - 21 \log (NWI) \quad (R^2 = 0.71) \quad \ldots 9.2$$
$$\text{Dry Density (kg m}^{-3}) = 2600 + 490 \log (NWI) \quad (R^2 = 0.86) \quad \ldots 9.3$$
$$\text{Porosity (\%)} = 2.7 + 9.2 \log (NWI) \quad (R^2 = 0.71) \quad \ldots 9.4$$
$$\text{California Bearing Ratio (\%)} = 86 + 40 \log (NWI) \quad (R^2 = 0.92) \quad \ldots 9.5$$

This New Weathering Index does not correlate well with shear strength, Atterberg limits, cohesion or angle of internal friction for the simple reason that those parameters are characteristics of clayey materials, and all weathering indices maintain more or less stable values from the time basalt is moderately weathered. This observation is insightful for understanding of early weathering behaviour, developed in Chapter 8.

9.2.2.2 Trace Elements

Correlations of trace elements with geotechnical parameters are established as follows: Rb with compressive strength (Schmidt); Zn, V, Cr, Rb and Sr with compressive strength (Point Load); Sr, Ga and Pb with dry density; Ba with permeability and Pb with

California Bearing Ratio. Comparisons made with the major elements suggest that the trace elements relate to geotechnical parameters in a fashion similar to their corresponding major elements in the periodic table as follows: Sr and Ba follow Ca; Rb follows K, while Nb and Zr follow Ti.

9.2.2.3 Abrasion pH Value

Abrasion pH value is indicative of the degree of weathering. It is highest in fresh rock (8.5) and gradually decreases to 4 due to weathering. This pattern is also followed in andesite too (Bassett, 1998) where abrasion pH drops from 7.25 to 5 due to weathering. Abrasion pH has significant positive correlations with dry density and California Bearing Ratio and negative correlations with cohesion, porosity and permeability. By obtaining the abrasion pH of a rock material, its degree of weathering can be determined and this may prove to be a very useful indicator.

9.2.3 Geotechnical Characteristics

Fresh Karamu Basalt is a strong rock with a uniaxial compressive strength of ~ 262 MPa. Based on field observations the weathering profile was divided into five grades as per the New Zealand Geomechanics Society Standards (1988). The residual soil horizon was absent probably owing to the overlying sequence of rhyolitic tephra and paleosols. Fresh rock shows near-vertical columnar jointing. It is assumed that the joints were present from the time of its formation. Vertical jointing facilitates the weathering process by exposing it to environment agents (factors affecting weathering) at the joint apertures. Along joint planes, discolouration occurs at slightly weathered stage. From fresh basalt to slightly weathered stage there is a significant drop in strength parameters which was not envisaged. Average point load strength index ($I_{s(50)}$) is 5.59 for fresh rock and 0.41 for slightly weathered basalt, and California Bearing Ratio drops from 100 % to 45 %.

Most geotechnical tests did not cover all weathering grades. Geotechnical parameters change in value from fresh rock to weathered, although the changes are not gradual. With depth, some parameters such as California Bearing Ratio show a two stage linear relationship, having a clear break of slope at the moderately weathered stage. Those properties that could be determined across the complete profile showed that from fresh to completely weathered basalt CBR dropped from 100 % to 1 % and the dry density

dropped from 2902 kg m^{-3} to 1502 kg m^{-3}. As previously depicted in Figure 7.1, permeability, porosity and cohesion increase with the intensity of weathering of Karamu Basalt.

Atterberg limit determination was confined to soil like weathered material only. The value ranges were LL: 57.61- 79.82 %; PL: 47.58 – 79.01 % and PI: 5.65 – 20.57 %. The activity of clay ranged from 0.39 to 2.5 from slightly to completely weathered basalt. No effective conclusions could be obtained from the changes of Atterberg limit values. Thus, Atterberg limits, which are of immense value for silts and clays of sedimentary origin, do not seem to work well with weathering profiles, mainly because of the nature of material required for these tests.

9.2.4 Chemical Predictors of Geotechnical Parameters

Statistical analysis reveals a proposed geochemical predictor (Predictor x) of geotechnical parameters that give easily calculable relationships with geotechnical parameters of Karamu Basalt.

Chemical predictor "x" = $225\ pH + 283\ TiO_2 + 7.4\ Sr - 80\ Fe_2O_3$ ... 9.6

Depending of the availability (or unavailability) of certain chemical data, the following chemical predictors too can be used to predict geotechnical parameters:

Chemical predictor No. 1 = $3.5\ TiO_2 - Fe_2O_3$ ... 9.7

Chemical Predictor No.1a = $2.8\ pH + 3.5\ TiO_2 - Fe_2O_3$ ... 9.8

Chemical Predictor No.1b = $0.1Sr + 3.5\ TiO_2 - Fe_2O_3$ ... 9.9

Chemical Predictor No. 2 = $25.2\ MnO - 1.6\ MgO + 16.2\ P_2O_5 - 0.5\ H_2O$ ... 9.10

As discussed in Chapter 6, these are applicable not only for Karamu Basalt, but in some cases for other rock types from New Zealand and overseas.

The following equations can be used to predict geotechnical properties of Karamu Basalt (R^2 values obtained at 95% confidence level are given within brackets) using these chemical predictors:

California Bearing Ratio = $130 + 120 \log$ Predictor x ($R^2 = 0.91$) ... 9.11

Dry Density, kg/m^3 = -82 + 1500 log Predictor x (R^2 = 0.92) ... 9.12

Porosity, % = 52 – 28 log Predictor x (R^2 = 0.73) ... 9.13

Comp. Strength (P.L), MPa = - 280 + 210 log Predictor x (R^2 =0.72) ... 9.14

Water content, % = 120 – 62 log Predictor x (R^2 = 0.74) ... 9.15

Permeability, m/s = 5300 – 4200 log Predictor x (R^2 = 0.64) ... 9.16

Water content, % = 39 – 1.1 Predictor 1b + 0.0072 (Predictor 1b)^2

(R^2 = 0.75) ... 9.17

Dry Density, kg/m^3 = 1900 + 27 Predictor 1b – 0.19 (Predictor 1b)^2

(R^2 = 0.89) ... 9.18

Comp. Strength (P.L), MPa = - 0.22 + 1.6 Predictor 1b (R^2 =0.78) ... 9.19

Cohesion, kPa = 0.03 + 1*Predictor 2 (R^2 = 0.78) ... 9.20

California Bearing Ratio = 36 – 6.3 * Predictor 2 (R^2 = 0.81) ... 9.21

Porosity, % = 14 + 1.4 * Predictor 2 (R^2 = 0.69) ... 9.22

One important observation is that major elements alone are generally inadequate as indicators of geotechnical behaviour, and a complete analysis including trace elements and abrasion pH is required (abrasion pH and Sr are important components of Predictor x).

Equations relating these predictors to geotechnical parameters for some other lithologies are presented in section 6.7. These predictors may be of use for a variety of lithologies, but since they were derived based on a limited set of available data, their wider applicability is not yet established.

9.2.5 Hypothesis for the Weathering Process

A causal relationship between the loss of cations Mg^{2+} and Ca^{2+} and initial loss of strength was hypothesised. This sees the early stage of weathering as diffusion-controlled whereby cations are lost from the constituent primary minerals and are replaced by H^+ and possibly Al^{3+}. This process is believed to affect the lattice structure due to radius to charge ratio imbalances, thus causing microfractures. The stress release mechanism causes macrofracturing of the thus weakened intact rock. After the moderately weathered stage, the weathering is controlled by hydrolysis, and later dissolution and leaching, leading to secondary mineral formation and further evolution of clay minerals. Initial indications imply that the same process may occur in other

lithologies, but sufficient information is not available to robustly evaluate the validity of this hypothesis for other rock types.

9.2.6 Classification of the Weathering Profile

According to New Zealand Geomechanics Society Standards (1988), weathering profiles are divided into 6 different groups according to their characteristics such as strength, discolouration, ratio of rock to soil, structure and other properties as follows: fresh, slight, moderate, high, complete and residual soil. In the Karamu profile, from fresh to slight there is a significant lowering of strength and density. Moreover, many parameters such as strength, density and chemical components seem to fall dramatically from fresh to moderately weathered, and then come to a more or less constant state. Completely weathered basalt does not contain any of the three primary minerals. It is thus possible to propose that the basalt weathering profile be more simply divided into 3 categories which better reflect the true geotechnical behaviour and weathering processes: fresh rock, weathered rock, and saprolitic soil. In this classification fresh rock would remain as it is; slightly weathered, together with moderately weathered material would be called weathered rock; highly and completely weathered material along with resdual soil would be called saprolitic soil. It must be noted that the residual soil (which does not contain any relict structure) was not developed on Karamu Basalt.

9.3 Ramifications of this Study

- It is now clear that slightly weathered rock is not necessarily a competent material and that the loss of some cations causes this incompetence. This has important ramifications for the engineering community: slightly weathered rock should be recognised as a potentially very weak material from the outset of any investigation. In all cases, proper caution should be exercised whenever slightly weathered rock is encountered in an engineering context.

- The current engineering field descriptions of weathering profiles do not reflect the weathering processes identified in this study, nor do they account for the important change after the moderately weathered stage from rock mass to soil behaviour. A modification of the standard classification scheme derived for Karamu Basalt is

simpler, and provides a better indication of material behaviour. This may be applicable to other lithologies.

- This study affirms the importance of abrasion pH as a good indicator of weathering. This is a convenient and simple test that can be used to predict the degree of weathering in a more objective manner than field description.

- The importance of carrying out complete chemical analysis with trace elements, determination of both ferrous and ferric iron contents in the samples, the abrasion pH and California Bearing Ratio is stressed if a full understanding of the weathering of rocks is required.

9.4 Recommendations for Future Research

This study has postulated a theory for the very early stages of weathering of basalts, which highlights the importance of cation diffusion as beginning the weathering process and having a dramatic effect on almost all geotechnical parameters. This theory has been developed from in-depth study of a single lithology, with an indication from some independent studies that the process may have a wider application. Further work to investigate the geochemical reactions taking place at the start of weathering in further detail (perhaps with simulation techniques) in order to better understand the processes involved is recommended.

Other areas of research which may prove fruitful include:

- The study of more basaltic rocks in order to determine the wider applicability of the New Weathering Index.

- Versatility of the chemical predictors for geotechnical parameters should be tested against other basalts or any other igneous rock types from all over the world.

- Weathering profiles of other rocks may be studied to investigate whether the proposed restructuring of the classification standards is universally applicable.

REFERENCES

Aires-Barros, L (1978). A comparative study between rates of experimental laboratory weathering of rocks and their natural environmental weathering decay. *Bulletin of the International Association of Engineering Geology* 18 pp 169-174.

Allbrook, R.F. (1980). The drop-cone penetrometer method for determining Atterberg limits. *New Zealand Journal of Science* 23 pp 93-97.

Althaus, E. and Tirtadinata, E. (1989). Dissolution of feldspar: The first step. *Water-Rock Interaction WRI – 6.* Blakema, Rotterdam. pp 15-17.

Anon (1981). *Code of Practice for Site Investigations* (BS5930). British Standards Institution, London.

Arel, E and Tugrul, A. (2001). Weathering and its relation to geomechanical properties of Cavusbasi granitic rocks in northwestern Turkey. *Bulletin of Engineering Geology and the Environment.* 60 pp 123-133.

Attewell, P.B. and Farmer, I.W. (1979). *Principles of Engineering Geology.* Halsted Press, New York.

Aylward, G and Findlay, T. (1998). *SI Chemical Data.* John Wiley and Sons, New York.

Baker, I and Haggerty, S (1967). Alteration of olivine in basaltic and associated lavas. II. Intermediate and low temperature alterations. *Contributions to Mineralogy and Petrology* 16 pp 258-273.

Bassett, P.B. (1998). Influence of weathering and hydrothermal alteration on engineering characteristics of Eastern Coromandel rocks. *M.Sc. Thesis.* University of Waikato, New Zealand.

Baynes, F.J. and Dearman, W.R. (1978). The microfabric of a chemically weathered granite. *Bulletin of the International Association of Engineering Geology* 18 pp 91-100.

Berner, R.A. (1978). Rate of control of mineral dissolution under earth surface conditions. *American Journal of Science* 278 pp 1235-1252.

Berner, R.A., Sjoberg, E.L., Velbel, M.A. and Krom, M.D. (1980). Dissolution of pyroxenes and amphiboles during weathering. *Science* 207 pp 1205-1206.

Berner, R.A. and Schott, J. (1982). Mechanism of pyroxene and amphibole weathering II. Observations of soil grains. *American Journal of Science* 282 pp 1214-1231.

Berner, R.A. (1995). Chemical weathering and its effects on atmospheric CO_2 and climate. *Mineralogical Society of America Reviews in Mineralogy.* 31 pp 543-583.

Bertin, E.P. (1975). *Principles and Practice of X-Ray Spectrometric Analysis.* Plenum Press, New York.

Betekhtin , A (1972). *A Course of Mineralogy.* Mir Publishers, Moscow.

Bieniawski, Z.T. (1975). The point load test in geotechnical practice. *Engineering Geology* 9 pp 1-11.

Bieniawski, Z.T. (1983). Mechanism of brittle rock fracture: Part 1. Theory of the fracture process. *International Journal of Rock Mechanics and Mining Sciences & Geomechanical Abstracts*. 4 pp 395-406.

Bigelow, W.C. and Smith, J.V. (1966). Powder diffraction file fink inorganic index. *American Society of Testing and Materials Publication.* Philadelphia.

Bishop, A.C. (1967). *An Outline of Crystal Morphology*. Hutchinson & Co. (Publishers) Ltd, London.

Blakemore, L.C., Searle, P.L. and Daly, B.K. (1987). *Methods for chemical analysis of soils.* New Zealand Soils Bureau, Lower Hutt, New Zealand.

Bland, W and Rolls, D (1998). *Weathering*. Arnold Publishers, London.

Bock, H. (1979). Experimental determination of the residual stress field in a basaltic column. *Proceedings of the International Congress on Rock Mechanics,* Rotterdam, Balkema. pp 45 – 49.

Bortz, S.A. and Wonneberger, B. (2000). Predicting the durability of building stone using accelerated weathering. *Durability 2000: Accelerated and Outdoor Weathering Testing*. pp 116-132.

Brand, E.W. (1985). Predicting the performance of residual soil slopes. *Proceedings of the 11th conference on Soil Mechanics and Foundation Engineering, San Francisco* 5 pp 2541-2578.

Briggs, R.M. (1983). Distribution, form, and structural control of the Alexandra volcanic group, north island, New Zealand. *New Zealand Journal of Geology and Geophysics* 26 pp 47-55.

Briggs, R.M. and Goles, G.G. (1984). Petrology and trace element geochemicalfeatures of the Okete volcanics, western north Island, New Zealand, *Contributions to Mineralogy and Petrology* 86 pp 77-88.

Briggs, R.M., Itaya, T., Lowe, D.J. and Keane, A.J. (1989). Ages of Pliocene-Pleistocene Alexandra and Ngatutura volcanics, western north island, New Zealand, and some geological implications, *New Zealand Journal of Geology and Geophysics* 32 pp 417-427.

Brown, E.T. (1981). Rock characterisation, testing and monitoring, *ISRM suggested methods* . International Society for rock mechanics, Pergamon Press, England.

Brown, G and Stephen, I (1959). A structural study of iddingsite from New South Wales, Australia. *American Mineralogist* 44 pp 251-260.

Carmichael, R.S. (1982). *Handbook of Physical Properties of Rocks.* CRC Press, Inc. Florida.

Carrol, D. (1970). *Rock Weathering.* Plenum Press New York.

Chang, R. (1998). *Chemistry.* WCB/McGraw-Hill, Boston.

Chichester, F.W., Youngberg, C.T. and Harward, M.E. (1969). Clay mineralogy of soils formed in Mazama pumice. *Soil Science Society of America Proc.* 33 pp 115-120.

Clayton, T and Pierce, R.B. (2000). Alteration mineralogy of Cretaceous basalt from ODP site 1001, Log 165 (Caribbean Sea). *Clay Minerals* 35 pp 719-733.

Colman, S.M. (1982). Chemical weathering of basalts and andesites: evidence from weathering rinds. *Geological Survey Professional Paper (U.S.)* 1246.

Colman, S.M. and Dethier, D.P. (1986). *Rates of Chemical Weathering of Rocks and Minerals*. Academic Press, New York.

Colman, S.M. and Pierce, K.L. (1981). Weathering rinds on andesitic and basaltic stones as a Quaternary age indicator, Western United States: *Geological Survey Professional Paper (U.S.)* 1210.

Conca, J.L. and Cubba, R (1986). Abrasion resistance and hardness testing of rock materials. *International Journal of Rock Mechanics and Mining Sciences* 23 pp 141-149.

Dearman, W.R. (1974). Weathering classification in the characterisation of rock for engineering purposes in British practice. *Bulletin of the International Association of Engineering Geology* 13 pp 123-127.

Dearman, W.R.(1976). Weathering classification in the characterisation of rock: a revision. *Bulletin of the International Association of Engineering Geology* 9 pp 33-42.

Dearman, W.R. (1995). Description and classification of weathered rocks for engineering purposes. *Quarterly Journal of Engineering Geology* 28 pp 267-276.

Deer, W.A., Howie, R.A. and Zussman, J. (1962). *An Introduction to the Rock Forming Minerals.* John Wiley and Sons, New York.

Deer, W.A., Howie, R.A. and Zussman, J. (1992). *An Introduction to the Rock Forming Minerals.* Longman Scientific and Technical Publications, England.

Duzgoren-Aydin, N.S.; Aydin, A. and Malpas, J. (2002). Reassessment of chemical weathering indices: case study on pyroclastic rocks of Hongkong. *Engineering Geology* 63 pp 99-119.

Eberhart, E, Stead, D., Stimpson, B and Latijai, E.Z. (1998). The effect of neighbouring cracks on elliptical crack initiation and propogation in uniaxial and triaxial stress fields. *Engineering Fracture Mechanics.* 59 pp 103-115.

Eggleston, C.M. and Hellmann, R. (1989). Altered layers on dissolving albite – 2. model. *Water-Rock Interaction WRI – 6.* Balkema, Rotterdam. pp 215-218.

Eggleton, R.A. (1984). Formation of iddingsite rims on olivine: a transmission electron microscopy study. *Clays and Clay Minerals* 32 No 1 pp 1-11.

Eggleton, R.A. (2001). *The Regolith Glossary: Surficial Geology, Soils and Lnadscapes.* CRC LEME, Australia.

ELE Catalogue (1993). *Engineering Laboratory Equipment Catalogue*. 9th Edition. ELE International Ltd., England.

Ferrari, G.A. and Magaldi, D (1983). Degree of soil weathering as determined by abrasion pH: applications in soil study in paleopedology. *Pedologie* 33 pp 94 -104.

Fieldes, M. and Perrot, K.W. (1966). Rapid field and laboratory tests for allophane. *New Zealand Journal of Science.* 9 pp 623-629.

Franklin, J. A. (1985). Suggested method for determining point load strength. *International Journal of Rock Mechanics, Mining Science and Geomechanics Abstracts.* 22 pp 53-60.

Frederickson, A.F. (1951). Mechanism of weathering. *Bulletin of Geological Society of America.* 62, pp 221-232.

Freund, J.E. (1974). *Modern Elementary Statistics.* Prentice-Hall Inc. London.

Frye, K. (1974). *Modern Mineralogy*. Prentice-Hall Inc. New Jersey.

Geological Society EngineeringGroup Working Party Report (1995). Description and classification of weathered rocks for engineering purposes. *Quarterly Journal of Engineering Geology* 28 pp 207-242.

Geonor, A. S. (1966). *Working Instructions for Geonor Inspection Vane Borer.* ROA, Norway.

Glassman, J.R. (1982). Alteration of andesite in wet, unstable soils of Oregon western cascades. *Clays and Clay Mineralogy.* 30 pp 253-263.

Goldich, S.S. (1938). A study of rock weathering. *Journal of Geology.* 46 pp 17-58.

Govett, G.J.S. (1983). *Handbook of Exploration Geochemistry* 2. Elsevier, Amsterdam.

Grant, W.H. (1969). Abrasion pH, an index of chemical weathering. *Clays and Clay Mineralogy* 17 pp 151-155.

Guan, P.; Ng, C.W.W.; Sun, M. and Tang, W. (2001). Weathering indices for rhyolitic tuff and granite in Hong Kong. *Engineering Geology.* 59 pp 147-159.

Gupta, A.S. and Rao, K.S. (1998). Index properties of weathered rocks: interrelationships and applicability. *Bulletin of Engineering Geology* 57 pp 161-172.

Gupta, A.S. and Rao, K.S. (2001). Weathering indices and their applicability for crystalline rocks. *Bulletin of Engineering Geology and the Environment.* 60 pp 201-221.

Haskins, D.R. and Bell, F.G. (1995). Drakensberg basalts: their alteration, breakdown and durability. *Quarterly Journal of Engineering Geology.* 28 pp 287-302.

Hetherington, J.R. (1989). A quantitative study of the weathering of the Manaia hill greywacke quarry. *M.Sc. Thesis.* University of Waikato, New Zealand.

Hencher, S.R. and McNicholl, D.P. (1995). Engineering in weathered rock. *Quarterly Journal of Engineering Geology,* 28 pp 253-266.

Hind, K.J. (1986). A geotechnical investigation of ignimbrite in the Ruahihi area, Tauranga. *M.Sc. Thesis.* University of Waikato, New Zealand.

Hochella, M.F. and Banfield, J.F. (1995). Microscopic perspective of silicate weathering. *Mineralogical Society of America Reviews in Mineralogy.* Volume 31 pp 353-406.

Hodder, A.P.W. (1984). Thermodynamic interpretation of weathering indices and its application to engineering properties of rocks. *Engineering Geology* 20 pp 241-251.

Hodder, A.P.W. and Hetherington, J.R. (1991). A quantitative study of the weathering of Greywacke. *Engineering Geology* 31 pp 353-368.

Hodder, A.P.W., De Lange, P.J. and Lowe, D.J. (1991). Dissolution and depletion of ferromagnesian minerals from Holocene tephra layers in an acid bog, New Zealand, and implications for tephra correlation. *Journal of Quarternary Science.* 6 pp 195-208.

Hoek, E. (1983). Strength of jointed rock masses. *Geotechnique* 33 pp 187-223.

Hoek, E. and Bieniawski, Z.T. (1965). Brittle fracture propogation in rock under compression. *International Journal of Fracture Mechanisms.* 1 pp 137-155.

Horrocks, J.L. (2000). Chronology and correlation of the Plio-Pliestocene Kauroa ash sequence, western-central north island, New Zealand. *Ph.D thesis*, University of Waikato, Hamilton.

Jayawardena, U. de S. and Izawa, E. (1994). A new chemical index of weathering for metamorphic silicate rocks in tropical regions. *Engineering Geology* 36 pp 303-310.

Johnson, G.G. and Vand, V. (1966). Kwic guide to the powder diffraction file. *American Society of Testing and Materials Publication.* Philadelphia.

Johnson, R. (1984). *Elementary Statistics*. Duxbury Press, Boston.

Johnson, R.A. and Wichern, D.W.(2001). *Applied Multivariate Statistical Analysis*. Prentice Hall, New Jersey.

Jumikis, A.R. (1982). *Rock Mechanics.* Gulf Publishing Company, Houston.

Keller, W.D. (1954). The Energy factor in sedimentation. *Journal of Sedimentary Petrology* 24 pp 62-68.

Kohn, B.P., Pillans, B. and McGlone, M.S. (1992). Zircon fission track age for middle Pleistocene Rangitawa tephra, New Zealand: stratigraphic and paleoclimatic significance. *Paleogeography, Paleoclimatology and Paleoecology*. 95 pp 73-94.

Koksoy, M. and Bradshaw, P.M.D. (1969). Secondary dispersion of mercury from cinnabar and stibnite deposits, West Turkey. *Colorado School of Mines Quarterly* 64 pp 333-356.

Krauskopf, K.B. (1979). *Introduction to Geochemistry*. McGraw-Hill, Inc. New York.

Krinsley, D.H. and Smalley, I.J. (1972). Sand. *American Scientist.* 60 pp 286-291.

Lambe, T.W. (1951). *Soil Testing for Engineers.* John Wiley and Sons, New York.

Lambe, T.W. and Whitman, R.V. (1969). *Soil Mechanics*. John Wiley & Sons, Inc.

Leeder, M.R. (1982). *Sedimentology*. Unwin Hyman, London.

Little, A.L. (1969). The engineering classification of residual tropical soils. *7th International conference on Soil Mechanics and Foundation Engineering, Mexico* pp 1-10.

Loughnan, F.C. (1969). *Chemical Weathering of Silicate Minerals*. Elsevier Publishing Company Inc. New York.

Lowe, D.J., Tippett, J.M., Kamp, P.J.J., Liddell, I.J., Briggs, R.M. and Horrocks, J.L. (2001). Ages on weathered Plio-Pleistocene tephra sequences, western north island, New Zealand. *Tephras: Chronology, Archeology.* 1 pp 45-60.

Lupini, J.F., Skinner, A.E. and Vaughan P.R. (1981). The drained residual strength of cohesive soils. *Geotechnique* 31 pp 181-213.

Macari, E.J. and Hoyos, L. (1996). Effect of degree of weathering on dynamic properties of residual soils. *Journal of Geotechnical Engiineering.* 122 pp 988-997.

Malomo, S. (1980). Abrasive pH as an engineeringindex for weathered granite. *Bulletin of the International Association of Engineering Geology.* 22 pp 207-211.

Malvern Mastersizer S (1996). *Mastersizer S PreliminaryMmanual.* Software Version 2.1. Malvern Instruments Ltd.

Manly, B.F.J. (1994). *Multivariate Statistical Methods.* Chapman & Hall, London.

Massey, J.B. and Pang, P.L.R. (1988). General report: stability of slope and excavations in tropical soils. *Proceedings 2nd International Conference on Geomechanics in Topical Soils Singapore* 2 pp 551-570.

Miller, R.P. (1965). Engineering classification and index properties for intact rock. *Ph.D Thesis.* University of Illinois. USA.

Ming, D.W. and Mumpton, F.A. (1989). Zeolites in soils. *Soil Science Society of America Book Series*, Madison, Wisconsin.

Miura, K. (1973). Weathering in plutonic rocks, *Journal of the Society for Engineering Geology of Japan* 14 pp 13-24.

Moon, V.G. (1989). Relationships between the geomechanics and petrography of ignimbrite. *Ph.D. Thesis*. University of Waikato, New Zealand.

Moore, C.L. (1996). Processes of chemical weathering of selected Cenozoic eastern Australian basalts. *Ph.D. Thesis*. Australian National University, Canberra.

Nahon, D., Colin, F. and Tardy, Y. (1982). Formation and distribution of Mg, Fe and Mn-smectities in the first stages of the lateritic weathering of forsterite and tephroite. *Clay Minerals* Vol. 17. No. 3 pp 339-348.

Nesbitt, H.W. and Wilson, R.E. (1992). Recent chemical weathering of basalts. *American Journal of Science* 292 pp 740-747.

New Zealand Geomechanics Society (1988). *Guidelines for the Field Description of Soils and Rocks in Engineering Use.* Institute of Professional Engineers of New Zealand, Wellington.

New Zealand Standard (1986). *Methods of Testing Soils for Civil Engineering Purposes.* Standards Association of New Zealand, Wellington

Nutter, L.J. and Otton, E.G. (1969). Ground-water occurrence in the Maryland Piedmont. *Maryland Geological Survey Report of Investigations* 10.

Obermeier, S.F. and Langer, W.H. (1986). Relationships between geology and engineeringcharacteristics of soils and weathered rocks of Fairfax county and vicinity, Virginia. *U.S. Geological Survey Professional Paper* 1344.

Ohtsubo, M., Egashira, K. and Kashima, K. (1995). Depositional and post-depositional geochemistry, and its correlation with the geotechnical properties of marine clays in Ariake Bay, Japan. *Geotechnique* 45 No.3 pp 509-523.

Ollier, C.D. (1984) *Weathering*. Longman, New York.

Ollier, C.D. (1988) *The Nature of Weathering*. Sozosha, Tokyo.

Ollier, C.D. (1991) *Weathering*. Longman, Harlow.

Oyama, T. and Chigira, M. (1999). Weathering rate of mudstone and tuff on old unlined tunnel walls. *Engineering Geology.* 55, pp 15-27.

Parfitt, R.L. and Kimble, J.M. (1989). Conditions for formation of allophane in soils. *Soil Science Society of America Journal* 53 pp 971-977

Parker, A. (1970). An index of weathering for silicate rocks, *Geological Journal 107* pp 501-504.

Price, D.G. (1995). Weathering and weathering processes, *Quarterly Journal of Engineering Geology* 28 pp 243-252.

Price, R.C., Gray, C.M., Wilson, R.E., Frey, F.A. and Taylor, S.R. (1991). The effects of weathering on rare-earth element, Y and Ba abundances in Tertiary basalts from southeastern Australia. *Chemical Geology* 93 pp 245-265.

Rawle, A (1993). *The Basic Principles of Particle Size Analysis.* Malvern Instruments Ltd. USA.

Rayment, G.C. and Higginson, F.R. (1992). Australian laboratory handbook of soil and water chemical methods. *Australian Soil and Landsurvey Handbook.* Inkata Press.

Reiche, P (1943). Graphic representation of chemical weathering. *Journal of Sedimentary Petrology,* 13 pp 53-68.

Reiche, P (1950). A Survey of weathering processes and products. *University of New Mexico Publications in Geology 3.* University of New Mexico Press.

Roaldset, E. (1972). Mineralogy and geochemistry of Quarternary clays in the Numedal area, Southern Norway. *Narsk Geol. Tidsskr,* 52 pp 335-369.

Rollinson, H. (1993). *Using Geochemical Data: Evaluation, Presentation and Interpretation.* Longman Group Ltd., United Kingdom.

Ruxton, B.P. (1968). Measures of the degree of chemical weathering of rocks. *Journal of Geology,* 76 pp 518-527.

Sahasrabudhe, Y.E. and Vaidyanath, L.N. (1981). Some Indian plateau laterites and their engineering properties. *Lateritisation Processes - Proceedings of the International Seminar on Lateritisation Processes in India.* pp 77-90.

Schott, J. and Berner, R.A. (1984). Dissolution mechanisms of pyroxenes and olivines during weathering. *The Chemistry of Weathering.* NATO ASI Series. pp 35-53.

Selby, M.J. (1993). *Hillslope Materials and Processes.* Oxford University Press.

Smith, K.L. and Eggleton, R.A. (1983). Goethite microstructure, a TEM study. *Clays & Clay Mineralogy* 31 pp 392-396.

Stegena, L (1983). Leaching in rocks: some physical principles. *Leaching and Diffusion in Rocks and their Weathering Products.* Theophrastus Publications, Athens. pp 81-92.

Stevenson, R.J. (1986). Geotechnical properties of Minden rhyolite at Paunui and Onemana, eastern Coromandel. *M.Sc. Thesis.* University of Waikato, New Zealand.

Stipp, J.J. (1968). The geochronology and petrogenesis of the Cenozoic volcanics of north island, New Zealand. *Unpublished Ph.D thesis*, Australian National University, Canberra.

Taylor, R.K. (1988). Coal measures mudrocks: composition, classification and weathering processes. *Quarterly Journal of Engineering Geology* 21 pp 85-100.

Tugrul, A. and Zarif, I.H. (1999). Correlation of mineralogical and textural characteristics with engineering properties of selected granitic rocks from Turkey. *Engineering Geology* 51 pp 303 - 317.

Ulusay, R , Tureli, K. and Ider, M.H. (1994). Prediction of engineeringproperties of a selected litharenite sandstone from its petrographic characteristics using correlation and multivariable statistical techniques. *Engineering Geology* 38 pp 135-158

Veblen, D.R. and Buseck, P.R. (1980). Microstructures and reaction mechanisms in biopyriboles. *American Mineral.* 65 pp 599-623.

Veblen, D.R. and Buseck, P.R. (1981). Hydrous pyriboles and sheet silicates in pyroxenes and uralites: intergrowth microstructures and reaction mechanisms. *American Mineral.* 66 pp 1107-1134.

Velde, B. (1992). *Introduction to Clay Minerals*. Chapman and Hall. London.

Veldkamp, E, Jongmans, A.J., Feijtel, T.C., Veldkamp, A. and van Breeman, N. (1990). Alkali basalt gravel weathering in Quaternary Allier river terraces, Limagne, France. *Soil Science Society of America Journal* 54 pp 1043-1048.

White, A.F. and Brantley, S.L. (1995). Chemical weathering rates of silicate minerals: an overview. *Mineralogical Society of America Reviews in Mineralogy. Volume 31* pp 1-22.

Whitehouse, I.E., McSaveney, M.J., Knuepfer, L.P.K. and Chin, T.J.H. (1986). The growth of weathering rinds on torlesse sandstone, southern Alps, NZ. *Rates of Chemical Weathering of Rocks and Minerals.* Academic Press. pp 419-435.

Whitten, D.G.A. and Brooks, J.R.V. (1972). *A Dictionary of Geology*. Penguin Books.

Wollast, R. and Chou, L. (1984). Kinetic study of the dissolution of albite with a continuous flow-through fluidised bed reactor. *The Chemistry of Weathering*. NATO ASI Series. pp 35-53.

Appendix 2.1 Chemical Weathering Indices (Duzgoren-Aydin *et al.*, 2002)

Table 5
Chemical weathering indices

Chemical index	Definition	Proposed by	Conditions and/or assumptions
'Absolute' weathering indices	$(A_w C_f)/(A_f C_w) - 100 = \%$ lost[a]	Merrill, 1906 in Reiche, 1943	Weight percentage of components
	$A_f - A_w(C_f/C_w)$[a]		The alteration, except H_2O, must be a subtractive process (Reiche, 1943) Some components are assumed to be constant during weathering (Reiche, 1943)
Comments on 'Absolute index'			
Assumptions are ill-founded (Reiche, 1943; this study)			
Parent rock composition must be known (Ruxton, 1968)			
SA (or Ki)	SiO_2/Al_2O_3	Harrassowitz, 1926: in Rocha Filho et al., 1985	Molecular ratio (mobile/immobile) Silica loss must be related to total element loss, and the Al and sesquioxide contents must remain constant during weathering (Ruxton, 1968)
Comments on 'silica to aluminium' ratio			
Valid for well-drained, acid and humid environments where the end products are kaolin group minerals, especially suitable for acid and intermediate rocks (Ruxton, 1968)			
Silica based; therefore unsuitable for acidic rocks, but can be suitable for basic rocks (Rocha Filho et al., 1985)			
Silica mobility within the profile is irregular and total loss is usually small (Parker, 1970)			
Good indicator of the degree of chemical weathering in volcanic and granitic rocks (Irfan, 1996; 1999)			
Poor correlation between 'SA' and the weathering grade (this study)			
Kr	$SiO_2/(Al_2O_3 + Fe_2O_3)$	Harrassowitz, 1926: in Rocha Filho et al., 1985; GSL, 1990	Molecular ratio (mobile/immobile)
Comments on 'sesquioxide ratio'			
It should be used in mature residual soils representing high clay content (Rocha Filho et al., 1985)			
Widely used to express relative differences between materials (Thomas, 1994)			
Poor correlation between 'Kr' and the weathering grade (this study)			
Ba	$(K_2O + Na_2O + CaO)/Al_2O_3$	Harrassowitz, 1926: in Rocha Filho et al., 1985	Molecular ratio (mobile/immobile)
Comments on 'potassium–sodium–calcium to aluminum' ratio			
Good correlation has been observed between 'ba' and the weathering grade (this study)			
ba_1	$(K_2O + Na_2O)/Al_2O_3$	Harrassowitz, 1926: in Rocha Filho et al., 1985	Molecular ratio (mobile/immobile)
Comments on 'potassium–sodium to aluminum' ratio			
Good correlation has been observed between 'ba_1' and the weathering grade (this study)			

Table 5 (*continued*)

Chemical index	Definition	Proposed by	Conditions and/or assumptions
ba_2	$(CaO + MgO)/Al_2O_3$	Harrassowitz, 1926: in Rocha Filho et al., 1985	Molecular ratio (mobile/immobile)
Comments on 'calcium–magnesium to aluminum' ratio			
Poor correlation has been observed between 'ba_2' and the weathering grade (this study)			
ba_3	$(K_2O + Na_2O + MgO)/Al_2O_3$	Harrassowitz, 1926: in Rocha Filho et al., 1985	Molecular ratio (mobile/immobile)
Comments on 'potassium–sodium–magnesium to aluminum' ratio			
Good correlation has been observed between 'ba_3' and the weathering grade (this study)			
B	$I_{weathered}/I_{sound}$ $I = [(K_2O + Na_2O + CaO)/Al_2O_3]$	Harrassowitz, 1926: in Rocha Filho et al., 1985	Molecular ratio $(mobile/immobile)_{parent\ normalized}$
Comments on 'parent normalized ba ratio'			
Good correlation has been observed between 'B' and the weathering grade (this study)			
β	$I_{weathered}/I_{sound}$ $I = [(K_2O + Na_2O)/Al_2O_3]$	Harrassowitz, 1926: in Rocha Filho et al., 1985	Molecular ratio $(mobile/immobile)_{parent\ normalized}$ The results are applicable to residual soil from granitic rocks (homogeneous profile) (Rocha Filho et al., 1985)
Comments on 'lixiviation index'			
A correlation has been established between lixiviation index and geotechnical properties of residual soil (Rocha Filho et al., 1985)			
It is not good indicator of the degree of weathering in granite (Irfan, 1996)			
It is not a good indicator of weathering even for the soil grades (Irfan, 1999)			
Good correlation has been observed between 'β' and the weathering grade (this study)			
a	K_2O/Na_2O	Jenny, 1931: in Ruxton, 1968	Molecular ratio (mobile/mobile)
Comments on 'potassium to sodium' ratio			
Index does not reflect the weathering changes in (Ruxton, 1968)			
Very poor correlation has been observed between 'a' and the weathering grade (this study)			
b	Al_2O_3/Fe_2O_3	Jenny, 1941	Molecular ratio (immobile/immobile)
Comments on 'aluminum to iron' ratio			
Very poor correlation has been observed between 'a' and the weathering grade (this study)			
SF	SiO_2/Fe_2O_3	Jenny, 1941	Molecular ratio (mobile/immobile) Silica loss must be related to total element loss and the sesquioxide contents must remain constant during weathering (Ruxton, 1968)
Comments on 'silica to iron' ratio			
Silica based, therefore unsuitable for acidic rocks (Rocha Filho et al., 1985)			
Poor correlation has been observed between 'Sf' and the weathering grade (this study)			

Table 5 (*continued*)

Chemical index	Definition	Proposed by	Conditions and/or assumptions
Silica:R_2O_3	$SiO_2/(Al_2O_3 + Fe_2O_3 + TiO_2)$	Jenny, 1941	Molecular ratio (mobile/immobile)
Comments on 'silica to R_2O_3' ratio			
Poor correlation has been observed between 'Silica to Sesquioxide ratio' and the weathering grade (this study)			
Leaching factor	$I_{weathered}/I_{fresh}$ $I = [(K_2O + Na_2O)/SiO_2]$	Jenny, 1941	Molecular ratio $(mobile/mobile)_{parent\ normalized}$
Comments on 'leaching factor'			
Good indicator (Birkeland, 1984)			
Good correlation has been observed between 'leaching factor' and the weathering grade (this study)			
WPI	$100\ (K_2O + Na_2O + CaO - H_2O^+)/(SiO_2 + Al_2O_3 + Fe_2O_3 + TiO_2 + CaO + MgO + Na_2O + K_2O)$	Reiche, 1943	Molecular ratio (mobile/immobile) Decrease of silica and mobile cations, and increase in LOI (Reiche, 1943)
Comments on weathering potential index (WPI)			
Good indicator of the degree of chemical weathering in volcanic and granitic rocks (Irfan, 1996; 1999)			
Poor correlation has been observed between 'WPI' and the weathering grade (this study)			
PI	$100\ SiO_2/(SiO_2 + TiO_2 + Fe_2O_3 + FeO + Al_2O_3)$	Reiche, 1943	Molecular ratio (mobile/immobile). During weathering, silica and mobile cations decrease, while LOI increases (Reiche, 1943)
Comments on 'weathering direction = Product index'			
Good indicator of the degree of chemical weathering in volcanic and granitic rocks (Irfan, 1996; 1999)			
Poor correlation has been observed between 'PI' and the weathering grade (this study)			
WI	$100(I_{weathered}/I_{fresh})$ $I = [(K_2O + Na_2 + CaO - H_2O^+)/(SiO_2 + Al_2O_3 + Fe_2O_3 + TiO_2 + CaO + MgO + Na_2O + K_2O)]$	Short, 1961	Molecular ratio $(mobile/immobile)_{parent\ normalized}$ Based on WPI (Short, 1961)
Comments on 'weathering index'			
Arbitrary scaling (Short, 1961; Ruxton, 1968; this study)			
Sensitive to hydroxyl water content (Ruxton, 1968)			
Poor correlation has been observed between 'WI' and the weathering grade (this study)			
Ab_f pH	$Ab_f\ pH = F[(Na + K + Ca + Mg)/Clay\ minerals]$	Grant, 1969	Expressing alteration in relation to a constant unchanging proportion of a single rock mineral (Thomas, 1994)
Comments on 'abrasive pH'			
Applicable to granitic rocks (Malomo, 1980)			
Minerals are subject to change and loss from the rock (Thomas, 1994)			
Assumptions are not valid — not recommended (this study)			

Table 5 (*continued*)

Chemical index	Definition	Proposed by	Conditions and/or assumptions
Parker's Index	[(Na/0.35) + (Mg/0.9) + (K/0.25 + Ca/0.7)]100	Parker, 1970	Atomic proportions (mobile) Based on bond strength and individual mobilities of most major elements (Parker, 1970) Hydrolysis is the main agent of silicate weathering (Parker, 1970)
Comments on Parkers's index			
Applicable to acid, intermediate and basic rocks (Parker, 1970)			
Good correlation has been observed between 'Parker's Index' and the weathering grade (this study)			
'Absolute' weathering index	% Change $(X_{sample}/I_{sample})/(X_{parent}/I_{parent}) - 1$ [b]	Nesbitt, 1979	Weight percentage of components Certain elements (e.g. Ti) must remain constant during weathering (Nesbitt and Young, 1982)
CIA	100x $Al_2O_3/(Al_2O_3 + CaO + Na_2O + K_2O)$	Nesbitt and Young, 1982	Molecular ratio (immobile/mobile)
Comments on 'chemical index of alteration'			
Ca, Na and K must decrease as the intensity of weathering increases (Nesbitt and Young, 1982)			
Bases:alumina	$(K_2O + Na_2O + CaO + MgO)/Al_2O_3$	Colman, 1982	Molecular ratio (mobile/immobile)
Comments on 'bases to alumina' ratio			
Proposed for mafic and ultramafic rocks (Colman, 1982)			
Good correlation has been observed between 'Bases to Al' the weathering grade (this study)			
Bases:R_2O_3	$(K_2O + Na_2O + CaO + MgO)/(Al_2O_3 + Fe_2O_3 + TiO_2)$	Colman, 1982	Molecular ratio (mobile/immobile)
Comments on 'bases to R_2O_3' ratio			
Good correlation has been observed between 'Bases to sesquioxide ratio' and the weathering grade (this study)			
K	$I_{weathered}/X_{sound}$ $I = SiO_2/Al_2O_3$ $X = (K_2O + Na_2O + CaO)/Al_2O$	Rocha Filho et al., 1985	Molecular ratio $(mobile/immobile)_{parent\ normalized}$ Silica loss must be related to total element loss, and the Al and sesquioxide contents must remain constant during weathering (Ruxton, 1968)
Comments on 'K'			
Poor correlation has been observed between 'K' the weathering grade (this study)			
b_1	Al_2O_3/TiO_2	Rocha Filho et al., 1985	Molecular ratio (immobile/immobile)
Comments on 'aluminum to titanium' ratio			
Very poor correlation has been observed between 'a' and the weathering grade (this study)			

Table 5 (*continued*)

Chemical index	Definition	Proposed by	Conditions and/or assumptions
LOI	H_2O(+and-)	Sueoka et al., 1985	Weight percentage LOI must increase as the intensity of weathering increases (Sueoka et al., 1985)
Comments on 'LOI'			
Good indicator of the degree of chemical weathering in volcanic and granitic rocks (Irfan, 1996; 1999)			
Poor correlation has been observed between 'LOI' and the weathering grade (this study)			
CIW = ACN	100 $Al_2O_3/(Al_2O_3 + Na_2O + CaO)$	Harnois, 1988	Molecular ratio (immobile/mobile) Al remains in the system and accumulates in the residue, while Ca and Na are leached (Harnois and Moore, 1988)
Comments on chemical index of weathering = CIW			
Not good indicator of the degree of weathering in granite (Irfan, 1996; 1999)			
Not sensitive to degree chemical of weathering (this study)			
ALK RATIO	$K_2O/(K_2O + Na_2O)100$	Harnois and Moore, 1988	Molecular ratio (mobile/mobile)
Comments on 'alkaline ratio'			
Good correlation has been observed between 'ALK RATIO' and the weathering grade (this study)			
CWI	$(Al_2O_3 + Fe_2O_3 + TiO_2 + LOI$/all chemical components)100	Sueoka, 1988	Molecular ratio Alkali, alkaline earths and silica components decrease, while sesquioxides and LOI increase during weathering (Sueoka, 1988)
Comments on 'chemical weathering index'			
It corresponds closely with physical properties of weathered granite (Sueoka, 1988)			
Valid for different climatic conditions (temperate as well as tropical) (Sueoka, 1988)			
Poor correlation has been observed between 'CWI' and the weathering grade (this study)			
Imob	$(I_{fresh} - I_{weathered})/I_{fresh}$ $I = (K_2O + Na_2O + CaO)$	Irfan, 1996	Molecular ratio $(mobile)_{parent\ normalized}$ Feldspar-bearing rocks, well drained conditions (Irfan, 1999) Parent rock composition must be provided (this study)
Comments on 'mobiles index'			
The index is not suitable for basic and ultrabasic rocks and for weathering conditions that result in smectite or vermiculate (Irfan, 1999)			
Good correlation has been observed between 'Imob' and the weathering grade (this study)			
CWD	100 $(W_w - W_f)/(W_u - W_f)\%$[c]	Esaki and Jiang, 1999	Weight percentage Based on H_2O^+content and assumes that H_2O^+reflects the chemical weathering degree (Esaki and Jiang, 1999)
Comments on 'chemical weathering degree'			
Assumptions are ill-founded. (this study)			
It is very subjective to define ultimate weathering product, not recommended (this study)			

[a] *A*: mobile component; *C*: non-variant constituent; w: weathered rock; f: fresh.
[b] X: mobile element; I: immobile element.
[c] W_w: water in weathered rock; W_f: water in fresh rock; W_u: water in the ultimate weathering product.

Appendix 2.2 Additional Chemical Weathering Indices

Chemical Index	Definition	Proposed by	Conditions and/or assumptions
Vogt Ratio **(VR)**	$(Al_2O_3 + K_2O) / (MgO + CaO + K_2O)$	Vogt, 1927; in Roaldset, 1972	Based on mole ratios of oxides of bases and aluminium
Ruxton's **(RR)** Ratio	$\frac{SiO_2}{Al_2O_3}$	Ruxton, 1968	Increase of alumina and loss in silica is considered
Miura **(MWI)** Weathering Index	$\frac{MnO + FeO + CaO + MgO + Na_2O + K_2O}{Al_2O_3 + Fe_2O_3 + H_2O}$	Miura, 1973	Ratio of concentrations of mobile elements vs immobile elements
Hodder **(W_h)** Weatherability Index	$\log \{ W^o m / W^o p \}$	Hodder, 1984	Comparison of Parker and Miura indices to check the weatherability of rock material
Silica-Titania Index	$\frac{SiO_2 / TiO_2}{(SiO_2 / TiO_2) + (SiO_2 / Al_2O_3) + (Al_2O_3 / TiO_2)}$	Jayawardena and Izawa, 1994	Molecular proportions of the elements taken. Used for metamorphic rocks of Sri Lanka
Weathering **(WR)** Index	$(MgO + CaO + Na_2O) / (ZrO_2)$	Bland and Rolls, 1998	Based on the resistant heavy minerals in 20-90 μm fraction
Mobility **(MI)** Index	$(R_p R^i_w) / (R_w R^i_p)$	Guan *et al.*, 2001	Percentages by weight of stable and non-stable constituents in the parent rock and weathered product

Appendix 3.1 Calibrative Study of Cone Penetrometer Readings with Standard Atterberg Limit Tests

Results of 6 samples tested by both methods are presented in table and graph form. Cone Penetrometer readings were obtained for all samples and then revised by subtracting appropriate average difference to obtain Liquid and Plastic Limits.

	LL Standard	LL Cone Penetrom	Difference	PL Standard	PL Cone Penetrom	Difference
MPJ 18	70.95	75.92	4.97	56.03	61.68	5.65
MPJ 18	70.03	75.61	5.58	56.84	61.43	4.59
MPJ 18	70.67	75.11	4.44	55.63	60.84	5.21
MPJ 34	72.21	75.76	3.55	63.85	69.67	5.82
MPJ 34	70.88	75.84	4.96	63.72	69.12	5.40
MPJ 34	72.29	75.76	3.47	63.51	69.33	5.82
Average			**4.50**			**5.42**

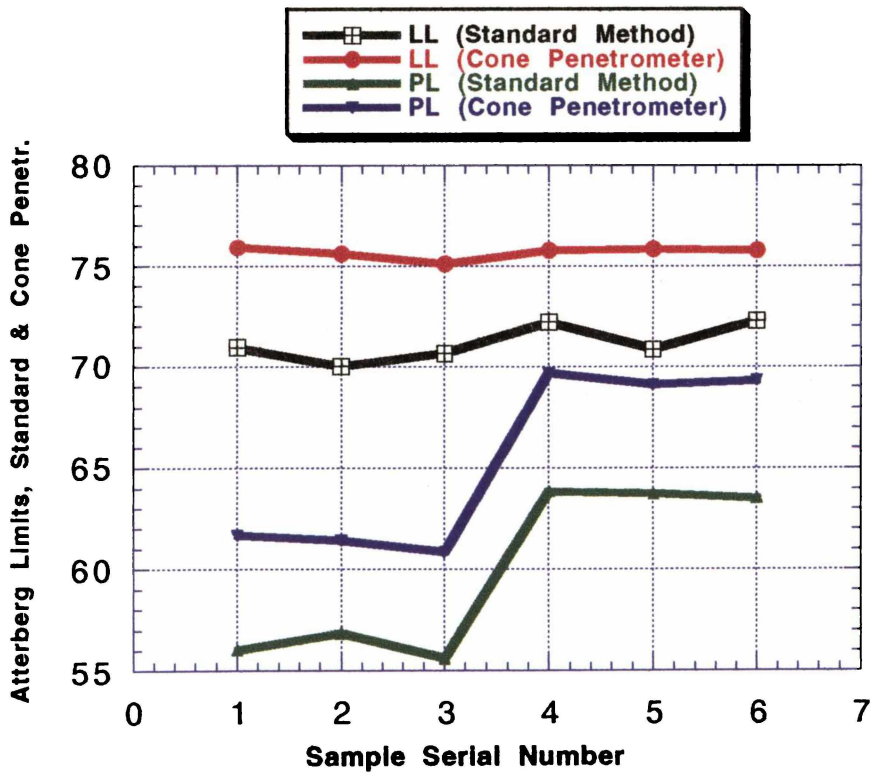

Figure Cone Penetrometer/Standard Limits Results Calibration

	APPENDIX	4.1 FIELD DESCRIPTION OF SAMPLES		
Serial No.	Sample No.	Colour Code	Colour Description	Material Description
1	MPJ 1	5Y3/2	Dark Greyish Black	Fresh Basalt Rock; Columnar joint spacing 0.5m;
				Phenocrysts of olivine & augite
2	MPJ 2	5Y3/2	Dark Greyish Black	Fresh Basalt Rock; as MPJ 1 but more cracks
3	MPJ 3	5Y3/2	Dark Greyish Black	Fresh Basalt Rock; columnar joint spacing 0.8 m
4	MPJ 4	5Y3/2	Dark Greyish Black	Fresh Basalt Rock; same as MPJ 3
5	MPJ 5	5Y3/2	Dark Greyish Black	Fresh Basalt Rock; same as MPJ 3
6	MPJ 6	5Y3/2	Dark Greyish Black	Fresh Basalt Rock; open joints of 1m spacing
7	MPJ 7	5Y3/2	Dark Greyish Black	Fresh Basalt Rock; same as MPJ 1
8	MPJ 8	10YR2/1 & 10YR4/4	Grey w. Brown on joint planes	Slightly Weathered Basalt; horizontal fracturing; open
				joints partly filled with brown clayey secondary minerals
9	MPJ 9	10YR6/6 & N1.5/0	Yellowish Brown w Black incls.	Moderately Weathered Basalt;brown soil material; large
				corestones; black manganese oxide lumps in soil
10	MPJ 10	10YR5/6	Yellowish Brown	Moderately Weathered Basalt;same as MPJ 9;no inclusions
11	MPJ 11	10YR5/6	Yellowish Brown	Moderately Weathered Basalt; brown soil material; large
				corestones; black manganese oxide lumps in soil
12	MPJ 12	10YR4/6 & 10YR6/8	Brown with Orange inclusions	Moderately Weathered Basalt; orange inclusions
13	MPJ 13	10YR5/6	Yellowish Brown	Moderately Weathered Basalt
14	MPJ 14	5YR3/2	Greyish Brown	Slightly Weathered Basalt; horizontal fracturing; open
				joints partly filled with brown clayey secondary minerals
15	MPJ 15	5Y4/3	Blackish Brown	Moderately Weathered Basalt
16	MPJ 16	10YR4/4 & 5YR4/6	Brown w Reddish Brown incls.	Moderately Weathered Basalt; hematite & clay inclusions
17	MPJ 17	10YR4/3	Brown	Moderately Weathered Basalt
18	MPJ 18	10YR3/2 & N8/0	Brown with White inclusions	Moderately Weathered Basalt; clay lumps
19	MPJ 19	5YR3/2	Dark Brown	Moderately Weathered Basalt
20	MPJ 20	5YR3/3 & N8/0	Dark Brown with White incls.	Moderately Weathered Basalt; clay lumps
21	MPJ 21	5YR4/6 & N8/0	Dark Brown with White incls.	Moderately Weathered Basalt; same as MPJ 20
22	MPJ 22	2.5Y8/8	Yellowish Brown	Weathered tephra; fragments of rhyolite;
				clays and goethite present
23	MPJ 23	2.5Y8/8	Yellowish Brown	Weathered Tephra; same as MPJ 22
24	MPJ 24	2.5YR5/8	Reddish Brown	Paleosol; hematite and clays present
25	MPJ 25	2.5Y8/8	Yellowish Brown	Weathered Tephra;fragments of rhyolite;
				clays & goethite present
26	MPJ 26	2.5Y7/8	Yellowish Brown	Weathered Tephra; clays and goethite present
27	MPJ 27	2.5Y7/8	Yellowish Brown	Weathered Tephra; same as MPJ 26
28	MPJ 28	5YR5/8	Reddish Brown	Paleosol; hematite and clays present
29	MPJ 29	7.5YR4/6	Dark Brown	Paleosol; hematite and clays present
30	MPJ 30	10YR8/8	Orangish Brown	Weathered Tephra; fragments of rhyolite;
				clays and goethite present
31	MPJ 31	5YR4/6	Reddish Brown	Completely Weathered Basalt; relict joints visible;
				clay minerals and limonite on relict joint planes
32	MPJ 32	7.5YR5/8	Reddish Brown	Completely Weathered Basalt; same as MPJ 31
33	MPJ 33	2.5YR3/4	Reddish Brown	Completely Weathered Basalt; relict joints visible;
				clays compose the matrix
34	MPJ 34	5YR3/4	Reddish Brown	Completely Weathered Basalt; same as MPJ 33
35	MPJ 35	10YR7/8	Yellowish Brown	Weathered Tephra; fragments of rhyolite; gibbsite,
				allophane & limonite present
36	MPJ 36	5YR4/6	Reddish Brown	Completely Weathered Basalt; relict joints visible;
				clay minerals and limonite on relict joint planes
37	MPJ 37	2.5YR5/8	Reddish Brown	Iron Oxides & Clays
38	MPJ 38	10YR7/8	YellowishBrown	Highly Weathered Basalt; corestones & soil in equal
				quantities; manganese & iron oxides, clays as incls.
39	MPJ 39	N1.5/0	Black inclusions	Manganese Oxide
40	MPJ 40	N8/0	White inclusions	Clay Minerals
41	MPJ 41	10YR8/1	Brown	Highly Weathered Basalt; core stones & soil in equal
				quantities; manganese & iron oxides, clays as incls.
42	MPJ 42	5YR5/4 7 N8/0	Brown with White inclusions	Clay minerals
43	MPJ 43	N1.5/0 & N8/0	Black and White inclusions	Manganese Oxide & Clays
44	MPJ 44	10YR6/8	Yellowish Brown	Highly Weathered Basalt; core stones & soil in equal
				quantities; manganese & iron oxides, clays as incls.
45	MPJ 45	10YR8/8	Yellow banded inclusions	Clays and Iron Oxides
46	MPJ 46	N1.5/0 & N8/0	Black & White inclusions	Manganese Oxide & Clays
47	MPJ 47	7.5YR4/6	Brown	Highly Weathered Basalt; corestones & soil in equal
				quantities; manganese & iron oxides, clays as incls.
48	MPJ 48	N1.5/0 & N8/0	Black & White inclusions	Manganese Oxide & Clays
49	MPJ 49	7.5YR4/6	Brown	Highly Weathered Basalt; corestones & soil in equal
				quantities; manganese & iron oxides, clays as incls.
50	MPJ 50	7.5YR4/6	Brown	Highly Weathered Basalt; same as MPJ 49
51	MPJ 51	5Y3/2	Greyish Brown	Slightly Weathered Basalt; open joints partly
				filled with brown clayey secondary minerals
52	MPJ 52	5Y3/2	Greyish Brown	Slightly Weathered Basalt; horizontal fracturing; open
				joints
53	MPJ 53	5Y3/2	Greyish Brown	Slightly Weathered Basalt; same as MPJ 52
54	MPJ 54	10YR8/1	Brown inclusions	Iron Oxides & Clays; more hematite than clays.
55	MPJ 55	N8/0 &5YR5/4	White and Orange inclusions	Clays and Iron Oxides; more clay than hematite
56	MPJ 56	10YR8/1	Brown inclusions	Iron Oxides and Clays; more hematite than clay
57	MPJ 57	N1.5/0 & N8/0	Black & White inclusions	Manganese Oxide & Clays
58	MPJ 58	5YR4/6	Reddish Brown	Completely Weathered Basalt; relict joints visible;
				clay minerals and goethite on relict joint planes
59	MPJ 59	5YR4/6	Reddish Brown	Iron Oxides and Clays;hematite and some clay
60	MPJ 60	5YR4/6	Reddish Brown	Completely Weathered Basalt; same as MPJ 58

APPENDIX 4.2 PETROGRAPHIC DESCRIPTION OF SAMPLES

Sample No.	Description of Samples
MPJ 1	Holocrystalline, fine grained, porphyritic with abundant subhedral phenocrysts of olivine, titanaugite and rare titanomagnetite set in a groundmass composed of labradorite laths, titanaugite and tiny granular titanomagnetite crystals. Accessory minerals are apatite and chromite. Olivine crystals show slight yellow outlines – iddingsite rims. Olivine 35 %; titanaugite 29 %; plagioclase 33 % and titanomagnetite 3 %.
MPJ 2	Same as MPJ 1.
MPJ 3	Hypocrystalline, fine grained, porphyritic with abundant euhedral to subhedral phenocrysts of olivine, plagioclase and subhedral titanaugite set in an intersertal groundmass composed of titanaugite, plagioclase laths, olivine, granular titanomagnetite, interstitial pools of zeolite and dark brown patches of glass. Olivine 34 %; titanaugite 26 %; plagioclase 35 %; glass 4 % and titanomagnetite 1 %.
MPJ 4	Holocrystalline, fine grained, porphyritic with abundant subhedral phenocrysts of olivine, titanaugite and rare titanomagnetite set in a groundmass composed of plagioclase laths, titanaugite, glass and tiny granular titanomagnetite crystals. Olivine crystals show pale yellow thin iddingsite rims (of ~10 μm thickness) and evidence of microfracturing. Olivine 30 %; titanaugite 31 %; plagioclase 35.5 %; glass 3 % and titanomagnetite 0.5 %.
MPJ 5	Hypocrystalline, fine grained, porphyritic with abundant euhedral to subhedral phenocrysts of olivine and subhedral titanaugite set in an intersertal groundmass composed of titanaugite, plagioclase laths, olivine, granular titanomagnetite and dark brown patches of glass. Olivine 29%; titanaugite 29 %; plagioclase 34 %; glass 6 % and titanomagnetite 2 %.
MPJ 6	Same as MPJ 3.
MPJ 7	Same as MPJ 1.
MPJ 8	Porphyritic texture. Alteration of olivine crystals: development of orange colour iddingsite rims (thickness ~17 μm) and widening of micro-fractures up to 10 μm. Micorfacturing more frequent. Turbid and speckly appearance on plagioclase due to clay formations. Some titanaugite crystal edges break off. Alteration of glass to smectite in interstitial positions (bright yellow interference colours). Titanomagnetite unaltered.
MPJ 9	Relict porphyritic texture. Olivine crystals have thicker (30 μm) iddingsite rims thicker than in slightly weathered basalt. Appearance of a network of cracks. Along fracture planes, olivine and titanaugite crystals in parts or completely removed. Plagioclase and glass vanished. Clays, hematite, titanomagnetite and goethite dominate.
MPJ 10	Parts of olivine and titanaugite crystals are removed due to weathering. Clay minerals present.

MPJ 11 Plagioclase is completely gone and clay minerals are formed.

MPJ 12 Presence of goethite is evident. Clay minerals abundant.

MPJ 13 Parts (in some places in whole) of olivine and titanaugite crystals are removed due to weathering. Clay minerals present.

MPJ 14 Porphyritic texture. Alteration of olivine crystals: development of orange colour iddingsite rims (thickness ~30 μm) and micro-fractures. Speckly appearance on plagioclase due to clay formations. Some titanaugite crystal edges break off. Alteration of glass to smectite in interstitial positions (bright yellow interference colours). Titanomagnetite is in abundance.

MPJ 15 Relict porphyritic texture. Olivine crystals have thicker (30 μm) iddingsite rims thicker than in slightly weathered basalt. Appearance of a network of cracks. Along fracture planes, olivine and titanaugite crystals in parts or completely removed. Plagioclase and glass vanished. Clays, hematite, goethite, titanomagnetite and manganese oxides are prominent.

MPJ 16 Same as MPJ 15.

MPJ 17 Relict porphyritic texture. Matrix contains clays, titanomagnetite and hematite. Olivine and titanaugite are altered to secondary minerals such as clays, goethite and hematite.

MPJ 18 Relict porphyritic texture. Olivine crystals have thicker (30 μm) iddingsite rims thicker than in slightly weathered basalt. Appearance of a network of cracks. Along fracture planes, olivine and titanaugite crystals in parts or completely removed. Plagioclase and glass vanished. Clays, hematite, titanomagnetite and goethite dominate.

MPJ 19 Same as MPJ 18.

MPJ 20 Relict porphyritic texture. Matrix contains clays, titanomagnetite and hematite. Most olivine and titanaugite phenocrysts are altered to secondary minerals such as clays, goethite and hematite.

MPJ 21 Same as MPJ 20.

MPJ 22 Clay minerals and goethite are predominant. Some fragments of rhyolite present.

MPJ 23 Clay minerals and goethite are predominant.

MPJ 24 Hematite and clay minerals are there.

MPJ 25 Clay minerals and goethite are predominant.

MPJ 26 Clay minerals and goethite are predominant.

MPJ 27 Clay minerals and goethite are predominant.

MPJ 28 Goethite and clay minerals are present.

MPJ 29 Hematite and clay minerals are present.

MPJ 30 Clay minerals and goethite are predominant.

MPJ 31 Relict porphyritic texture. Only relict outlines of olivine and titanaugite crystals visible. Clay minerals, hematite and goethite constitute the material.

MPJ 32 Same as MPJ 31.

MPJ 33 Hematite, goethite and clay minerals. Only traces of original basalt-forming minerals.

MPJ 34 Relict porphyritic texture. Only relict outlines of olivine and titanaugite crystals visible. Clay minerals, hematite and goethite constitute the material.

MPJ 35 Clay minerals and goethite are predominant.

MPJ 36	Hematite and clay minerals. Only traces of original basalt-forming minerals.
MPJ 37	Hematite is the predominant mineral. Tiny crystals of olivine, titanaugite and some plagioclase present.
MPJ 38	Relict porphyritic texture. Olivine and titanaugite phenocrysts altered to goethite and hematite. Only a small fraction of olivine can be seen in relict phenocrysts. Pyroxenes in the groundmass broken down to clays. Clays abundant. Extensive crack network.
MPJ 39	Manganese oxide concretions.
MPJ 40	Clay minerals are predominant.
MPJ 41	Relict porphyritic texture. Olivine and titanaugite phenocrysts altered to goethite and hematite. Only a small fraction of olivine can be seen in relict phenocrysts. Pyroxenes in the groundmass broken down to clays. Clays abundant. Extensive crack network.
MPJ 42	Clay minerals.
MPJ 43	Manganese oxide nodules and lumps of clay minerals present.
MPJ 44	Relict porphyritic texture. Clay minerals and altered olivine & titanaugite crystals can be observed.
MPJ 45	Clay minerals & goethite in the matrix. Remnants of olivine and titanaugite present.
MPJ 46	Manganese oxide and clay minerals present.
MPJ 47	Relict porphyritic texture. Clay minerals, goethite and hematite are predominant.
MPJ 48	Manganese oxide and clay minerals.
MPJ 49	Relict porphyritic texture. Olivine and titanaugite phenocrysts altered to goethite and hematite. Only a small fraction of olivine can be seen in relict phenocrysts. Pyroxenes in the groundmass broken down to clays. Clays abundant. Extensive crack network.
MPJ 50	Same as MPJ 49.
MPJ 51	Porphyritic texture. Alteration of olivine crystals: development of orange colour rims (thickness ~17 μm) and micro-fractures. Turbid appearance on plagioclase due to clay formations. Some titanaugite crystals show irregular edges.
MPJ 52	Porphyritic texture.Alteration of olivine crystals: development of orange colour iddingsite rims (thickness ~17 μm) and micro-fractures. Speckly appearance on plagioclase due to clay formations. Some titanaugite crystal edges break off. Alteration of glass to smectite in interstitial positions (bright yellow interference colours). Titanoagnetite is in abundance.
MPJ 53	Same as MPJ 52
MPJ 54	Hematite and clay minerals.
MPJ 55	Goethite and clay minerals.
MPJ 56	Hemaite and clay minerals.
MPJ 57	Manganese oxide and clay minerals
MPJ 58	Relict porphyritic texture. Only relict outlines of olivine and titanaugite crystals visible. Clay minerals, hematite and goethite constitute the material.
MPJ 59	Hematite and clay minerals.
MPJ 60	Relict porphyritic texture. Only relict outlines of olivine and titanaugite crystals visible. Clay minerals, hematite and goethite constitute the material.

APPENDIX 4.3 PERCENTAGES OF MINERALS DETECTED BY X-RAY DIFFRACTION ANALYSIS

Description	Fresh Basalt									Slightly Weathered Basalt							Std. Dev.	Moderately Weathered Basalt														Highly Weathered Basalt			
Sample Details	bulk							Average	Std. Dev.	bulk		core	joint infill		Average			bulk			core		matrix		Average	Std. Dev.	bulk		core					
Sample Nos.	MPJ 1	MPJ 2	MPJ 3	MPJ 4	MPJ 5	MPJ 6	MPJ 7			MPJ 51	MPJ 14	MPJ 8	MPJ 52	MPJ 53				MPJ 9	MPJ 10	MPJ 12	MPJ 17	MPJ 20	MPJ 11	MPJ 13	MPJ 16	MPJ 15	MPJ 21			MPJ 44	MPJ 47	MPJ 49	MPJ 50		
Mineral Name																																	
olivine	20.9	21.5	19.3	19.6	21.0	21.3	18.3	**20.3**	1.2	37.5	36.3	14.7	29.7	5.7	**24.8**	14.0	6.8	9.1	0.0	0.0	5.2	22.4	73.6	27.9	0.0	17.9	**16.3**	**22.4**	0.0	0.0	3.0	7.7		
augite	28.2	27.9	28.2	29.6	29.6	27.2	28.5	**28.5**	0.9	18.7	22.3	26.5	17.8	23.8	**21.8**	3.6	0.0	0.0	4.7	3.3	0.0	14.1	10.5	13.4	0.0	8.0	**5.4**	**5.7**	2.9	3.4	3.5	3.7		
plagioclase	38.6	38.9	40.0	38.5	38.2	39.2	40.4	**39.1**	0.8	0.0	0.0	17.9	0.0	0.0	**3.6**	8.0																		
volcanic glass	7.1	7.2	7.5	7.6	6.9	7.8	8.0	**7.4**	0.4	4.5	4.3	5.9	0.0	0.0	**2.9**	2.8																		
magnetite	2.2	2.2	2.3	2.3	2.2	2.1	2.2	**2.2**	0.1	0.0		2.6		9.5	**4.1**	4.9	0.0	8.8	0.0	0.0	4.1	11.8	0.0	11.7	0.0	0.0	**3.6**	**5.1**	0.0	0.0	0.0	0.0	25.4	16.2
chromite																	0.0	0.0	9.4	0.0	6.4	0.0	0.0	0.0	0.0	0.0	**1.6**	**3.4**						
hematite																	9.9	0.0	0.0	14.0	34.7	0.0	0.0	0.0	0.0	5.4	**6.4**	**11.1**						
goethite																	0.0	0.0	14.6	0.0	13.1	14.1	0.0	17.5	0.0	5.1	**6.5**	**7.5**	6.7	4.2	2.9	0.0	10.8	5.3
manganosite										0.0	0.0	2.6	3.7	0.0	**1.3**	1.8	0.0	10.7	0.0	2.7	0.0	0.0	0.0	0.0	0.0	0.0	**1.3**	**3.4**	4.1	0.0	0.0	0.0	7.9	2.6
phlogopite										0.0	0.0		5.3	0.0	**1.3**	2.7																		
montmorillonite	0.0	2.3	0.0	0.0	2.1	2.3	2.5	**1.3**	1.2	11.8	11.3	2.9	13.6	21.0	**12.1**	6.5	24.5	39.0	34.3	24.5	9.3	37.5	0.0	0.0	62.6	36.0	**26.8**	**19.6**	0.0	6.4	0.0	0.0	27.5	16.8
nontronite										0.0	0.0	4.4	0.0	0.0	**0.9**	2.0																		
beidellite										0.0	0.0	7.8	0.0	0.0	**1.6**	3.5													15.9	17.7	20.5	23.1	0.0	0.0
saponite	3.0	0.0	2.7	2.4	0.0	0.0	0.0	**1.2**	1.2	9.8	8.8	4.9	4.4	12.1	**8.0**	3.3	0.0	16.4	0.0	0.0	11.1	0.0	0.0	29.4	0.0	5.5	**6.2**	**10.0**					5.5	
kaolinite										17.7	17.0	2.4	11.5	14.7	**12.7**	6.2	18.3	0.0	27.9	18.4	5.9	0.0	0.0	0.0	37.4	6.3	**11.4**	**13.4**	24.7	27.6	23.6	22.5	19.4	26.9
vermiculite										0.0	0.0	0.0	3.7	0.0	**0.7**	1.7										2.5								
illite										0.0	0.0	7.3	0.0	0.0	**1.5**	3.3	40.5	0.0	9.1	21.6	0.0	0.0	0.0	0.0	0.0	13.1	**8.4**	**13.5**	28.1	24.1	28.5	23.1	0.0	19.8
halloysite										0.0	0.0	0.0	10.2	13.3	**4.7**	6.5	0.0	16.0	0.0	15.5	10.1	0.0	15.9	0.0	0.0	0.0	**5.8**	**7.6**	17.5	16.5	18.0	19.8	0.0	12.4
allophane																																		
TOTAL	100.0	100.0	100.0	100.0	100.0	100.0	100.0			100.0	100.0	100.0	100.0	100.0				100.0	100.0	100.0	100.0	100.0	100.0	100.0	100.0	100.0			100.0	100.0	100.0	100.0	100.0	100.0
% clay minerals	3.0	2.3	2.7	2.4	2.1	2.3	2.5	**2.5**	0.3	39.3	37.1	29.9	43.4	61.0	**42.2**	11.7	83.3	71.4	71.3	80.0	36.4	37.5	15.9	29.4	100.0	63.5	**58.9**	**27.4**	86.3	92.3	90.7	88.6	52.4	75.9

Description	Completely Weathered Basalt																		Tephra	Paleosol	Inclusions			
Sample Details	matrix		Average	Std. Dev.	bul bulk								Average	Std. Dev.										
Sample Nos.	MPJ 38	MPJ 41			MPJ 31	MPJ 32	MPJ 33	MPJ 34	MPJ 36	MPJ 58	MPJ 60								MPJ 22	MPJ 29	MPJ 54	MPJ 57		
Mineral Name																								
olivine	0.0	0.0	**1.8**	**3.1**																	11.6	12.5		
augite	3.5	0.0	**2.8**	**1.4**																	2.6	8.5		
plagioclase																								
volcanic glass																								
magnetite					6.0	13.7	0.0	0.0	10.7	0.0	0.0	**4.3**	**5.9**											
chromite																								
hematite					6.4	0.0	0.0	8.3	0.0	0.0	7.7	**3.2**	**4.0**								6.4	7.2		
goethite	10.8	5.3	**5.0**	**3.7**	8.8	0.0	16.3	11.3	7.3	2.9	7.2	**7.7**	**5.3**							51.3				
manganosite	7.9	2.6	**2.5**	**3.2**	0.0	0.0	0.0	0.0	0.0	16.1	0.0	**2.3**	**6.1**											
phlogopite																					4.8	4.6		
montmorillonite	27.5	16.8	**8.4**	**11.4**	24.2	33.6	40.3	22.1	37.0	31.0	32.3	**31.5**	**6.5**						41.1		47.0	44.6		
nontronite																								
beidellite	0.0	0.0	**12.9**	**10.3**	8.6	0.0	12.7	15.5	0.0	3.6	4.0	**6.3**	**6.1**											
saponite	19.4	26.9	**24.1**	**3.0**	3.7	0.0	0.0	0.0	0.0	28.9	30.0	**8.9**	**14.1**						22.4		6.8	8.9		
kaolinite					0.0	0.0	0.0	0.0	7.3	6.2	7.5	**3.0**	**3.8**								1.1	1.0		
vermiculite																								
illite	0.0	19.8	**20.6**	**10.6**	19.6	10.3	7.2	19.8	30.6	11.3	11.3	**15.7**	**8.1**							48.7	19.8	12.8		
halloysite	0.0	12.4	**14.1**	**7.3**	19.9	26.2	23.6	16.3	0.0	0.0	0.0	**12.3**	**11.9**						30.6					
allophane																			5.9					
TOTAL	100.0	100.0			100.0	100.0	100.0	100.0	100.0	100.0	100.0								100.0	100.0	100.0	100.0		
% clay minerals	52.4	75.9	**81.0**	**15.2**	78.7	86.3	83.7	80.4	82.1	81.0	85.1	**82.5**	**2.7**						100.0	48.7	74.6	67.2		

Appendix 4.4 CHEMICAL ANALYSIS OF SAMPLES (X-RAY FLUORESCENCE METHOD), WEATHERING INDICES AND CHEMICAL PREDICTORS (some trace element concentrations were not determined for tephra, paleosol and inclusions)

Serial No.	Sample No.	Sample description	SiO2 %	Al2O3 %	MnO %	MgO %	CaO %	Na2O %	K2O %	TiO2 %	P2O5 %	Fe2O3 %	FeO %	LOI %	Total
1	MPJ 1	Fresh Basalt	42.74	11.71	0.19	12.97	10.94	1.59	1.02	2.39	0.44	3.09	10.34	2.63	100.05
2	MPJ 2	Fresh Basalt	45.92	12.43	0.18	11.28	10.18	1.93	1.10	2.18	0.38	2.91	9.76	2.11	100.36
3	MPJ 3	Fresh Basalt	41.46	12.09	0.19	12.88	10.94	1.00	0.45	2.52	0.38	3.22	10.79	4.71	100.64
4	MPJ 4	Fresh Basalt	41.25	12.10	0.18	12.83	10.80	1.03	0.51	2.50	0.38	3.20	10.72	4.48	99.99
5	MPJ 5	Fresh Basalt	41.21	12.06	0.18	12.77	10.78	1.03	0.51	2.48	0.38	3.19	10.69	4.48	99.77
6	MPJ 6	Fresh Basalt	42.42	12.06	0.19	12.62	11.12	1.27	0.64	2.42	0.39	3.14	10.52	3.65	100.44
7	MPJ 7	Fresh Basalt	41.71	11.84	0.18	12.34	10.99	1.25	0.64	2.40	0.38	3.11	10.42	3.68	98.95
	Average		**42.39**	**12.04**	**0.18**	**12.53**	**10.82**	**1.30**	**0.70**	**2.41**	**0.39**	**3.12**	**10.46**	**3.68**	**100.03**
	Std. Dev.		**1.66**	**0.23**	**0.00**	**0.59**	**0.31**	**0.35**	**0.26**	**0.11**	**0.02**	**0.10**	**0.35**	**0.99**	**0.56**
8	MPJ 8	Slightly Weath.	35.69	14.23	0.19	11.45	6.11	0.19	0.11	3.01	0.33	3.75	12.54	11.49	99.09
12	MPJ 14	Slightly Weath.	31.87	22.07	0.32	3.71	0.64	0.00	0.22	3.94	0.57	19.10	1.01	13.95	97.33
9	MPJ 51	Slightly Weath.	28.87	23.37	0.29	0.94	0.00	0.00	0.00	4.89	0.57	19.50	4.20	14.13	96.63
10	MPJ 52	Slightly Weath.	28.94	24.09	0.48	0.79	0.00	0.00	0.00	4.88	0.60	19.76	3.80	13.60	96.80
11	MPJ 53	Slightly Weath.	28.68	23.83	0.31	0.71	0.00	0.00	0.00	4.86	0.58	19.47	4.00	13.92	96.22
	Average		**30.81**	**21.52**	**0.32**	**3.52**	**1.35**	**0.04**	**0.07**	**4.32**	**0.53**	**16.32**	**5.11**	**13.42**	**97.21**
	Std. Dev.		**3.03**	**4.15**	**0.10**	**4.61**	**2.68**	**0.08**	**0.10**	**0.83**	**0.11**	**7.03**	**4.36**	**1.09**	**1.12**
13	MPJ 9	Moderately w.	40.63	29.59	0.03	0.12	0.06	0.05	0.13	0.92	0.05	6.66	0.35	20.08	98.67
14	MPJ 10	Moderately w.	40.91	30.72	0.03	0.10	0.06	0.04	0.10	0.87	0.04	6.68	0.35	18.88	98.78
15	MPJ 11	Moderately w.	34.54	27.97	0.27	0.31	0.07	0.00	0.08	2.85	0.38	14.49	0.76	16.36	98.04
16	MPJ 12	Moderately w.	32.11	27.39	0.30	0.65	0.07	0.00	0.05	3.47	0.49	16.85	0.89	15.44	97.64
17	MPJ 13	Moderately w.	39.19	28.76	0.07	0.19	0.07	0.02	0.13	1.26	0.13	7.97	0.42	20.45	98.66
18	MPJ 15	Moderately w.	29.75	23.56	0.32	1.36	0.07	0.00	0.09	4.41	0.53	20.88	1.10	15.26	97.24
19	MPJ 16	Moderately w.	34.39	27.42	0.16	0.44	0.10	0.00	0.06	2.45	0.28	12.62	0.66	19.74	98.29
20	MPJ 17	Moderately w.	35.44	27.52	0.17	0.94	0.40	0.00	0.07	2.42	0.28	12.67	0.67	18.10	98.67
21	MPJ 18	Moderately w.	27.24	23.26	0.35	0.84	0.01	0.00	0.00	4.31	0.40	20.05	1.06	19.93	97.37
22	MPJ 19	Moderately w.	28.10	24.32	0.40	0.96	0.01	0.00	0.00	4.63	0.51	21.53	1.13	15.46	96.97
23	MPJ 20	Moderately w.	27.00	24.66	0.30	1.13	0.01	0.00	0.00	4.61	0.48	21.53	1.13	17.27	98.04
24	MPJ 21	Moderately w.	30.20	26.77	0.27	0.71	0.03	0.00	0.03	3.63	0.43	17.39	0.92	17.74	98.05
	Average		**33.29**	**26.83**	**0.22**	**0.65**	**0.08**	**0.01**	**0.06**	**2.98**	**0.33**	**14.94**	**0.79**	**17.89**	**98.04**
	Std. Dev.		**5.05**	**2.40**	**0.13**	**0.42**	**0.10**	**0.02**	**0.05**	**1.42**	**0.18**	**5.67**	**0.30**	**1.94**	**0.62**
25	MPJ 38	Highly Weath.	28.22	28.24	0.36	0.54	0.00	0.00	0.00	3.57	0.83	18.00	0.95	16.17	96.78
26	MPJ 41	Highly Weath.	27.37	26.19	0.39	0.50	0.00	0:00	0.00	4.85	0.74	22.16	1.17	14.04	97.30
27	MPJ 44	Highly Weath.	39.38	30.69	0.04	0.15	0.01	0.00	0.06	1.50	0.08	10.07	0.53	15.64	98.14
28	MPJ 47	Highly Weath.	41.07	25.44	0.14	0.28	0.00	0.00	0.16	2.33	0.28	13.59	0.72	14.27	98.23
29	MPJ 49	Highly Weath.	32.88	30.25	0.36	0.23	0.00	0.00	0.00	2.78	0.52	14.22	0.75	15.74	97.66
30	MPJ 50	Highly Weath.	27.75	26.00	0.41	0.54	0.01	0.00	0.13	4.57	0.74	21.36	1.12	14.63	97.12
	Average		**32.78**	**27.80**	**0.28**	**0.37**	**0.00**	**0.00**	**0.06**	**3.27**	**0.53**	**16.57**	**0.87**	**15.08**	**97.54**
	Std. Dev.		**6.13**	**2.28**	**0.16**	**0.17**	**0.01**	**0.00**	**0.07**	**1.31**	**0.30**	**4.75**	**0.25**	**0.88**	**0.58**
31	MPJ 31	Completely W.	46.77	26.68	0.04	0.18	0.00	0.02	0.19	1.13	0.12	8.45	0.44	14.25	98.26
32	MPJ 32	Completely W.	46.01	22.07	0.02	0.22	0.00	0.00	0.16	2.02	0.15	13.31	0.70	13.81	98.46
33	MPJ 33	Completely W.	25.82	26.47	0.27	0.34	0.00	0.00	0.00	4.94	0.50	23.03	1.21	14.82	97.28
34	MPJ 34	Completely W.	30.28	29.18	0.13	1.10	0.00	0.00	0.00	3.68	0.34	17.23	0.91	15.16	97.92
35	MPJ 36	Completely W.	43.86	26.66	0.01	0.19	0.00	0.00	0.17	1.61	0.08	10.83	0.57	14.41	98.37
36	MPJ 58	Completely W.	39.54	30.04	0.01	0.10	0.00	0.00	0.04	1.27	0.02	9.35	0.50	16.62	97.45
37	MPJ 60	Completely W.	38.42	32.58	0.02	0.08	0.00	0.00	0.01	0.94	0.03	8.15	0.40	16.71	97.28
	Average		**38.67**	**27.67**	**0.07**	**0.32**	**0.00**	**0.00**	**0.08**	**2.23**	**0.18**	**12.91**	**0.68**	**15.11**	**97.86**
	Std. Dev.		**7.99**	**3.34**	**0.10**	**0.36**	**0.00**	**0.01**	**0.09**	**1.51**	**0.18**	**5.49**	**0.29**	**1.14**	**0.52**
38	MPJ 22	Weath. Tephra	41.58	34.64	0.00	0.02	0.00	0.01	0.00	0.62	0.02	2.69	2.69	16.68	98.93
39	MPJ 23	Weath. Tephra	43.52	30.56	0.01	0.14	0.00	0.01	0.12	0.90	0.03	3.63	3.63	15.83	98.38
40	MPJ 25	Weath. Tephra	41.21	32.73	0.01	0.07	0.02	0.00	0.13	0.84	0.01	3.48	3.48	16.63	98.60
41	MPJ 26	Weath. Tephra	41.72	31.73	0.01	0.11	0.00	0.01	0.14	0.96	0.02	3.82	3.82	16.20	98.52
42	MPJ 27	Weath. Tephra	43.75	34.34	0.03	0.07	0.00	0.01	0.07	0.57	0.01	1.94	1.94	16.12	98.83
43	MPJ 28	Weath. Tephra	44.01	31.65	0.00	0.04	0.00	0.01	0.00	0.71	0.02	3.34	3.35	15.35	98.38
44	MPJ 30	Weath. Tephra	42.96	33.30	0.01	0.07	0.00	0.00	0.04	0.59	0.04	3.13	3.13	15.29	98.55
45	MPJ 35	Weath. Tephra	50.25	25.84	0.05	0.18	0.00	0.00	0.17	1.07	0.10	3.97	3.97	13.24	98.83
	Average		**43.63**	**31.85**	**0.02**	**0.09**	**0.00**	**0.01**	**0.08**	**0.78**	**0.03**	**3.25**	**3.25**	**15.67**	**98.63**
	Std. Dev.		**2.88**	**2.80**	**0.02**	**0.05**	**0.01**	**0.01**	**0.07**	**0.19**	**0.03**	**0.66**	**0.67**	**1.11**	**0.21**
46	MPJ 24	Paleosol	15.41	15.80	0.15	0.00	0.00	0.00	0.00	0.64	0.10	50.10	0.64	15.03	97.77
47	MPJ 29	Paleosol	28.28	28.16	0.30	0.25	0.00	0.00	0.00	4.23	0.46	20.22	0.39	15.38	97.58
	Average		**21.85**	**21.98**	**0.23**	**0.13**	**0.00**	**0.00**	**0.00**	**2.43**	**0.28**	**35.16**	**0.52**	**15.21**	**97.68**
48	MPJ 37	Hematite incl	34.67	31.73	0.09	0.47	0.00	0.15	0.00	2.00	0.29	6.13	6.13	16.69	98.33
49	MPJ 39	MnO inclusions	27.95	27.50	0.67	0.80	0.00	0.00	0.00	4.15	0.73	19.19	1.01	14.96	96.85
50	MPJ 40	Clay fillings	27.06	25.87	0.39	0.51	0.00	0.00	0.00	4.83	0.76	11.56	11.56	14.20	96.62
51	MPJ 42	Clay fillings	39.64	30.87	0.04	0.15	0.02	0.00	0.06	1.52	0.08	5.30	5.30	15.56	98.53
52	MPJ 43	MnO;clay	27.19	26.02	0.39	0.51	0.00	0.00	0.00	4.86	0.76	11.68	11.68	13.93	96.92
53	MPJ 45	Clay;goethite	28.29	27.86	0.54	0.34	0.00	0.00	0.03	3.99	0.82	10.08	10.08	15.45	97.36
54	MPJ 46	MnO;clay	27.25	26.30	0.43	0.56	0.01	0.00	0.00	4.81	0.78	11.60	11.60	14.33	97.58
55	MPJ 48	MnO; clay	25.62	25.45	0.32	0.51	0.00	0.00	0.00	5.05	0.85	12.33	12.33	14.76	97.14
56	MPJ 54	Hematite; clay	39.54	30.04	0.01	0.10	0.00	0.00	0.04	1.27	0.02	9.35	0.50	16.62	97.45
57	MPJ 57	MnO; clays	38.42	32.58	0.02	0.08	0.00	0.00	0.01	0.94	0.03	8.15	0.40	16.71	97.28
	Average		**31.56**	**28.42**	**0.29**	**0.40**	**0.00**	**0.02**	**0.01**	**3.34**	**0.51**	**10.54**	**7.06**	**15.32**	**97.41**
	Std. Dev.		**5.80**	**2.66**	**0.23**	**0.23**	**0.01**	**0.05**	**0.02**	**1.69**	**0.36**	**3.88**	**5.02**	**1.06**	**0.61**

Serial No.	Sample No.	Nb ppm	Zr ppm	Th ppm	Sr ppm	Ba ppm	Rb ppm	V PPM	Cr ppm	Ni ppm	Zn ppm	La ppm	Ce ppm	Nd ppm	Ga ppm	Pb ppm	Y ppm
1	MPJ 1	40	202	7	947	349	27	298	796	336	105	21	65	32	19	1	23
2	MPJ 2	34	184	3	668	332	28	287	626	269	112	21	65	33	19	2	23
3	MPJ 3	42	205	4	679	295	12	301	751	336	108	36	59	45	19	<1	24
4	MPJ 4	42	207	5	676	294	14	308	741	341	107	34	62	30	20	<1	24
5	MPJ 5	43	206	4	674	314	14	301	729	320	105	27	48	44	19	<1	23
6	MPJ 6	40	201	4	656	301	15	286	717	312	105	25	62	42	20	<1	23
7	MPJ 7	41	200	4	653	319	15	301	721	314	106	25	67	51	21	2	23
	Average	**40**	**201**	**4**	**708**	**315**	**18**	**297**	**726**	**318**	**107**	**27**	**61**	**40**	**20**	**2**	**23**
	Std. Dev.	**3**	**8**	**1**	**106**	**20**	**7**	**8**	**51**	**25**	**3**	**6**	**6**	**8**	**1**	**1**	**0**
8	MPJ 8	48	228	7	166	604	6	360	903	423	134	48	50	31	23	2	30
12	MPJ 14	58	299	6	35	761	8	429	1134	808	221	137	86	229	30	6	235
9	MPJ 51	72	330	9	20	680	4	512	1318	828	183	74	110	86	34	7	49
10	MPJ 52	71	330	11	10	740	2	526	1418	837	177	49	92	68	36	3	37
11	MPJ 53	71	320	12	10	700	5	512	1432	895	178	46	83	62	36	6	37
	Average	**64**	**301**	**9**	**48**	**697**	**5**	**468**	**1241**	**758**	**179**	**71**	**84**	**95**	**32**	**5**	**78**
	Std. Dev.	**11**	**43**	**3**	**67**	**61**	**2**	**71**	**223**	**190**	**31**	**39**	**22**	**77**	**5**	**2**	**88**
13	MPJ 9	18	407	31	13	302	12	105	48	18	40	<5	65	<10	35	35	10
14	MPJ 10	19	436	32	12	295	10	90	29	16	34	6	59	<10	36	37	9
15	MPJ 11	45	378	17	17	482	10	277	449	301	77	26	99	27	36	22	17
16	MPJ 12	55	368	17	34	468	8	373	765	464	107	122	125	65	36	16	18
17	MPJ 13	23	383	29	16	310	13	130	106	56	45	<5	74	14	34	35	11
18	MPJ 15	66	326	27	11	714	6	529	1313	793	199	25	65	79	37	7	63
19	MPJ 16	41	373	19	15	419	8	253	422	181	70	20	91	28	36	27	14
20	MPJ 17	40	374	20	20	407	7	281	586	315	87	18	90	33	37	24	27
21	MPJ 18	69	325	10	5	631	5	524	1192	933	151	8	114	48	36	9	22
22	MPJ 19	70	330	27	27	693	5	492	1385	722	170	46	110	55	36	5	41
23	MPJ 20	72	330	12	8	499	5	459	1160	734	158	10	100	37	37	5	13
24	MPJ 21	58	352	18	9	439	6	410	868	585	111	17	101	27	37	16	15
	Average	**48**	**365**	**22**	**16**	**472**	**9**	**327**	**694**	**427**	**104**	**30**	**91**	**41**	**36**	**20**	**22**
	Std. Dev.	**20**	**35**	**7**	**8**	**144**	**3**	**162**	**497**	**325**	**55**	**34**	**21**	**20**	**1**	**12**	**16**
25	MPJ 38	60	355	18	31	373	5	443	609	437	73	75	231	70	42	12	13
26	MPJ 41	73	337	10	26	551	7	662	1400	670	135	82	136	45	37	8	21
27	MPJ 44	18	300	23	9	333	6	214	160	62	33	<5	47	<10	34	25	8
28	MPJ 47	40	402	27	19	228	16	672	1484	510	157	91	124	27	41	6	14
29	MPJ 49	46	420	19	16	359	5	350	690	245	76	51	73	28	28	19	11
30	MPJ 50	61	380	14	28	303	7	664	1451	496	164	107	128	41	39	7	12
	Average	**50**	**366**	**19**	**22**	**358**	**8**	**501**	**966**	**403**	**106**	**81**	**123**	**42**	**37**	**13**	**13**
	Std. Dev.	**19**	**44**	**6**	**8**	**108**	**4**	**195**	**556**	**216**	**53**	**21**	**63**	**17**	**5**	**8**	**4**
31	MPJ 31	24	384	41	6	140	23	178	56	9	37	18	134	19	40	14	16
32	MPJ 32	31	504	36	21	162	24	328	100	13	42	8	64	15	57	17	17
33	MPJ 33	73	337	10	8	327	5	655	1099	160	121	51	94	16	38	60	5
34	MPJ 34	57	283	10	5	118	5	351	652	97	56	<5	22	<10	25	25	7
35	MPJ 36	24	453	38	12	104	16	239	97	13	33	<5	73	15	53	21	12
36	MPJ 58	15	250	20	5	180	7	229	77	37	31	<5	22	<10	35	27	8
37	MPJ 60	8	150	14	2	280	4	238	115	65	30	<5	32	13	28	32	7
	Average	**33**	**337**	**24**	**8**	**187**	**12**	**317**	**314**	**56**	**50**	**26**	**63**	**16**	**39**	**28**	**10**
	Std. Dev.	**23**	**122**	**14**	**6**	**84**	**9**	**161**	**405**	**56**	**33**	**23**	**42**	**2**	**12**	**15**	**5**
38	MPJ 22	21	540	37	2	210	2										
39	MPJ 23	21	496	36	7	247	10										
40	MPJ 25	23	644	39	5	410	13										
41	MPJ 26	24	670	41	5	335	13										
42	MPJ 27	13	300	28	5	349	7										
43	MPJ 28	18	351	48	5	355	11										
44	MPJ 30	14	268	41	5	296	39										
45	MPJ 35	25	374	35	6	123	17										
	Average	**20**	**455**	**38**	**5**	**291**	**14**										
	Std. Dev.	**4**	**155**	**6**	**1**	**93**	**11**										
46	MPJ 24	19	159	10	5	188	5										
47	MPJ 29	63	301	10	12	308	5										
	Average	**41**	**230**	**10**	**9**	**248**	**5**										
48	MPJ 37	37	364	29	15	208	5										
49	MPJ 39	64	302	10	54	607	5										
50	MPJ 40	74	336	10	26	545	6										
51	MPJ 42	18	301	23	10	317	7										
52	MPJ 43	73	336	10	26	551	6										
53	MPJ 45	62	326	10	26	457	6										
54	MPJ 46	72	334	10	28	509	5										
55	MPJ 48	74	353	10	13	386	5										
56	MPJ 54	15	250	n/a	5	180	7										
57	MPJ 57	8	150	n/a	2	280	4										
	Average	**50**	**305**	**14**	**21**	**404**	**6**										
	Std. Dev.	**27**	**63**	**8**	**15**	**152**	**1**										

Serial No.	Sample No.	Ruxton's Ratio	Reiche P.I.	Reiche W.P.I.	Miura W.I.	Parker W.I. %	New W.I.	Predic-. tor x	Predic- tor 1	Predic- tor 1a	Predic- tor 1b	Predic- tor 2
1	MPJ 1	3.65	10.45	28.42	2.13	27.52	1.97	9257	5.28	29.55	99.98	-8.11
2	MPJ 2	3.69	11.61	26.10	1.97	25.61	1.79	7285	4.72	30.82	71.52	-5.94
3	MPJ 3	3.43	11.70	25.06	1.81	27.52	1.73	7291	5.60	29.75	73.50	-10.28
4	MPJ 4	3.41	11.68	25.32	1.82	27.17	1.74	7256	5.55	29.58	73.15	-9.78
5	MPJ 5	3.42	11.05	25.27	1.82	27.12	1.74	7189	5.49	28.89	72.89	-9.73
6	MPJ 6	3.52	11.75	26.42	1.93	27.97	1.82	7086	5.33	29.30	70.93	-8.93
7	MPJ 7	3.52	11.03	26.31	1.92	27.65	1.81	7065	5.29	29.32	70.59	-8.61
	Average	**3.52**	**11.33**	**26.13**	**1.92**	**27.22**	**1.80**	**8505**	**5.32**	**29.60**	**76.08**	**-8.77**
	Std. Dev.	**0.11**	**0.49**	**1.15**	**0.11**	**0.77**	**0.08**	**785**	**0.30**	**0.60**	**10.60**	**1.46**
8	MPJ 8	2.51	5.40	8.91	1.04	15.37	1.02	3450	6.79	29.05	23.39	-12.34
12	MPJ 14	1.44	3.80	-12.09	0.11	1.61	0.10	1133	-2.39	13.10	-0.39	4.39
9	MPJ 51	1.24	3.82	-18.15	0.10	0.00	0.09	1033	-2.68	12.77	-1.68	0.62
10	MPJ 52	1.20	3.54	-17.41	0.09	0.00	0.08	1042	-2.46	12.87	-1.46	4.53
11	MPJ 53	1.20	3.69	-18.17	0.09	0.00	0.08	987	-5.30	9.91	-1.80	-0.80
	Average	**1.52**	**4.05**	**-11.38**	**0.28**	**3.40**	**0.27**	**2544**	**-1.21**	**15.54**	**3.61**	**-0.72**
	Std. Dev.	**0.56**	**0.76**	**11.62**	**0.42**	**6.73**	**0.42**	**1075**	**4.63**	**7.66**	**11.07**	**6.90**
13	MPJ 9	1.37	10.70	-25.53	0.01	0.15	0.01	1056	-3.45	12.99	-2.15	0.54
14	MPJ 10	1.33	10.93	-23.64	0.01	0.15	0.01	961	-3.65	11.83	-2.45	1.26
15	MPJ 11	1.23	6.15	-20.53	0.03	0.18	0.02	848	-4.53	9.81	-2.83	1.67
16	MPJ 12	1.17	5.86	-19.02	0.03	0.18	0.03	970	-4.70	9.76	-1.30	2.70
17	MPJ 13	1.36	10.12	-26.25	0.02	0.18	0.01	889	-3.55	10.46	-1.95	0.70
18	MPJ 15	1.26	3.75	-18.15	0.05	0.18	0.04	787	-5.46	9.60	-4.36	1.60
19	MPJ 16	1.25	6.94	-25.51	0.02	0.25	0.02	863	-4.06	10.20	-2.56	0.72
20	MPJ 17	1.29	7.31	-21.66	0.04	1.01	0.03	882	-4.19	9.97	-2.19	0.62
21	MPJ 18	1.17	3.86	-26.72	0.04	0.03	0.03	821	-4.98	10.62	-4.48	-2.72
22	MPJ 19	1.16	3.64	-19.34	0.04	0.03	0.03	932	-5.33	9.94	-2.63	-0.13
23	MPJ 20	1.09	4.68	-21.70	0.04	0.03	0.04	832	-5.39	10.48	-4.59	0.73
24	MPJ 21	1.13	5.84	-22.59	0.03	0.08	0.03	799	-4.71	9.93	-3.81	1.00
	Average	**1.24**	**6.65**	**-22.55**	**0.03**	**0.20**	**0.03**	**1902**	**-4.50**	**10.47**	**-2.94**	**0.73**
	Std. Dev.	**0.09**	**2.66**	**2.98**	**0.01**	**0.26**	**0.01**	**80**	**0.72**	**0.99**	**1.10**	**1.30**
25	MPJ 38	1.00	6.26	-20.84	0.03	0.00	0.02	1713	-5.50	6.47	-2.40	6.48
26	MPJ 41	1.05	4.33	-17.76	0.03	0.00	0.03	1771	-5.20	7.67	-2.60	5.38
27	MPJ 44	1.28	9.50	-19.19	0.01	0.03	0.01	1679	-4.82	8.23	-3.92	3.25
28	MPJ 47	1.61	13.23	-17.17	0.02	0.00	0.02	1696	-5.45	7.48	-3.55	4.58
29	MPJ 49	1.09	7.49	-19.99	0.02	0.00	0.02	1757	-4.48	8.51	-2.88	2.06
30	MPJ 50	1.07	7.25	-18.41	0.04	0.03	0.03	1753	-5.38	7.25	-2.58	4.44
	Average	**1.18**	**8.01**	**-18.89**	**0.03**	**0.01**	**0.02**	**1728**	**-5.14**	**7.60**	**-2.99**	**4.37**
	Std. Dev.	**0.23**	**3.06**	**1.38**	**0.01**	**0.01**	**0.01**	**37**	**0.40**	**0.73**	**0.61**	**1.56**
31	MPJ 31	1.75	20.97	-16.84	0.02	0.00	0.01	590	-4.50	7.53	-3.90	4.50
32	MPJ 32	2.08	18.75	-16.42	0.02	0.00	0.02	547	-6.23	5.56	-4.13	5.69
33	MPJ 33	0.98	6.34	-19.14	0.03	0.00	0.02	532	-5.75	6.49	-4.95	4.45
34	MPJ 34	1.04	15.26	-18.07	0.03	0.00	0.03	636	-4.35	8.13	-3.85	3.96
35	MPJ 36	1.65	23.46	-17.19	0.02	0.00	0.01	597	-5.18	7.06	-3.98	4.48
36	MPJ 58	1.32	15.20	-20.84	0.01	0.00	0.01	618	-4.91	8.03	-4.41	2.54
37	MPJ 60	1.18	10.67	-20.97	0.01	0.00	0.01	592	-4.86	7.98	-4.66	2.43
	Average	**1.43**	**15.81**	**-18:50**	**0.02**	**0.00**	**0.02**	**1602**	**-5.11**	**7.25**	**-4.27**	**4.01**
	Std. Dev.	**0.41**	**5.92**	**1.87**	**0.01**	**0.00**	**0.01**	**37**	**0.68**	**0.96**	**0.42**	**1.17**
38	MPJ 22	1.20	14.36	-21.09	0.05	0.00	0.05	1045	-0.52	13.94	-0.32	3.55
39	MPJ 23	1.42	13.37	-19.96	0.08	0.00	0.08	850	-0.47	10.78	0.23	3.62
40	MPJ 25	1.26	8.44	-21.14	0.07	0.05	0.07	829	-0.54	10.72	-0.04	3.01
41	MPJ 26	1.31	10.10	-20.56	0.08	0.00	0.08	914	-0.45	11.85	0.05	3.35
42	MPJ 27	1.27	10.18	-19.92	0.04	0.00	0.04	847	0.06	10.92	0.56	2.96
43	MPJ 28	1.39	10.12	-19.35	0.07	0.00	0.07	744	-0.84	9.60	-0.34	4.19
44	MPJ 30	1.29	11.43	-19.09	0.06	0.00	0.06	854	-1.08	11.10	-0.58	4.24
45	MPJ 35	1.94	24.62	-16.03	0.10	0.00	0.10	960	-0.23	12.34	0.37	4.98
	Average	**1.39**	**12.83**	**-19.64**	**0.07**	**0.01**	**0.07**	**1895**	**-0.51**	**11.41**	**-0.01**	**3.74**
	Std. Dev.	**0.24**	**5.14**	**1.64**	**0.02**	**0.02**	**0.02**	**91**	**0.35**	**1.31**	**0.39**	**0.69**
46	MPJ 24	0.98	5.71	-18.48	0.01	0.00	0.01		-47.88		-47.38	1.90
47	MPJ 29	1.00	7.27	-19.67	0.01	0.00	0.01	546	-5.40	6.45	-4.20	3.30
	Average	**0.99**	**6.49**	**-19.08**	**0.01**	**0.00**	**0.01**	**1561**	**-26.64**	**6.45**	**-25.79**	**2.60**
48	MPJ 37	1.09	12.27	-21.97	0.13	0.00	0.12		0.89		2.39	4.83
49	MPJ 39	1.02	4.08	-18.77	0.04	0.00	0.03		-4.66		0.74	-2.14
50	MPJ 40	1.05	4.40	-21.06	0.24	0.00	0.23		5.35		7.95	6.27
51	MPJ 42	1.28	10.05	-20.16	0.11	0.05	0.11		0.01		1.01	3.92
52	MPJ 43	1.04	4.38	-20.52	0.24	0.00	0.24		5.32		7.92	6.23
53	MPJ 45	1.02	5.37	-22.64	0.21	0.00	0.20		3.87		6.47	3.08
54	MPJ 46	1.04	4.71	-20.94	0.24	0.03	0.23		5.24		8.04	5.39
55	MPJ 48	1.01	5.64	-22.30	0.25	0.00	0.24		5.36		6.66	9.01
56	MPJ 54	1.32	15.20	-20.84	0.01	0.00	0.01		-4.91		-4.41	3.20
57	MPJ 57	1.18	10.67	-20.97	0.01	0.00	0.01				0.20	3.10
	Average	**1.10**	**7.68**	**-21.02**	**0.15**	**0.01**	**0.14**		**1.83**		**3.70**	**4.29**
	Std. Dev.	**0.12**	**4.02**	**1.12**	**0.10**	**0.02**	**0.10**		**4.25**		**4.31**	**2.93**

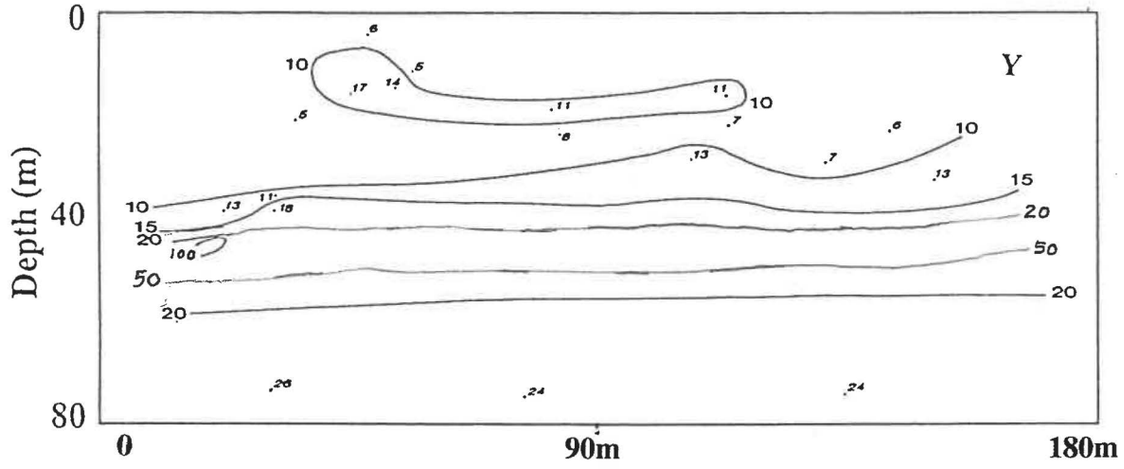

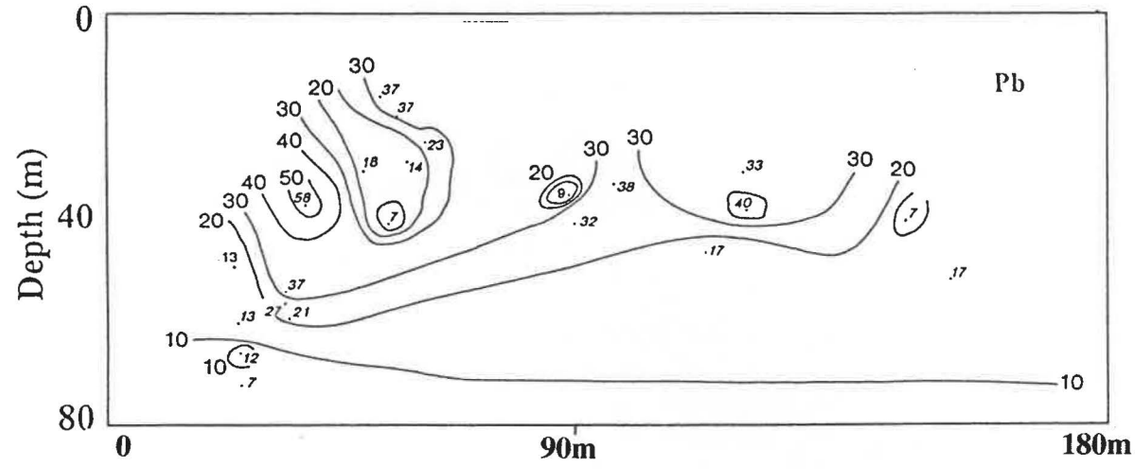

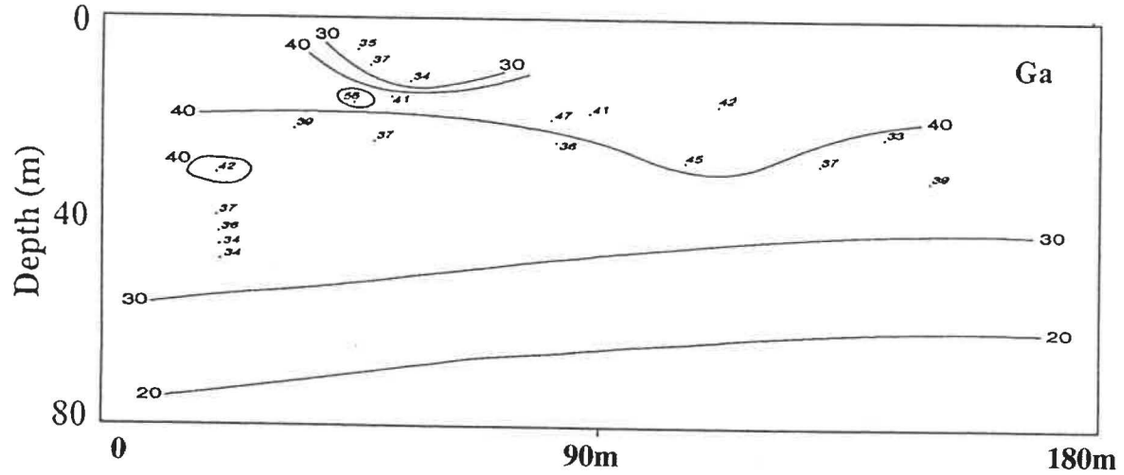

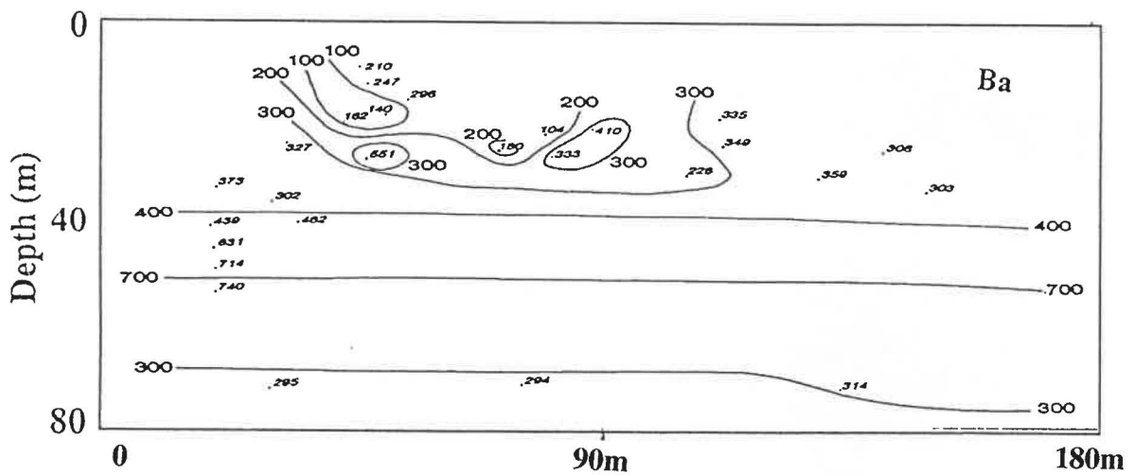

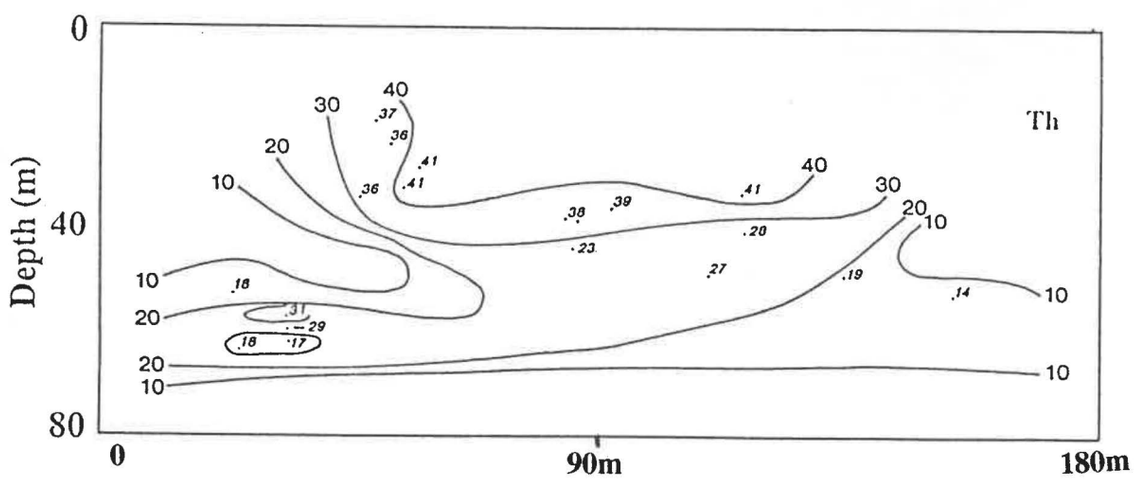

Appendix 4.5 Iso-con Contour Cross Sections of Trace Elements Y, Pb, Ga, Ba & Th

APPENDIX 4.6 CHEMICAL ANALYSIS OF SAMPLES RECALCULATED FOR CONSTANT ALUMINIUM

Serial No.	Sample No.	Sample Description	SiO_2	MgO	CaO	FeO	Fe_2O_3	TiO_2	P_2O_5	LOI
1	MPJ 1	Fresh Basalt	42.74	12.97	10.94	10.34	2.63	2.39	0.44	3.09
2	MPJ 2	Fresh Basalt	46.30	11.37	10.26	9.84	2.13	2.20	0.38	2.94
3	MPJ 3	Fresh Basalt	41.64	12.94	10.99	10.83	4.73	2.53	0.38	3.24
4	MPJ 4	Fresh Basalt	41.43	12.89	10.85	10.77	4.50	2.51	0.38	3.22
5	MPJ 5	Fresh Basalt	41.37	12.82	10.82	10.73	4.50	2.49	0.38	3.21
6	MPJ 6	Fresh Basalt	42.59	12.67	11.16	10.56	3.66	2.43	0.39	3.15
7	MPJ 7	Fresh Basalt	41.77	12.36	11.01	10.43	3.69	2.40	0.38	3.12
		Average	**42.55**	**12.57**	**10.86**	**10.50**	**3.69**	**2.42**	**0.39**	**3.14**
		Standard Deviation	**1.74**	**0.57**	**0.29**	**0.34**	**1.00**	**0.11**	**0.02**	**0.10**
8	MPJ 8	Slightly Weath	36.74	11.79	6.29	12.91	11.83	3.10	0.34	3.86
9	MPJ 51	Slightly Weath	33.26	1.08	0.00	4.84	16.28	5.63	0.66	22.47
10	MPJ 52	Slightly Weath	33.66	0.92	0.00	4.42	15.82	5.68	0.70	22.98
11	MPJ 53	Slightly Weath	33.24	0.82	0.00	4.64	16.13	5.63	0.67	22.57
12	MPJ 14	Slightly Weath	36.11	4.20	0.73	1.14	15.80	4.47	0.65	21.64
		Average	**34.60**	**3.76**	**1.40**	**5.59**	**15.17**	**4.90**	**0.60**	**18.70**
		Standard Deviation	**1.68**	**4.70**	**2.75**	**4.37**	**1.88**	**1.13**	**0.15**	**8.31**
13	MPJ 9	Moderately w.	50.95	0.15	0.08	0.44	25.18	1.15	0.06	8.35
14	MPJ 10	Moderately w.	52.14	0.13	0.08	0.45	24.06	1.10	0.05	8.51
15	MPJ 11	Moderately w.	42.34	0.38	0.09	0.93	20.05	3.49	0.47	17.76
16	MPJ 12	Moderately w.	39.04	0.79	0.09	1.08	18.77	4.22	0.60	20.49
17	MPJ 13	Moderately w.	48.57	0.24	0.09	0.52	25.34	1.57	0.16	9.88
18	MPJ 15	Moderately w.	34.36	1.57	0.08	1.27	17.63	5.09	0.61	24.12
19	MPJ 16	Moderately w.	41.83	0.54	0.12	0.81	24.01	2.98	0.34	15.35
20	MPJ 17	Moderately w.	43.17	1.15	0.49	0.81	22.05	2.95	0.34	15.44
21	MPJ 18	Moderately w.	31.34	0.97	0.01	1.21	22.93	4.95	0.46	23.07
22	MPJ 19	Moderately w.	32.78	1.12	0.01	1.32	18.04	5.40	0.59	25.11
23	MPJ 20	Moderately w.	31.64	1.32	0.01	1.33	20.24	5.40	0.56	25.23
24	MPJ 21	Moderately w.	36.41	0.86	0.04	1.10	21.39	4.37	0.52	20.97
		Average	**40.38**	**0.77**	**0.10**	**0.94**	**21.64**	**3.56**	**0.40**	**17.86**
		Standard Deviation	**7.39**	**0.48**	**0.13**	**0.33**	**2.72**	**1.61**	**0.21**	**6.35**
25	MPJ 38	Highly Weath.	34.72	0.66	0.00	1.17	19.89	4.39	1.02	22.15
26	MPJ 41	Highly Weath.	32.74	0.60	0.00	1.40	16.79	5.80	0.89	26.51
27	MPJ 44	Highly Weath.	50.16	0.19	0.01	0.68	19.92	1.91	0.10	12.83
28	MPJ 47	Highly Weath.	48.63	0.33	0.00	0.85	16.90	2.76	0.33	16.10
29	MPJ 49	Highly Weath.	41.62	0.29	0.00	0.95	19.92	3.52	0.66	18.00
30	MPJ 50	Highly Weath.	33.11	0.64	0.01	1.34	17.46	5.45	0.88	25.48
		Average	**40.16**	**0.45**	**0.00**	**1.06**	**18.48**	**3.97**	**0.65**	**20.18**
		Standard Deviation	**7.85**	**0.21**	**0.01**	**0.29**	**1.59**	**1.52**	**0.36**	**5.43**
31	MPJ 31	Completely W.	56.32	0.22	0.00	0.54	17.16	1.36	0.14	10.17
32	MPJ 32	Completely W.	52.13	0.25	0.00	0.79	15.65	2.29	0.17	15.08
33	MPJ 33	Completely W.	31.00	0.41	0.00	1.46	17.79	5.93	0.60	27.65
34	MPJ 34	Completely W.	37.75	1.37	0.00	1.13	18.90	4.59	0.42	21.48
35	MPJ 36	Completely W.	52.80	0.23	0.00	0.69	17.35	1.94	0.10	13.04
36	MPJ 58	Completely W.	49.90	0.13	0.00	0.63	20.97	1.60	0.03	11.80
37	MPJ 60	Completely W.	50.31	0.10	0.00	0.52	21.88	1.23	0.04	10.67
		Average	**47.17**	**0.39**	**0.00**	**0.82**	**18.53**	**2.71**	**0.21**	**15.70**
		Standard Deviation	**9.20**	**0.45**	**0.00**	**0.35**	**2.22**	**1.82**	**0.22**	**6.52**

APPENDIX 5.1 RESULTS OF SCHMIDT REBOUND HARDNESS TEST											
Sample Number	MPJ 1	MPJ 2	MPJ 3	MPJ 4	MPJ 5	MPJ 6	MPJ 7	MPJ 8	MPJ 51	MPJ 52	MPJ 53
Schm. L. Reb. Ham. Val.	51	45	38	39	44	28	29	31	19	16	16
,,	50	45	38	38	44	28	28	30	19	16	16
,,	46	44	34	37	35	28	26	29	19	16	16
,,	45	44	32	32	35	28	25	25	19	16	16
,,	43	41	31	32	32	28	25	24	19	16	15
,,	42	40	29	32	32	27	25	22	19	16	15
,,	42	40	28	32	30	26	24	20	19	16	15
,,	41	39	27	30	30	26	24	20	19	16	15
,,	37	39	25	27	29	26	24	20	19	15	15
,,	37	38	25	25	29	22	22	19	19	15	15
,,	36	37	24	24	28	21	22	18	17	15	15
,,	36	36	24	22	28	21	22	18	17	15	15
,,	31	35	23	22	26	20	21	17	17	15	15
,,	31	35	21	21	26	20	20	17	17	15	15
,,	29	34	18	17	25	19	20	17	16	15	15
,,	28	34	18	15	25	17	14	16	16	15	15
,,	26	33	12	14	24	16	14	15	16	15	15
,,	25	32	12	13	21	15	12	14	16	14	15
,,	23	26	12	12	13	15	12	13	15	11	15
,	22	24	12	12	13	14	11	12	12	11	11
Average(10 higher)	43.4	41.5	30.7	32.4	34.0	26.7	25.2	24.0	19.0	15.8	15.4
Std. Dev.	4.74	2.72	4.81	4.55	5.70	1.89	2.04	4.57	0.00	0.42	0.52

	APPENDIX 5.2 PARTICLE SIZE DISTRIBUTION OF SAMPLES										
serial	sample	sample	% gravel	% coarse sand	% medium sand	% fine sand	% coarse silt	%medium silt	% fine silt	% clay	TOTAL
number	number	description	> 2mm	2-0.6mm	0.6-0.2mm	0.2-0.06mm	0.06-0.02mm	0.02-0.006mm	2-6 microns	<2 microns	
1	MPJ 14	slightly weath	42.17	11.41	0.38	3.35	6.16	9.68	8.27	18.58	100
2	MPJ 9		0.00	10.02	0.37	3.62	13.81	23.21	17.77	31.20	100
3	MPJ 10		0.00	10.11	0.31	3.55	12.17	22.52	17.73	33.62	100
4	MPJ 11	moderately	0.00	10.23	0.68	7.92	16.83	20.70	14.57	29.07	100
5	MPJ 12		0.63	27.28	0.43	3.72	13.07	17.59	11.11	26.18	100
7	MPJ 13	weathered	0.00	30.10	0.40	4.08	10.11	16.27	13.19	25.84	100
8	MPJ 15		55.07	16.90	0.10	1.37	1.67	6.68	7.89	10.32	100
9	MPJ 16	basalt	10.10	9.78	0.00	2.50	6.55	15.10	15.29	40.67	100
10	MPJ 17		11.02	10.10	0.12	2.64	8.31	17.29	14.51	36.01	100
11	MPJ 18		0.00	10.31	0.00	1.69	14.40	28.85	17.62	27.14	100
12	MPJ 19		1.51	10.41	0.05	2.03	7.96	20.49	17.73	39.82	100
13	MPJ 20		0.00	10.00	0.63	6.05	15.19	17.18	14.11	36.84	100
14	MPJ 21		1.21	15.02	0.88	7.46	17.89	19.63	11.90	26.01	100
Average			6.63	14.19	0.33	3.89	11.50	18.79	14.45	30.23	
Std. Dev.			15.76	7.17	0.29	2.18	4.72	5.35	3.10	8.26	
31	MPJ 38	highly	29.05	38.41	0.00	0.02	0.71	5.03	6.52	20.26	100
33	MPJ 41		0.00	0.00	2.10	9.17	17.35	22.15	15.55	33.68	100
35	MPJ 44	weathered	0.47	41.72	0.50	2.66	4.22	9.09	10.76	30.58	100
36	MPJ 47		1.31	10.74	0.00	10.35	15.73	14.20	10.28	37.39	100
37	MPJ 49	basalt	5.90	11.94	0.00	10.81	16.52	12.85	9.81	32.17	100
38	MPJ 50		2.62	4.68	0.00	12.90	19.20	13.16	10.34	37.10	100
Average			6.56	17.92	0.43	7.65	12.29	12.75	10.54	31.86	
Std. Dev.			11.22	17.72	0.84	5.11	7.78	5.72	2.90	6.29	
24	MPJ 31	completely	35.42	45.01	0.01	0.19	0.93	3.86	4.44	10.14	100
25	MPJ 32		52.26	29.69	0.01	0.32	1.49	4.36	3.34	8.52	100
26	MPJ 33	weathered	15.18	30.99	0.29	3.04	7.51	9.12	8.08	25.78	100
27	MPJ 34		12.00	36.48	0.18	0.56	2.24	14.97	9.93	23.65	100
29	MPJ 36	basalt	0.37	68.46	0.01	0.29	1.31	4.59	5.64	19.33	100
44	MPJ 58		0.00	0.00	0.92	5.59	15.22	17.58	15.19	45.50	100
45	MPJ 60		0.00	0.00	0.92	7.20	12.05	18.17	19.70	41.96	100
Average			16.46	30.09	0.33	2.46	5.82	10.38	9.47	24.98	
Std. Dev.			20.26	24.32	0.41	2.91	5.86	6.42	6.01	14.35	
15	MPJ 22		0.00	0.00	0.00	0.69	4.12	28.39	25.60	41.20	100
16	MPJ 23	weathered	0.00	0.00	0.00	0.31	2.70	20.06	22.29	54.64	100
18	MPJ 25		0.00	0.00	0.30	3.64	12.60	28.02	22.31	33.13	100
19	MPJ 26	tephra	0.00	0.00	0.11	2.35	12.70	26.96	20.68	37.20	100
20	MPJ 27		0.00	0.00	0.00	5.54	29.36	31.34	16.92	16.84	100
21	MPJ 28		0.00	0.00	3.46	15.98	28.84	24.88	11.65	15.19	100
23	MPJ 30		0.00	0.00	0.71	5.66	14.63	38.65	16.49	23.86	100
28	MPJ 35		31.84	43.80	0.01	0.33	1.25	4.96	5.66	12.14	100
Average			3.98	5.48	0.57	4.31	13.27	25.41	17.70	29.28	
Std. Dev.			11.26	15.49	1.19	5.19	10.98	9.82	6.52	14.83	
17	MPJ 24	paleosol	0.00	0.00	0.94	3.56	3.43	12.94	14.40	64.73	100
22	MPJ 29		17.07	20.03	0.52	7.08	14.70	15.66	8.84	16.10	100
Average			8.54	10.02	0.73	5.32	9.06	14.30	11.62	40.41	
Std. Dev.			12.07	14.16	0.30	2.49	7.97	1.92	3.93	34.39	
30	MPJ 37		0.00	0.00	0.00	0.04	2.23	20.28	21.74	55.71	100
32	MPJ 39	inclusions	0.95	16.01	1.00	7.40	8.85	9.94	11.94	43.91	100
34	MPJ 42		0.35	25.63	0.00	2.89	10.10	16.02	12.38	32.63	100
42	MPJ 54		37.75	21.26	0.21	3.50	6.25	7.30	7.61	16.13	100
43	MPJ 57		26.72	19.69	0.00	2.48	8.29	10.07	9.22	23.53	100
Average			13.15	16.52	0.24	3.26	7.14	12.72	12.58	34.38	
Std. Dev.			17.85	9.86	0.43	2.66	3.08	5.30	5.49	15.81	

APPENDIX 5.3 GEOTECHNICAL PARAMETERS OF KARAMU BASALT SAMPLES

Ser. No.	Sample No.	Weath. degree	Depth meters	Water content	Compr. Str. MPa Schmidt	Compr. Str. MPa Point L.	Penetra resist.	Shear Strength	% Clay	Liquid Limit	Plastic Limit	Plast. Index	Activity of Clay	Cohesion kPa	Angle of Int. Fr.	Dry Density	Porosity	Perm-lity m/s X 10^{-4}	CBR
1	MPJ 1	Fresh	75.0	0.00	115	170										2814	0.25		100
2	MPJ 2	Fresh	75.0	0.00	108	156										2902	0.31		
3	MPJ 3	Fresh	77.0	0.00	60	75										2816	0.18		
4	MPJ 4	Fresh	72.0	0.00	65	85										2827	0.25		100
5	MPJ 5	Fresh	67.0	0.00	70	87										2792	0.46		
6	MPJ 6	Fresh	75.0	0.00	48	151										2754	0.54		
7	MPJ 7	Fresh	75.0	0.00	45	138										2774	0.29		
	Average		**73.7**	**0.0**	**73.0**	**123**										**2811**	**0.33**		**100**
	Std. Dev.		**3.3**	**0.0**	**27.8**	**39**										**48**	**0.13**		**0**
8	MPJ 8	Slight	65.0	12.04	41	16										2492	2.96		
9	MPJ 14	Slight	56.9	34.86					18.58	79.82	72.56	7.26	0.39	0.0	36	1845	13.34		40
10	MPJ 51	Slight	61.3	33.87	35	6										2175	6.53		45
11	MPJ 52	Slight	60.0	31.11	26	5										2059	10.32		
12	MPJ 53	Slight	58.5	30.62	24											2008	6.65		
	Average		**60.3**	**28.5**	**31.5**	**9.0**			**18.58**	**79.82**	**72.56**	**7.26**	**0.39**	**0.0**	**36**	**2116**	**7.96**		**43**
	Std. Dev.		**3.1**	**9.4**	**7.9**	**6.1**										**241**	**3.98**		**4**
13	MPJ 9	Moderate	48.3	45.89			3.89	95.0	31.20	89.56	75.09	14.47	0.46	1.0	33	2066	11.37	2.45	
14	MPJ 10	Moderate	47.5	44.09			3.89	96.2	33.62	86.74	72.31	14.43	0.43	1.0	34	2066	11.02	2.44	25
15	MPJ 11	Moderate	49.8	54.41			3.86	110.3	29.07	85.65	71.42	14.23	0.49	2.0	33	2031	13.72	2.43	
16	MPJ 12	Moderate	49.3	50.34			3.89	98.6	26.18	88.63	76.04	12.59	0.48	1.0	33	2045	13.68	2.43	
17	MPJ 13	Moderate	48.8	41.91			3.87	95.2	25.84	89.75	79.01	10.74	0.42	1.0	32	1832	11.84	2.45	
18	MPJ 15	Moderate	55.8	39.49					10.32	79.05	71.07	7.98	0.77	0.0	34	1845	16.17		
19	MPJ 16	Moderate	54.8	32.20			4.39		40.67	77.28	56.71	20.57	0.51	0.0	35	1841	16.88	1.52	
20	MPJ 17	Moderate	53.9	37.52			4.39		36.01	74.12	60.83	13.29	0.37	0.0	36	1842	17.73	1.52	
21	MPJ 18	Moderate	53.3	51.47			4.23	183.3	27.14	75.92	61.68	14.24	0.52	0.0	35	1887	14.46	1.52	30
22	MPJ 19	Moderate	52.5	50.97			4.25	162.7	39.82	72.98	63.54	9.44	0.24	0.0	33	1867	15.56	1.52	
23	MPJ 20	Moderate	51.5	61.91			4.26	119.1	36.84	72.12	63.14	8.98	0.24	0.0	34	1868	12.83	1.52	
24	MPJ 21	Moderate	50.5	48.98			4.21	119.2	26.01	68.15	40.00	28.15	1.08	0.0	36	1706	16.08	1.52	
	Average		**51.3**	**46.6**			**4.1**	**120.0**	**30.23**	**80.00**	**65.90**	**14.09**	**0.50**	**0.5**	**34**	**1908**	**14.28**	**1.94**	**28**
	Std. Dev.		**2.7**	**8.1**			**0.2**	**32.0**	**8.26**	**7.68**	**10.74**	**5.55**	**0.23**	**0.7**	**1**	**116**	**2.24**	**0.48**	**4**
25	MPJ 38	High	45.0	79.31			4.38	146.6	20.26	77.88	58.31	19.57	0.97	7.2	36	1787	21.38	77.3	
26	MPJ 41	High	33.5	35.12			4.02		33.68	63.87	58.22	5.65	0.17	7.0	35	1787	21.83	77	
27	MPJ 44	High	33.5	34.00			4.05	116.3	30.58	74.12	58.51	15.61	0.51	2.0	36	1767	14.35	76.8	15
28	MPJ 47	High	42.5	34.92			4.11	118.5	37.39	75.68	55.91	19.77	0.53	3.0	38	1754	21.63	76.9	
29	MPJ 49	High	43.0	35.00			4.12	112.8	32.17	65.67	57.13	8.54	0.27	2.5	38	1745	22.34	77.9	
30	MPJ 50	High	43.5	29.74			4.21	120.4	37.10	57.61	47.58	10.03	0.27	3.0	38	1735	23.33	77	15
	Average		**40.2**	**41.3**			**4.1**	**122.9**	**31.86**	**69.14**	**55.94**	**13.20**	**0.45**	**4.1**	**37**	**1763**	**20.81**	**77.2**	**15**
	Std. Dev.		**5.2**	**18.7**			**0.1**	**13.5**	**6.29**	**7.96**	**4.21**	**5.97**	**0.29**	**2.3**	**1**	**22**	**3.24**	**0.4**	**0**
31	MPJ 31	Complete	6.0	33.21				121.0	10.14	81.01	61.23	19.78	1.95	7.0	33	1554	26.66	454.5	1
32	MPJ 32	Complete	6.5	42.51				106.5	8.52	80.01	58.75	21.26	2.50	7.0	33	1576	25.94	432.9	
33	MPJ 33	Complete	9.0	49.41				110.4	25.78	69.01	56.92	12.09	0.47	5.0	36	1502	27.19	427.3	
34	MPJ 34	Complete	6.5	42.54				112.8	23.65	75.76	69.67	6.09	0.26	4.0	35	1642	25.80	456.6	4.5
35	MPJ 36	Complete	23.5	59.32				121.0	19.33	86.72	72.01	14.71	0.76	5.0	34	1591	25.45	500.0	1
36	MPJ 58	Complete	27.5	35.25			4.39		45.50					2.0	36	1554	21.71	268.0	
37	MPJ 60	Complete	28.5	36.37			4.34		41.96					2.0	36	1556	24.94	279.3	3.5
	Average		**15.4**	**42.7**			**4.4**	**114.3**	**24.98**	**78.50**	**63.72**	**14.79**	**1.19**	**4.6**	**35**	**1568**	**25.38**	**402.7**	**2.5**
	Std. Dev.		**10.6**	**9.2**			**0.0**	**6.5**	**14.35**	**6.59**	**6.73**	**6.12**	**0.98**	**2.1**	**1**	**43**	**1.78**	**91.2**	**1.8**

Appendix 6.1 Principal Component Analysis Results Sheet

Principal Component Analysis: SiO2, Al2O3, MnO, MgO, CaO, Na2O, K2O, TiO2, P 2O5,

Eigenanalysis of the Correlation Matrix

23 cases used 6 cases contain missing values

Eigenvalue	9.9849	3.0301	2.7808	1.2395	0.9261	0.6861
Proportion	0.499	0.152	0.139	0.062	0.046	0.034
Cumulative	0.499	0.651	0.790	0.852	0.898	0.932
Eigenvalue	0.4232	0.2760	0.2054	0.1573	0.1191	0.0731
Proportion	0.021	0.014	0.010	0.008	0.006	0.004
Cumulative	0.954	0.967	0.978	0.985	0.991	0.995
Eigenvalue	0.0373	0.0296	0.0151	0.0099	0.0060	0.0004
Proportion	0.002	0.001	0.001	0.000	0.000	0.000
Cumulative	0.997	0.998	0.999	1.000	1.000	1.000
Eigenvalue	0.0002	0.0000				
Proportion	0.000	0.000				
Cumulative	1.000	1.000				

Variable	PC1	PC2	PC3	PC4	PC5	PC6
SiO2	-0.297	-0.106	-0.140	-0.018	0.034	-0.124
Al2O3	-0.135	0.221	0.345	0.042	-0.567	0.128
MnO	0.291	0.004	0.013	0.253	-0.009	0.147
MgO	0.172	0.062	-0.425	-0.319	-0.140	0.043
CaO	0.055	0.154	-0.481	-0.206	-0.337	0.037
Na2O	-0.199	0.264	-0.016	0.056	0.140	0.585
K2O	-0.174	-0.141	-0.429	-0.059	0.043	0.038
TiO2	0.307	-0.087	0.042	-0.003	0.133	0.018
P2O5	0.279	-0.111	0.019	0.239	-0.180	0.224
LOI	-0.081	0.471	0.103	0.072	0.193	0.093
Nb	0.305	-0.061	0.054	0.027	0.159	0.020
Zr	-0.210	-0.180	-0.039	0.439	0.217	0.151
Th	-0.299	-0.124	-0.052	0.103	0.062	0.037
Sr	0.113	-0.084	-0.310	0.543	-0.367	0.207
Rb	-0.232	-0.249	-0.227	0.195	0.180	-0.112
Ba	0.226	0.242	-0.232	0.084	0.182	-0.024
Fe2O3	0.301	-0.140	0.027	-0.001	0.150	0.003
FeO	0.301	-0.139	0.026	-0.003	0.148	0.002
pH	0.032	0.487	-0.196	0.057	0.327	0.104
El.Cond.	0.032	0.355	-0.066	0.416	-0.091	-0.670

```
MTB > PCA c4-c21;
SUBC>   NComponents 6;
```

Principal Component Analysis: SiO2, Al2O3, MnO, MgO, CaO, Na2O, K2O, TiO2, P 2O5,

Eigenanalysis of the Correlation Matrix

Eigenvalue	8.1308	2.6108	2.2547	1.4351	1.2286	0.6944
Proportion	0.452	0.145	0.125	0.080	0.068	0.039
Cumulative	0.452	0.597	0.722	0.802	0.870	0.909
Eigenvalue	0.5753	0.3133	0.2495	0.1636	0.1431	0.0791
Proportion	0.032	0.017	0.014	0.009	0.008	0.004
Cumulative	0.941	0.958	0.972	0.981	0.989	0.993
Eigenvalue	0.0624	0.0330	0.0166	0.0083	0.0009	0.0003
Proportion	0.003	0.002	0.001	0.000	0.000	0.000
Cumulative	0.997	0.999	0.999	1.000	1.000	1.000

Variable	PC1	PC2	PC3	PC4	PC5	PC6
SiO2	-0.313	0.110	0.180	0.025	-0.188	-0.216
Al2O3	-0.233	-0.185	-0.234	-0.099	0.387	-0.085
MnO	0.324	-0.007	-0.031	0.139	0.152	0.055
MgO	0.205	0.359	0.083	-0.406	-0.034	0.158
CaO	0.046	0.497	0.061	-0.388	0.130	0.055
Na2O	-0.193	0.209	-0.235	0.272	-0.218	0.299
K2O	-0.164	0.393	0.338	0.021	-0.131	0.035
TiO2	0.341	-0.080	0.021	0.053	-0.028	0.120
P2O5	0.318	-0.031	0.092	0.142	0.215	0.070
LOI	-0.138	0.135	-0.481	0.085	0.184	0.397
Nb	0.337	-0.050	0.003	0.119	-0.009	0.175
Zr	-0.077	0.197	0.238	0.649	-0.067	0.164
Sr	0.128	0.325	0.242	0.223	0.393	-0.211
Ba	0.285	0.186	-0.211	-0.060	-0.160	-0.176
Fe2O3	0.332	-0.084	0.085	0.032	0.049	0.196
FeO	0.231	-0.104	-0.049	0.065	-0.488	-0.410
pH	0.120	0.294	-0.458	0.057	-0.327	0.009
El.Cond.	0.047	0.261	-0.336	0.230	0.311	-0.555

APPENDIX 6.1 Best Subset Regression Result Sheet (Response – Water Content)

Best Subsets Regression

Response is Water Content

Vars	R-Sq	Adj. R-Sq	C-p	s	SiO2	Al2O3	MnO	MgO	CaO	Na2O	K2O	TiO2	P2O5	LOI	Nb	Zr	Th	Sr	Rb	Ba	Fe2O3	FeO	pH	El. Cond.
1	79.7	79.0	18.7	9.7277					X															
1	79.0	78.3	20.1	9.8773				X																
2	83.2	82.0	12.7	8.9885	X												X							
2	81.0	79.6	17.8	9.5779					X															X
3	86.1	84.5	8.3	8.3461	X												X							X
3	84.3	82.6	12.2	8.8508	X												X					X		
4	86.8	84.8	8.7	8.2801	X												X				X			X
4	86.5	84.5	9.2	8.3539	X										X		X							X
5	87.5	85.0	9.1	8.2176	X							X			X						X	X		
5	87.3	84.8	9.5	8.2760	X							X									X	X		X
6	89.8	87.3	5.9	7.5668	X							X					X				X	X		X
6	89.7	87.2	6.1	7.5950	X							X			X						X	X		X
7	91.2	88.5	4.8	7.1897	X							X			X		X				X	X		X
7	90.8	88.1	5.6	7.3267	X					X		X					X				X	X		X
8	92.1	89.2	4.7	6.9555	X					X		X			X		X				X	X		X
8	91.7	88.6	5.7	7.1482	X		X					X			X		X				X	X		X
9	93.2	90.3	4.2	6.5908	X		X			X		X			X		X				X	X		X
9	92.9	89.9	4.9	6.7365	X					X		X			X		X		X		X	X		X
10	93.8	90.7	4.9	6.4695	X			X	X	X	X	X					X				X	X		X
10	93.7	90.6	5.1	6.5009	X		X					X		X	X		X				X	X	X	X
11	94.4	91.2	5.5	6.2769	X		X	X	X	X	X	X					X				X	X		X
11	94.2	90.8	6.1	6.4347	X			X	X	X		X			X		X		X		X	X		X
12	94.8	91.4	6.7	6.2353	X		X	X	X	X	X	X			X		X				X	X		X
12	94.8	91.3	6.7	6.2430		X	X		X	X	X		X	X			X	X	X		X			X
13	95.1	91.3	8.1	6.2593	X	X	X		X	X	X	X	X	X			X	X	X					X
13	95.0	91.1	8.3	6.3168	X		X	X	X	X	X	X			X		X		X		X	X		X
14	95.2	91.0	9.7	6.3502	X	X	X		X	X	X	X	X	X	X		X	X	X					X
14	95.2	90.9	9.9	6.3859	X		X	X	X	X	X	X			X		X	X	X		X	X		X
15	95.3	90.7	11.5	6.4756		X	X	X	X	X	X	X	X		X		X	X	X		X	X		X
15	95.3	90.5	11.6	6.5238	X	X	X		X	X	X	X	X	X	X	X	X	X	X					X
16	95.4	90.1	13.4	6.6678	X	X	X	X	X	X	X	X	X		X		X	X	X		X	X		X
16	95.3	90.0	13.4	6.6941		X	X	X	X	X	X	X	X		X		X	X	X		X	X	X	X
17	95.4	89.5	15.2	6.8751	X	X	X	X	X	X	X	X	X	X	X		X	X	X		X	X		X
17	95.4	89.4	15.3	6.9062	X	X	X	X	X	X	X	X	X		X		X	X	X	X	X	X		X
18	95.5	88.7	17.2	7.1312	X	X	X	X	X	X	X	X	X	X	X		X	X	X	X	X	X		X
18	95.5	88.7	17.2	7.1405	X	X	X	X	X	X	X	X	X	X	X		X	X	X		X	X	X	X
19	95.5	87.9	19.0	7.3894	X	X	X	X	X	X	X	X	X	X	X		X	X	X	X	X	X	X	X
19	95.5	87.7	19.1	7.4382	X	X	X	X	X	X	X	X	X	X	X	X	X	X	X	X	X	X		X
20	95.5	86.6	21.0	7.7487	X	X	X	X	X	X	X	X	X	X	X	X	X	X	X	X	X	X	X	X

APPENDIX 8.1 GEOCHEMICAL AND GEOTECNICAL DATA EXTRACTED FROM BASSETT (1998)

Table 4.2: XRF and pH results from Kuaotunu Hill.

Unit	pH	SiO_2	Al_2O_3	MnO	MgO	CaO	Na_2O	K_2O	P_2O_5	TiO_2	Fe_2O_3	LOI	Total
		Wt. %	Wt. %	Wt. %	Wt. %	Wt. %	Wt. %	Wt. %	Wt. %	Wt. %	Wt. %	Wt. %	Wt. %
AL.GW	4.69	60.67	18.66	0.08	0.93	0.1	0.06	2.51	0.07	0.97	6.78	8.01	98.84
CW.GW	4.83	59.03	17	N.D.	0.75	0.04	N.D.	3.07	0.09	1.06	10.46	7.44	98.94
HW.GW	4.55	59.83	19.81	0.01	0.94	0.02	0.23	3.41	0.04	1.11	5.44	7.39	98.25
MW.GW	4.53	63.79	16.3	0.03	0.84	0.21	2.17	4.70	0.1	0.81	4.77	4.52	98.24
SW.GW	6.57	60.02	15.99	0.1	2.18	1.89	3.56	2.41	0.15	0.9	6.88	4.10	98.18
UW.GW	6.85	66.87	13.39	0.1	1.56	3.15	4.90	1.07	0.07	0.72	4.68	1.91	98.42
AL.AN	4.69	59.28	17.88	0.04	1.62	0.05	0.02	0.02	N.D.	0.74	6.73	11.88	98.24
CW.AN	5.14	55.16	19.75	0.18	1.73	0.10	0.19	0.63	N.D.	0.78	7.64	11.99	98.12
HW.AN	5.00	56.22	19.42	0.1	1.62	0.54	0.86	1.6	N.D.	0.66	6.09	10.84	97.94
MW.AN	5.72	61.41	16.28	0.08	1.26	4.4	2.78	2.08	0.04	0.61	6.07	4.19	99.2
SW.AN	7.12	60.61	16.12	0.1	1.39	5.08	2.80	2.03	0.04	0.63	6.25	3.37	98.42
UW.AN	7.25	61.43	15.92	0.11	2.01	5.33	2.91	1.98	0.04	0.6	6.30	2.94	99.57

Table 4.4: Bulk Rock Properties of Kuaotunu Hill Sampled Material.

Unit	Moisture Content	Density				Porosity
		Dry	Bulk	Saturated	Particle	Total
	%	kgm^{-3}	kgm^{-3}	kgm^{-3}	kgm^{-3}	%
AL.GW	30.9±2.0	1260±46	1651±28	2259±46	2711±12	53.5±1.7
CW.GW	24.6±1.1	1474±36	1829±28	2473±36	2761±7	46.6±1.3
HW.GW	16.4±0.7	1643±44	1913±51	2020±85	2725±9	39.7±1.6
HW Cor	5.0±2.6	2324±162	2435±114	3224±162	2690±7	13.6±6.0
MW.GW	2.9±0.2	2330±23	2398±23	3329±23	2662±5	12.5±0.9
SW.GW	1.0±0.1	2573±14	2598±11	3572±14	2707±9	5.0±0.5
UW.GW	0.5±0.0	2662±1	2676±1	3661±1	2703±2	1.5±0.1
AL.AN	46.8±0.7	1093±15	1605±18	2093±15	2722±3.9	59.8±0.1
CW.AN	27.9±01.0	1141±21	1459±34	2141±21	2671±11.8	57.3±0.8
HW.AN	22.6±0.5	1669±14	2047±19	2118±114	2618±16.4	36.3±0.5
MW.AN	4.6±0.4	2365±13	2471±8	3364±13	2670±9.7	11.4±0.5
SW.AN	2.8±0.1	2443±20	2511±20	3442±20	2666±10	8.4±0.7
UW.AN	3.2±0.0	2496±7	2577±6	3496±7	2700±3	7.6±0.3

Table 4.5: Strength Results.

Unit	Shear Strength		OWC	CBR			UCS	Point Load	Slake
	Cohesion	Friction Angle		At Optimum	Soaked	Swell			Durability
	kPa	°	%	%	%	%	MNm^{-2}	$I_{S(50)}$	Id_2 (%)
AL.GW	29±1	27±1	29±1	28±1	12±1	1±1	—	—	52±1
CW.GW	29±1	48±1	26±1	30±1	14±1	1±1	—	—	54±1
HW.GW	87±1	55±1	25±1	32±1	8±1	3±1	—	—	77±1
MW.GW	—	—	11±1	45±1	45±1	0±1	—	1.5±0.2	97±1
SW.GW	—	—	6±1	55±1	55±1	0±1	—	3.4±0.2	99±1
UW.GW	—	—	—	—	—	—	248±7	5.2±0.2	100±1